Characterization of mass transfer by condensation on a horizontal plate

Akhilesh Tiwari

▶ **To cite this version:**

Akhilesh Tiwari. Characterization of mass transfer by condensation on a horizontal plate. Other. Université Blaise Pascal - Clermont-Ferrand II, 2011. English. NNT : 2011CLF22211 . tel-00708562

HAL Id: tel-00708562

https://theses.hal.science/tel-00708562

Submitted on 15 Jun 2012

HAL is a multi-disciplinary open access archive for the deposit and dissemination of scientific research documents, whether they are published or not. The documents may come from teaching and research institutions in France or abroad, or from public or private research centers.

L'archive ouverte pluridisciplinaire **HAL**, est destinée au dépôt et à la diffusion de documents scientifiques de niveau recherche, publiés ou non, émanant des établissements d'enseignement et de recherche français ou étrangers, des laboratoires publics ou privés.

N° d'ordre : D.U. : **2211** Année 2011
E D S P I C : **548**

UNIVERSITE BLAISE PASCAL – Clermont II

ECOLE DOCTORALE
SCIENCES POUR L'INGENIEUR DE CLERMONT-FERRAND

Thèse

Présentée par

Akhilesh TIWARI

pour obtenir le grade de

DOCTEUR D'UNIVERSITE

Spécialité: **GÉNIE DES PROCÉDÉS**

Characterization of mass transfer by condensation on a horizontal plate

---

Soutenue publiquement le 21 Décembre 2011 devant le jury :

Président:
M. **DUSSAP** C-G., Professeur, Université Blaise Pascal, Clermont-Fd.

Rapporteurs:
M. **ASTOLFI** J. A., MCF-HdR, Ecole Navale, IRENav, Brest.
Mlle **DULUC** M-C., MCF-HdR, CNAM, Paris.

Membres de Jury:
M. **GROS** J-B., Professeur Emérite, Université Blaise Pascal, Clermont-Fd.
M. **KONDJOYAN** A., Directeur de Recherche, INRA, Theix, Clermont-Fd.
M. **LASSEUR** C., Docteur, ESA, ESTEC, Noorwijk, Pays Bas.
M. **SPIERO** F., Docteur, Etudes Spatiales, CNES, Paris.

Directeur de thèse:
M. **FONTAINE** J-P., Professeur, Université Blaise Pascal, Clermont-Fd.

Laboratoire de Génie Chimique et Biochimique – Université Blaise Pascal

ABSTRACT

For the development of successful long term space flights, and the establishment of permanent bases in space, a well controlled self sustained closed environment is required. In order to optimize a closed-loop bio-regenerative life support system, it is necessary to control the hydrodynamics and the coupled heat and mass transfer, which develop in a space habitat concerned with humans and plants. We have designed a ground based experimental setup and protocol to measure the air flow velocities and concomitant mass transfer by condensation of water vapour from humid air on a horizontal flat plate of small size (area 25 cm^2), in a controlled air flow conditions (flow regime, hygrometry, temperature). An active isothermal surface was kept below the dew point, by using thermoelectricity, and precise weighing of the condensate in order to evaluate the rate of mass flux. An air-conditioned closed circuit wind tunnel has been used to produce laminar to weakly turbulent flows. Almost 70 condensation experiments have been performed at an ambient temperature (19-23 °C) for a relative humidity between 35-65 %, and for the velocity range 1.0-3.0 m/s. The condensing unit behaves as a blunt-faced body and mass transfer coefficients were deduced. When increasing the flow intensity it was found that the Sherwood number had a dependence on $Re^{2/3}$. An empirical relation was proposed to estimate the surface temperature. The flow behaviour within the boundary layer and the analysis of the drop growth on the flat plate surface under weakly turbulent flows has been discussed. This experimental work will be helpful to develop theoretical models for further studies with other geometries.

Keywords: condensation; mass transfer; humid air; small size horizontal plate; weakly turbulent flow; experimental characterisation; climatic tunnel; thermoelectricity.

Titre de la thèse

Caractérisation du transfert de matière par condensation sur une plaque horizontale

RÉSUMÉ

La réussite du développement de vols spatiaux de longue durée, ainsi que de l'établissement de stations permanentes nécessite des systèmes fermés autonomes bien contrôlés. L'optimisation d'une boucle fermée d'un système support vie bio-régénératif, impose le contrôle de l'hydrodynamique et des transferts de chaleur et de masse couplés qui se développent au sien d'un habitacle spatial comprenant des hommes ou des plantes. Un protocole expérimental (expérience terrestre et méthode de mesure) a été conçu pour quantifier les vitesses de l'air et les transferts hétérogènes qui se développent par condensation d'air humide sur une surface plate horizontale de petite taille (25 cm^2), en conditions contrôlées (régime d'écoulement, hygrométrie, température). Une surface active était maintenue isotherme sous le point de rosée par thermoélectricité et le flux de masse était mesuré par pesée. Un tunnel climatique a été utilisé pour générer des écoulements laminaires ou faiblement turbulents. Environ 70 expériences de condensation ont été réalisées à température ambiante (19-23°C) avec une humidité relative de 35-65 % et pour des vitesses comprises entre 1.0 et 3.0 m/s. Le dispositif de condensation a un comportement de type profil épais pour l'écoulement et les coefficients de transferts de masse ont été évalués. L'augmentation de l'intensité de l'écoulement se traduit par une dépendance du nombre de Sherwood en $Re^{2/3}$. Une relation empirique est proposée pour estimer la température de la surface. Le comportement de l'écoulement au sein de la couche limite et de la croissance des gouttes sur la surface de la plaque sont discutées. Ce travail expérimental sera utile pour le développement de modèles théoriques adaptés à d'autres géométries.

Mots clés: transfert de masse; condensation; air humide; plaque horizontale de petite taille; écoulement faiblement turbulent; caractérisation expérimentale; tunnel climatique; thermoélectricité.

Acknowledgements

First and foremost I would like to thank **Almighty God**, great souls, guidance of professionals, support from dear one and the affection from my family members, specially my wife Anuradha and daughter Esha, I missed her childhood for this exhilarating and everlasting experience, all paved the way to reach the final quest.

The pursuit was headed by Professor Jean-Pierre Fontaine; his constant support and continuous encouragement only has made it possible to complete this work. It is very difficult to verbalize his elder brother like affection, which he showered upon me during the period of my research work and cooperation with a motive to make me independent. His scientific advice and support during my stay in France make me very comfortable; I am grateful and pay respect to him from the core of my heart.

I am very much grateful to Prof Claude-Gilles Dussap, Head, LGCB & Director of Polytech'Clermont-ferrand, France for welcoming me in LGCB and Prof. Ashok Pandey, Deputy director and Head Biotechnology division, NIIST, Trivandrum, India, for giving this opportunity, and encouragement by providing useful suggestions and inspiration to carry out the present work, the main source and confidence behind this work. My sincere thanks to Prof. Christian Larroche for his friendly behaviour, and helping me by giving the guidelines for the administrative needs.

I wish to express my sincere thanks to our collaborator Dr Alain Kondjoyan, Senior Scientist, Directeur de Recherche (HDR), INRA, St Genès Champanelle, France for his continued help by providing wind tunnel facility and for fruitful discussions. I am extremely grateful to all the faculty members of LGCB, Polytech'Clermont-Ferrand and especially to Prof Jean-Bernard Gros for productive discussions, also Pascal and David for technical support and others with whom I had prolific debates. Thanks to Béatrice in extending administrative support and corrections in my French, Fabrice for his presence and immediate helps. Missing the lunch time friends at "Repas du mercredi" – Denis, Issa, Stéphanie, Darine. Also thanks to Hélène for cheering up, Catherine for information's, Pierre for cultural discussions, Bérangère for MELiSSA project related information's, Laurent for his help in computers and Gwendoline for her company sometimes at tea. I am thankful to Pauline for

discussions in French, Swathy for her companionship, Kaies as a colleague, and also to Alain, Matthieu, Cindie, Marie-Agnès, Oumar, Aurore, and Numidia for their company.

I wish to thank to all of my friends from our India-Pakistan community who made our weekends memorable – specially would like to mention Anil, Vinod, Reeta, Arpit, and Sunny. The unforgettable months in France could not have been possible without Sushma mamiji, my deepest thoughts for her.

I am extremely thankful to Teresa and Dominique for her affections and my love to Céline, Patrice, Guillaume and Estelle. I shall never forget the parental love of Claire aunty and Patrick uncle, who make me relaxed with French culture and history.

I have an affectionate family my mother (Amma), Bhabhiji, Maya didi, Girijesh Bhaisahab, Manju Bhabhi, Usha didi, Anviksha, Mukta, Anupam, Anand, Abhyudaya. At this moment, I am remembering my Father and Dadaji, whose sacrifice and love, I shall never forget. I **dedicate this work to my eldest brother "Bhaisahab" (Prof. Dinesh Prasad Tiwari)**, who is the main source of inspiration behind my all educational growth.

Table of contents

List of abbreviations and symbols 13

List of Tables 16

List of Figures 17

Introduction **25**

Chapter 1: Literature survey **29**

1.1 Introduction **31**

1.2 Fundamentals of condensation **32**

1.3 **Filmwise condensation** **35**
1.3.1 Theoretical developments 35
1.3.1.1 Effect of variable physical properties 36
1.3.1.2 Effect of non-condensable gases 39
1.3.2 Experimental developments 43
1.3.2.1 Effect of variable physical properties 43
1.3.2.2 Effect of non-condensable gases 44

1.4 Dropwise condensation **49**
1.4.1 Theoretical developments 49
1.4.2 Experimental developments 51

1.5 Mass transfer **53**
1.5.1 Diffusion 54

1.6 Characteristics of the fluid medium **55**
1.6.1 Air 55
1.6.2 Some physical constants of air 56
1.6.3 Temperature dependence of physical constants of air 57
1.6.3.1 Density 57
1.6.3.2 Viscosity 57
1.6.3.3 Vapour pressure 58
1.6.3.4 Saturation vapour pressure 58
1.6.4 Mass fraction of water vapour in air 58
1.6.5 Dewpoint 59
1.6.6 Forced flow over an isothermal plate 59
1.6.7 Psychometric chart 60

1.7 Mars **61**
1.7.1 Atmosphere 61

1.8 Moon **62**
1.8.1 Atmosphere 62

1.9 Dimensionless Numbers **62**
1.9.1 Sherwood number 62
1.9.2 Reynolds number 63
1.9.3 Schmidt number 64
1.9.4 Stanton number 64
1.9.5 Friction factor 64
1.9.6 Chilton and Colburn J factor analogies 65

1.10 Conclusion **65**

Chapter 2: Materials and Methods **67**

2.1 Introduction **69**

2.2 Wind Tunnel **69**
2.2.1 Main Characteristics 69
2.2.2 Measurement of wind velocity 71

2.3 Condensation unit **73**
2.3.1 Global system 73
2.3.2 Plate size and thickness 75
2.3.3 Thermoelectric cooler – Peltier element 76
2.3.3.1 Basic principle 76
2.3.3.2 Modelling of the Peltier effect 77
2.3.3.3 Specifications of the used Peltier modules 80
2.3.4 Weighing of condensate 82

2.4 Calibration of temperature sensors **83**
2.4.1 Resistance temperature detector (RTD) 83
2.4.2 Thermistor thermometer 83
2.4.3 Thermocouples 84

2.5 Conclusion **84**

Chapter 3: Surface temperature profile studies **85**

3.1 Introduction **87**

3.2 Plate size and thickness **87**

3.3 Temperature distribution on the surface of the Plate and Peltier **88**
3.3.1 Peltier Element 50 x 50 mm^2 90
3.3.2 Peltier Element 40 x 40 mm^2 90
3.3.3 Peltier Element 30 x 30 mm^2 90

3.4 Preparation of metal substrate **94**
3.4.1 Choice of test plate 96
3.4.2 Choice of heat sink and its orientation with air flow 98

3.5 Conclusion **102**

Chapter 4: Velocity Profile Studies Inside a controlled environment **105**

4.1 Introduction **107**

4.2 Calibration of hotwire anemometers **108**

4.3 Measurement of velocity profile and turbulent intensity **108**
4.3.1 Dry conditions 108
4.3.1.1 Horizontal position 108
4.3.1.1.1 Simple plate without any cooling device 108
4.3.1.1.2 Plate with cooling arrangement 110
4.3.1.2 Vertical position 110
4.3.2 Wet conditions 110

4.4 Results and discussions **111**
4.4.1 Dry conditions 111
4.4.1.1 With simple plate 111
4.4.1.2 Plate with all the accessories 121
4.4.2 Wet conditions 126

4.5 Flow about blunt-faced flat plate **131**

4.6 Conclusion **134**

Chapter 5: Condensation experiments in an open environment **137**

5.1 Introduction **139**

5.2 Initial condensation experiments in ambient conditions **139**

5.3 Results and Discussions **143**

5.4 Conclusion **153**

Chapter 6: Condensation experiments in the wind tunnel **155**

6.1 Introduction **157**

6.2 Experimental characteristics **158**
6.2.1 Mean velocity control 158
6.2.2 Environmental control 158
6.2.3 Mass condensate measurement 158

6.3 Experiments with a mean entrance velocity 1.0 m/s (15.6 Hz fan 156frequency) **160**
6.3.1 Analysis of the evolution of the condensation rate versus time 163
6.3.2 Analysis of the condensation rate versus the temperature difference (ΔT_c) 169

6.4 Influence of the mean entrance velocity **173**

6.4.1 Experiments with a mean entrance velocity of 1.5 m/s (21.5 Hz fan frequency) 173
6.4.2 Experiments with a mean entrance velocity of 2.0 m/s (27.6 Hz fan frequency) 174
6.4.3 Experiment with a mean entrance velocity of 2.5 m/s (32.1 Hz fan frequency) 174
6.4.4 Experiment with a mean entrance velocity of 3.0 m/s (40.0 Hz fan frequency) 174

6.5 Theoretical calculations and discussion 174
6.5.1 Surface temperature estimation 175
6.5.2 Calculation of the Sherwood number (*Sh*) 177
6.5.3 Partial pressure difference (ΔP) estimation 179
6.5.4 Velocity boundary layer and temperature profile 179

6.6 Discussion 190
6.6.1 Experimental measurements of the rate of condensation at 1.0 m/s 190
6.6.2 Comparison with theoretical results at 1.0 m/s 193
6.6.3 Mass flux evaluation at 1.0 m/s 197
6.6.4 Influence of the flow intensity on the condensation mass flux 197

6.7 Image analysis 208

6.8 Flow patterns 217

6.9 Conclusion 218

Conclusion – Future prospects 219

References 225

Publications 243

List of abbreviations and symbols

BLSS	=	Biological life support system
CEI	=	Condensation experiments performed at INRA
CEL	=	Condensation experiments performed at LGCB
CFD	=	Computational fluid dynamics
DWC	=	Dropwise condensation
DIMI	=	Dynamic ion-beam mixed implantation
EPMA	=	Electron probe micro-analyser
FWC	=	Filmwise condensation
HTC	=	Heat transfer coefficient
ID	=	Internal diameter
INRA	=	Institute national de recherché agronomy
LEO	=	Low Earth orbit
LGCB	=	Laboratoire de génie chimie et biochimique
NCG	=	Non-condensable gas
NASA	=	National aeronautics and space administration
RH	=	Relative humidity
TEC	=	Thermoelectric cooler
PIV	=	Particle image velocimetry
ent.	=	Entrance
Temp.	=	Temperature
wt	=	Weight
diff.	=	Difference
vel.	=	Velocity
Turb.	=	Turbulence

Symbols

A	=	area, m^2
C_p	=	specific heat capacity, J/ kg K
D	=	binary diffusion coefficient at interface m^2/s
e	=	thickness, m
E	=	voltage, volt

f	=	friction factor
F	=	geometry factor
h	=	heat transfer coefficient, J/m^2 K s
I	=	current, Ampere
g	=	gravitational acceleration, m/s^2
J_{diff}	=	diffusive mass flux,
k	=	thermal conductivity, W/m K
L	=	characteristic length of the plate, m
l_v	=	latent heat of vaporisation, J/kg
m	=	mass of condensate, kg
N_A	=	mass flux, kg/m^2 s
P	=	partial pressure, Pa or Power, (watt)
Q	=	heat, Joule
q	=	mean heat flux for surface
R	=	gas constant or resistance, ohm
t	=	time, s
T	=	temperature, K
T_c	=	temperature constraint set on controller, °C
T_s	=	surface temperature, °C
Tu	=	turbulence intensity of air, %
U	=	mean air velocity in the free stream, m/s
u	=	velocity fluctuations around U in the main flow direction, m/s
W	=	mass fraction
x	=	distance from the starting edge of the plate, m
z	=	figure-of-merit

Dimensionless quantity

Sh	=	Sherwood number
Re	=	Reynolds number
Sc	=	Schmidt number
Nu	=	Nusselt number
Pr	=	Prandtl number
St	=	Stanton number

Greeks

α	=	Seebeck coefficient, (V/K)
ρ	=	density, $kg.m^{-3}$
μ	=	dynamic viscosity, Pa.s
ω	=	mass fraction of water vapour in air
Δ	=	difference
ν	=	kinematic viscosity, $m^2.s^{-1}$
δ	=	boundary Layer thickness, m
θ	=	angle of inclination of flat plate from horizontal, rad
τ	=	shear stress
π	=	Peltier coefficient, Volt

Subscripts

a	=	air or ambient
c	=	controller
d	=	dewpoint
F, *f*	=	film
I	=	liquid vapour interface
l	=	liquid
m	=	mean
n	=	number
s	=	surface or interface of air and flat plate
SAT	=	saturation
T	=	total
v	=	vapour
W	=	wall
wv	=	water vapour
x	=	local or (x-coordinate)
z	=	z-component or towards upper surface of the wind tunnel
atm	=	atmosphere
conv	=	convection
cond	=	conduction
ref	=	reference
∞	=	at infinity or at ambient or free flow

List of Tables

I-1	Summary of previous experimental investigations with non-condensable gas	47
I-2	The composition of dry air at sea level	56
I-3	Some physical constants of air	56
I-4	Composition of atmosphere at Mars	61
I-5	Composition of elements at Moon	62
II-1	Technical parameters of single stage thermoelectric coolers	80
II-2	Details of Peltier modules used in this experiment	81
III-1	Temperature distribution table (The key parameters of main exp. carried out.)	91
IV-1	Values of parameters used in calculations and taken at the time of the experiment.	120
V-1	A Condensation Experimentation (LGCB) - (approx. wind velocity 1.0-1.2 m/s)	141
V-1	B Condensation Experimentation (LGCB) - (approx. wind velocity 1.0-1.2 m/s)	142
VI-1	A Condensation Experimentation (Mean wind vel.-1,0 m/s)	164
VI-1	B	165
VI-2	A Condensation Experimentation (Mean wind vel.- 1.5 m/s)	182
VI-2	B	183
VI-3	A Condensation Experimentation (Mean wind vel.- 2.0 m/s)	184
VI-3	B	185
VI-4	A Condensation Experimentation (Mean wind vel.- 2.5 m/s)	186
VI-4	B	187
VI-5	A Condensation Experimentation (Mean wind vel.- 3.0 m/s)	188
VI-5	B	189
VI-6	A Relative Humidity Chart	205
VI-6	B Temperature Difference chart	205

List of Figures

I-1	Flow of laminar film on a plate	35
I-2	Characteristic profiles due to the presence of a non-condensable	40
I-3	Othmer's experiments on the effect of a non-condensable gas on condensation heat transfer (under natural convection) (Asano 2006)	45
I-4	Psychometric chart	60
I-5	The properties of moist air normally represented by the Psychometric chart	61
II-1	Schematic of Wind tunnel	70
II-2	Hot wire sensor probe (DANTEC 55P15)	71
II-3	A view of the test chamber with telescope	72
II-4	Representation of different temperature levels on the active condensing unit	73
II-5	Schematic of the whole condensation unit: (a) front view, (b) side view of the upper part, which faces the airflow	75
II-6	(a) Single stage Peltier element with a basis of thermocouple (b) A typical four stage Peltier element (By KRYOTHERM) (c) Schematic representation (d) Peltier element with sealant.	77
II-7	Sketch of a Peltier element	78
II-8	Sketch of the dimensions of Peltier element	81
II-9	Photographs of thermocouple adaptor	84
III -1	Sketch of the plates with points, where surface temperature has been measured	89
III-2	(a, b, c) Evolution of surface temperature (centre and edge), dewpoint and temperature given by controller (temp controller) for all size of the plates	93
III-3	Temperature distribution experiment with a plate having a slight concavity	94
III-4	Temperature homogeneity plots on the surface of the ceramic plate of Peltier element on the cold side (without metal plate).	95
III-5	(a, b) Distribution of surface temperature with (a) aluminium plate and (b) steel plate	97
III-6	Distribution of surface temperature with a plate of 3 mm thickness	98
III-7	Dimensions of the heat sink	99

III-8 Three different orientations of the heat sink with Peltier and plate 99
III-9 Temperature distribution plots for orientation of Figure III-8 (a, b, c) 100
III-10 Temperature distribution plots 102

IV-1 Orientation of the plate and its velocity measurement points 109
IV-2 Photograph of test chamber and a closer look of condensing unit 111
IV-3 (a-b) A comparative surface plots for the flat plate in horizontal position, velocity profiles in (m/s) for ambient temperature (T_a) = 21.8 °C 112
IV-3 (c-d) A comparative surface plots for the flat plate in horizontal position, a velocity profiles in (m/s) for ambient temperature at (T_a) =21.2 °C 113
IV-3 (e-f) A comparative surface plots for the flat plate in horizontal position, a turbulence intensity in (%) for ambient temperature at (T_a) = 21.8 °C 114
IV-3 (g-h) A comparative surface plots for the flat plate in horizontal position, a turbulence intensity in (%) for ambient temperature at (T_a) = 21.2 °C and entrance velocity 2.02 m/s 115
IV-3 (*i-l*) Comparative surface plots above the flat plate in horizontal position at 1 mm (*i*, *k*) and at 3 mm (*j*, *l*): (*i-j*) velocity profiles in meter per second and (*k-l*) turbulence intensity in per cent 116
IV-4 (a-b) A comparative surface plots of a flat plate in vertical position, velocity profile in m/s for (a) ambient temperature (T_a) = 21.1 $^{\circ}$C and (b) at (T_a) =19.9 $^{\circ}$C 117
IV-4 (c-d) A comparative surface plots of a flat plate in vertical position for turbulence intensity in % for (c) ambient temperature (T_a) = 21.1 $^{\circ}$C and (d) at (T_a) =19.9 $^{\circ}$C at entrance velocity 2.0 m/s 118
IV-5 (a-b) A comparative plots of boundary layer thickness calculated using Blasius solution (continuous line) and observed experimentally (square points) (b) its relative percentage error 120
IV-6 (a-d) A comparative surface plots of velocity profile (m/s) on a horizontal flat plate at 1 mm height for four different entrance velocities. 121
IV-7 (a-d) A comparative surface plots of turbulence intensity (%) on a horizontal flat plate at 1 mm height for four different entrance velocities. 122
IV-8 (a-d) A comparative surface plots of velocity profile (m/s) on a horizontal flat plate at 11 mm height for four different entrance velocities. 123
IV-9 (a-d) A comparative surface plots of turbulence intensity (%) on a horizontal 124

flat plate at 11 mm height for four different entrance velocities

IV-10 (a-b) Plot of velocity versus height above the plate for 1.0, 1.5, 2.0 2.5, and 3.0 m/s entrance velocity 125

IV-11 (a-d) A comparative surface plots of (a, c) velocity profile (m/s) and (b, d) turbulence intensity (%) on a horizontal flat plate at 5 mm height during condensation, after a constant value 2.0 g of condensate collected on the surface of the plate for 2.5 m/s velocity in two different experiments - (a-b) CEI-38, and (c-d) CEI-39. 127

IV-12 (a-d) A comparative surface plots of (a, c) velocity profile (m/s) and (b, d) turbulence intensity (%) on a horizontal flat plate at 5 mm height during condensation on increasing weight (from 0.5 g to 0.7 g) of condensate on the surface of the plate for 2.5 m/s velocity in two different experiments- (a-b) CEI-37, and (c-d) CEI-39. 128

IV-13 (a-d) A comparative surface plots of (a, c) velocity profile (m/s) and (b, d) turbulence intensity (%) on a horizontal flat plate at 5 mm height during condensation on increasing weight (from 1.5 g to 1.7 g) of condensate on the surface of the plate for 2.5 m/s velocity in two different experiments- (a-b) CEI-38, and (c-d) CEI-39 129

IV-14 (a-b) Photographs of condensing horizontal flat plate with a condensate (a) 2.0g (b) 2.1g of condensate on the surface of the plate in flow of 2.5 m/s velocity in two different experiments- (a) CEI-38, and (b) CEI-39 130

IV-15 Comparative plots of two experiments (CEI-38, CEI-39) showing variation of velocity at last middle point of the plate (i.e. X = 5.0 cm, Y = 2.5 cm, Z = 0.3 – 2.3 cm) from inside the boundary layer to free flow stream. 131

IV-16 (a, b, c, d, e, f) 3D curves of the velocity profile at fan frequency 32.1 Hz and mean entrance velocity 2.5 m/s at different heights from the surface of the plates. X and Y –Axis representing the plate cross section on which the velocity measurements have been taken. Z- Axis as velocity (m/s). 133

V-1 Photograph of the experimental arrangement in LGCB 140

V-2 (a-b) Amount of condensate and temperature as a function of time. The value of ambient temperature is also given in the graph after reducing 10 °C to fit in scale. 145

V-3 (a-b) The temperature difference and mass flux as a function of total time 146

V-4	(a) Amount of condensate as a function of total time of experiment for 8 experiments in open environment (b) inside the wind tunnel for 3 experiments at given temperature differences	147
V-5	(1-4) Photographs of the flat plate with condensation on it at different duration of time (in hours) from starting point of condensation.	148
V-6	a) Amount of condensate and temperature as a function of time. The value of ambient temperature is also given in the graph after reducing 10°C to fit in scale b) Mass flux and temperature difference as a function of time	150
V-7	(a-b) Average mass flux as a function of average partial pressure difference at ambient temperature and interface temperature for the plate sizes a) 5 x 5 cm^2 and b) 4 x 4 cm^2 for experimental data shown in Table V-1A, 1B	152
VI-1	Closure view photograph of the experimental arrangement (1) inside wind tunnel, and (2) below the test chamber, temperature controller with electronic weight balance	159
VI-2	Photographs of the flat plate during condensation, at different times and different weights of the condensate on the surface of the plate, showing how the drops develop and their localization	161
VI-3	Photographs of flat plate showing the falling drops of condensate before applying sponge from the vertical surface of the plate (a) after 40 min of the exp (b) after 5 h and (c) after 7 h 30 min of the condensation exp (CEI-7)	162
VI-4	Plot of amount of condensate and secondary Y-axis as temperature ambient (-10°C), dewpoint, and set on controller with respect to time	163
VI-5	(a, b) Plot of the amount of condensate and secondary Y-axis as temperatures ambient (-10°C), dewpoint, and set on controller, as a function of time	167
VI-6	(a, b) Plot of the amount of condensate and secondary Y-axis as temperatures ambient (-10°C), dewpoint, and set on controller, as a function of time	168
VI-7	(a, b) Amount of condensate as a function of time for different average temperature differences (ΔT_c), both are for the 1.0 m/s mean entrance velocity	170
VI-8	(a, b, c) Amount of condensate and temperature as a function of time	172
VI-9	(a) Velocity function $f(z)$ versus height from the surface of the flat plate; (b) estimated temperature using eq. (VI-8) as a function of height from the surface of the plate (c) turbulence intensity versus height from the plate surface.	180

VI-10 (a, b) Rate of condensation (g/h) for a mean entrance velocity of 1.0 m/s as a function of (a) temperature difference (ΔT_c °C) (b) temperature difference (ΔT_s °C) 191

VI-10 (c) Rate of condensation (g/h) for a mean entrance velocity of 3.0 m/s as a function of temperature difference (ΔT_s °C) 192

VI-11 Rate of condensation as a function of temperature difference (ΔT_c °C). The theoretical values calculated using the surface temperature formula given as eqs (VI-3, 4, 5) 193

VI-12 Rate of condensation as a function of temp difference (ΔT_s) for 1.0 m/s velocity 195

VI-13 Rate of condensation as a function of average of difference in partial pressure of water vapour in humid air 196

VI-14 (a, b) Mass flux for mean entrance velocity 1.0 m/s (a) as a function of the mean partial pressure difference, and (b) of the temperature difference (ΔT_s). 198

VI-15 Mass flux as function of (a) ΔT_s (°C), and (b) mean partial pressure difference (kPa) for a mean entrance velocity 1.5 m/s 199

VI-16 (a, b) Plots of $N_A/\Delta P$ as a function of the mean entrance velocity, for (a) the experimental data, and (b) the theoretical data. All the experimental data are shown in here including the experiments performed in unregulated open environment marked as LGCB 200

VI-17 (a, b): Plots of $N_A/\Delta T_s$ as function of the mean entrance velocity for (a) the experimental data, and (b) the theoretical data. All the experimental data are shown in here including the experiments performed in unregulated open environment marked as LGCB 201

VI-18 (a, b) Plots of $N_A/\Delta P$ as a function of the mean entrance velocity for the (a) the experimental data, and (b) the theoretical data. Scattered experimental data have been removed including the experiments performed in unregulated open environment to reduce the discrepancy 203

VI-19 (a, b) Plots of $N_A/\Delta T_s$ as a function of the mean entrance velocity with (a) the experimental data, and (b) the theoretical data. Scattered experimental data have been removed including the experiments performed in unregulated open environment to reduce the discrepancy. 204

VI-20 Calculated Sherwood numbers as a function of the Reynolds number and their 206

trend line as a power series

VI-21 Re-plotted data of figure VI-19, by using Sh_i / Re^{m_i} as ordinate and mean entrance velocity as abscissa 207

VI-22 (a) Images of condensing plate for velocity 1.0 m/s. 209

VI-22 (b) Images of condensing plate for velocity 2.0 m/s. 210

VI-22 (c) Images of condensing plate for velocity 2.5 m/s. 211

VI-22 (d) Images of condensing plate for velocity 3.0 m/s. 212

VI-23 The thermal distribution on the surface of the flat plate at 23.4°C ambient temperature and (a) 43% relative humidity (b) 33% relative humidity. 213

VI-24 Photographs of the condensing plate (a) without sponge and tape (b) with only tape on its vertical surface (c) 7 mm wide and 6 mm thick sponge before the plate (d) 3 mm wide and 6 mm thick sponge (e-f) 3 mm wide and 3 mm thick sponge before the plate. 214

VI-25 Photographs of the plates with condensate (1, 2) shows flow pattern, and (3,4) shows schematic of the plate with horizontal and vertical flow patterns on the plate surface 217

Introduction

Introduction

Space is hostile to human life and the availability of water, oxygen, food, optimum temperature, radiation, and other life supporting factors are affected. Thus, the development of advanced life support systems aims to provide enough food, water, and oxygen for a crew to operate indefinitely in space with little resupply from Earth using specially-designed regenerative, or recycling technologies. While life support systems can use physical methods alone to purify water and create oxygen from exhaled carbon dioxide, only bio-regenerative systems, those involving plants, can also produce food and thereby qualify as completely self-sufficient systems. The most important advantage of a bio-regenerative life support system (BLSS) is that it does not require to be resupplied with food, water, and air, nor does it need expendable water or air filtration systems as existing mechanical spacecraft life support systems do. Indeed, throughout the history of manned-space flight, one of the key problems has been the development of bio-regenerative life support systems, to provide autonomy to piloted spacecraft and planetary outposts for multiyear missions. A comparison of BLSS has been given by Bartsev et al. (1997), and the use of biological organisms was employed in the development of such systems (Mergeay et al 1988, Gros et al 2003). As a matter of fact, if no chemical transformation is included, physicochemical systems are sufficient (adsorption of CO_2, water purification, etc.). In that case all consumables need to be refurnished (O_2, food, part of water). If O_2 is regenerated (by Sabatier process for example), chemical transformations are mandatory. If carbon and nitrogen recycling are envisaged, the LSS must include food production; in that case it requires biological transformations, such as higher plants growth in specific chambers and/or bioconversion in bioreactors (Wheeler et al 1996, Tamponnet and Savage 1994, Lasseur et al 1996).

Today's technology is capable of supporting human crews in space for missions in low earth orbit (LEO) of short or indefinite duration as long as resupply is readily available, as evidenced by the International Space Station (ISS). All crewed space missions rely on resupply from Earth for some or nearly all of the required consumable resources (oxygen, water, food). The technology used on the ISS is capable of recovering water from humidity condensate, waste hygiene water, and crew urine with 80 to 90 percent efficiency (Bagian 1997). The air and water treatments are performed with physicochemical processes. However, no space-qualified technologies are capable of recycling food or oxygen from waste materials, and wastes have to be discarded or stored for return to Earth. Resupplying future missions beyond LEO, missions to Mars or to the moon for example, will be even more intricate, if not

impossible.

The importance of recycling within the spacecraft, with crews consuming the products of autotrophic synthesis, needs recycling of materials, requires exchanges between photoautotrophic organisms, which synthesize organic substances using solar or artificial light, and heterotrophic organisms. Hence, growing plants is a vital component and its performance in BLSS for space missions will be principally dependent on the progress of plant cultivation technology for space and the achievement of associated equipment. The growth of higher plants in a green house is optimized by the environmental conditions among which the effect of ventilation, condensation and evaporation phenomena on the surfaces of leaves, plants, windows, and walls. Moreover, condensation on walls or human skin has to be controlled as well as the ambient air for optimized living conditions in the spacecraft, even if the humidity level is not as high in a greenhouse. Furthermore, forced convection is known to be a good solution to prevent condensation while maintaining optimized conditions for life. The optimization of BLSS require a global coupled hydrodynamics, heat and mass transfer modeling that could simulate precisely the atmosphere in space greenhouses, or in manned-capsule and to prevent mould, rot or rust. Further, the coupling with microbiological development models will help for the protection of the crew from nosocomial infections, the optimization of the microclimate prevailing in a space greenhouse and a better control of higher plant growth.

Numerical simulation or theoretical models could give insights into the dynamics of transport phenomena and assist in the design of an optimized and reliable air-conditioning system. However, a precise mathematical model requires the knowledge of the local mass transfer coefficient (for condensation or evaporation) for the specific configurations, and a validated turbulent model. Such data can only be given by experimental works or by literature. The primary goal of this study was to develop an experimental set-up to measure heterogeneous mass flux on a horizontal surface in a well controlled air-conditioned system. The final goal was to estimate the local mass transfer coefficients on such a basic configuration.

We have used thermoelectricity to generate a homogenous cold surface, maintained isothermal and below the dewpoint to induce condensation of water vapour from humid air. A small size horizontal plate was selected first as a basic configuration for local mass transfer

evaluation. This water condensate on the active surface was weighed precisely during the condensation process by an electronic balance, on which the entire experimental device has been placed. The process of condensation was monitored and the condensing unit placed inside a closed wind tunnel, where hygrometric and hydrodynamic parameters were controlled. The condensation experiments were performed for different flow velocities, to know the velocity dependence of the mass flux on the blunt-faced flat plate surface. The analysis of the flow field on the surface of the flat plate, with and without condensation has also been investigated for a better understanding of the condensation phenomenon and its dynamics on the surface of such geometries.

Three main difficulties had to be overcome

1. to generate an isothermal surface (air/plate interface), even when condensation occurred, in order to be able to evaluate precisely the mass flux and its dynamics;
2. to accurately weigh the growing condensate versus time on a small size plate, for the measurement to be considered as local;
3. to reach a good control of the main flow field and to obtain sound knowledge of the boundary layer flow above the obstacle, for the experiments to be considered as standard and to be used further as test benches for the validation of numerical models (mass flux, turbulence, ...).

The design was conceived in a way that other basic or more complex configurations (vertical plate, cylinder, sphere, porous material, chemically or biologically active components) could be dealt with later on. The technologies used to study heat and mass transfer coefficients, usually involve heat transfer measurements and then by analogy the mass transfer coefficients are deduced. Our aim in this work was to use a mass transfer measurement technology instead for use in further developments of mathematical modelling.

The first chapter is a review of the information and the resources available from the literature on the various aspects of the study. The materials and methods considered are detailed in chapter two. The third chapter details the experiments performed to design the condensation unit. The fourth chapter describes the various velocity profile studies inside the wind tunnel on the surface of the blunt-faced flat plate. The fifth and sixth chapters present the condensation studies, respectively, in an open environment and in a well controlled environment.

Chapter I

Literature survey

1.1 Introduction

Water is essential to life on Earth, and as such it is present in the form of oceans, lakes, rivers, and also in the air. The sustainability of life on Earth is reliant on water, even 90% of the human body is comprised of water. Water transports nutrients and electrolytes from one part of the body to another; it also washes waste and toxins. It makes the atmosphere humid, it is one of the greenhouse gases, and its presence in the atmosphere is necessary as water vapour plays many key roles in the life form on Earth. The relative humidity of the atmosphere also defines the comfort level in the living environment, and it affects the growth of plants as well. In the confined environment of a spacecraft ecosystem, based on the average quantity of water, oxygen and food that crew and living organisms use everyday, water constitutes 95% of the total consumable mass vital for human life support. In order to regulate the water cycle inside a closed space environment many basic phenomena need to be well understood and their adaptation to microgravity, which occur naturally in the Earth atmosphere; for example: condensation and evaporation of water vapour from humid air. Condensation of water vapour from humid air will occur when the temperature of the ambient atmosphere will go down to the dew point or even below. Normally, the relative humidity is high in space habitats (25 to 75%), which can cause condensation on surfaces (Schwarzkopf 1994). Such condensates can damage electronic instruments and increase fungal and microorganisms' growth that can be difficult to control. It also inhibits the cooling of human body by the evaporation of perspiration. Without proper air convection, in a microgravity environment, the water droplets reside on the skin or the surface of the plant leaves or any solid surface.

For long duration space flights with humans and plants together, and to position them beyond the Earth orbit as a self-sufficient space habitat, air and water must be recycled. Usually, humidity condensates, wash-water and urine are the three primary sources available for recycling waste water. To purify these waste water sources, technology involves physicochemical processes such as distillation, filtration, phase change, or bio-regenerative processes, which use photosynthetic plants grown in aquaculture (Mergeay 1988, Waligora et al 1994). Transpiration is the process by which plants supply pure water to its environment: generally, plants can absorb waste water (water from showers and laundry) and release water,

which can be condensed and reused by humans and plants after being disinfected it with ultraviolet light (Waligora et al 1994).

Hence, condensation on solid walls or on plants has to be controlled to provide optimized living conditions (for astronauts or plants), although the humidity level may be particularly high in a greenhouse (75-80%). Air-conditioning systems have always been known as good solutions to prevent condensation while maintaining optimized conditions for life, but an adapted ventilation system (forced convection) is needed, particularly in a micro-gravity environment as no-gravity force could help a condensate to leave a non- horizontal surface. Thus, a precise control of the hydrodynamics and the concomitant heat, humidity and mass transfer developing in the space-station has to be performed. Numerical simulation or theoretical models could provide insights into the dynamics of transport phenomena and assist in the design of an optimized and reliable air-conditioning system. However, a precise mathematical model requires the knowledge of the local mass transfer coefficient (for condensation or evaporation) for the specific configuration, and a validated turbulent model. Such data can only be given by experimental works or by literature.

The main objective of this study is to give insights into the heat and mass transfer with condensation of air and to control the ventilation of humid air in space environment. The issues are the quality and the subsequent treatment of the air in a greenhouse or a manned capsule, the control of condensation-evaporation phenomenon, the characterization of gas/plant transfer, the hydrodynamics and concomitant heat and mass transfer, and the influence on the growth of high-plants. The other related effects are health risks (nosocomial infections), mould, rot/corrosion, light transmission etc. A ventilation system includes interaction between weakly turbulent air flows and water vapour transfer at condensation interfaces. This chapter presents a review of the existing results, both analytical and experimental, dealing with heat and mass transfer for the condensation of humid air, with a focus on the modelling of mass exchange.

1.2 Fundamentals of condensation

Condensation, the physical process of converting a material from a gaseous or vapour phase to liquid phase, commonly results when the temperature is lowered and/or the vapour pressure of the material is increased below or above saturation values. Indeed, if the pressure of the vapour is larger than its saturation pressure (or the temperature lower than its saturation

temperature), vapour is in a metastable state and will eventually condense into a liquid phase, its state of minimal energy. In general the tendency exists for condensation to occur when the partial pressure of a given component of a gaseous mixture at a given temperature exceeds the vapour pressure of that component at the given temperature. It can be considered as taking place either within the bulk material or on a cooled surface, and is accompanied by simultaneous heat and mass transfer.

Condensate (condensed vapour) may form from vapour in a number of ways (Butterworth et al. 1983):

1. Filmwise condensation (FWC): It is the most famous mode of condensation occurring in industrial equipments and it forms a continuous film of condensate on a cooled surface.
2. Dropwise condensation (DWC): More than 4 to 8 times higher heat transfer coefficients can be obtained with DWC in comparison to FWC, but this is difficult to maintain continuously in heat exchangers for a long duration. It occurs on a cooled surface as droplets instead of as a continuous film.
3. Homogeneous condensation: This forms a fog, when the vapour condenses out as droplets suspended in the gas phase. A necessary condition for this to occur is that the vapour is below the saturation temperature, which may be achieved by increasing the pressure as the vapour flows through a smooth expansion in a flow area. In condensers, however, it usually occurs when condensing high molecular-weight vapours in the presence of non condensable gas.
4. Direct contact condensation: It occurs when vapour is brought directly into contact with a cold liquid.
5. Condensation of vapour mixtures forming immiscible liquids: a typical example of this is when a steam-hydrocarbon mixture is condensed.

Dew is also a form of condensate and it is a natural phenomenon where humid air condenses on a substrate and transforms into liquid water. However, the occurrence of dew in nature has long been a mystery as it is precisely, when the sky is free of clouds that dew forms (Beysens 1995). Many researchers have contributed to the understanding of dew formation. But, it is only in the middle of the 20^{th} century that, a precise theory was proposed by Monteith (1957). For the workers of different fields dew has had different interpretation as in the laboratory studies dew is characterised as ‘breath figures’, i.e. the patterns formed when droplets condense onto a cold surface (Merigoux 1937, Beysens & Knober 1986, Fritter et al

1991). According to Beysens and Knober (1986), the formation of dew can be controlled by two key parameters, i.e. the temperature and the wetting properties of the substrate. These two parameters control the nucleation rate and the latter has in addition major consequences on the form and growth of droplet patterns.

To describe the mechanism of the formation of initial condensate drops on a solid surface, two kinds of mechanisms have been presented (i) liquid fracture hypothesis (ii) surface nucleation hypothesis. The first one proposed by Jakob (1936), who suggested that a thin film condenses on a cool surface and grows in thickness up to a critical value, where it brakes and forms the initial drops with the action of surface tension. Several other workers, (Ruckenstein & Metiu 1965, Haraguchi 1992) have supported this hypothesis. Ruckenstein and Metiu (1965) considered that the condensation surface contained numerous active centres so close as to form a continuous film of the condensate. Moreover, they found the critical thickness of the fractured film to be about 0.27 μm and the critical time to form this critical film to be in the magnitude of 10^{-2} s through thermodynamic calculations. Haraguchi (1992) applied microscopy technology and observed the initially formed droplet size to be about 1 μm and the critical thickness of the fractured condensate film to be 0.1-0.3 μm. The second hypothesis, surface nucleation site mechanism was proposed by Tammann and Boehme (1935). They suggested that dropwise condensation DWC was a nucleation process with nuclei randomly existing on solid surfaces. A thermal fluctuation causes the formation of the smallest nucleus, a liquid drop that is thermodynamically stable, which does not evaporate. Although many experimental studies have been devoted to the origin of the mechanism of dropwise condensation, all of them have been performed with microscopy or with a high speed camera, which are limited to microscale phenomena above 100 nm. McCormick and Westwater (1965, 1966), Umur & Griffith (1965), and Peterson & Westwater (1966), Grahm & Griffith (1973), Tanaka (1975a,b), Song et al (1990), Peter & Wayner (2002), proved the evidence of droplet nucleation and identified the nucleation sites during dropwise condensation with microscopes and movie cameras. Recently, Tianquing et al (2007) used an electron probe microanalyser (EPMA) at different scales, on magnesium surfaces that can react with hot water (condensation of hot water). The hot condensate produced magnesium hydroxide. The average surface roughness was about 20 nm, as observed by an atomic force microscope. EPMA was used to analyse the chemical composition of the surface before and after condensation. The authors concluded that the distribution of sites where drops develop is not uniform and the size of the initial condensate nuclei is in the range of 3-10 nm, in

agreement with thermodynamics for new phase formation which predicts that the size of an initial liquid nucleus is in nanometer scale if the initial condensate forms in nucleation state.

Condensation heat transfer is a vital process in the power generation industries as it is used to transfer a large quantity of heat. The focus of this thesis is devoted to the condensation of water in air mainly on solid surfaces, since this has the greatest engineering significance and the emphasis is on the evaluation of mass transfer both for FWC or DWC. FWC is currently used by industry while DWC is an alternative that is still under development (Pang et al 2005) as durability is not easy to reach.

1.3 Filmwise condensation

1.3.1 Theoretical developments

The first analytical solution for heat transfer on a plane vertical surface was given by Nusselt (1916) for the filmwise condensation with the following four major assumptions (Collier & Thorne 1996)

- The temperature distribution in the liquid film is linear
- The physical properties are constant
- The vapour phase consists of stationary saturated pure vapour
- The effect of vapour shear on the surface of the condensate is negligible

Fig.1 shows the physical representation of the film condensation of a pure vapour on a flat plate. The global heat transfer coefficient (h_m) for the flat plate was given by Nusselt (1916)

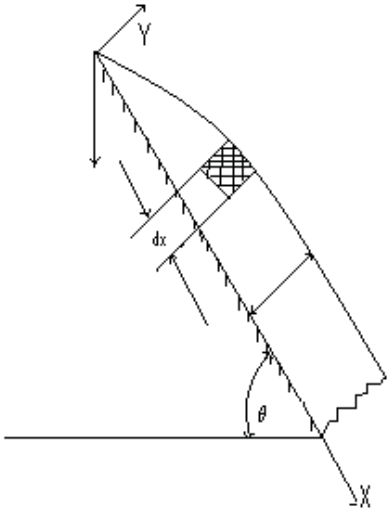

Fig.I-1: Flow of laminar film on a plate.

$$h_m = 0.943\left(\frac{g\sin\theta\rho_l(\rho_l-\rho_v)l_v k_l^{\,3}}{\mu_l(T_{sat}-T_w)L}\right)^{\frac{1}{4}} \qquad \text{(I-1)}$$

where k_l is the condensate thermal conductivity, ρ_l is the condensate density, ρ_v is the vapour density, g is the gravitational acceleration, μ_l is the condensate dynamic viscosity, l_v is the latent heat of vaporisation, T_{sat} is the saturation temperature, T_w is the wall temperature, and L is the total length, and θ is angle (Dhir and Lienhard 1971, Incropera and DeWitt 1990) between the horizontal and the surface. However, it must be used with caution for very low or large values of θ and does not apply if $\theta = 0$ or π.

Defining the Nusselt number (*Nu*), eq. (I-1) is expressed in dimensionless form as

$$Nu = \frac{h_m L}{k_l} = 0.943 \left(\frac{g \sin\theta \rho_l (\rho_l - \rho_v) l_v k_l^{\,3} L^3}{\mu_l k_l (T_{sat} - T_w)} \right)^{\frac{1}{4}} \qquad \text{(I-2)}$$

Nusselt (1916) also proposed the heat transfer coefficient in laminar film condensation for horizontal tubes. The characteristic length L is replaced by the tube diameter, (outer diameter for condensation outside the tube and inner diameter for condensation inside the tube), and the coefficient 0.943 becomes 0.725. The constant 0.725 was obtained by numerical integration, and a more accurate value of 0.728 has since been derived (Butterworth et al 1983). The Nusselt model can be used to predict the rates of condensation of pure vapours fairly accurately, if the physical properties of the liquid and the temperature at the vapour liquid interface are evaluated in a suitable manner, in which case agreement between experimental data and the theory is quite good.

1.3.1.1 Effect of variable physical properties

The formulation of the analytical Nusselt model assumes constant physical properties of the liquid, which are very sensitive to variations in temperature, such as, its viscosity. Furthermore, there exists a temperature difference between the vapour-liquid interface and the surface of the condensing wall. The condensation heat transfer coefficient of pure steam calculated with the physical properties at the condensing wall (approx. 25°C) is more than 35% higher than that calculated from the physical properties at the interface temperature (Asano 2006). The influence of inertia forces, convection terms in liquids, shear at the liquid vapour interface, sub-cooling within the condensate etc. was added by several workers to the classic Nusselt theory, which will be discussed in this section.

The initial corrections to the Nusselt theory was done to take into account the latent heat of vaporisation and the effect of sub-cooling within the liquid film (Bromley 1952). The heat transfer at the wall is greater than the energy from the latent heat by the sub-cooling of the liquid film that takes place; it is being saturated only at the liquid vapour interface. A non-linear distribution of temperature through the film due to energy convection (Rohsenow 1956) was also included. The latent heat of vaporization, l_v, in eq. (I-1) should be replaced by

$$l_v' = l_v \left(1 + D\beta\right) \qquad \text{(I-3)}$$

where $\beta = \left(\frac{(T_{sat} - T_w)C_p}{l_v} \right)$, and C_p the specific heat capacity. However, it should be noted that in most engineering applications, the value of β is very small (< 0.001) and can be ignored. Bromley (1952) proposed the value of constant D = 0.4 and the value of β up to about 3 and Rohnesow (1956) suggested D = 0.68 and β upto one.

The problem of film condensation on a vertical surface has been discussed by Sparrow and Gregg (1959) who included the influence of inertia forces and convection terms in liquid, but still neglected shear at the liquid vapour interface. In a further work, the shear forces at the liquid-vapour interface were taken into full account by Koh et al (1961) and the above results show that the interfacial shear stress can reduce heat transfer due to the effect of holdup of the condensate film for low values of *Pr* (Prandtl number of condensate), but this effect is small and decreases with increasing *Pr* above unity. An independent solution was obtained for this case, but using a perturbation scheme on a modified integral boundary layer equation (Chen 1961). Poots & Miles (1967) applied the boundary layer theory to film condensation on vertical surfaces to solve the problem for variable physical properties of the liquid condensate, notably viscosity and Kwang-Tzu (1966) did it for the case where the plate is non-isothermal. The effect of temperature difference between the surface of the wall and the liquid vapour interface creates variable physical properties. Minkowycz (1965) and Minkowycz and Sparrow (1966) also included natural convection arising from temperature gradients. On the basis of their detailed and elaborate calculations, they recommend the use of reference temperature, T_{ref} for this problem, which is calculated as

$$T_{ref} = T_w + C\,(T_I - T_w) \qquad \text{(I-4)}$$

where T_w is the wall temperature and T_I stands for liquid vapour interface temperature. The value of constant C = 0.31 was given by Minkowycz and Sparrow (1966) and C = 0.25 was suggested by Drew (1954). Minkowycz and Sparrow (1966) reported that the Nusselt model calculated from the physical properties at the reference temperature with the use of eq. (I-4) gives good results. In addition, the effects of interfacial resistance, superheating, thermal diffusion and property variation in the condensate film and in the vapour-gas mixture were considered and concluded to be less important except for superheating.

The laminar film condensation on the underside of horizontal and inclined surfaces was studied analytically and experimentally by Gerstman and Driffith (1967). The case of the

upper side condensation on a horizontal plate was first studied by Leppert and Nimmo (1968) and Nimmo and Leppert (1970). They have given an approximate solution for film condensation on top of a horizontal cooled surface of finite width in terms of the liquid film thickness at the edge. The film condensation thickness at the plate edge is either assumed or specified by a particular boundary condition. In this condition, for laminar film condensation, the condensate flows from the plate with a maximum film thickness, across the plate under the influence of a hydrostatic pressure gradient, and off the edge with the critical (minimum thickness. Shigechi et al (1990) obtained the condensate thickness and heat transfer results on a horizontal plate by adjusting the inclined angle of the vapour-liquid interface at the plate edge. The thickness of the film at the plate edge can not be zero, Yang and Chen (1992) used the concept of minimum mechanical energy to search the boundary condition at the horizontal plate edge. The concept states that a fluid flowing across a hydrostatic pressure gradient and off the plate will adjust itself so that the rate of mechanical energy within the fluid will be minimal with respect to the boundary layer at the plate edge (Bakhmeteff 1966, Chang 2005). Yang et al (1997) considered the condensation on a finite-size horizontal wavy disk and on a plate facing upward based on the Bakhmeteff's (1932) assumption, which is the minimum mechanical energy with respect to the boundary layer thickness at the edge of the plate. Wang et al (2003) discussed the problem of boundary layer condensation along a horizontal flat plane embedded in a porous medium and they got exact solutions. A new general flow pattern based heat transfer model for condensation inside horizontal, plain tubes has been proposed by Thome et al (2003) and it includes the effect of interfacial roughness of the liquid–vapour on heat transfer. The model resorts to very few empirical constants and exponents compared to other previous methods. The model accurately predicts local condensation heat transfer coefficients for the following flow regimes: annular, intermittent, stratified-wavy, fully stratified, and mist flow and it predicts a very broad experimental database for fifteen fluids obtained in nine different laboratories. The model has been tested over the conditions of mass velocities from 24 to 1022 kg/(m^2 s), vapour qualities from 0.03 to 0.97, reduced pressures from 0.02 to 0.80 and tube internal diameters from 3.1 to 21.4 mm.

To include the effects of vapour velocity and its associated drag on the condensate film, which has been found to be significant in many practical problems, Cess (1960) presented uniform property boundary layer solutions for the case of vapour flow parallel to a horizontal flat plate, obtained by neglecting the inertia and energy convection effects within the condensate film and assuming that the interfacial velocity was negligible in comparison

with the free stream vapour velocity. Similar assumptions have been considered by Shekriladze and Gomelauri (1966) for the case of an isothermal vertical plate. An attempt to expand Nusselt's approach to take account of vapour friction and momentum drag was made by Mayhew et al (1965-66, 1987). South and Denny (1972) proposed a simpler interpolation formula for the interfacial shear stress.

Jacobs (1966) considered the combination of body force and vapour forced convection-induced motion of the liquid film over a flat plate and used an integral method to solve the boundary layer by matching the mass flux, shear stress, temperature and velocity at the interface. The inertia and convection terms in the boundary layer equations of the liquid film were neglected. The variation of the physical properties and the thermal resistance at the vapour-liquid interface were also neglected. Further, the case of free, forced, and mixed convection has been considered (Fujii and Uehara 1972) and the results showed good agreement with Cess (1960) approximate solution. In a recent study, Liao et al (2009) considered the transition from natural to mixed convection for steam-gas flow condensing along a vertical plate.

1.3.1.2 Effect of non-condensable gases

It is well known that the presence of non-condensable gases in vapour can significantly lower the rate of condensation. The presence of non-condensable gas reduces the partial pressure of the vapour and the saturation temperature at which condensation occur. The analysis of the heat and mass transfer in the presence of non-condensable gas has generally involved either boundary layer analysis or heat and mass transfer analogy methods. The most common test geometries for the theoretical and experimental studies are external plate flow geometries or condensation outside a horizontal tube and the resulting correlations and models use overall or mean values of the heat transfer only applicable to special system with little or trace non-condensable gas at a horizontal plate, vertical plate or in-tube condensation heat transfer.

The studies (Siow 2002, Oh and Revnkar 2005) on condensation with a non-condensable gas employing a boundary layer analysis focussed on different flow configurations, the effects of turbulence, liquid-phase inertia and energy convection, and neglected the problem of convection regime identification.

The existence of non-condensable gas, like air, in a condensing environment reduces heat and mass transfer during condensation. A boundary layer of air-vapour forms next to the condensate layer and the partial pressures of air (p_a) and vapour (p_v) vary through the boundary layer as shown in Fig. I-2. The collection of non-condensable gas near the condensate film, due to condensation of vapour acts as a barrier and prevents the vapour molecules from reaching the liquid film easily, and thus impedes the rate of mass and heat transfer. The presence of less than 1% (in mass) of air in steam can lead to a reduction of 50% in heat transfer coefficient (Othmer 1929). Therefore, it is necessary to solve the conservation equations of mass, momentum and energy simultaneously for both the condensate film and the vapour-gas boundary layer together, with continuity conditions at the interface.

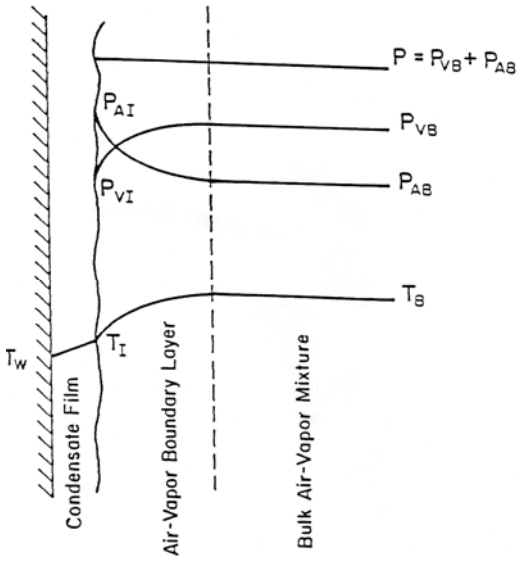

Fig. I-2: Characteristic profiles due to the presence of a non-condensable gas.

The equations for laminar film condensation on an isothermal surface have been solved by Sparrow and Lin (1964) and Sparrow and Eckert (1961) for a stagnant vapour-gas mixture. They included the free convection term arising from the density difference associated with different composition and considered the vapour-gas mixture as composite for the film condensate moving downward. The condensing rate is dependent on the bulk gas mass fraction, (i.e. the fraction of total mass and the mass of gas) and the vapour-gas mixture Schmidt number ($Sc = \mu/D$, D being the diffusion coefficient). Theoretical studies showed that on increasing the Schmidt number the effect of non-condensable gas increases. It has been noticed that, when the non-condensable gas and vapour have different relative molecular weights and increasing bulk gas mass fraction, the free convection arises because of both temperature and concentration difference. An approximate integral boundary layer solution was given by Rose (1969) assuming uniform properties except for density in the buoyancy term, like in the Boussinesq approximation and also to reduce the computation time. Possible velocity and concentration profiles for the vapour-gas boundary layer were used and it was assumed that these two layers had equal thickness. The results showed quite good agreement with those of Minkowycz and Sparrow (1966).

The focus on air-conditioned systems is directly related to the study of a moving vapour with a non condensable gas. Sparrow et al (1967) studied forced convection condensation over a flat plate using a boundary layer type of analysis to take into account the presence of non-condensable gases and interfacial thermal resistances), and solved conservation equations for both phases. They assumed zero velocity at the interface for the computation of the velocity field in the vapour gas boundary layer, and neglected inertia and convection in liquid layer. Most of the properties were estimated at the reference temperature and the results showed that the effect of non-condensable gas is much less than the corresponding stationary vapour gas mixture. When comparing with the moving vapour gas mixture, it results in a little more gas concentration at the interface and has a sweeping effect. Also, it is considered that the ratio of the heat flux with a non-condensable gas and without a non-condensable gas was calculated to be independent of bulk velocity. The numerical results showed that the interfacial resistance has a negligible effect on the heat transfer and that superheating has much less effect than in the corresponding free convection studies.

In an approximate analysis, this problem was again considered by Koh (1962) without taking into account the assumption of Rose (1969) except for uniform properties and had similar results. Rose (1980) used experimental results for a flow over the horizontal plate with suction effect (Rose 1979) without solving the complete set of conservation equations. In the gas-vapour boundary layer, the condensation process leads to a thinning of the said boundary layer, which is called suction effect (Maheshwari et al 2004). For the study of condensation on vertical flat plate Denny et al (1971), Denny & Jousionis (1972), and Denny & South (1972) have solved mass, momentum and energy equations considering downward flow of vapour gas mixture parallel to the flat plate and reference temperature concept has been used to evaluate the variable physical properties in the condensate film, while those in the vapour gas layer were treated exactly. The consideration of interfacial shear stress of a single phase flow over an impermeable plate was done by Asano & Nakano (1979) for the film condensation as in the Nusselt analysis. Heat and mass transfer analogy has been used by Whitley (1976), who proposed a simple model for forced convection condensation of a turbulent mixture boundary layer neglecting interfacial shear and considering surface of condensate film to be smooth. Kim and Corradini (1990) adapted this model to forced and natural convection applications by extending it to a wavy turbulent film. The analytical model

described above was solved using only a laminar vapour-gas (or pure vapour) boundary layer except for Mayhew et al (1965-66).

Corradini (1997) proposed the following approach by using well accepted correlations for flat plate geometry, the solution procedure is simplified to computing the condensate film thickness and the local Reynolds and Sherwood numbers in the downstream direction. It guides to a computationally better solution, which can be easily expanded to include more detailed models of the condensate film. Total heat flow is controlled by the gas phase heat transfer and the heat flow through the condensate film. Therefore, the total condensation heat transfer coefficient can be written as:

$$\frac{1}{h_T} = \frac{1}{h_{film}} + \frac{1}{h_{gas}} \qquad \text{(I-5)}$$

Gas phase heat transfer consists of convection heat transfer and the latent heat released as a result of mass transfer. Radiation heat transfer can be neglected in the temperature range of interest (20 - 50°C). Hence h_{gas} is given by

$$h_{gas} = h_{conv} + h_{cond} \qquad \text{(I-6)}$$

where h_{cond} is defined as :

$$h_{cond} = \frac{m''(l_{bulk} - l_I)}{T_{bulk} - T_I} \qquad \text{(I-7)}$$

The condensation heat transfer coefficient h_{cond} can then be obtained by substituting the following definition into above eqn,

$$m'' = K\left(\frac{W_I - W_{bulk}}{1 - W_I}\right) \qquad \text{(I-8)}$$

where K is the mass transfer coefficient and W is the mass fraction. Chilton and Colburn analogy (1934) between heat and mass transfer is used in order to deduce the following local Nusselt and Sherwood numbers for turbulent flow along a smooth horizontal flat plate:

$$Nu_x = 0.0296\,\mathrm{Re}_x^{4/5}\,\mathrm{Pr}^{1/3} \qquad \text{where } 5\times10^5 \le Re_x \le 10^7 \qquad \text{(I-9)}$$

$$Sh_x = 0.0296\,\mathrm{Re}_x^{4/5}\,Sc^{1/3} \qquad \text{where } 5\times10^5 \le Re_x \le 10^7 \qquad \text{(I-10)}$$

The boundary layer thickness is reduced due to the apparent suction effect of the condensation process. This leads to larger temperature and concentration gradients close to the interface that, consequently, increase heat and mass transfer rates. Kim and Corradini (1990) proposed correction factors to account for the suction effect. They also introduced a roughness parameter as droplets or waves that form on the condensate interface can increase the shear stress and lead to enhanced turbulent mixing at the interface. These correlations can be used for the simple engineering applications according to the authors.

1.3.2 Experimental developments

1.3.2.1 Effect of variable physical properties

Most of the experimental results have shown greater heat transfer coefficients than those derived by theoretical and numerical prediction (Park et al 1997). The earliest attempt to consider the condensation heat transfer rate on a horizontal surface was experimentally done by Popov (1951). The experimental investigations before this period (Johnson 1998), showed some difference with the predictions of the Nusselt theory as in McAdams (1954) and these differences were because of the reasons such as significant forced-convection effects, presence of non-condensable gas, waviness and turbulence within the condensate film, and the presence of DWC.

In an experimental study on a copper vertical flat plate Slegers and Seban (1969) condensed n-butyl alcohol at stationary conditions. The steam was condensed by Mills and Seban (1967) and Mayhew and Agarwal (1973) at stationary and moving conditions respectively. The results support the Nusselt theory for pure stationary vapour condensation, and it was concluded that the Nusselt's assumptions can be accepted for the condensation of pure steam water without non-condensable gas at stationary conditions in practical engineering situations. Also, Asano & Nakano (1979) reported their data for the condensation of pure saturated vapours on a vertical flat copper plate and showed good agreement with their model.

The stability analysis and experimental observations on falling film on a vertical wall have shown that various surface waves according to film Reynolds number appeared due to intrinsic instabilities (Chu and Dukler 1974, Kang and Kim 1992a, Chang 1994, Park et al 1997). This mechanism will enhance the heat and mass transfer in the filmwise condensation (Chun and Seban 1971, Kutateladze and Gogonin 1979, Kellenbenz and Hahane 1994). Also,

these surface waves are expected to enhance the heat and mass transport in the vapour phase and liquid phase. In an experimental study (Yun et al 2006) of laminar film condensation heat transfer coefficient on horizontal tubes and a low heat transfer rate was measured and analyzed with the variations of surface roughness, tube material, tube thickness and wall subcooling. The condensation heat transfer coefficient was significantly lower than that estimated by the Nusselt analysis when the ratio of the condensate liquid film thickness to the surface roughness was relatively low.

Recently, Dalkilic et al (2009), investigated the film heat transfer coefficients during laminar flow at high mass flux and discussed that the modified Nusselt theory's (Carey 1992) deviation is between 60.7% and 64.1%, the McAdams correlation's (1954) deviation is between 52.8% and 56.9%, and the classical Nusselt theory's (1916) deviation is between 74.7% and 76.6%. This shows that they are not suitable for laminar flow at high mass flux. These correlations are usually applied to stationary vapour flow. They are not valid when the vapour velocity is much greater than the film velocity along the test tube. High vapour velocity can also cause dragging on the downward motion of the condensate. The Nusselt-type analysis does not take account of high vapour friction or momentum drag. In addition, it is useful to know that for the solution of laminar flow at high mass flux, the deviations of the Dobson and Chato model (Dobson and Chato 1998), the Fujii correlation (Walladares 2003) and Cavallini et al's correlation (Cavillini et al 1974) are within the range of ±25%.

1.3.2.2 Effect of non-condensable gases

The heat transfer coefficients have been observed to decrease strongly with increased noncondensable gas mass fraction under various conditions and test geometries. This is caused by the accumulation of a noncondensable gas layer near the condensing film through which the vapour molecules must diffuse. Many workers have investigated the case of stationary vapour with a non condensable gas. An early experimental approach by Othmer (1929) to describe the effect of non-condensable gas and introduced air mole fraction below 7%, he also studied the condensation of stationary steam mixed with small amounts of air on a horizontal tube at constant pressure (Fig. I-3).

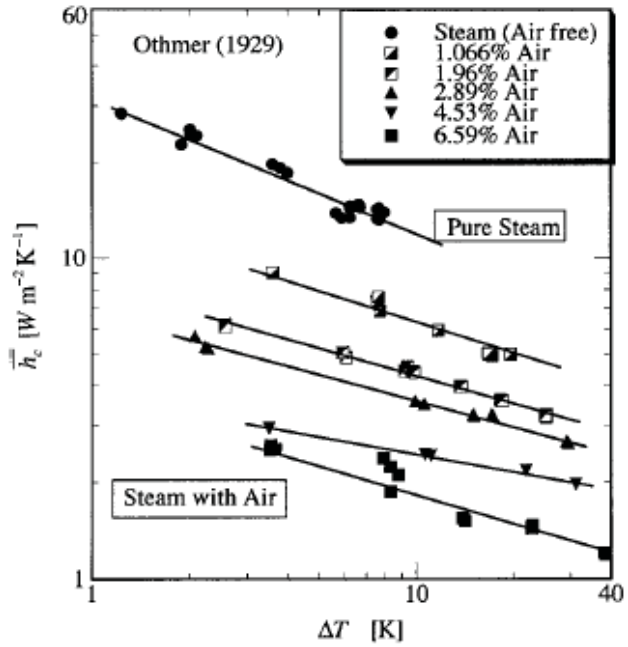

Fig.I-3: Othmer's experiments on the effect of a non-condensable gas on condensation heat transfer (under natural convection) (Asano 2006).

Heat-transfer measurements for film condensation of steam on a vertical plane surface in the presence of air, argon, neon and helium, under free-convection conditions are reported by Al-Diwany and Rose (1973). The results indicate greater reductions in heat transfer, for given non-condensing gas concentrations, than suggested by earlier reports. The vapour-gas mixture was passed into the steam chamber via flow straighteners, which provided uniform flow of the mixture towards the condensing surface so as to preclude forced convection effects. The experimental data for steam-air, steam-argon and steam-neon showed satisfactory agreement with the predicted theoretical values of Sparrow & Eckert (1961) but for steam-helium showed a lower value than the theoretical ones. Rauscher et al. (1974) performed experiments of filmwise condensation from steam-air mixtures undergoing forced flow over 18.8 mm outer diameter horizontal tube. The heat transfer coefficient at the stagnation point was reported for bulk air mass fractions of 0 to 7. DuVuono and Christensen (1984) carried out experiments at pressure slightly above atmospheric to 0.7MPa to know the effect of pressure and considered natural convection of a steam-air mixture. The experiments were performed on a horizontal copper tube with 0.0794 m outer diameter by 1.22 m of active condensation length. The tube was mounted in a cylindrical pressure vessel of 1.52 m outer diameter by 3.35 m long. From an external source the saturated steam has been supplied and,

than, it allowed to diffuse in the tube resulting in steady-state, natural convection conditions. This experiment showed a significant effect of pressure, but the pipe geometry considered prevents from suggesting the use of their correlations to a large scale system.

Some experimental studies regarding the condensation in the presence of non-condensable gas in a vertical tube were performed by several workers (Vierow and Schrock 1991, Siddique et al 1993, Araki et al 1995, Kuhn et al 1997, Park and No 1999, Lee and Kim 2008) and they have condensed steam in air or helium using secondary jacket cooling technique. Maheshwari et al (2004) investigated condensation in presence of non-condensable gas for wide range of Reynolds number.

Several other workers (Cho and Stein 1988, Robinson and Windebank 1988, Dehbi 1991) have investigated the effect of system pressure and reported that an increase in the system pressure will enhance the rate of heat transfer. Cho and Stein (1988) increased system pressure from 0.31 MPa to 1.24 MPa and showed that it influenced the mode of condensation also on a downward facing polished surface with helium as the non-condensable gas. Higher pressures led to a mixed mode of condensation i.e. filmwise and dropwise condensation coexisted. Robinson and Windebank (1988) studied the effect of pressure in the range of 0.27-0.62 MPa with an air-stream mixture and the non-condensable gas mass fraction was varied from 24 to 88 percent. The heat transfer rates were measured with a cooled disk that was placed inside a pressure vessel. The results showed that heat transfer rates increase with pressure and decrease with the mass ratio of non-condensable gas. Dehbi (1991) conducted similar tests on a cooled tube and measured heat transfer rates at three different pressures (0.15, 0.275 and 0.45 MPa). The non-condensable gas mass fraction in the tests ranged from 25 to 90 percent. The summary of some experiments is given in Table I-1.

In a similar geometry as Cho and Stein (1988), Kroger and Rohsenow (1968) condensed potassium vapour in the presence of argon and helium. The diffusion theory successfully predicted the experimental data with helium. Vapour phase instabilities and secondary flow cells were also reported by Spencer et al (1970) for condensation of Freon-113 in presence of helium, nitrogen and carbon-dioxide on a vertical surface under stagnant flow conditions. The visual observations and heat transfer measurements indicated a modest effect of non-condensable gas molecular weight.

Table I-1: Summary of previous experimental investigations with non-condensable gas (NCG).

Exp Performed	Type of Fluid and flow			Geometry, Size and Orientation	Remarks on the findings
	Gas	Vapour	Flow		
Ma et al. (2008)	Air	Steam	Stationary	Vertical copper plate, (cylindrical shape) D = 30 mm, L=310 mm	Results show that DWC heat transfer coefficients of steam and air concentration of 0.5-5% can be increased by 30-80% compared with FWC.
Oh and Revankar (2006)	Air	Steam	Moving	Vertical tube D = 47.5 mm, L = 1.8 m	A model for FWC with NCG developed and compared with Kuhn (1997) gave a satisfactory agreement
Maheshwari et al. (2004)	Air	Steam	Moving	Vertical tube ID=42.76 mm, L=1.6 m	Experiments were performed with natural convection of a vertical tube. Correlation is developed and a dependency of heat transfer coefficient on Reynolds number was shown.
Kuhn (1997)	Air, helium	Steam	Moving	Vertical SS tube ID=50.8 mm, L=2.4 m	The local Nusselt number was correlated as a function of local mixture Reynolds number, Jakob number and gas mass fraction and Schmidt number.
Park et al. (1997)	Air	Steam	Moving	Vertical tube	Correlation for local HTC in terms of degradation factor is developed. The range of validity for Jakob number in the correlation is smaller than that of the correlation developed by Siddique et al (1993)
Araki (1995)	Air	Steam	Moving	Vertical tube ID = 49.5 mm L = 1.21 m	Correlations for condensation HTC for laminar and turbulent range are developed in terms of Reynolds number and air mass fraction
Siddique (1993)	Air, Helium	Steam	Moving	Vertical tube ID= 25.27 mm, L=1.22 m	Developed correlations and for similar mole fraction, compared to helium air has more inhibiting effect on condensation heat transfer, but for the same mass ratio, helium is found to be more inhibiting.
Dehbi (1991)	Air, helium -steam	Steam,	Stationary	Vertical copper tube D=38 mm, L=3.5 m	Given correlations and it agrees well with experimental data for heat transfer coefficient estimated by heat and mass transfer model

Vierow (1991)	Air	Steam	Moving	Vertical copper tube ID=22.1 mm, L=2.13 m	At an air inlet mass fraction of 14% the HTC were reduced to one-seventh the values of pure steam. Instabilities were observed at high air contents. Also developed a correlation for calculating local HTC
Al-Diwani and Rose (1973)	Air, Argon and Helium	Steam	Stationary	Cooled vertical copper plate, 97 x 97 mm	Experimental data showed good agreement with the published data
Gerstman & Griffith (1967)	Air	Freon-113	Stationary	Horizontal and inclined plate L = 457.2 mm	HTC obtained by condensing Freon-113 were found to agree quite well with their model.
Othmer (1929)	Air	Steam	Stationary	Copper tube D = 76.2 mm, L=1.22 m	Reduction in HTC by 50% when 0.5% air is present in steam.

The effect of forced flow was studied by Dallmeyer (1970) for condensation of CCl_4 and C_6H_6 on a vertical plate in the presence of air flowing in laminar or turbulent regime. The results showed that heat transfer rates increased with the Reynolds number and the vapour concentration. Measured profiles illustrated the apparent suction effect of condensation that increases the gradients near the wall and thus leads to higher heat and mass transfer rates in the laminar flow region. Barry (1987) performed condensation experiments with the mixture of steam and air. His apparatus consisted of a horizontal plate facing upwards. The velocity and mass ratio range were chosen so that they covered the conditions that are likely to exist in containment during an accident in a developing parallel flow situation. Kutsuna et al (1987) studied condensation of steam on a horizontal plate (facing up) in the presence of air. They also reported increased heat transfer rates due to forced convection. Their results showed the expected effects of non-condensable gas concentration and velocity on the heat transfer coefficients. The condensate film characteristics depend on its flow field and the nature of the condensing surface, e.g. roughness, wetting, and orientation. The surface finish has a major effect on the mode of condensation for all kind of surfaces especially for a downward facing surface and it is the wetting characteristics of the surface that ultimately determine this. The dropwise condensation is likely to exist on non-wetting surfaces and filmwise condensation is likely on wetting surfaces. In dropwise condensation mode with polished metal surfaces, the heat transfer characteristics are likely to change with time due to the oxidation of the surface or tarnishing. Thus, one cannot precisely know the wetting characteristics as surface aging occurs (Rose 1998).

1.4 Dropwise condensation

It is well known that if the condensate does not completely wet the solid surface, individual liquid droplets form rather than a continuous condensate film. Dropwise condensation (DWC) is an attractive mode of heat transfer because the heat transfer coefficients are much higher. In the condensation of steam, the heat transfer coefficients measured in DWC have been a factor of four to eight times larger (Butterworth 1983) than the FWC. In film condensation, the surface is blanketed by a liquid film of increasing thickness between the solid surface and the vapour which serves as a resistance to heat transfer. The heat of vaporization released, as the vapour condenses, must diffuse through this resistance before it can reach the solid surface. In DWC, part of the surface is in contact with vapour leading to higher heat transfer rates. The active condensation interface is also much larger in DWC. In attempting to predict or correlate heat transfer rates with DWC on solid surfaces or in evaluating experimental results, several factors should considered to count for the non-condensable gases, the promoter surface thermal properties and the droplet removal mechanism. Since the discovery of the advantages of DWC, many trials have been performed to induce this form of condensation on metallic surfaces, but up to now none of the methods could be implemented in real technical applications because in most cases long term stability over several years cannot be obtained (Rausch et al 2008).

1.4.1 Theoretical developments

Fatica and Katz (1949) were the earliest to propose a model to compute the rate of heat transfer. They assumed that on a given area all drops have the same size, are uniformly spaced and grow by direct condensation. In later attempts, different researchers dealt with the problem of dropsize distribution in a variety of ways. Wu and Maa (1976) used the population balance method to derive the drop size distribution of small drops which grow mainly by direct condensation based on the assumption of steady size distribution. They estimated a vapour side heat transfer coefficient of DWC by assuming heat conduction through the drop as the only resistance to drop growth. In Maa (1978) the number of nucleation sites was varied so that the results would fit the experimental data. Later, Abu-Orabi (1998) modified the concept used by Maa (1978) by incorporating the resistance due to the promoter layer into his model. He included a theoretical derivation for the sweeping period in his model but, actually the sweeping period could be determined experimentally by knowing the maximum

drop radius and the contact angle it made with the condensing surface. Le Fevre and Rose (1966) derived a time-averaged distribution which had the correct behaviour for the limiting cases of very large and very small drops. Rose and Glicksman (1973) proposed a universal form of the distribution function for large drops which grow primarily by coalescence with smaller drops. However, the predicted distribution was not valid for small drops, which grow by direct condensation. Rose (1981) tried to improve the form by incorporating the resistances to heat transfer due to the drop and various contact angles. He suggested changing the radius of the smallest viable drop or the maximum drop radius or adding a resistance due to the promoter layer to match the experimental data. Tanaka (1975a, 1979) proposed a theory based on transient condensation and derived a set of simultaneous differential equations from statistical and geometrical considerations.

A detailed discussion and its theoretical and experimental developments were given by Le Fevre & Rose (1965), and Rose (1988, 1994). As it was discussed by Rose in the 70's it was clear that the early results suffered from errors due to the presence of air in the vapour as well as insufficiently accurate measurement of the small vapour to surface temperature difference. The studies of different research groups were in good agreement and indicated heat-transfer coefficients for dropwise condensation of steam around 10 and 20 times those for film condensation at power station condenser pressures and at atmospheric pressure respectively. Moreover the heat-transfer coefficient was found to increase with an increase in the temperature difference or heat flux. The empirical equations (Rose, 1998) for DWC of steam are summarized by the correlations,

$$q = \theta^{0.8}\left[5\frac{\Delta T}{K} + 0.3\frac{\Delta T^2}{K^2}\right] \qquad \text{(I-11)}$$

where q = mean heat flux for surface (kWm^{-2})
ΔT = vapour to surface temperature difference
$K = (8/3)\,(2\pi)^{1/2}\,[\Gamma(1/3)]^{-9/4} = 0.728018$
θ = Celsius temperature

And for the heat transfer coefficient h ($kWm^{-2}K^{-1}$),

$$h = \theta^{4/5}\left[5 + 0.3\frac{\Delta T}{K}\right] \qquad \text{(I-12)}$$

As reported by Rose (1998) this correlation is in good agreement with experimental results for steam, which include data from several different sources. A theory of DWC (Maa, 1978) is also in good agreement with these data for steam and other fluids (Rose, 1988, 1994,

1998, 1999). Rose (1999) recommended that future investigators validate their experimental techniques by first using a well-known monolayer promoter such as dioctadecyl disulphide, or even olelic acid, and checking that results consistent with eqs. (I-11) and (I-12) are obtained.

1.4.2 Experimental developments

As discussed by Rausch et al (2008), for producing DWC on metals, a reduction of their free energy in order to reduce wetting properties is necessary, which could either be obtained by applying hydrophobic layers of organic substances (Erb & Thelen 1966, Marto et al 1986, Vemuri & Kim 2006), inorganic compounds (Mori et al 1991), polymers (Koch et al 1997, 1998a) or hard coatings (Koch et al 1998b, Leipertz & Koch 1998, Zhao et al 1991) to surface or by the formation of surface alloys (Zhao et al 1991, Zhao & Burnside 1994). To develop a reliable DWC promoter, organic materials such as waxes, oils, and greases have been applied to achieve DWC of steam in the early 1960s; however, these promoters can be washed off rapidly and the condensation reverts to filmwise quickly. Noble metal coatings such as gold, silver, rhodium, palladium, and platinum have been found to produce excellent DWC (Woodruff & Westwater 1979, 1981, O'Neill & Westwater 1984, Bernett & Zisman 1970).

Since the 1980s, thin-layer organic coatings with low surface energies have received more attention. For organic coatings, three factors restrict their applications to promote DWC. First, there must be a good, long-term adhesion between the coatings and metal substrates. However, it is well known that organic materials are more difficult to be sustained on metal substrates at elevated temperatures. Second, in general, if the coating is thicker, it is a better resistance to oxidation and erosion. However, the thickness of these organic coatings should not be larger than a few micrometers in order to minimize thermal resistance; otherwise, the enhancement of the heat transfer coefficient will be compensated by the increase in thermal resistance of the coating itself (Marto et al 1986).

The development of ultra-thin and stable coatings for DWC are still of interest to researchers. Ma et al (1994) coated ultra-thin polymers that were created by plasma polymerization and dynamic ion-beam mixed implantation (DIMI) method on vertical brass tubes for heat transfer experiment. It was concluded that, while the heat transfer enhancement was 20 times higher, the promotion and the adhesion of the ultra-thin film with the substrate were strongly dependent on the process conditions of the two methods and require further

study to optimize its performance. Subsequently, a lifetime test experiment was conducted (Ma et al 1999). These experimental results demonstrated that one surface had sustained DWC for about 1000h. It was also found that polymer films prepared by DIMI had good adhesion with the metal substrate. In a different study, Ma et al (2002) investigated the influence of processing conditions for polymer films by means of the DIMI technique on dropwise condensation heat transfer. Their experimental results indicated that as heat flux was increased by 0.3-4.6 times, condensation heat transfer coefficient could increase 1.6-28.6 times when compared with those from FWC for the brass tubes treated with various conditions. The experimental results given by Vemuri & Kim (2006) using self-assembled monolayer (SAM) technique for the coating of n-octadecyl mercaptan solution showed DWC for more than 2600 h.

Erb and Thelen (1966) used coatings of inorganic compounds such as metal sulfides and found out that a sample of sulfided silver on mild steel showed excellent DWC. Extensive studies were made by Woodruff & Westwater (1979, 1981) on condensation by using noble metal plated surfaces and showed that noble metal plated surfaces have consistently showed excellent dropwise characteristics. However, the hydrophobic characteristics of these noble metals as DWC promoters had been controversial in the literature (Bernett & Zisman 1970), and also the cost incurred in manufacturing such surfaces have limited their applications. Organic materials (Marto et al 1986, Holden et al 1987, Haraguchi et al 1991) like hydrocarbons and polyvinylidene chloride coatings had also received considerable attention for their hydrophobic capabilities to promote DWC. Many researchers (Ma et al 1993, 2002, Zhao et al 1991a, b) have used different types of technologies to employ polymer coatings for promoting DWC and reported that heat transfer enhancements were up to 30 times higher than film condensation. Das et al (2000) used an organic mono-layer coating and they concluded that SAM coatings increased the condensation heat transfer coefficient by a factor of 4. However, the durability of the coated surfaces has not been determined. In general, organic coatings are difficult to maintain, and require strong, long term adhesion forces between the coating and the metal substrate.

The interest and the development of dropwise condensation waned following failures, despite the fact that many attempts have been made to find an industrially effective and reliable means of promoting dropwise condensation. However, Zhao and co-workers (1991b, 1994) have given encouraging reports from China and proposed a means of process called

'dynamic mixing magnetron sputtering/ion plating'. In this process a hydrophobic surface alloys has been formed and used for the promotion of DWC. This technique has been successfully used in Dalian and Jilin power plants and has been patented in China (Wang et al 1992, Zhao & Wang 1993). A dropwise-promoted, vertical-tube condenser/feed heater has operated successfully since 1989 with an overall heat-transfer coefficient of 6000 Wm^{-2} K^{-1} and with the same performance as a similar condenser operating under the same steam and coolant conditions and with twice the number of untreated tubes. Zhao et al (1991c) achieved DWC successfully by using ion implantation of N, Ar, He, H, and Cr in copper tubes. Zhao and Burnside (1994) implanted polytetrafluoroethylene (PTFE) coated tube surfaces with Cr^+ and obtained heat transfer coefficients 5 times larger than those of unimplanted tubes. The method of simultaneous magnetron sputtering ion-plating of Cr^+ and N^+ and then of CH_4 in copper U-tubes (Zhao et al 1991b) and C_2H_6 in white copper (70%Cu:30%Ni) U-tubes (Zhao et al 1994) produced excellent DWC of steam.

Kananeh et al. (2006) experimentally studied DWC on plasma-ion implanted stainless steel tubes. They proposed that the stable DWC was obtained on stainless steel tubes implanted with ion doses of 10^{15} and 10^{16} N cm^{-2} at low cooling water flow rates which converted at higher cooling water flow rates to a mixed condensation form of FWC and DWC. The measured heat transfer coefficient h_c for DWC was found to be larger by a factor of about 3 compared with the FWC values calculated from corrected Nusselt's film theory and could be enhanced by increasing the ion dose. An increasing steam pressure has a positive effect on DWC by lowering the interfacial resistance of mass transfer at the liquid-vapour interface as well as the surface tension of the condensate.

1.5 Mass transfer

When a system contains two or more components whose concentration vary from point to point, there is a natural tendency for mass to be transferred, minimizing the concentration difference within the system (Benitez, 2009). The transport of one constituent component from a higher concentration region to that of lower concentration is called mass transfer. The transfer of mass within a fluid mixture or across a phase boundary is a process that plays a major role in many industrial processes, such as dispersion of gases from stacks, removal of pollutants from plant discharge streams by absorption, stripping of gases from waste water, air conditioning. Also many of day-by-day experiences involve mass transfer,

some example: A lump of sugar added to a cup of coffee eventually dissolves and then diffuses to make the concentration uniform, water evaporates from ponds and sea to increase the humidity of passing-air-stream, and its reverse the condensation of water vapour present in humid air, perfumes present a pleasant fragrance which is imparted throughout the surrounding atmosphere.

The mechanism of mass transfer involves both molecular diffusion and convection. Diffusion can be defined as the relative motion of molecules from the centre of mass of the mixture, moving at the local velocity of the fluid, whereas convective mass flux is the transfer of material through an interface of two phases. Convective mass transfer between two phases is always accompanied by energy transfer associated with phase change, which will affect the interface boundary layer conditions. In this regards mass transfer is always associated with simultaneous heat transfer.

Condensation and evaporation are processed of simultaneous heat and mass transfer, which involves a phase change. These are the transport phenomena in which vapours or vapour mixtures are in contact with liquids or solids, and a large amount of energy is released or absorbed with phase change, which is called latent heat. Condensation of water vapour on a cold surface, it involves a film of condensed liquid followed by a cold surface and a film of gas through which the condensate is transferred by molecular diffusion.

1.5.1 Diffusion

Diffusion of water vapour in air is an important property involving mass transport phenomena with humid air. Diffusion of mass is dependent on the differences in concentration, temperature, and pressure (Reid et al. 1987). The general expression for diffusive flux of one dilute gas (A) in another (B) at low velocities can be written as (Landau and Lifshitz 1987, chaps. 57 and 58)

$$J_{Diff} = -\rho_0 \left[D_{AB} \frac{\partial}{\partial z} \frac{\rho_A}{\rho_0} + \frac{D_T}{T} \frac{\partial T}{\partial z} + \frac{D_p}{p_0} \frac{\partial p_0}{\partial z} \right] \qquad \text{(I-13)}$$

where J_{Diff} is the diffusive mass flux of gas A, D_{AB} the mutual diffusion coefficient, D_T the coefficient for 'thermodiffusion', T the temperature, and D_p the coefficient of 'barodiffusion'. Thermodiffusion (diffusion driven by thermal energy) and barodiffusion (diffusion driven by pressure) are usually small compared with concentration diffusion, and the above equation

holds in a reference frame where the centre of mass velocity of the gas mixture is zero. In an environment where temperature and total pressure change little, and the vapour concentration is low, the concentration diffusion J_{Diff} would be simply described by

$$J_{Diff} = -D_{AB}\frac{\partial \rho_A}{\partial z} \tag{I-14}$$

Cunningham and Williams (1980) discussed in detail about the reference frames and non-isothermal diffusion.

Diffusion coefficient may be calculated from Kinetic theory of gases, which requires the evolution of parameters such as reduced collision integral for diffusion and mean molecular free path (Mason and Monchick 1963). Hirschfelder et al (1952) derived a theoretical equation for the binary diffusion coefficients from the kinetic theory of gases:

$$D_{AB} = \frac{1.858\times10^{-7}.T^{3/2}(1/M_A + 1/M_B)^{1/2}}{(P/101325)\sigma_{AB}^2\Omega(T_D^*)} \tag{I-15}$$

where D_{AB} is in $m^2.s^{-1}$,

M_A, M_B are molecular weights of component A and B,

$\sigma_{AB} = (\sigma_A + \sigma_B)/2$ collision diameters of components A & B,

$T_D^* = kT/\varepsilon_{AB}$ and $k/\varepsilon_{AB} = \sqrt{(k/\varepsilon_A)(k/\varepsilon_B)}$ where k is the Boltzmann constant,

ε_A/k or ε_B/k is the characteristic energy of component of A & B [K].

$\Omega(T_D^*)$ collision integral for diffusion, and P is pressure in Pascal.

Also Rossie (1953) has proposed equations for diffusion of water vapour in air for the temperature range -20 °C to 300 ºC, the equations are

$$D = 104.91143\times10^{-6}\frac{T^{1.774}}{P} \quad \text{for t} \le 80\ ^{\circ}\text{C} \tag{I-16}$$

$$D = \frac{805.2375\times10^{-6}}{P}\frac{T^{2.5}}{(T+190)} \quad \text{for } 80 < \text{t} < 300\ ^{\circ}\text{C} \tag{I-17}$$

where D is in m^2/s and P in Pascal.

1.6 Characteristics of the fluid medium

1.6.1 Air

Air is a complex mixture of gases, its pressure and temperature have a tendency to

vary constantly at one point, and also minor changes have been found in its composition with time and space according to the release and use of some of its components. The standard composition of dry air considering on ideal gas and having negligible humidity as given by International civil aviation organisation (OACI)

Table I-2**:** The composition of dry air at sea level

Gases	Molar Mass (g/mol)	Molar Fraction	Concentration by vol.
Nitrogen (N_2)	28.0134	0.7809	78.09 (%)
Oxygen (O_2)	31.9988	0.2095	20.95 (%)
Argon (Ar)	39.948	0.0093	0.93 (%)
Carbon-di-Oxide (CO_2)	44.0099	0.0003	385 (ppm)
Neon (Ne)	20.183	0.000018	18 (ppm)
Helium (He)	4.0026	0.00000524	5.2 (ppm)
Krypton (Kr)	83.80	0.0000010	1.1 (ppm)
Methane (CH_4)	16.04	0.00000177	1770 (ppb)
Hydrogen(H_2)	2.0159	0.00000050	500 (ppb)
Xenon (Xe)	131.30	0.000000086	86 (ppb)
Ozone (O_3)	47.998	0.00000001	10 (ppb)
Radon (Rn)	222	10^{-20}	6×10^{-11}(ppb)

1.6.2 Some Physical Constants of air: (at 15 ºC Sea level)

Table I-3: Some physical constants of air

Gas Property	Value	Unit
Molecular Weight	28.9645	kg/kmol
Atmospheric Pressure	101325	N/m^2 (Pascal)
Density	1.226	kg/m^3
Universal gas constant (R)	8314.32	J/(K · kmol)
Viscosity	1.73×10^{-5}	$N.s/m^2$

Also the variation in atmospheric pressure (P_{atm}) with height can be represented by the relation (Duminil 2006)

$$P_{atm} = 1.19745 \times 10^{-8} (288.15 - 0.0065h)^{5.25588} \qquad \text{(I-18)}$$

where h is the height above sea level. The average molecular mass of air at standard temperature and pressure is 28.57 g/mol and of water vapour 18.02 g/mol.

1.6.3 Temperature dependence of physical constants of air

1.6.3.1 Density (ρ)

Density of air is the mass per unit volume of the surrounding atmosphere. It depends on the altitude above sea level and decreases with increasing altitude, and depends also on the ambient temperature. According to the ideal gas equation the density is defined as

$$\rho_a = \frac{P_{atm}}{R.T} \tag{I-19}$$

where ρ_a is the air density [kg.m^{-3}], P_{atm} is the atmospheric pressure [Pascal], R is the specific gas constant, and T [K] is Temperature. The specific gas constant for dry air is 287.05 [J.kg^{-1}.K^{-1}]. Thus, the density of dry air

$$\rho_d = \frac{P_v}{287.05T} \tag{I-20}$$

where ρ_d is the density [kg.m^{-3}] of dry air, P_v is the partial pressure [Pascal] of dry air.

And the density of water vapour is

$$\rho_{wv} = \frac{P_{wv}}{461.495T} \tag{I-21}$$

where ρ_{wv} is the density [kg.m^{-3}] of water vapour, P_{wv} is the partial pressure [Pascal] of water vapour, and according to the Dalton law $P_{atm} = P_v + P_{wv}$. The constant 461.495 is the specific gas constant for water vapour. Now, the density of humid air may be calculated considering a mixture of ideal gases (dry air and humid air)

$$\rho_{humidair} = \frac{P_v}{287.05T} + \frac{P_{wv}}{461.495T} \tag{I-22}$$

The density of air reduces after addition of water vapour in dry air, which is because of difference in molecular masses of water (18.02) and the humid air (28.57).

1.6.3.2 Viscosity (μ)

Viscosity is the property that measures the resistance of the fluid to deforming due to a shear force. It is also defined as the internal friction of the fluid, which creates a resistance to

the flow of fluid layers over each other. The viscosity of the fluid is significantly dependent on the temperature of the fluid, and relatively independent on the pressure. The temperature dependence for the range 0 - 54 ºC is given as (Weast 1986)

$$vis\cos ity(\mu) = (17.1 + 0.067.T - 0.0004.T^2) \times 10^{-6} \quad \text{(I-23)}$$

1.6.3.3 Vapour Pressure

Vapour pressure of water vapour in air can be defined as

$$P_{wv} = RH.P_{sat} \quad \text{(I-24)}$$

where P_{wv} is the partial pressure of water vapour in air and RH is the relative humidity, while P_{sat} is the saturation vapour pressure.

1.6.3.4 Saturation Vapour Pressure

The saturation vapour pressure of water at any given temperature is the vapour pressure when the relative humidity equals 100%. As described in Duminil (2006) that Cadiergues (1978) has proposed empirical relations for the temperature dependence of the saturation vapour pressure over ice and over water, which are always different on 0 ºC ice and on 0 ºC water

Over water

$$\log P_{sat} = \frac{7.625.T}{241.0 + T} + 2.7877 \quad \text{(I-25)}$$

Over ice

$$\log P_{sat} = \frac{9.756.T}{272.7 + T} + 2.7877 \quad \text{(I-26)}$$

where P_{sat} [Pascal] is saturation vapour pressure, and temperature T is in ºC.

1.6.4 Mass Fraction of water vapour in Air

The mass fraction of water vapour in air (ω) is defined as

$$\omega = \frac{PartialP.ofwater \times Mol.wt.ofwater}{(partialP.ofAir \times Mol.wt.ofAir) \times (partialP.ofwater \times Mol.wt.ofwater)}$$

$$\omega_{freestream} = \frac{PartialP.ofwatervapour \times 18}{(PartialP.ofAir \times 29) \times (PartialP.ofwatervapour \times 18)} \quad \text{(I-27)}$$

Mass Fraction at free stream flow

$$\omega_{freestream} = \frac{P_{wv} \times 18}{((P_{atm} - P_{wv}) \times 29) \times (P_{wv} \times 18)} \quad \text{(I-28)}$$

Mass Fraction at surface temperature

$$\omega_{surface} = \frac{P_{sat} \times 18}{((P_{atm} - P_{sat}) \times 29) \times (P_{sat} \times 18)} \quad \text{(I-29)}$$

1.6.5 Dewpoint

Dewpoint temperature is a saturation point, at constant atmospheric pressure, at which the water vapour in air starts condensing. When the dewpoint temperature falls below the freezing point of water, it is called frost point and water vapour no longer creates dew, it directly forms frost by deposition on a cooled surface. It is related to the relative humidity, when the relative humidity equals 100% the dewpoint is equal to the current temperature. At a constant pressure, the dewpoint indicates the mole fraction of water vapour in air; therefore it gives the specific humidity of air.

1.6.6 Forced Flow over an Isothermal Plate

Forced air flow over a hot plate will remove heat from the plate, and a cool plate below dewpoint will condensate water vapour and takes heat from the surroundings including latent heat of water vapour. If velocity of the air is slow enough and the plate length short enough, we can expect the flow in the boundary layer near the plate to be laminar. In our experiments due to the thickness of the heat sink below the Peltier element, there was turbulence on the surface of the plate. To know the flow profile over a flat plate, if we analyse a two-dimensional flow over a flat plate, it serves well to illustrate several key concepts in forced convection, but a one-dimensional flow analysis will also serves the purpose. For boundary layer analysis the viscosity of the fluid requires that the fluid at the plate's surface have zero velocity. As a result a boundary layer exists where the fluid velocity changes from U_∞ in the free stream (far from the plate) to zero at the plate. Within this boundary layer, the flow is initially laminar but can proceed to turbulence once the Reynolds Number *Re* of the flow is sufficiently high. The transition from laminar to turbulent for flow over a flat plate occurs in the range defined above.

1.6.7 Psychrometric chart

The psychrometric chart gives thermal and physical properties of moist air in a representation of graphical form. A psychometric chart contains a lot of information with boundaries of dry bulb temperature scale on horizontal axis, humidity ratio (moisture content) on the vertical axis, and an upper curved boundary which represents saturated air or 100 percent moisture holding capacity. A general look of the psychometric chart is shown in the fig.I-4 (it is for standard atmospheric pressure (14.7 psi) and temperatures of 30° to 120°F). Some other important properties of humid air, which are normally shown by these charts, have been given in fig.I-5 (http://sp.uconn.edu). The Psychrometric properties are also available as charts, data tables, equations, and slide rulers.

Usually to read these psychrometric charts, we find the intersection of two known properties and then run through the lines passing from this intersection to the way headed for the unknown property as given in the fig.I-5.

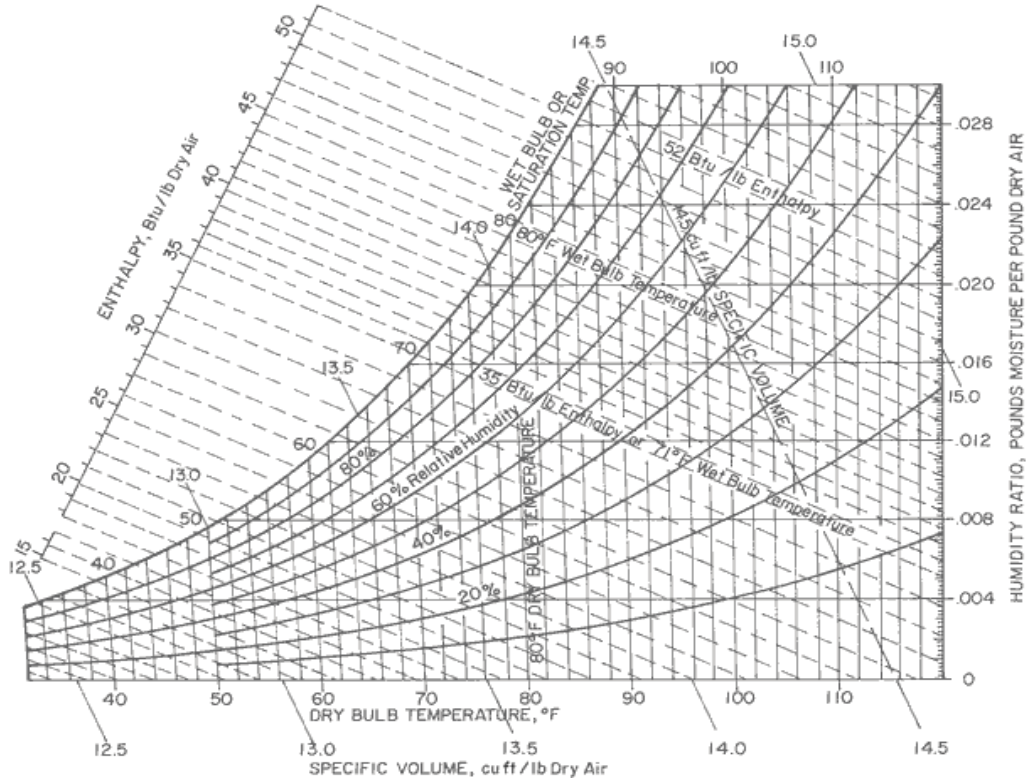

Fig. I-4**:** Psychrometric chart

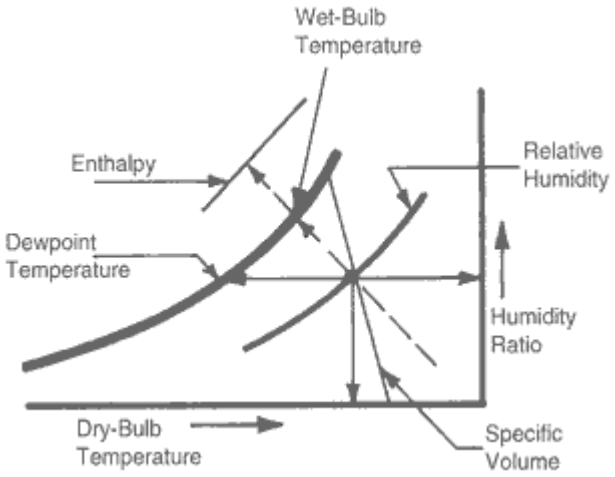

Fig. I-5**:** The properties of moist air normally represented by the Psychometric chart**.**

1.7 Mars

Mars is a planet nearest to Earth and fourth from the Sun in our solar system, often called red planet, because of iron oxide prevalent on its surface, gives it a reddish emergence. It is officially the main future targets for human space exploration missions. The existence of life on Mars is a big question for today's scientists, and till now no sign have been evidenced for life. The similar seasonal cycles and rotational period of Mars and Earth, also is the tilt which produces the season makes it encouraging to explore the possibilities of developing an atmosphere favourable to sustain life on Mars.

1.7.1 Atmosphere

The basic information on Mars and about its atmosphere is the result of several Mars missions of NASA and Russian Space Agency. The average atmosphere height of Mars is little higher approx. 11 Kms in comparison to Earth as 7 Kms. The atmosphere consists of a mixture of gases given below

Table I-4: Composition of atmosphere at Mars

Gases	**Concentration by vol.**
Carbon-dioxide (CO_2)	95.3 (%)
Nitrogen (N_2)	2.7 (%)
Argon (Ar)	1.6 (%)
Oxygen (O_2)	0.13 (%)

Carbon-mono-Oxide (CO)	0.07 (%)
Nitric Oxide	0.013 (%)
Neon (Ne)	2.5 μmol/mol
Krypton (Kr)	300 nmol/mol
Formaldehyde (CH_2O)	130 nmol/mol
Xenon (Xe)	80 nmol/mol
Ozone (O_3)	30 nmol/mol
Methane (CH_4)	10.5 nmol/mol

1.8 Moon

1.8.1 Atmosphere

It is the Earth's only satellite, and fifth largest satellite in solar system. Moon is the single celestial body on which humans have landed. The atmosphere of the moon is so tenuous, as to consider nearly vacuum. The traces of Argon-40, Helium-4, Oxygen (O_2), Methane (CH_4), Carbon monoxide (CO), Carbon dioxide (CO_2), Nitrogen (N_2) detected in-situ by detector placed by Apollo astronauts (Stern, 1999). The average daytime abundance of the elements present in the atmosphere of moon are given as follows

Table I-5: Composition of elements at Moon

Elements	**Atoms per cubic centimetre**
Argon	40,000
Sodium	2,000-40,000
Potassium	70
Hydrogen	Fewer than 17

1.9 Dimensionless numbers

1.9.1 Sherwood number

It is a dimensionless number, which usually gives the mass transfer rate, known as the *Sherwood Number (Sh)*. Conventionally, it is taken to be dimensionless, and composed of the mass transfer coefficient, the diffusivity, and the characteristic length of the system, in analogy to similar number in heat transfer, namely the Nusselt number. In general it is defined

as

$$\text{Sherwood number (Sh)} = \frac{\text{Convective mass transfer coefficient}}{Diffusive \cdot mass \cdot transfer \cdot coefficient} = \frac{kL}{D} \quad \text{(I-30)}$$

where k is mass transfer coefficient (m/s), L is the characteristic length (m), D is the diffusivity (m^2/s). Due to various definitions of concentrations, which are used in practical applications, such as mole fraction, partial pressure, partial molar density, mass fraction, and absolute humidity, in a case-by-case way, hence various definitions of Sherwood numbers and mass transfer coefficients exists. Because of this variety, the numerical values of the Sherwood number obtained from the same numerical data, but calculated with a different definition of concentrations do not have to be same under certain conditions, although in case of Nusselt number, there is no such trouble. For the purpose of generalization, Asano (2006) has proposed a definition, which depends on mass flux or molar flux:

$$\text{Sherwood number (Sh)} = \frac{\text{mass flux or molar flux}}{characteristic \cdot diffusion \cdot flux \cdot at \cdot the \cdot boundary} \quad \text{(I-31)}$$

$$Sh = \frac{m_x}{\rho D(\omega_s - \omega_\infty)/L} \quad \text{(I-32)}$$

Here, m_x is the mass flux of component x (kg m^{-2} s^{-1}), ρ is the density of fluid (kg m^{-3}), ω_s and ω_∞ are the mass fraction at surface and free stream respectively. Interface

1.9.2 Reynolds number (*Re*)

It indicates the relative order of magnitude of the inertia forces to the viscous forces in the fluid flow. The local Reynolds number is defined by the following equation:

$$\text{Re}_x = \frac{\rho x U_\infty}{\mu} \quad \text{(I-33)}$$

Where *Re* is a dimensionless Reynolds number, x is the distance from the leading edge of the plate (m), U_∞ is free stream velocity (m/s), ρ is the density of the fluid (kg m^{-3}), μ is the viscosity (Pa.s). Its value also indicates the transition from laminar to turbulent flow, if the Reynolds number exceeds a certain value, which is called the critical Reynolds number. The critical value of *Re* for a flow over a horizontal flat plate, whether the flow is laminar,

transient or turbulent, given for a flow in a boundary layer along a flat plate is in the range of 3.5 x 10^5 to 1 x 10^6.

1.9.3 Schmidt number (Sc)

It is a dimensionless number, which represents the relative order of magnitude of the thickness of concentration boundary layer in comparison with that of the velocity boundary layer.

$$\left(\frac{\delta_c}{\delta}\right) \approx \left(\frac{\mu}{\rho D}\right)^{-1/3} = Sc^{-1/3} \qquad \text{(I-34)}$$

$$Sc = \left(\frac{\mu}{\rho D}\right) \qquad \text{(I-35)}$$

Where δ_c is the concentration boundary layer (m), δ is the velocity boundary layer.

1.9.4 Stanton number (St)

The dimensionless number named after British scientist Thomas Edward Stanton (1865-1931), commonly used in the study of forced convection, and in heat transfer calculations, it measures the ratio of heat transferred into a fluid to the thermal capacity of the fluid. The Stanton number (St_m) for mass transfer gives the rate of turbulent mass transfer and can be expressed as:

$$St_m = \frac{Sh}{\mathrm{Re}\,Sc} \qquad \text{(I-36)}$$

1.9.5 Friction factor

The viscous drag due to friction in a boundary layer along a horizontal flat plate can be obtained by using some dimensionless functions (Asano 2006). The local friction factor (f_x) for **laminar** boundary layer at a distance x (m) from the leading edge of the plate, can be written as:

$$f_x = 0.664\,\mathrm{Re}_x^{-1/2} \qquad \text{(I-37)}$$

where Re_x is the local Reynolds number. The average friction factor over total length of the plate L:

$$f_x = \frac{1}{L}\int_0^L \frac{0.664}{\mathrm{Re}_x^{1/2}} dx = 1.328\,\mathrm{Re}^{1/2} \qquad \text{(I-38)}$$

The equation for the local friction factor in a **turbulent** boundary layer can be written as:

$$f_{x.} = 0.0576\,\mathrm{Re}_x^{-0.2}$$

Schlichting (1968) proposed that if the coefficient on the right hand side of the equation is replaced with 0.0592 instead of 0.0576 in original derivation, then a better agreement has been obtained with observed data:

$$f_{x.} = 0.0592\,\mathrm{Re}_x^{-0.2} \qquad \text{(I-39)}$$

The average friction factor over the total length of the plate, L can then be obtained by integration

$$f = \frac{1}{L}\int_0^L f_x dx = 0.074\,\mathrm{Re}^{-0.2} \qquad \text{(I-40)}$$

where Re is the Reynolds number over the entire length of the plate.

1.9.6 Chilton and Colburn J factor analogies:

It is a well known correlation and probably the most successful and widely used analogy for heat, mass and momentum transfer. Because of the similar nature of mathematical correlations and basic mechanisms of heat, mass and momentum transport, several analogies have been suggested such as Reynolds analogy, Prandtl-Taylor analogy, von Karman analogy (1939), Deissler analogy (1955). The correlation proposed by the Chilton and Colburn (1934) on the basis of a wide range of data on heat and mass transfer, is given below:

$$\frac{f}{2} = j_H = \frac{Nu_x}{\mathrm{Pr}^{1/3} f(\mathrm{Re}_x)} = j_D = \frac{Sh_x}{Sc^{1/3} f(\mathrm{Re}_x)} \qquad \text{(I-41)}$$

The above equation helps to predict an unknown transfer coefficient when one of the other coefficients is known.

1.10 Conclusion

The evaluation of heat and mass transfer related to the condensation of humid air has been extensively investigated for the past 50 years. Various technological applications are concerned but with different issues: enhancement of heat transfer in condensers, quality of air in living areas (automotive, houses, operating rooms, cold chambers, greenhouses, etc.),

collection of water in deserted zones, etc. The complex physics of the condensation process has lead to fine and very specific studies, both experimental and theoretical. Some of them are still being conducted for the origin of the formation of the initial drops for the dropwise condensation regime.

However, most of the studies intend to measure heat transfer at interfaces only. Mass transfer is then deduced from empirical laws. For the prediction of precise mass transfer rates the determination of the local mass transfer coefficients is needed. Today's knowledge lacks accurate data for gas/liquid transfer on solid walls (simple or complex shapes), on plants or on human bodies. Moreover no data are available concerning such configurations in non-terrestrial gravity.

The optimisation of BLSS require those local mass transfer coefficients for implementation in a global coupled hydrodynamics, heat and mass transfer modelling that could simulate the atmosphere in space greenhouses, or in manned-capsule and to prevent mould, rot or rust also. Further, the coupling with microbiological development models will help for the protection of the crew from nosocomial infections, the optimisation of the microclimate prevailing in a space greenhouse, a better control of high-plant growth.

Chapter II

Materials and Methods

2.1 Introduction

To generate and control the mass flux of humid air that condenses on the surface of a flat plate, a system of controlled thermoelectric cooling has been developed. The temperature of this plate is kept constant in order to induce a steady flow of condensation on the air at the air/plate interface, and the produced condensate is regularly monitored by weighing the whole system. The system consists of a square shaped Peltier module sandwiched between a square shaped aluminium flat plate and a heat exchanger device, and a temperature regulator that controls the power supply of the Peltier module. The overall arrangement was placed in a vein of a wind tunnel in which the hydrodynamics, temperature and hygrometry were regulated (Fontaine and Tiwari 2009).

2.2 Wind Tunnel

2.2.1 Main Characteristics

The wind tunnel facility built by INRA in Theix by Dr Alain Kondjoyan (1993) aimed at generating from nearly laminar to highly turbulent flows. The detailed description of the wind tunnel is given in the literature (Kondjoyan, 1995). The data for laminar flows were compared to reference works; the studied turbulent flows were similar to those encountered in agribusiness. The temperature, humidity and wind velocity can all be regulated inside the wind tunnel.

The main characteristics of the wind tunnel are:

- The testing chamber has a cross section of 0.8 x 0.8 m^2 measurements and a length of 1.6 m in the direction of the flow.
- It was designed to generate air flow velocities from an average of 0.5 ms^{-1} to 5.0 ms^{-1} and index of turbulence $Tu = \sqrt{\overline{u}^2}\,/U$ between 1% and 20%.
- Temperature and humidity (characterized by the dew point) regulated to ±0.1°C (air temperatures and dewpoint are homogeneous to 0.1°C within the area of experimental specimen).

The wind tunnel is shown schematically in Figure II-1, which is a closed loop of 12 m long and 4 m high. The flow is initially made as laminar as possible and to get a very weak turbulence intensity in the order of 1% in the test chamber (1), the diffusers (2, 6, 8 and 10) and elbows (4 and 7) were designed to bring the air of the ventilator (5) to the damping screen (11) without generation of turbulence due to separations on the walls of ducts. The fine mesh

grid located in the damping chamber dissipates turbulence by viscous effects. The contraction area (12) makes the flow more uniform at the entrance of the experimental chamber through a contraction ratio of 9.

Two drawers (12, 14) located respectively upstream and downstream of the contraction area may optionally be used as generators of turbulence by adding or removing extra perforated plates, perpendicular to the direction of the flow. The use of two drawers at different distances from the experimental test chamber strongly increases the possibility of obtaining flows whose index of turbulence is uniform around the experimental specimen.

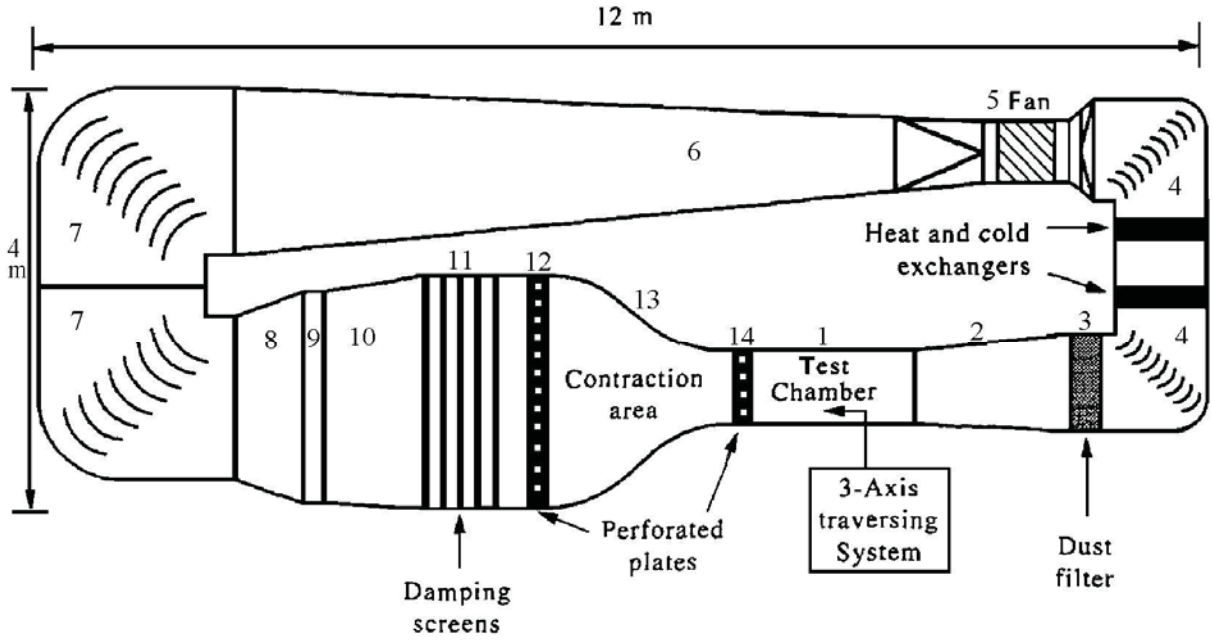

Fig. II-1: Schematic of Wind tunnel

Two devices of air-conditioning assistant are associated with the wind tunnel installation to ensure the temperature and humidity control. The measurement of the dew point is carried out using a cooled mirror hygrometer with a precision of ± 0.1°C (Dew 10 of National Instrument). The wind tunnel is a closed loop, sealed, strongly isolated and the devices of conditioning are located upstream of the ventilator.

The hydrodynamic homogeneity of the experimental test chamber was validated by velocity measurements taken in many points of this chamber, these measurements showed

that the mean velocities differ by less than 5% within the total volume, the intensity of turbulence varies by less than 3% in the area, where we should place our prototype of condensation, for mean velocities located in our speed range. Previous measurements showed a very good uniformity in temperature and humidity in the test area, the variations were lower than ±0.1°C for the temperature of the air and the dew point, even for a nearly laminar flow (Kondjoyan 1995).

2.2.2 Measurement of wind velocity

The characterization of the flow, mean flow velocity and fluctuations, was carried out by hot wire anemometry. Single-wire anemometers (one component) with constant temperature (and therefore constant resistance) were selected. The velocity variations in the incidental flow induce variations of voltage across the terminals of the wire, which are directly proportional to the variation of the value of the current. The hot wires are normally 5 µm in diameter and 1.25 mm long suspended between two needle-shaped prongs. The sensor possesses a large flow sensitivity and a wide frequency response in turbulent flow. Miniature wire probes with offset prongs and with the sensor perpendicular to probe axis (DANTEC 55P15) were selected because they are designed to take measurements within the boundary layer, the sensor is placed perpendicular to the axis of the probe. This shape of prongs allows measurements close to a solid wall without disturbance from the body of the probe, which remains beyond the boundary layer.

Fig.II-2: Hot wire sensor probe (DANTEC 55P15)

The wind tunnel is equipped with a three-axis traversing system that enables the displacement of the hot wire probe in an area of chosen dimension and location with a selected displacement in the order of about 0.01 mm.

A telescope (magnification ×24) placed at a distance (about 3 m) was used to locate the point remotely, made possible to set its position with precision (± 0.05 mm) closed to the wall of the plate in order to avoid any contact with the probe. See figure II-2.

The sample frequency was chosen between 0.5 kHz and 2 kHz. The hot wires available were calibrated with room temperature for velocity measurements averaged ranging between 0.5 ms^{-1} to 4.5 ms^{-1} with an accuracy of 1-3%. Below 0.4 ms^{-1} hot wire measurements lack accuracy because of thermal exchange (Kondjoyan 1995). The data acquisition for the localization of the hot wire probe and the average velocity fluctuations was ensured using a computer connected to the system.

The single wire probes were calibrated using King's law (King, 1914), which is frequently used for calibrating hot-wire anemometry written as

$$E^2 = A + B\,u^n \qquad \text{(II-1)}$$

where A, B and n are parameters to be determined through the fitting process. Traditionally A and B were obtained fitting a straight line to E^2 and u^n data, and here n was chosen as n =0.45. For calculating two coefficients, measurements were performed with standard TSI sensor on more than fifteen points distributed between 0.2 and 4.5 ms^{-1}. A least square fit was performed on this data set with a generalized form of king's law, and then the coefficients of calibration were used to convert the instantaneous voltages into instantaneous velocity components. The above equation is easily inverted analytically, giving

$$u = \sqrt[0.45]{\frac{E^2 - A}{B}} \qquad \text{(II-2)}$$

Fig.II-3: A view of the test chamber with telescope

2.3 Condensation unit

2.3.1 Global system

The whole system of cooling a square flat plate was controlled by a thermoelectric cooler and a temperature regulator with several assisted components is shown in Figure II-5. The temperature of the active surface is controlled by a Peltier element and a thermistor, which is itself inserted inside the aluminium flat plate (middle) for the regulation of the input current of the Peltier element adapted by the controller.

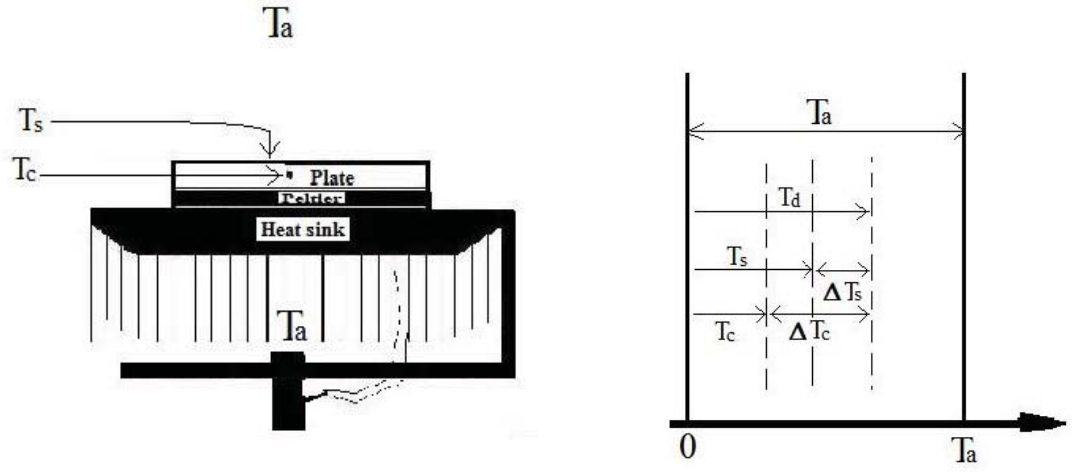

Fig.II-4: Representation of different temperature levels on the active condensing unit.

A square aluminium flat plate (2) was glued on a Peltier module (3) of the same size, with a thermal paste. The other side of the Peltier module was pasted on a heat sink (4). This heat sink made up of single-piece extruded aluminium had a strong density of wings aligned with the direction of the flow to reinforce the convective exchange (Figure III-5(b)). To increase the effectiveness of the Peltier module, the use of a heat sink on the hot side of the Peltier element is an important parameter. The objective is to dissipate the heat flux produced on the "hot" side by the Peltier element in order to maintain this side at a temperature as close as the ambient temperature $T_{a,}$ which can thus be used as a reference temperature. The value of the electric current in a Peltier module theoretically makes it possible to create an

absorption of heat on one side ("cold") and an equivalent heat emission on the opposite side ("hot"). Keeping this surface at room temperature, which is the reference temperature, makes it possible to create the necessary temperature difference with the dew point T_d in order to induce the desired rate of condensation on the cold surface temperature T_s. Indeed, the rate of condensation is directly related to this difference in temperature $\Delta T_s = T_d - T_s$.

In order to control this rate of condensation, we need, on the one hand, to maintain this temperature contrast constant $\Delta T_s = T_d - T_s$ throughout the experiment. For this purpose, a thermistor of small size (1) is inserted in the plate to measure the temperature in its centre under the plate/air interface; it is connected to the temperature regulation controller (7), which adjusts the electric current transmitted to the Peltier module to maintain T_s constant. In addition, to obtain a uniform mass flux on the whole surface for a precise measurement of this mass flux, we must maintain the temperature of the active surface (plate/air) as isothermal as possible. Aluminium plates (strong thermal conductivity) of thickness 1 mm, 2 mm and 3 mm were studied. The thickness of the aluminium plates should make possible the homogenization of the heterogeneous thermal distribution that is produced at the ceramic Peltier module (variations of several degree Celsius for a 5 x 5 cm^2 plate) at the cold surface side.

A programmable temperature regulation controller (LFI-3751 of Wavelength Electronics) for the Peltier module was chosen for its stability over time and accuracy (± 0.1°C). In addition, it can be possible to add an auxiliary thermocouple (as for the control of temperature on the upper surface).

The main goal of this experimental arrangement is to evaluate the local mass transfer coefficients. Thus, we must study active surfaces of small sizes in order to obtain a sufficiently uniform temperature at the active interface, but which sizes are however sufficiently large to condense a quantity of water that can be weighted with sufficient precision.

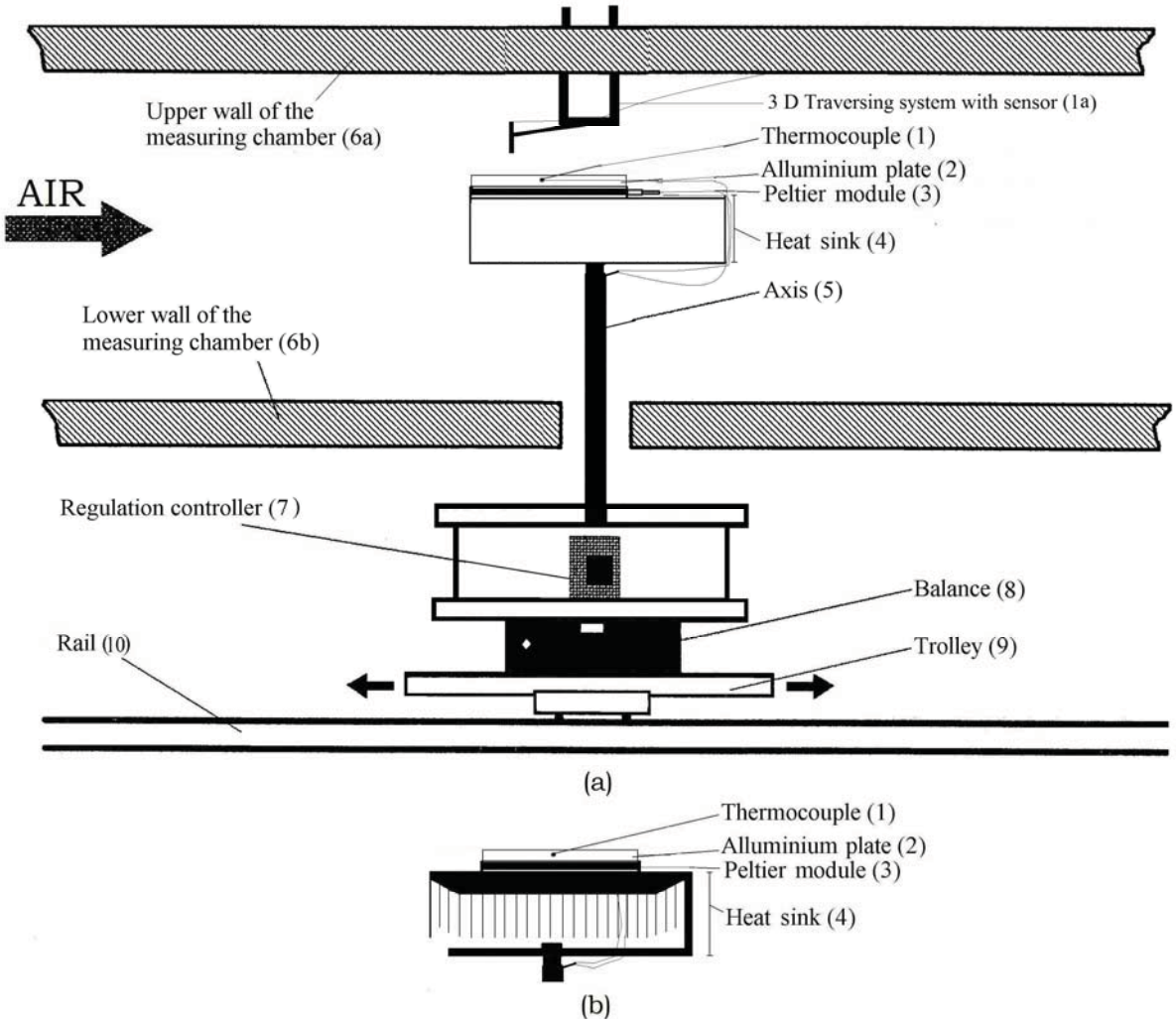

Fig.II-5: Schematic of the whole condensation unit: (a) front view, (b) side view of the upper part, which faces the airflow

2.3.2 Plate size and thickness

For the condensation of humid air on an active surface, aluminium metal was chosen to make the flat square plates for its good thermal conductivity. To maintain the thermal homogeneity of the active surface, the two parameters that were studied are the plate size and its thickness. Indeed, the external surface would be even more thermally homogeneous if its size were small, but the mass flow induced by the condensation of humid air would also be small, and therefore more difficult to measure the condensate mass on a balance. Moreover, the thickness of the plate was designed to reduce the thermal in-homogeneity that appears on each side: due to the various condensation nucleation sites at the upper side and especially at the underside which is in contact with the ceramic thermoelectric module. Such an element is by design an assembly of a large number of thermocouples connected in series and kept sandwiched between two ceramic plates (Fig. II-6); it generates a substantial geometrical inhomogeneity of the flow of cold produced. However, thick plates have a large thermal

inertia, which will impact directly the response time and thus the temporal control of the temperature of the interface plate / air.

Plates measuring 30 x 30 mm^2, 40 x 40 mm^2 and 50 x 50 mm^2 were considered for the 3 mm thickness. Three different thicknesses of 1, 2 and 3 mm have been considered for the plates of sizes 40 x 40 mm^2 and 50 x 50 mm^2. The details of these temperature distribution experiments will be discussed in the chapter III.

2.3.3 Thermoelectric cooler – Peltier element

2.3.3.1 Basic principle

A thermoelectric cooler uses the principle of 'Peltier Effect' to create a heat pump between the junctions of the two different types of materials. Basically, the Peltier effect is the inverse of the Seebeck effect. The Seebeck effect was discovered (Seebeck 1823) by Estonian-German Scientist Thomas Johann Seebeck: dissimilar metals, which are connected at two different locations (junctions), will develop a micro-voltage if the two junctions are held at different temperatures. This effect is the basis for thermocouple thermometers. A French physicist, Jean Charles Athanase Peltier discovered (Peltier 1834) the inverse of it and found that if you take a thermocouple and apply a voltage, this causes a temperature difference between the junctions, known as 'Peltier Effect'. In 1838 Lenz showed that depending on the direction of current flow, heat could be either removed from a junction to freeze water into ice, or by reversing the current, heat can be generated to melt ice, this results in a small heat pump also known as a 'thermoelectric cooler' (TEC). Altenkirch (1909, 1911) pointed out that thermoelectric cooling material needed to have high Seebeck coefficients, good electrical conductivity to minimize Joule heating, and low thermal conductivity to reduce heat transfer from junctions to junctions. Goldsmid and Douglas (1954) demonstrated that cooling from ordinary ambient temperatures down to below 0°C was possible.

The amount of heat released or absorbed at the conductors' junctions is proportional to the current that passes through the heterogeneous conductors. The proportionality constant (π) is known as the Peltier coefficient. The basic TEC unit is a thermocouple, which consists of p-type and n-type semiconductor elements, or pellets, which are traditionally made of Bismuth Telluride (Bi_2Te_3)-based alloy and normally copper commutation tabs are used to interconnect these pellets. Thus, a typical TEC consists of thermocouples connected electrically in series and sandwiched between two Alumina ceramic plates.

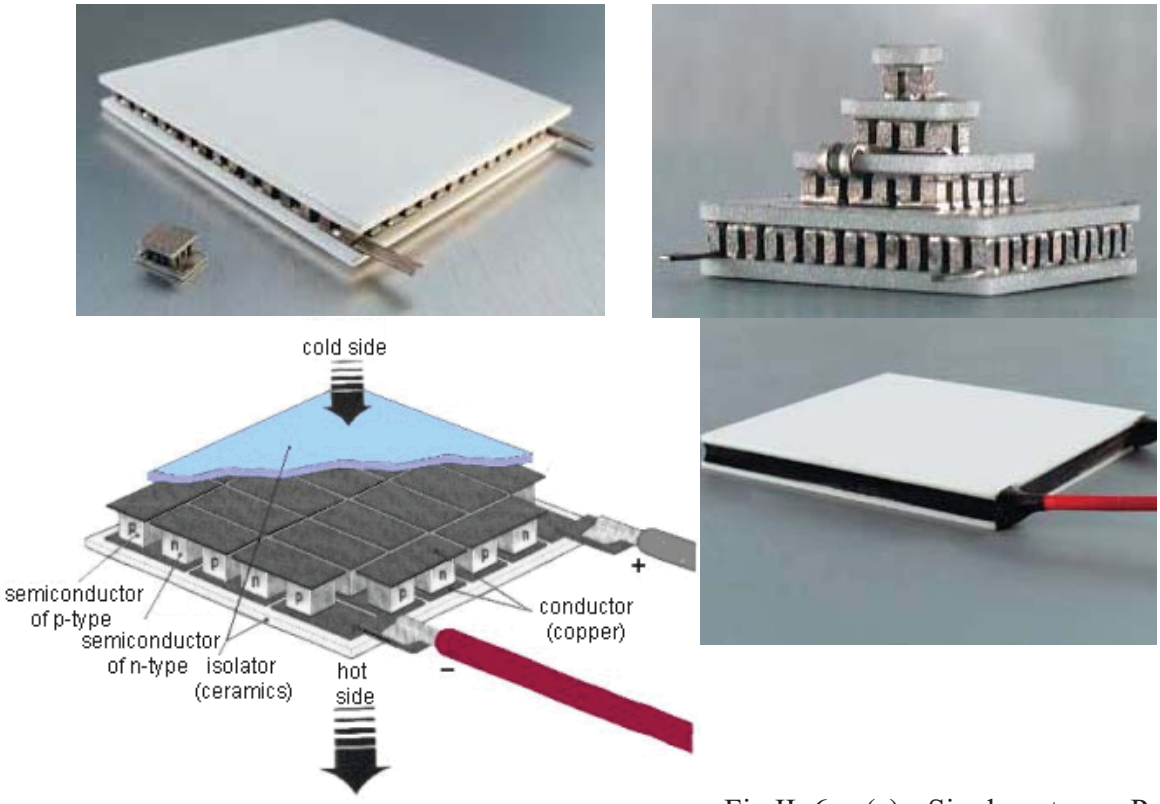

Fig.II–6: (a) Single stage Peltier element with a basis of thermocouple (b) A typical four stage Peltier element (By KRYOTHERM) (c) Schematic representation (d) Peltier element with sealant.

The number of thermocouples may vary from several elements to hundreds of units; it is related to the desirable cooling capacity ranging from fractions of Watts to hundreds of Watts. When a constant electric current passes through the thermoelectric module a temperature difference is generated between its sides. If efficient heat withdrawal is provided for on TEC hot side, for example, by heat sink, the temperature obtained on its cold side can be by tens of degrees below the ambient temperature. The rate of cooling will be proportional to the amount of current, but it has a limiting factor to create a lowest achievable temperature at cold side. A single-stage thermoelectric cooler permits the generation of temperature differences up to about 70 K; larger temperature differences can be obtained with multistage thermoelectric coolers (Rowe 1995).

2.3.3.2 Modelling of the Peltier effect

If the amount of heat absorbed at the cold end is $\dot{Q}_{12}$, at an interface between two conductors (say 1 and 2), it can be expressed as a linear function of the electric current

$$\dot{Q}_{12} = \pi_{12} I = (\pi_1 - \pi_2) \cdot I \qquad \text{(II-1)}$$

where I is the electric current, through the interface, and π_{12} is the Peltier coefficient (V) of the entire thermocouple and π_1 and π_2 are the Peltier coefficients of the two materials. Heat is generated if $\pi_1 > \pi_2$ and the electric current flows from 1 to 2. If the direction of the electric current is reversed, so is the direction of the heat absorbed. By combining two interfaces, 1 to 2 and 2 to 1, a hot and a cold junction can be created. In this case, heat is generated at one of the interfaces and the same amount is absorbed at the other.

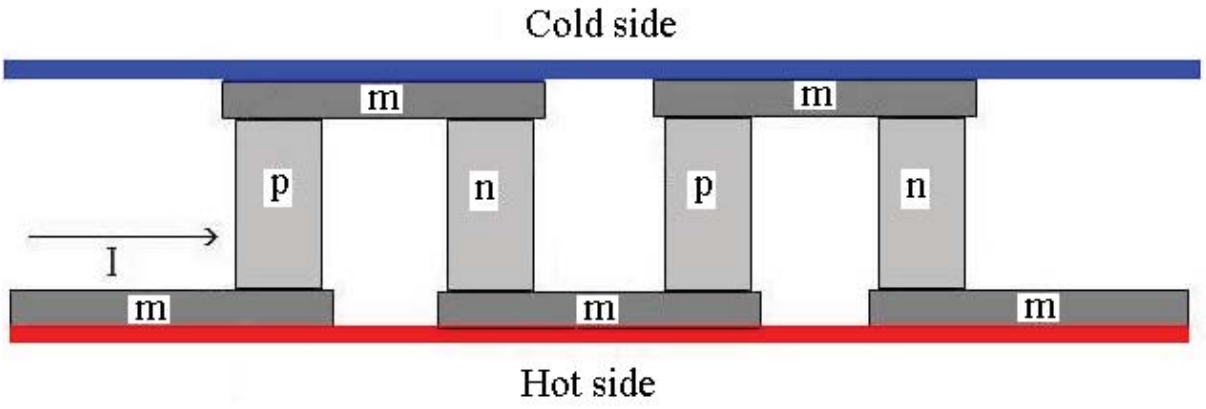

Fig. II–7: Sketch of a Peltier element.

Three different materials are commonly used in Peltier elements (a p-doped semiconductor (p), a metal (m) and an n-doped semiconductor (n)). The Peltier coefficients of the three materials are different, $\pi_n > \pi_m > \pi_p$. If the materials are arranged according to fig. II-6, a hot and a cold side are created, using several interfaces between the materials (and thus maximizing the cooling) with simple series electric connections. The arrangement functions due to the fact that (for the materials given in this example) heat is generated at junctions of the type m to p and n to m and absorbed at junctions' m to n and p to m.

Even though the Peltier cooling increases linearly with the electric current through the element, the cooling ability of a Peltier element is limited by several factors. As the electric current increases, so does the resistive heating of the entire element (Joule effect). At some point, the resistive heating caused by an increasing electric current will be larger than the cooling caused by the Peltier effect. For each pair of hot/cold interfaces (eg. metal-semiconductor-metal), the cooling, *P (W)*, (eg. the flow of thermal energy from the cold to the hot side) is related to the Peltier coefficients of the two materials, π_1 and π_2 (where it is assumed that $\pi_1 > \pi_2$), the electric resistivity of the element, R (ohm m), the electric current, I

(A), the thermal conductivity of the element, *k* (W/m K), and the temperature difference between the sides of the element, *ΔT*, according to eq. (II-2).

$$P = (\pi_1 - \pi_2) \cdot I - \frac{R \cdot I^2}{2} - k\Delta T \qquad \text{(II-2)}$$

From the above equation, the Peltier cooling (1st term) depends linearly on the electric current, whereas the resistive heating (2nd term) is related to the square of the electric current. The third term describes the conduction of heat through the Peltier element and relates to the temperature difference between the cold and hot sides, *ΔT*. The relationship between *ΔT* and the electric current is unknown. At low electric currents, the Peltier cooling is the dominating term, but as the electric current increases, the resistive heating will increase faster than the Peltier cooling. At a certain value of the electric current, the resistive heating will be larger than the Peltier cooling, and any further increase in electric current will actually decrease the generated cooling.

For an element consisting of n_{mp} pairs of interfaces between metal and p-doped semiconductor, and n_{mn} pairs of interfaces between metal and n-doped semiconductor, the total cooling power would be

$$P_{total} = n_{mp} \cdot (\pi_m - \pi_p) \cdot I + n_{mn} \cdot (\pi_n - \pi_m) \cdot I - \frac{R \cdot I^2}{2} - k \cdot \Delta T \qquad \text{(II-3)}$$

In eq. (II-3), the Peltier element is considered as a single unit regarding the heat conduction and resistive heating. The resistance, R, in the equation describes the total electric resistance of the Peltier element. It is worth noting that the current is the same through each of the interfaces as through the entire element (since they are connected in series). For practical purposes, it would also be possible to assign a total Peltier coefficient to the entire element, thus incorrectly regarding it as a single pair of material interfaces. In this case, eq. (II-2) can be used, with the total Peltier coefficient replacing the term (π_1-π_2):

$$P_{total} = \pi_{total} \cdot I - \frac{R \cdot I^2}{2} - k \cdot \Delta T \qquad \text{(II-4)}$$

The analysis of the basic one-dimensional thermal balance equations for the thermoelectric coolers has been discussed in the literature (Phelan et al. 2002, Bierchenk and Gilly 2006, Hasan and Toh 2007, Rowe 1995, Zhang et al. 2010) and they have included the effect of geometrical factors, when the effect of temperature on the thermoelectric properties,

the effects of ceramic plates, and joining copper traces and electrical contact resistances, are assumed to be small, then the equation for the cooling power absorbed at the cold side of the Peltier element is expressed by:

$$P_c = 2N\left(\alpha I T_c - \frac{I^2 R}{2F} - kF\Delta T\right) \qquad \text{(II-5)}$$

where N represents the number of TEC thermocouples, α the Seebeck coefficient (V/K), T_c the temperature at cold side, and F is the geometry factor (defined by the ratio of area over length (m)) (Zhang 2010). The electrically driven TEC power:

$$P_{te} = 2N\left(\alpha I\Delta T + \frac{I^2 R}{2F}\right) \qquad \text{(II-6)}$$

Now the total heat generated at the hot side of the TEC:

$$P_{Total} = P_c + P_{te} = 2N\left(\alpha I T_h + \frac{I^2 R}{2F} - kF\Delta T\right) \qquad \text{(II-7)}$$

2.3.3.3 Specifications of used Peltier modules

The Peltier modules used in this study were manufactured by Kryotherm (Russia) and Quickcool (Germany). The different parameters are given below.

Table II -1: Technical parameters of single stage thermoelectric coolers

	I_{max} A	**Q_{max} W**	**U_{max} V**	**ΔT_{max} (K)**	**R_{ac} Ohm**	**Dimension mm^2**	**Thickness mm**
Snow Ball – 71-S	3.6	36	16.1	71	3.2	30 x 30	3.6
ICE-71 HT(120) E L3	8	80	16.1	71	1.5	40 x 40	3.4
TB-127-2.0-2.5	7.6	76.0	16.3	72	1.65	48 x 48	4.8
QC-127-2.0-15.0	15	110	15.5	71		50 x 50	3.6

The parameters in Table II-1 are:

ΔT_{max} = Maximum achievable temperature difference between the hot and cold sides of a thermoelectric cooler

I_{max} = Input current through a thermoelectric cooler resulting in the greatest ΔT (ΔT_{max})

U_{max} = Voltage on a thermoelectric cooler contacts at ΔT_{max}

Q_{max} = Maximum cooling capacity of a thermoelectric cooler. It is determined at maximum current through a thermoelectric cooler and at zero temperature difference between hot and cold sides

$\mathbf{R_{ac}}$ = Electric resistance of a thermoelectric cooler measured with an alternating current of 1 kHz frequency.

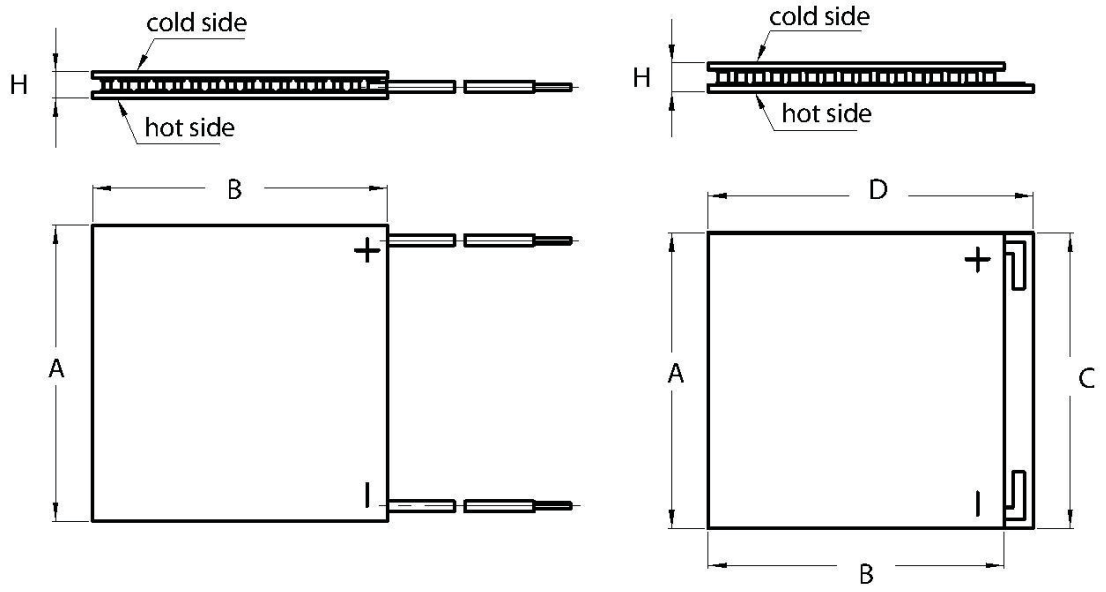

Fig.II-8: Sketch of the dimensions of Peltier element.

Table II -2: Details of Peltier modules used in this experiment

Peltier element	supplier	no of thermocouples	(A x B x H mm^3)
1. QC-127-2.0-15.0	Quickcool (Germany)	127	50 x 50 x 3.6
2. TB-127-2.0-2.5	Kryotherm (Russia)	127	48 x 48 x 4.8
3. ICE-71	Kryotherm (Russia)	71	40 x 40 x 3.4
4. Snowball – 71	Kryotherm (Russia)	71	30 x 30 x 3.6

Advantages of using a Peltier module as cooling device:

- A thermoelectric cooler module has no moving parts, therefore, it needs virtually no maintenance.
- Its life testing indicates the capability of modules to exceed more than hundred thousand hours of steady-state operation according to the producer.
- It is a very compact instrument for cooling and heating.
- Accurate temperature control within fractions of degree can be obtained with appropriate circuitry.
- It has a very fast response time, within a few minutes you can even produce ice.
- Thermoelectric coolers are not orientation or position dependent.
- Heat pumping in the system is fully reversible. A cooler can be a heater with no physical movement of the whole device or any part of it.

But despite all the above mentioned advantages, Peltier modules have some specific features, which must be taken into account when using them as a part of a cooling unit.

Difficulties to overcome for using efficiently a Peltier module as cooling device:

- The modules, dissipating much heat, require the use of fans and heat sinks, to carry off efficiently the heat generated at the hot side.
- The thermoelectric modules have a quite low performance factor.
- The usage of these modules might cause overheating of the other components inside the system block, without proper ventilation facility.
- And at the same time on the cool side low temperatures might cause moisture condensation inside the Peltier element, which might lead to short circuits between the elements.

To prevent the condensation inside the Peltier elements different sealants were tested. Here, in these experiments Peltier modules were sealed with Silicon and Epoxy; Silicon for Snowball-71 S and TB-127-2.0-2.5, and Epoxy for ICE-71.

2.3.4 Weighing of condensate

The condensation unit is placed horizontally (active horizontal plate) at the centre of the test chamber (Fig.II-3). It is maintained in the measuring chamber by a shaft (5) fixed itself at the balance pan (8), located under the test chamber. There are two horizontal parallel plates connected by four screws and placed on the balance, in between these two plates the temperature regulation controller (7) is placed. The wire of the Peltier module and the thermistor inserted in the active plate (1) walk along the axis and are connected to the temperature controller. The balance is put on a mobile platform, a chariot (9) which makes it possible to slide the whole system on a rail (10) parallel to the direction of the flow. This device allows a continuous signal acquisition recorded by a precision balance (Mettler 30, precision of ±0.1 g), for monitoring the increase in mass as the humid air will condense on the active surface. A ring made of sponge was added around the upper part of the sealant of the Peltier module in order to collect the drops that were produced on the vertical side of the plate. Otherwise the drops would flow down by gravity and eventually fall on the heat sink or lower surface of the tunnel and then evaporate as the heat sink is warmer. As a result part of the produced mass would disappear. For measurements with a vertical plate (the incident air flow will be parallel or perpendicular to the active surface), a system of condensate recovery will have to be added with the device because of the effect of streaming or runoff.

2.4 Calibration of temperature sensors

Calibration is the process of standardizing a temperature monitoring instrument to ensure that it will measure within a specific temperature range in which the instrument is designed to operate. Accuracy of a thermometer is its ability to measure temperature correctly without error. Three types of sensors were used in our experiments, thermistors, thermocouples, and PT100 RTD sensors.

2.4.1 Resistance temperature detector (RTD)

A resistance temperature detector is a thin platinum wire wrapped around a glass or ceramic rod. Platinum wire coils can also be imbedded in a ceramic matrix. A protective coating of glass or ceramic completely houses the detector. The accuracy of temperature readings for a RTD is very good. The RTD device is stable and accurate, however it is fragile and not easy to calibrate. Surface temperature sensors (PT100 SURFASIQUE, class B – NFC 4Z330) were tested but did not give good estimates because of forced convection. For these experiments, all sensors were calibrated in ice and boiling water and for a range of room temperature (5 ºC – 25 ºC) in a water bath. The sensors were plunged in a can of metallic powder held in the water bath. Basically, during calibration these sensors were close enough (approx. 0.5-1.0 °C) for measuring the temperature.

2.4.2 Thermistor Thermometer

Thermistor is a generic term for “thermally sensitive resistors”. The key word in this phrase is sensitive. Thermistor thermometers are the most sensitive temperature measuring devices, able to detect small changes in temperature. Transitional metal oxides are semi-conductive materials used in thermistors. Manganese and nickel, or manganese, nickel and cobalt are the most common component metals. Thermistors can be used over a wide range of temperatures without affecting accuracy. Thermistors are fragile and can lose calibration at extremely high temperatures.

2.4.3 Thermocouples

A level converter for Voltcraft thermocouple thermometers has been used for thermocouple sensor.

Fig.II-9: Photographs of thermocouple adaptor

The thermistor was put below the aluminium flat plate surface with thermal paste for good contact and attached to the controller, which gives the online display of the sensor. PT100 and thermocouples were used to characterize the surface temperature of the plate and Peltier element.

2.5 Conclusion

The use of a Peltier element to produce a homogeneous surface temperature for the condensation of humid air on a small size plate proved to be efficient. The efficiency of a Peltier element is not very good nowadays; its solid state nature, effectiveness and reliability which are also not affected by the orientation of the Peltier element makes it very useful for our application. The measurement by different kinds of sensors and their relative accuracy sometimes are different lead us to select the most appropriate ones. But after the calibration of these sensors in different environments, similar values were obtained. The availability of a wind tunnel experimental facility for low air velocities that was also regulated in temperature and humidity is needed to evaluate accurately the mass transfer coefficients around small obstacles with precise measurements of the velocity profiles and turbulence intensity around the obstruction. This global experimental set-up will be very helpful for the development of theoretical models. The calibrations of constant temperature anemometers inside the wind tunnel gave their characteristics of measurement, and were used for further experiments.

Chapter III

Design of the condensation plate and thermal profile of the active surface

3.1 Introduction

The knowledge of the temperature distribution on the upper and lower surface of the Peltier element is one of the important factors in this experiment. To obtain a thermally homogeneous surface on the active side of the plate, we have used an arrangement composed of a Peltier element, a heat sink to dissipate the heat from the hot side of the Peltier, a same size metal plate on the cold side and a temperature controller, which regulates the Peltier element by supplying a proper current to maintain a fixed temperature on the cold surface (active). These are very small size square flat plates of surface area 9, 16 and 25 cm^2. The size should be small enough for the active surface to be thermally homogeneous, and large enough for the amount of condensate to be measured accurately (Fontaine and Tiwari 2010).

3.2 Plate size and thickness

For the condensation of humid air on the surface, aluminium metal has been chosen to make a flat square plate with a high thermal conductivity. The goal was to induce condensation on an active surface, which is thermally homogeneous and to measure local mass transfer coefficient. The two parameters that were studied are the plate size and its thickness to keep it as homogeneous as possible. Indeed, the external surface will be even more thermally homogeneous if its size is small, but the mass flow induced by condensation of humid air will not be enough, therefore it will be more difficult to measure the mass on a balance. Moreover, the thickness of the plate has been designed to reduce the thermal inhomogeneity that appears on the ceramic side of the Peltier module. At the upper side, due to the various condensation nucleation sites and especially at below side, which is in contact with ceramic thermoelectric module, which by design (an assembly of a large number of thermocouples connected in series and sandwiched between two ceramic plates, Fig. II-2) generates a substantial inhomogeneity of the flow of cold formed. However, thick plates have a large thermal inertia, which will impact directly the response time and thus, the temporal control of the interface plate surface / air.

Three different thicknesses have been tested 1, 2 and 3 mm. Plates measuring 30 x 30 mm^2, 40 x 40 mm^2 and 50 x 50 mm^2 were considered for the 3 mm thickness. The outcome of the temperature distribution experiments to verify the homogeneity of the plate surface is given in Table III-1, which summarizes the various trends observed over many trials. The

distribution of temperature on the upper surface (solid / air) is quantified by measuring the difference between the maximum temperature (at the corners) and minimum temperature (at the centre of the square plate) i.e. $\Delta T_{in} = T_{max}$ (plate corner) – T_{min} (plate centre) (given as Temp difference in the Table III-1) as the plate is cooled down by the Peltier element. The temperature measurement was carried by a classical type of thermocouple. To measure the temperature profile on the surface of the plate, the surface was divided into meshes comprising of 49, 25 and 17 points, on the plate of 50 x 50 mm^2, 40 x 40 mm^2 and 30 x 30 mm^2, respectively as given in Fig. III-1. During the first phase the in-homogeneity of the surface of the plate was studied under permanent regimes i.e. a fixed amount of voltage was imposed on the Peltier module and the temperature distribution measurements were made after stabilization. In the second phase most of the experiments were carried out after connecting a controller to the Peltier. A thermistor had been inserted inside the plate at the centre just below the upper interface, to regulate the current in order to keep the air/plate surface temperature constant.

3.3 Temperature distribution on the surface of the plate and Peltier

The temperature distribution experiments have been performed on the surface of the aluminium plate with a Peltier element glued underneath, and also on the surface of the Peltier element directly. These experiments were carried out for the three different thicknesses of 1, 2, and 3 mm with surface area of 900 mm^2, 1600 mm^2, 2500 mm^2 to know the temperature homogeneity on the surface of the square metal plate. At the beginning, a plate of 50 x 50 mm^2 was glued on the Peltier element of size 40 x 40 mm^2. The temperature was measured every 0.5 mm to 1.0 mm distance. Similar measurements were repeated without the plate (on Peltier element surface directly). Then the 50 x 50 mm^2 square plate was replaced by a square plate of similar size as the Peltier element. Two types of temperature distribution experiments have been carried out:

1. Fixed values of current and voltage were supplied to the Peltier element by 12 Volts power supply, which brought the square metal plate to a certain value of temperature, then the temperature was measured on the surface of the flat plate every 0.5 mm to 1.0 mm distance at different points as given in the sketch of Fig. III-1. Finally the surface temperature profiles rely on 17 to 49 measurement points depending on the size of the plate.

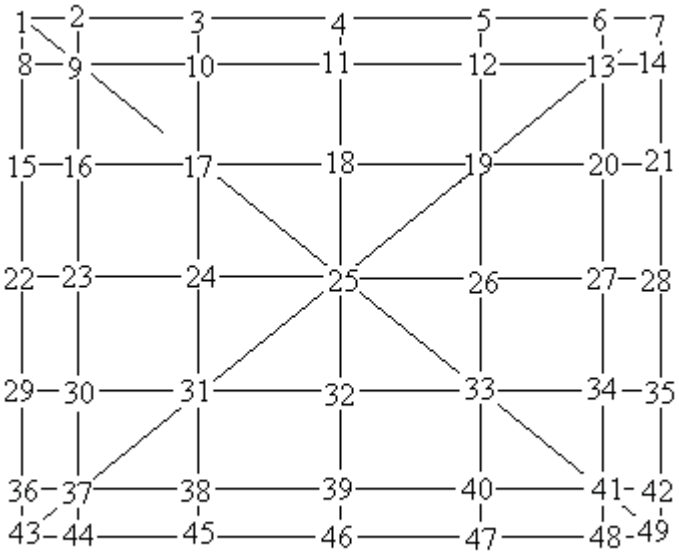

50 x 50 mm^2 Plate

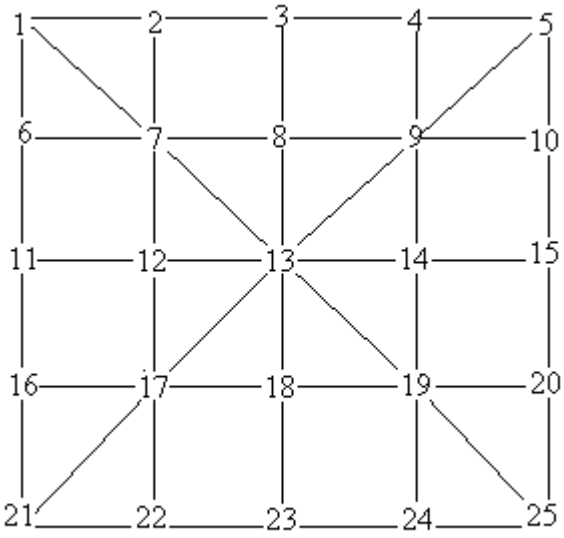

40 x 40 mm^2 Plate

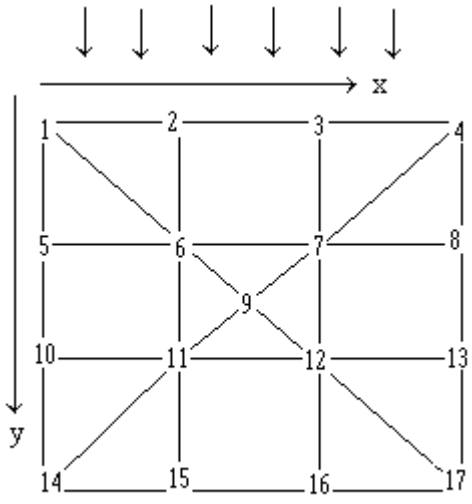

30 x 30 mm^2 Plate

Fig.III-1. Sketch of the plates with points, where surface temperature has been measured

2. A fixed value of temperature was set on the controller and then measured at 5 points on the surface: at the centre of the square plate and at the middle of each four sides, for a whole range of available temperature values below the ambient temperature till a few degrees below the dewpoint temperature. Basically, this experiment gave us the value of temperature difference set on the controller and actually measured on the surface of the plate at different surface temperatures, which is not a constant value for all surface temperatures, and also gives the temperature difference between the centre and the sides of the plate.

3.3.1 Peltier element 50 x 50 mm^2

The plates of thickness at 1 mm, 2 mm and 3 mm have been used for this size of Peltier element as well as only Peltier element without plate for the profile of temperature distribution on the surface of the Peltier.

3.3.2 Peltier element 40 x 40 mm^2

This size of the Peltier element has been used with plates of sizes 50 x 50 mm^2 and 40 x 40 mm^2. The aluminium plate of 50 x 50 mm^2 size with the thickness at 1, 2, and 3 mm, and one steel plate of thickness 1 mm have been used. The remaining experiments of this Peltier size were performed with a same size, 3 mm thick plate

3.3.3 Peltier element 30 x 30 mm^2

This was the smallest Peltier element size used in this work, and has been tested without plate and with a 3 mm thick aluminium plate. Also, copper and aluminium heat sinks were utilized to study the effect of wind velocity flowing around the heat sink (fins), in order to remove hot air transfer to forced ambient flow.

The Table III-1 represents the following parameters (according to column number):

1. Dimension of Peltier module (in bold) and dimension of the plate (in italics)
2. Thickness of the plate
3. Temperature difference $\Delta T_{in} = T_{max}$ (plate) - T_{min} (plate)
4. Range of variation of surface temperature (interface plate / air)
5. Dewpoint temperature T_d

Table III - 1: Temperature distribution table (The key parameters of main experiments carried out.)

Peltier Element and Plate size	Plate Thickness	Temp Difference (°C)	Temp Range (°C)	Dew Point (°C)	diff from min (°C)	Plate Metal	Heat Sink	Temp ambient (°C)	Remarks	Exp no,	Date performed	Experimented with	Data Acquisition time (h-min)
1	2	3	4	5	6	7	8	9	10	11	12	13	14
50 x 50 Peltier	OnlyPeltier	3,2	13,3-16,5	13,7	-0,4		Al	23,6		9	14/05/2009	Power supply	0-54
50 x 50 Plate	1 mm	1,2	17,2-18,4	15,7	+1,5	Al	Al	25,7	little condensate	14	13/07/2009	Power supply	1-25
		1,8	9,8-11,6	9,1	+0,1	Al	Al	26,2	Dry	12	25/05/2009	Power supply	0-58
		2,4	11,9-14,3	8,4	+3,5	Al	Al	25,8	Dry	13	08/07/2009	Power supply	0-32
	2 mm	0,8	18,3-19,1	16,3	+2,0	Al	Al	27,9	very small drops appear	16	13/07/2009	Power supply	2-55
		1,1	13,2-14,3	11,8	+1,4	Al	Al	22,2	condensate on whole plate	10	14/05/2009	Power supply	5-23
	3 mm	0,7	17,4-18,1	15,5	+1,9	Al	Al	25,9	very small drops appear	15	13/07/2009	Power supply	0-30
		1,0	10,6-11,6	10,5	+0,1	Al	Al	23,2	condensate on whole plate	11	19/05/2009	Power supply	0-49
		1,0	13,9-14,9	5,3	+8,6	Al	Al	22,3	Dry	29	05/11/2009	controller	2-10
		1,4	11,5-12,9	5,9	+6,6	Al	Al	23,4	Dry	30	05/11/2009	controller	0-35
		1,5	13,7-15,2	6,0	+7,7	Al	Al	22,2	Dry	28	04/11/2009	controller	6-41
		1,8	12,5-14,3	9,4	+3,1	Al	Al	23,4	Dry -with different face	27	03/11/2009	controller	0-30
40 x 40 Peltier	OnlyPeltier	3,5	10,9-14,4	5,5	+5,4		Al	25,0	Dry	2	28/04/2009	Power supply	0-47
		3,6	16,9-20,5	14,1	+2,85	Al	Al	24,3	Dry	4b	06/10/2009	controller	0-20
40 x 40 Plate	3 mm	0,6	14,9-15,5	12,8	+2,1	Al	Al	23,8	very small drops appear	**9b**	07/10/2009	controller	1-26
		0,7	17,9-18,6	12,2	+5,7	Al	Al	23,2	Dry	7b	07/10/2009	controller	0-24
		1,5	15,1-16,6	12,4	+2,7	Al	Al	23,6	Dry	**8b**	07/10/2009	controller	0-21
50 x 50 Plate	1 mm	8,0	9,6-17,6	7,6	+2,0	Steel	Al	22,3	Dry	1	27/04/2009	Power supply	1-32
	2 mm	1,5	11,9-13,4	11,1	+1,8	Al	Al	24,3	Dry	4	06/05/2009	Power supply	0-14
		1,8	10,4-12,2	11,2	-0,8	Al	Al	24,8	little condensate	7	07/05/2009	Power supply	0-15
		2,1	7,3-9,4	10,7	-3,4	Al	Al	20,8	with condensate on whole plate	5	07/05/2009	Power supply	1-06
		2,4	9,6-12,0	10,2	-0,6	Al	Al	25,0	small drops on whole plate	8	07/05/2009	Power supply	1-11
		2,8	6,0-8,8	10,9	-4,9	Al	Al	23,7	with condensate on whole plate	6	07/05/2009	Power supply	1-55
	3 mm	1,4	13,0-14,4	6,7	+6,3	Al	Al	23,2	Dry	3	28/04/2009	Power supply	1-17
30 x 30 Peltier	OnlyPeltier	3,1	16,1-19,2	14,7	+1,4		Al	24,1	Dry	5b	06/10/2009	controller	0-20
30 x 30 Plate	3 mm	0,9	18-18,9	15,8	+2,2	Al	Al	25,2	Dry	6b	06/10/2009	controller	0-31
		0,9	13,2-14,1	6,5	+6,7	Al	Cu	23,0	Dry-Finned side faced flow	26	28/10/2009	controller	0-25
		1,2	13,2-14,4	6,4	+6,8	Al	Cu	22,9	Dry-Finned side faced flow	24	28/10/2009	controller	0-25
		1,5	13,0-14,5	6,5	+6,5	Al	Cu	23,2	Dry-Finned side perp. flow	25	28/10/2009	controller	0-25

6. Temperature difference from the minimum temperature of the plate and the dewpoint:
   T_{min} (plate) $-T_d$; condensation possible if T_{min} (plate) $- T_d < 0$
7. Material of the plate
8. Material of the heat sink
9. Ambient temperature T_a
10. Visual observation
11. Reference experimentation
12. Date of execution
13. Mode of input to Peltier element: power supply (constant voltage), controller (variable voltage)
14. Transient time before experimentation including data acquisition time (experimentation time was approx. 15-20 min.)

A brief analysis shows that the inhomogeneity of temperature naturally increases by lowering the temperature of the plate (i.e. by increasing the gap with the ambient temperature). This non uniformity of the surface temperature T_s is closely related to the cooling capacity generated by the thermoelectric module (the module is constituted with many thermocouples, Table II-1). Fig. III-2 shows the evolution of characteristic temperatures when we changed the controller temperature (set by controller); for each measuring point the steady state was reached. Primarily, it was found that the difference between the two surface temperatures (in the centre of the plate and edge of the sides) decreases, more or less continuously from 1°C to 0°C , when the controller temperature (surface temp) moves from 8°C (T_d = 15°C) to 24°C (T_a = 27°C). Secondly, it was noted that when the surface temperature at the centre (measured at the centre point on the surface of the plate) reached a value slightly above or equal to the dewpoint, i.e. a condition where the surface of the plate induces a local condensation process, that the measured surface temperature (both at the centre and the sides) “moved away” from the controller temperature, meaning that the temperature difference seems to be increased.

It could reflect that the surface temperature gets warmer because of the release of latent heat due to condensation, or that accuracy of the measurement is significantly affected by the occurrence of the water drops.

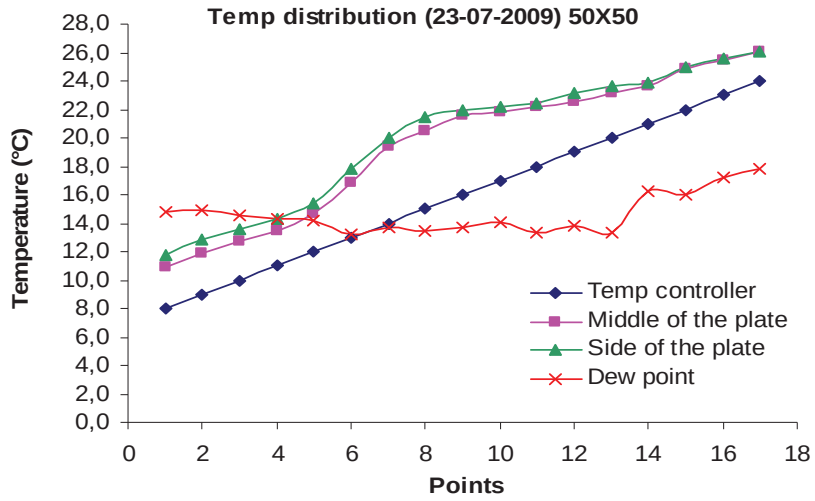

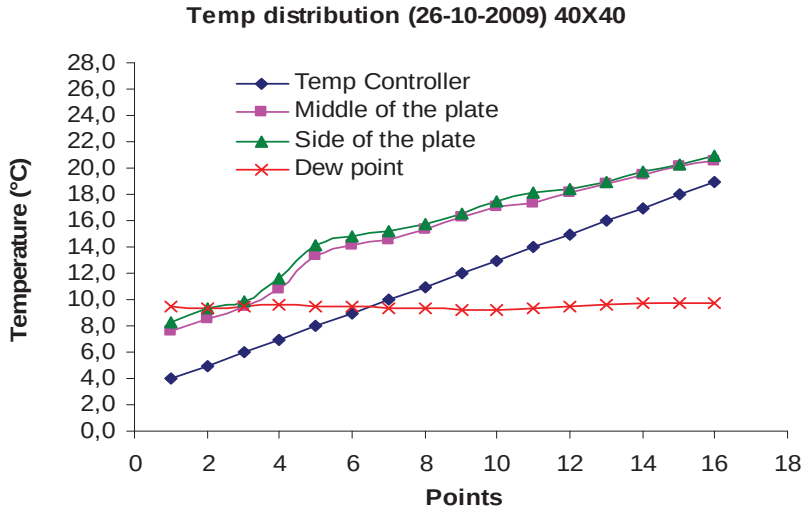

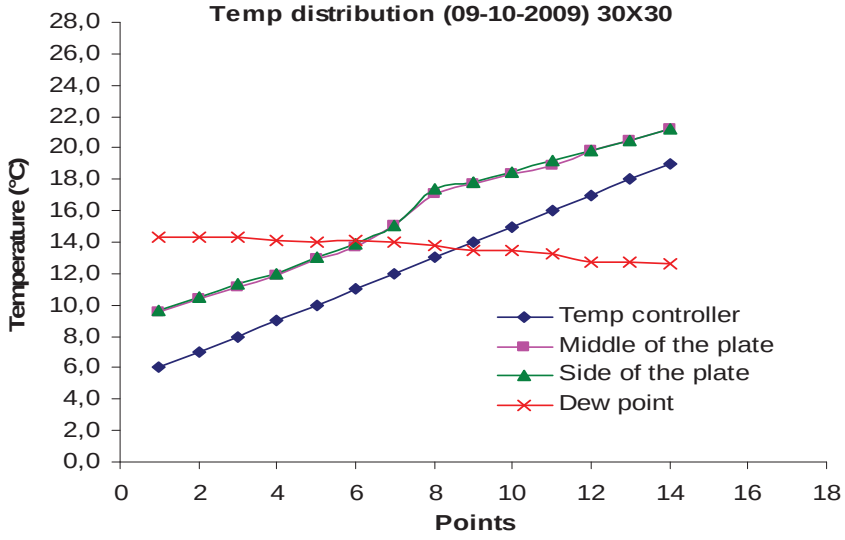

Fig.III–2 (a, b, c): Evolution of surface temperature (centre and edge), dewpoint and temperature given by controller (temp controller) for all size of the plates.

The presence of condensate on the surface of the plate also has an effect of allowing more accurate surface temperature measurements (the layer of air circulating just above the plate has less influence). Fig.III-2 gives the plots of temperature distribution for all three sizes of the plates, it shows a similar type of trend for all surfaces.

3.4 Preparation of metal substrate

The method for preparing the metal substrate was critical: the sample was cut on a large plate, the first sample showed a slight concavity, which was caused by cutting with shear cutting tools. Once the sample was mounted, this concavity induced a thick heat seal between the ceramic plate (top of the Peltier module) and this non-regular metal plate. Various attempts to reduce the concavity of this plate have not been successful because of its small size; especially as any polishing to flatten the surface would have also caused a reduction of local thickness, which in turn would have induced a non uniform thermal mass uniform in thickness below the solid/air interface. The effect of the concavity on the distribution of the surface temperature was very significant. The plates were then machined by milling process. The figure III-3 shows the effect of concavity.

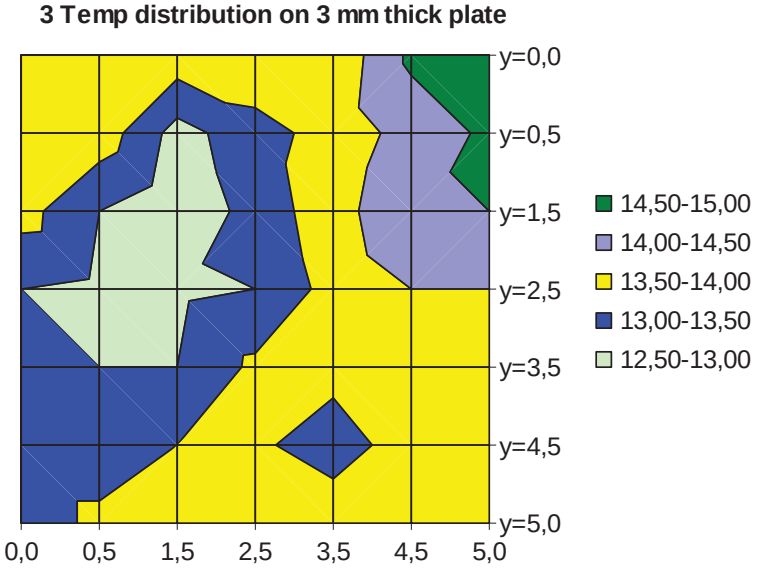

Fig.III-3**:** Temperature distribution experiment with a plate having a slight concavity.

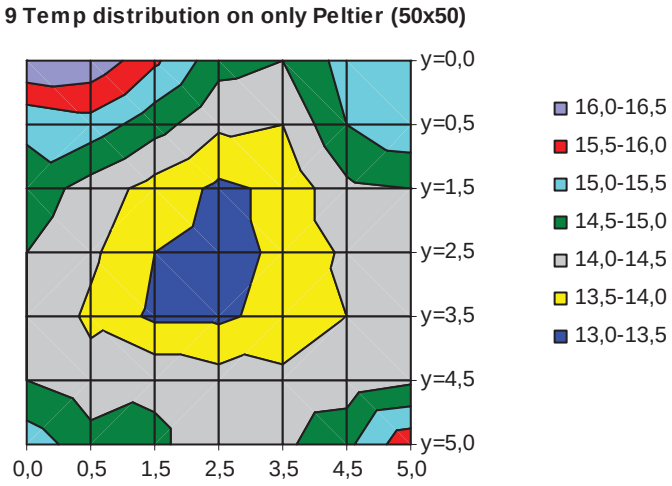

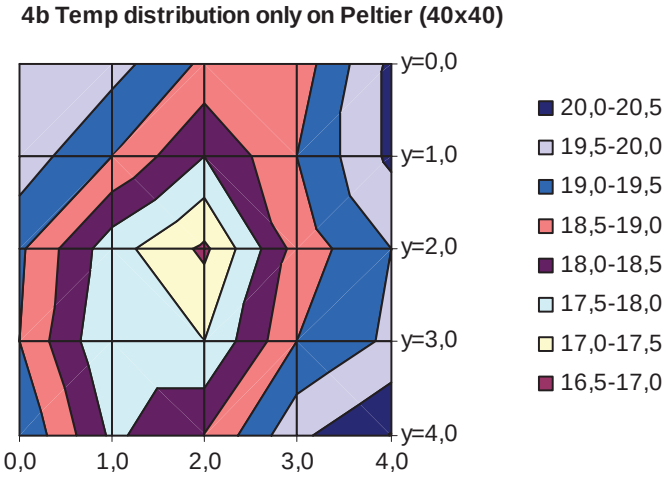

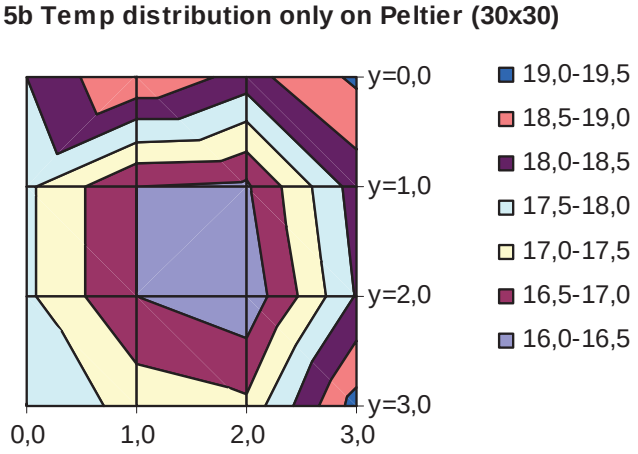

Fig.III-4: Temperature homogeneity plots on the surface of the ceramic plate of Peltier element on the cold side (without metal plate).

3.4.1 Choice of test plate

The trials without a metal plate over the ceramic plate of Peltier element (exp 9, 2, 4b, 5b) show a strong inhomogeneity of the interfacial temperature: the temperature difference ΔT_{in} is greater than 3°C (Fig.III-4). This is because the thermocouples are connected in series and regularly arranged in space, thus an identical electric current leads to a cooling capacity greater at the centre of the module that generates a regular thermal gradient with concentric isotherms which represent a surface profile of conical type. The role of the ceramic plates (both sides of Peltier element) is the mechanical robustness of the set. However, it is very thin and has a very little thermal conductivity that prevents the absorption of such an inhomogeneity.

The influence of the conductive properties of the plate is shown in the Figure III-5 (a, b) by comparing 1 mm thick plates of aluminium (alloy of grade 2017 as rolled condition) and steel, which is less thermally conductive than aluminium. The experiments 1 and 1b conducted under similar conditions (room temperature, dew point, average surface temperature), show a difference in temperature gradients much higher on the steel substrate (8.0 °C temperature difference over the steel plate and 2 °C over the aluminium plate), although its temperature distribution is axially symmetric relative to the centre of the plate (Fig.III-5b). However, the ceramic / plate contact was not optimised, a thermal paste which had been used to glue both of them, it amplified a little the thermal non-uniformity. Fig.II-5a shows a temperature distribution, which has a less symmetric profile but more uniform over the surface of the plate.

Copper plates could also be used for their higher conductivity, though copper corrosion after successive phases of condensation would have generated a non negligible oxide layer with time, thus insulating the active air / solid interface with a thermal buffer. The corrosion of aluminium has a lower impact on the geometry itself (an oxide layer of a few μm, but the evolution of this layer will develop after a year of testing).

The adjustment of the dimensions of the plate to those of the thermoelectric module is needed for better temperature uniformity. Initially the experiments have been performed with a 40 x 40 mm^2 Peltier below a 50 x 50 mm^2 plate. When comparing the experiments 9b and 7b performed with the similar dimension plate (40 x 40 mm^2), and experiment 3 performed

with the 50 x 50 mm^2plate, it can be observed that ΔT_{in} is doubled. The experiment 8b was not significant because the steady state was not reached, the controller temperature was near the dew point, and it has already been shown in fig.III-3 that when those temperatures converge the surface temperature tend to increase. In the same experiment, after one hour of experimentation the condensate drops appeared (exp 9b), which caused again the change in temperature difference.

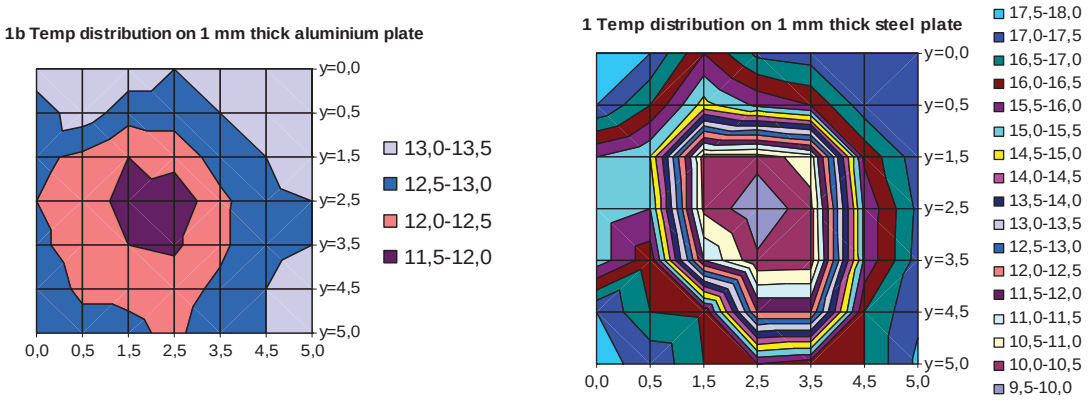

(a) (b)

Fig.III-5 (a, b): Distribution of surface temperature with (a) aluminium plate and (b) steel plate.

The influence of the plate thickness (t) is clearly visible by comparing the experiments 14 (t = 1 mm, ΔT_{in} = 1.2 °C), 16 (t = 2 mm, ΔT_{in} = 0.8 °C) and 15 (t = 3 mm, ΔT_{in} = 0.7°C) performed with similar thermal conditions ($T_a - T_{(plate)}$). An increased thickness helps in absorbing much of the thermal inhomogeneity present at the ceramic plate of the thermoelectric module, and results in a more uniform surface temperature (Figure III-6) in comparison to the 1 mm thick plate. Our goal is to perform mass measurements as local as possible, thus such an almost homogeneous configuration is more appropriate; subsequently, 3 mm thick plates were used.

The area of the plate seems not very significant for the homogenization of the surface temperature distribution for the various configurations considered. The experiments 15 (50 x 50 mm^2), 7b (40 x 40 mm^2) and 6b (30 x 30 mm^2) induced similar temperature differences for similar thermal conditions. To facilitate the weighing of the condensate, the plate 50 x 50 mm^2 was chosen for mass flow measurements in order to generate sufficient amounts of mass, which can be measured more accurately (sensitivity of the balance), knowing that the phenomenon of condensation is very slow.

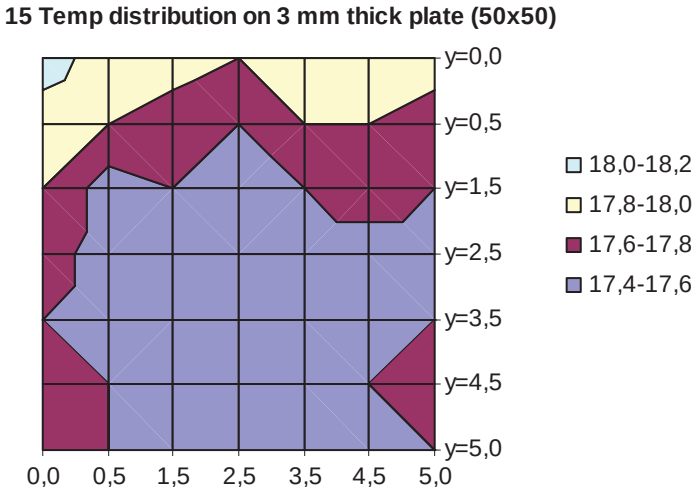

Fig.III-6: Distribution of surface temperature with a plate of 3 mm thickness.

3.4.2 Choice of heat sink and its orientation with air flow

The heat generated on the opposite side of the Peltier module must be well dissipated in order to obtain a distribution of temperature near room temperature (which is the reference temperature in this work) and thus generate a known and stable temperature gradient between the hot and cold sides of the Peltier module. This is necessary to obtain a good thermal control of the cold solid / air interface. Within the wind tunnel, the air flow rate is sufficient to cool down the fins of the heat sink. At LGCB, a fan was added to accelerate the ambient air flow rate that circulated in the laboratory, and its speed (controlled by the input voltage) was chosen so as to dissipate the highest heat flux, and kept constant for all tests.

Concerning the design of the heat sink, two different configurations of the same size were tested: a conventional extruded aluminium heat sink, with a large number of fins (fig.III-7a), and another one in copper consisting of very thin fins cooled down with a circulation of coolant. The various tests have yielded similar results (tests 24-26).

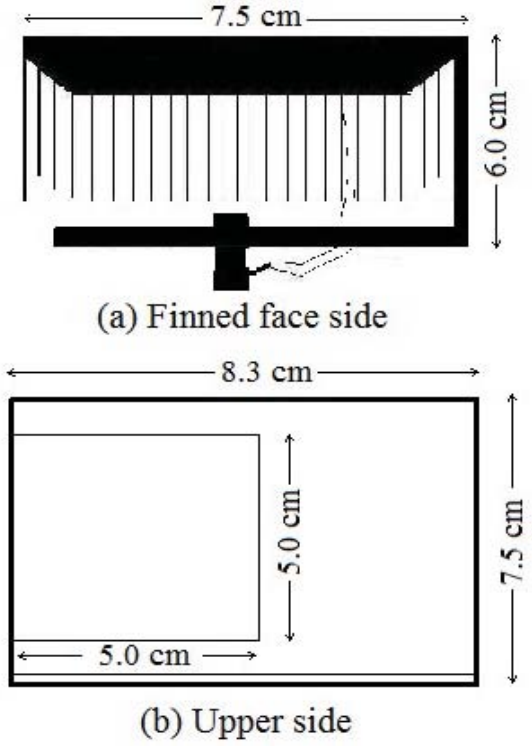

Fig.III-7: Dimensions of the heat sink

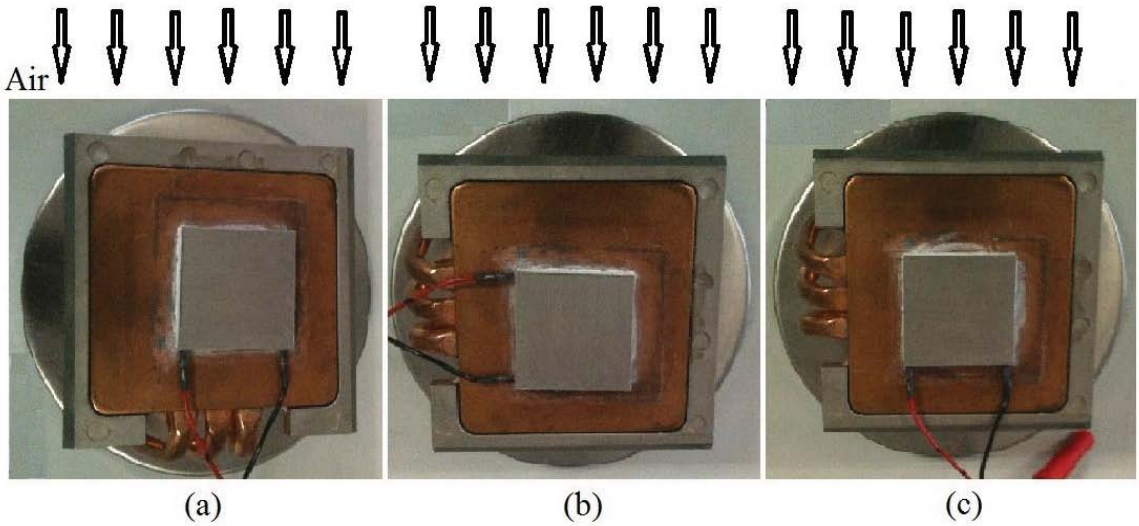

Fig.III-8: Three different orientations of the heat sink with Peltier and plate.

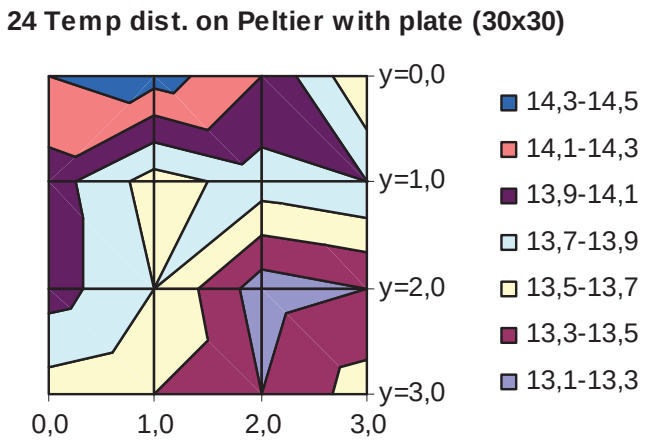
24 Temp dist. on Peltier with plate (30x30)
y=0,0
y=1,0
y=2,0
y=3,0
0,0
1,0
2,0
3,0
14,3-14,5
14,1-14,3
13,9-14,1
13,7-13,9
13,5-13,7
13,3-13,5
13,1-13,3

(a)

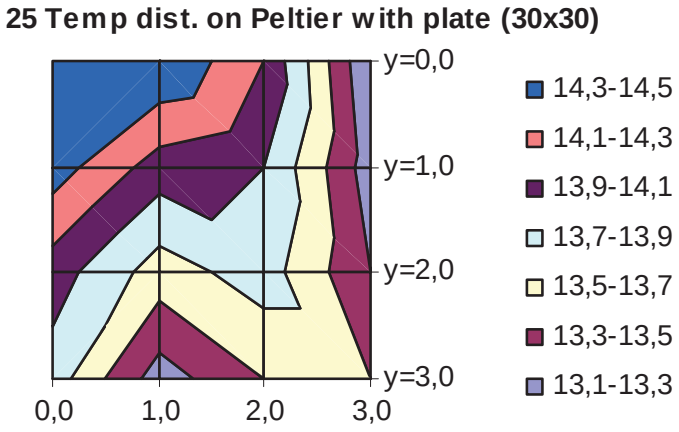
25 Temp dist. on Peltier with plate (30x30)
y=0,0
y=1,0
y=2,0
y=3,0
0,0
1,0
2,0
3,0
14,3-14,5
14,1-14,3
13,9-14,1
13,7-13,9
13,5-13,7
13,3-13,5
13,1-13,3

(b)

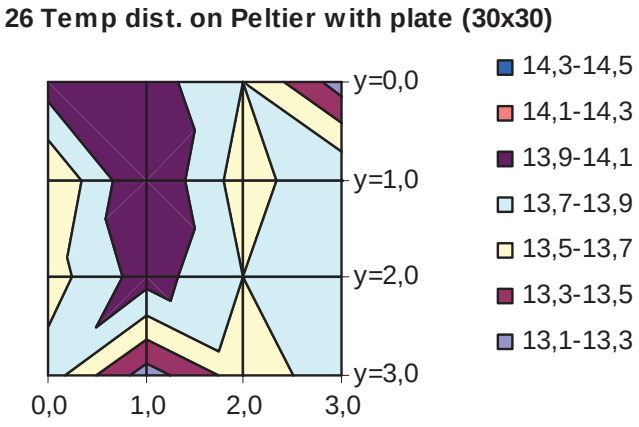
26 Temp dist. on Peltier with plate (30x30)
y=0,0
y=1,0
y=2,0
y=3,0
0,0
1,0
2,0
3,0
14,3-14,5
14,1-14,3
13,9-14,1
13,7-13,9
13,5-13,7
13,3-13,5
13,1-13,3

(c)

Fig.III-9 (a, b, c): Temperature distribution plots for orientation of Fig.III-8 (a, b, c).

The best conditions are obtained, quite logically, by placing the module in the centre of the heat sink. But, in the wind tunnel, the module was placed at the edge facing the flow (fig.III-7b) for hydrodynamic considerations (boundary layer development mainly).

The orientation of the heat sink towards the direction of the flow also plays a role in the homogeneity of the surface of the plate (fig.III-8). A few experiments with a 30 x 30 mm^2 plate and copper heat sink have been performed to verify this and the plots are given as fig.III-9 (a, b, c). The temperature difference from minimum to maximum value was recorded as 1.2 °C, 1.5 °C, and 0.9°C. The fig.III-9(a) corresponds to the position in fig.III-8 (a), fig.III-9 (b) corresponds to fig. III-8 (b), and fig.III-9 (c) to fig.III-8 (c). The difference was maximum for fig.III-8 (b) position because its finned sides were not parallel to the air flow. And the position of fig.III-8 (a) and (c) are similar but the temperature profiles as shown in the fig.III-9 (a) and (c) are quite different and the difference recorded was 1.2 °C and 0.9 °C, which gives us an indication on how to position the Peltier element on top of the surface of the heat sink. The position of fig.III-9 (c) has given minimum temperature difference in comparison to other two positions, and it seems a better position chosen for further experiments and also it favours the air flow, in which the fins of heat sink are parallel to the flow direction.

The experiments 24, 25, and 26 have been performed in an average air velocity of 0.8-0.9 m/s, a relative humidity of 34-35%, and an ambient temperature of 22-23 °C. The relative humidity and ambient temperature were the ones of the room, where the experiment was performed but the air velocity was local as a forced flow was generated by a small ventilator to remove the hot air from the fins of the heat sink, but such a local flow disturbance also affected the active plate.

Some other experiments have been performed to know the temperature distribution profile, when the Peltier element was placed at the centre or along the sides of the heat sink. The plots for only two experiments 27, 28 have been given here for the 50 x 50 mm^2 plate and the plots are given as fig.III-10 (a, b). The experiments 27 has been carried out by placing the Peltier element on one side of the heat sink facing the flow and in 28 it was placed in the centre of the heat side.

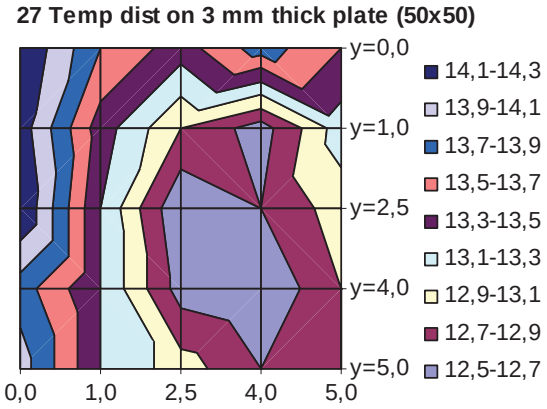

(a)

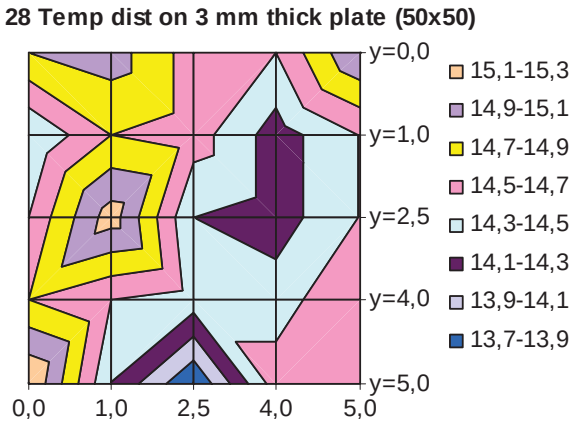

(b)

Fig.III-10: Temperature distribution plots.

The plots shown here indicate the differences in the temperature profiles, the points of minimum and maximum temperature values are shifted, the profiles are not similar, also the difference from minimum to maximum values on the surface was 1.8 °C for 27 and 1.6 °C for 28. The difference was a little higher for experiment 27 in comparison to 28 but the location of Peltier and plate on the heat sink surface was better in regard to the velocity boundary layer that develops on the active surface. If the Peltier and plate are placed in the centre portion of the heat sink, the velocity boundary layer will be much more turbulent.

3.5 Conclusion

The above experimental findings on temperature profile of the square flat plate show that the minimum variation of temperature was 0.6 °C and the maximum was 2.4 °C with the same

size plate on the Peltier and it was more than 3 °C without plate. It has been experienced here that the increased mass helps to reduce the thermal inhomogeneity on the surface of the plates. The area of the plate also plays a role, an increase helped us to produce more condensate without significantly affecting the inhomogeneity, only minor changes have been seen. It was also observed that adjusting the size of the plate to the one of the Peltier element helped in reducing the inhomogeneity of the surface of the plate.

Chapter IV

Velocity Profile Studies Inside a controlled environment

4.1 Introduction

The air flowing over the surface of a living objects, plants or human being affect it's growth and behaviour. Most of their activities require thorough understanding of the local atmospheric conditions. The agricultural process depends on temperature, sunshine, absence or presence of clouds, air velocity, and on the amount of water available in the local atmosphere. The net photosynthetic rate of the plant canopy increases with increasing air velocities inside plant canopies (Kitaya, 2004). In bio-regenerative life support system (BLSS), the plant culture will play an important role in food production, CO_2/O_2 conversion, and water purification. Life support of crews in space is dependent on both the amount of food and atmospheric O_2 produced by plants in a limited space. In a closed chamber the enhancement of the gas exchange in leaves and growth of plants would be dependent on several factors, including control of air current. Insufficient air movement around plants generally limits their growth by reducing the gas diffusion in the leaf boundary-layer thereby decreasing photosynthetic and transpiration rates (Monteith and Unsworth 1990, Yabuki and Miyagawa 1970). Airflow affects plant growth through energy and mass transfer, latent heat exchanged through the processes of water evaporation (transpiration) and condensation onto plant surfaces is also directly affected by air movement.

Normally, the higher wind velocity causes greater effects of airflow on plant growth. However, responses are not linear over the range of airflow generally experienced, but tend to a maximum or optimum. Observed closed chamber or greenhouse airflow velocities within the plant canopy ranging from 0.15 to 1.70 m s^{-1} caused variation (Korthals et al 1990). An air velocity of 0.5 to 0.7 m s^{-1} was reported as optimum for plant growth under controlled conditions (Grace 1977); however, there are minimal data to support this conclusion. Some researchers have even suggested air velocities as high as 1.5 m s^{-1} to be used without unfavourable effects to most plants (Grace 1977). This inconsistency in response can be attributed to species canopy and physiological differences, interaction with other environmental factors, or inaccurate control or measurement of air flow.

In this chapter, the details of velocity profile experiments performed in a closed wind tunnel are described. The local effect of velocity and turbulence intensity, and its variation on a small flat plate are discussed. Here, we have performed the following types of velocity profile experiments (Fontaine and Tiwari 2010):

1. **Dry conditions (without condensation on the surface of the plate)**

   (i) On an simple aluminium square flat plate

   (ii) With all the accessories required for condensation experiments

2. **Wet conditions (with condensation on the surface of the flat plate)**

   (i) After constant amount of condensate collected on the surface

   (ii) In course of condensation with a certain amount of condensate on the surface

For the dry condition for a simple square flat plate, the square flat plate geometry was similar to the one used in the other experiments, nothing was added or connected to the plate, only a perpendicular rod attached to it for support and all other experiments were with the whole cooling arrangement, as it has been discussed in detail in chapter II of this thesis such as with Peltier element, aluminium heat sink, sponge, and temperature sensor. In all the experiments the chosen plates have the same dimensions for the velocity profile studies. Before, starting the experiments the hot wire sensors have been calibrated inside the wind tunnel.

4.2 Calibration of hot wire anemometer

To study the velocity profile and turbulence intensity, we have used a single hot-wire probe (see chapter II). Calibration of each wire probe with air temperature enabled mean velocity measurements to be made with an accuracy of l – 3 % in the range of 0.4 - 4.5 m/s (Kondjoyan 1993). In the clear test chamber the mean velocity at any point within the chamber differed by less than 0.5 % from its average value over the entire chamber. The turbulence intensity was less than 1.3 % and uniform in a part of the test chamber large enough to contain the sample. Repeated calibrations of the response of the hot wire system with respect to air temperature ensured that the absolute error on the velocity measurements was less than +/−0.1 $m.s^{-1}$ (Fontaine and Tiwari 2010).

4.3 Measurement of velocity profile and turbulent intensity

4.3.1 Dry conditions

4.3.1.1 Horizontal position

4.3.1.1.1 Simple Plate without any cooling device

The square flat plate of aluminium was located inside the test chamber of the wind

tunnel and subjected to air flows of different velocities. In a first set of experiments, the average velocity and fluctuated velocity profiles were measured in the boundary layer, which developed along the surface of the horizontal flat plate and parallel to the direction of the air flow. In another set of experiments the surface of the flat plate was taken as vertical and perpendicular to the direction of the air flow (see 4.3.1.2). The flat plate used to study the velocity profile was 5 cm long, 5 cm wide and 3 mm thick as shown in figure IV-1. It was located halfway up the test chamber i.e., 40 cm above the base of the tunnel, 40 cm down from the upper surface of the tunnel, and 74 cm downstream from its entrance. The square shaped flat plate of aluminium held in position by a cylindrical rod glued perpendicularly on its back.

The measurement of a velocity profile began by choosing the frequency of the fan, which fixed the fan speed to reach an average air velocity of about 0.5 $m.s^{-1}$ inside the test chamber (this air velocity was measured accurately afterwards). The turbulence intensity ($Tu = \sqrt{\overline{u}^2}/U$) and the free stream flow were determined. The three axis traversing system was reset to zero in the flow direction X, Y, and 1 mm in Z by conveying the tip of the hot wire prongs on a line parallel to the edge of the flat plate surface. On the flat plate we have taken 25 points as shown in the top view of the flat plate in figure IV-1. Z was fixed and then the probe was conveyed at 1 cm towards Y, and at a given distance X of 1, 2.5, 4 or/and 5 cm from the leading edge of the plate. A telescope (×24) was used to accurately locate the point of contact (the error of this visual observation through the magnifying glass was +/−0.05 mm). From this point upward the air velocity and fluctuation in the main flow direction were measured at 3 mm and until the frontier of the boundary layer was reached (average velocity value became constant).

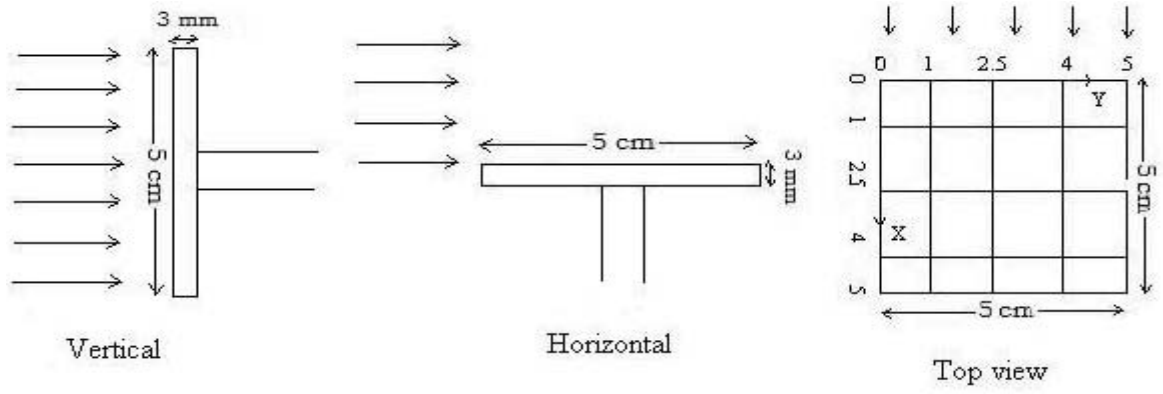

Fig.IV-1: Orientation of the plate and its points of velocity measurement.

4.3.1.1.2 Plate with cooling arrangement

The Peltier element was pasted below the plate, the heat sink was underneath, and a thin layer of sponge circled the outside vertical surface of the Peltier element to prevent the water condensate from falling down on the top of the heat sink. The use of sponge was developed after several experiments, which helped us to characterise its thickness, wideness and proper position, so that the velocity profile on the active surface were minimally affected. The whole arrangement and its dimensions have been already shown in fig. II-5(b) and fig.III-7. It was supported by a hollow rod of aluminium having a total length above the balance of 48.1 cm, in which 34.2 cm were inside the tunnel. All the electrical wires ran inside this hollow rod and were connected to the plate and Peltier on the backside of the arrangement in the direction of the flow, so that it would not affect the profile of the flow on the plate.

4.3.1.2 Vertical position

The plate has been kept in vertical position as shown in fig.IV-1, perpendicular to the direction of the air flow inside the wind tunnel. The measurements were taken at similar points as for the horizontal position given in the top view of the plate in fig.IV-1.

4.3.2 Wet conditions

The arrangement of cooling the metal plate has been described in detail in the chapter II, a photograph showing the test chamber and a closer look of condensing unit with all the necessary components is given in fig.IV-2. To prevent the condensate from falling from the sides of the square plate, a 3 mm thick and 2 mm wide sponge has been applied on the outer side of the plate surface, which also affected the turbulent intensity and flow profile on the surface of the plate.

Two types of velocity measurement experiments were planned in wet conditions:

(i) above the active surface of the plate at constant height (from the plate surface) with the growing thickness of the condensate layer, and

(ii) with a constant amount of condensate layer on the active surface with increasing height from 3-5 mm above the plate surface to the outside of the boundary layer.

Fig.IV-2: Photograph of test chamber and a closer look of condensing unit

At every height the measurement has been taken at each 25 points on the same horizontal plane as described before.

4.4 Results and discussions

4.4.1 Dry conditions

4.4.1.1 With simple plate

We have performed velocity measurements at 1 mm and 3 mm away from the square flat plate surface in both horizontal and vertical positions. The velocity measurement using hot-wire are known to be erroneous very close to the wall because of the influence of thermal exchanges by conduction and radiation between the wall and the hot wire (Brun 1995). Overall 25 measurement points for each height plane were considered as shown in the top view of the flat plate in fig.IV-1.

The surface plots of the velocity profile are given for the flat plate in horizontal position in fig.IV-3 (a, b, c, d, i, j) and in vertical position in fig.IV- 4 (a, b). The turbulence intensity is given for the same positions in fig.IV-3 (e, f, g, h, k, l) and in fig.IV-4 (c, d). The experiments were performed for a mean entrance velocity of 0.5, 1.1, 1.5, and 2.0 m/s and the wind velocity as well as the turbulence intensity was measured. It is observed from the fig.IV-3 (a, b) and IV-3 (c, d), on moving from surface of the flat plate to free stream velocity, the fluctuations in the velocity decrease and the shape of the velocity profile is conical, and centred towards the middle to back part of the flat plate. It is also observed in fig.IV-3 (e, f, g, h), that for a velocity of 0.5 m/s the maximum turbulence intensity at 0.001 m above the surface of the plate reaches 6-8%, and at 3 mm above the surface drops to 3-4%. In addition

for 2.0 m/s, the maximum turbulence intensity is above 30% at a 1 mm height and more than 20% at 3 mm above the flat plate. At the same time the turbulence intensity at the entrance of the tunnel is 2.2% for 0.5 m/s and 1.4% at 2.0 m/s. We have taken the readings for a height of 5 mm and little more, the turbulence intensity at 5 mm started decreasing and then suddenly reached the range of the turbulence intensity measured at the entrance of the tunnel, which shows that the probe was outside the boundary layer. These preliminary experiments have been performed inside the wind tunnel for the study of velocity and turbulence intensity profiles in dry conditions at room temperature ($T_a \approx 22°C$) (Tiwari et al. 2009, 2010). The mean velocity measurements have been performed at 1 mm and 3 mm above the surface of the horizontal plate. A comparative surface plots of the velocity profile and for the turbulence intensity has been given in fig.3 (*i-l*) for mean entrance velocity of 1.5 m/s.

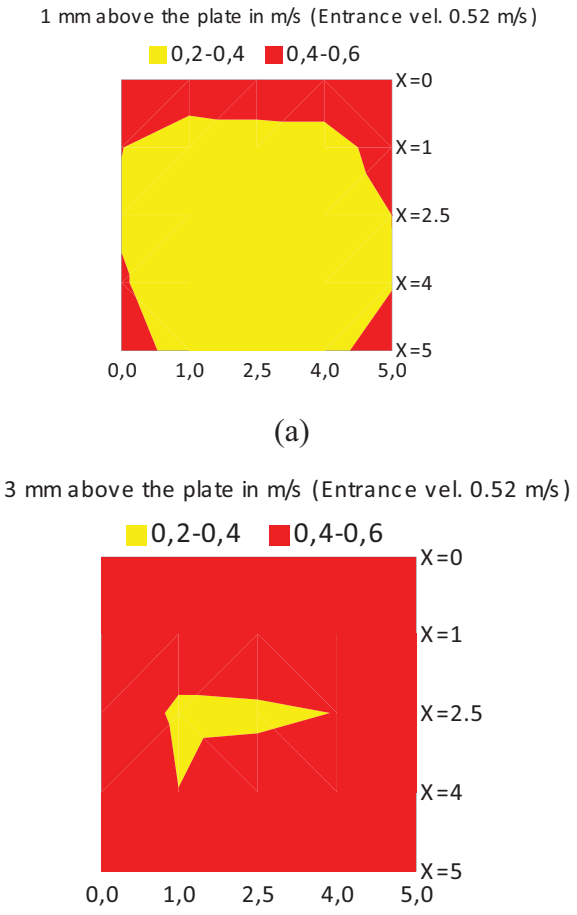

Fig.IV-3 (a-b): A comparative surface plots for the flat plate in horizontal position, velocity profiles in (m/s) for ambient temperature (T_a) = 21.8 °C.

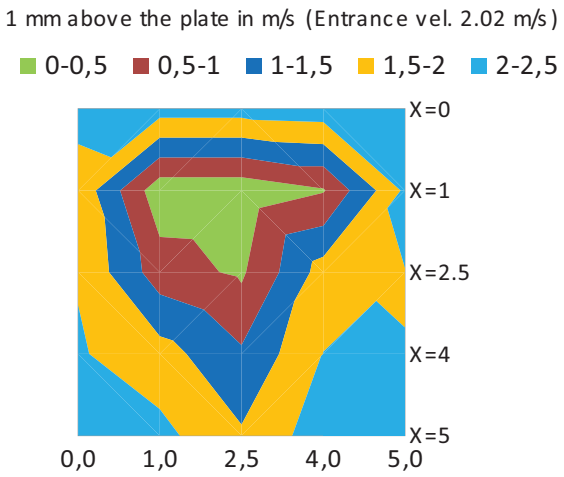

(c)

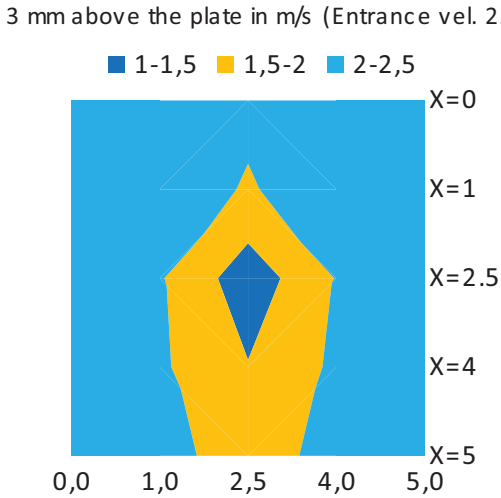

(d)

Fig.IV-3 (c-d): A comparative surface plots for the flat plate in horizontal position, a velocity profiles in (m/s) for ambient temperature at (T_a) =21.2 °C.

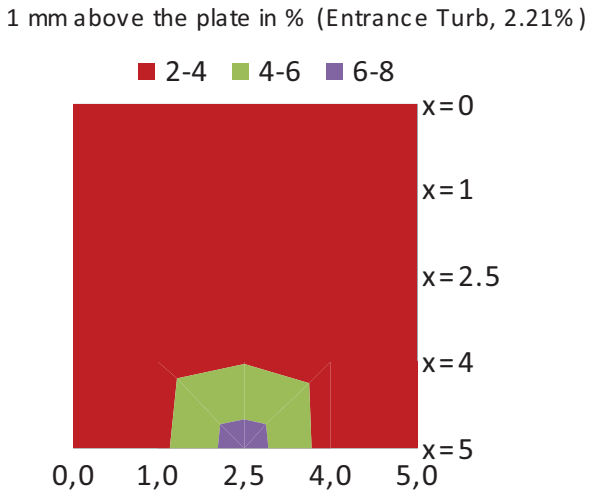

(e)

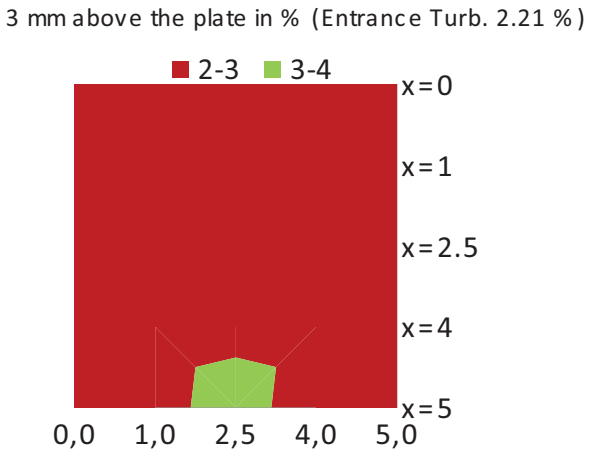

(f)

Fig. IV-3 (e-f): A comparative surface plots for the flat plate in horizontal position, a turbulence intensity in (%) for ambient temperature at (T_a) = 21.8 °C and entrance velocity 0.52 m/s..

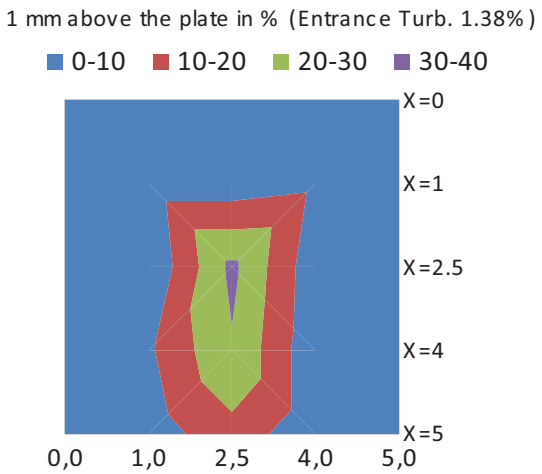

(g)

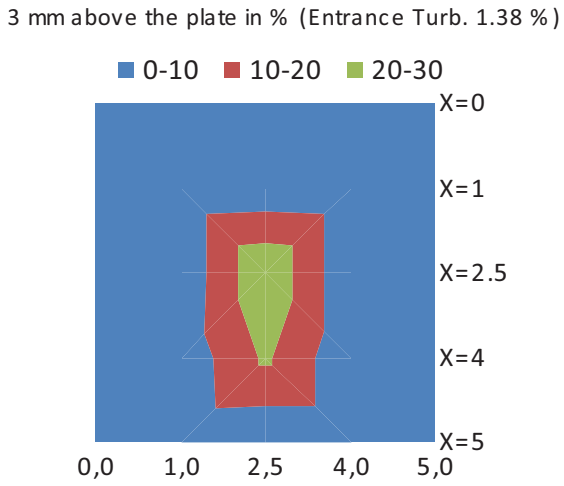

(h)

Fig.IV-3 (g-h): A comparative surface plots for the flat plate in horizontal position, a turbulence intensity in (%) for ambient temperature at (T_a) = 21.2 °C and entrance velocity 2.02 m/s.

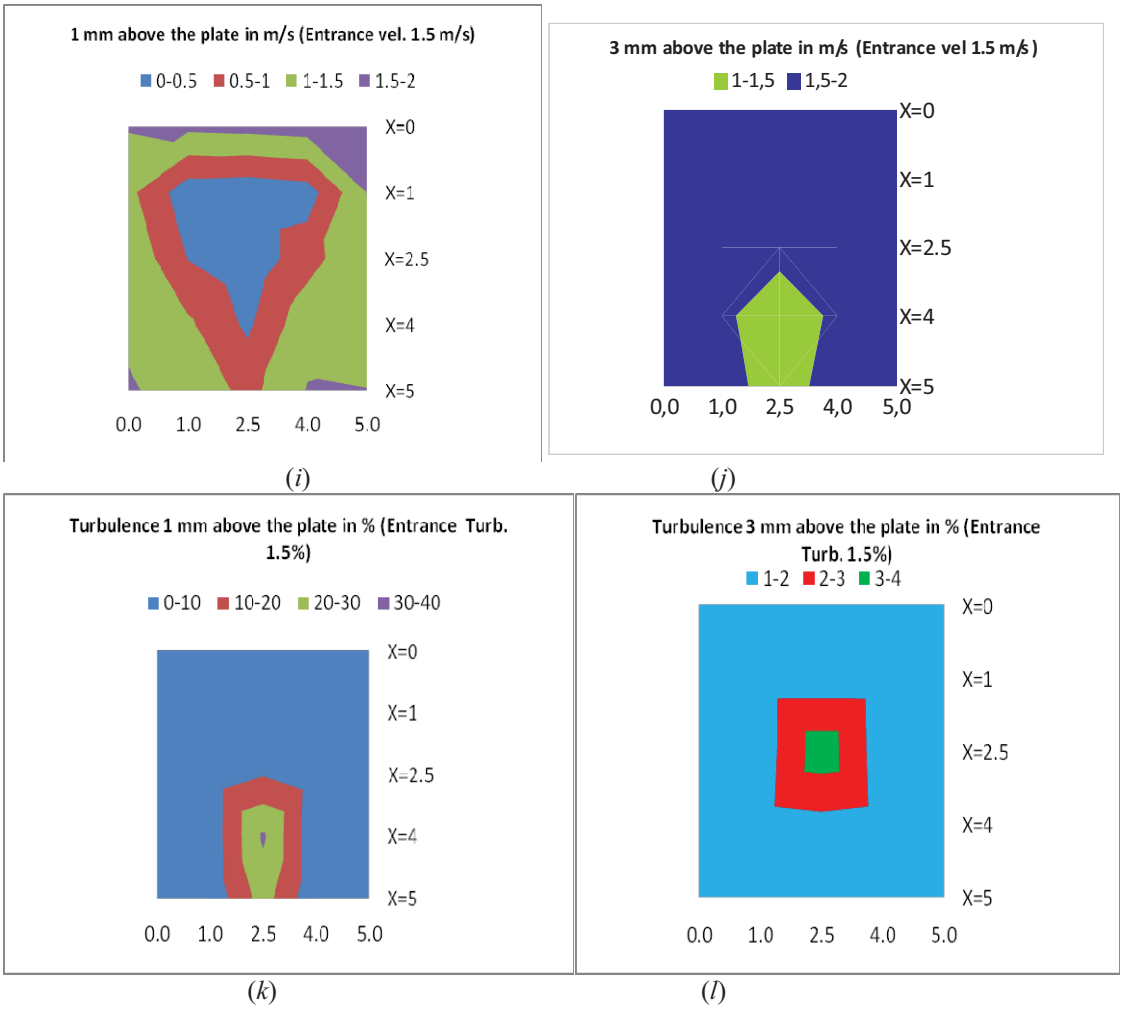

Fig.IV-3(*i-l*): Comparative surface plots above the flat plate in horizontal position at 1 mm (*i*, *k*) and at 3 mm (*j*, *l*): (*i-j*) velocity profiles in meter per second and (*k-l*) turbulence intensity in per cent.

It is observed from fig.IV-3 (*i, j*) that, on moving from the surface of the flat plate to free stream velocity, the fluctuations in the velocity decrease and the shape of the velocity profile is almost similar as in the previous figure. The fig.IV-3(*k, l*) showing here that the maximum turbulence intensity at 1 mm above the surface of the plate reaches 30-40%, and at 3 mm above the surface drops to 3-4%, whereas the turbulence intensity at the entrance of the tunnel was about 1.5%. Slightly above a height of 3.2 mm of the plate, the turbulence intensity suddenly reached the range of the turbulence intensity measured at the entrance of the tunnel (1.5%), which shows that the probe was outside the boundary layer. The symmetry of the measured profiles (velocity and turbulence intensity) reflects the accuracy of the experimental set-up (position, manufacturing etc.).

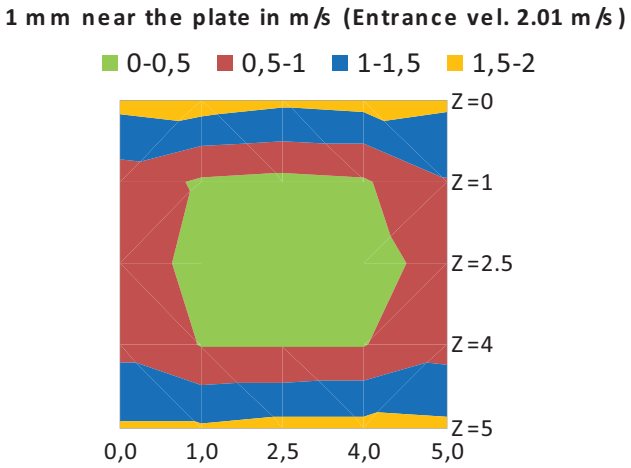

(a)

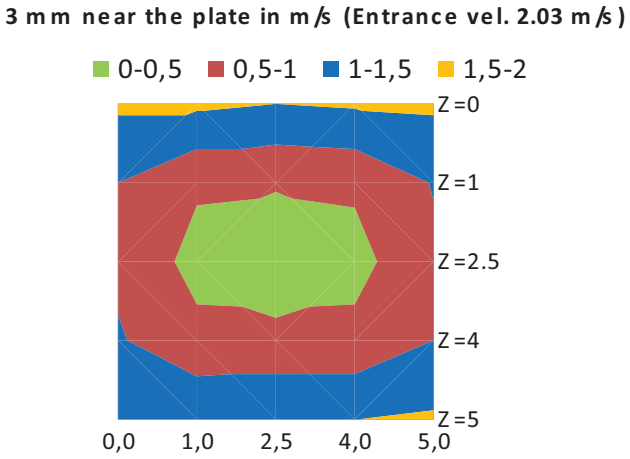

(b)

Fig.IV-4 (a-b): A comparative surface plots of a flat plate in vertical position, velocity profile in m/s for (a) ambient temperature (T_a) = 21.1 $^{\circ}$C and (b) at (T_a) =19.9 $^{\circ}$C.

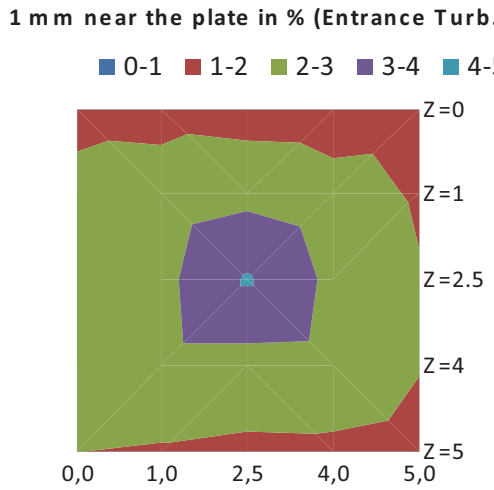

(c)

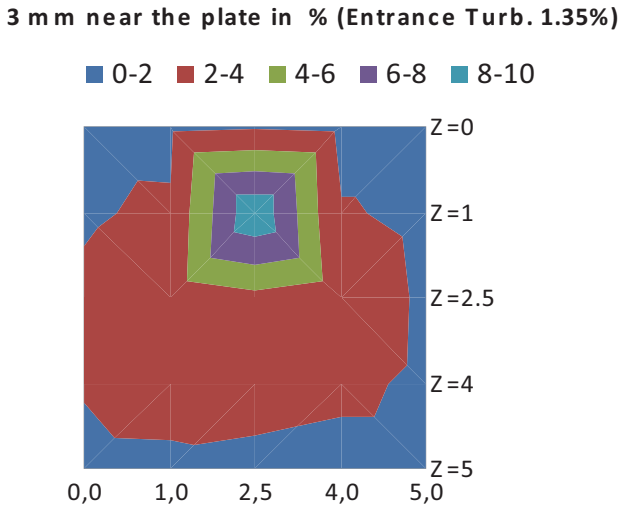

(d)

Fig.IV-4(c-d): A comparative surface plots of a flat plate in vertical position for turbulence intensity in % for (c) ambient temperature (T_a) = 21.1 $^{\circ}$C and (d) at (T_a) =19.9 $^{\circ}$C at entrance velocity 2.0 m/s.

The plots given in the fig. IV-4 (a, b, c, d) concern a vertical flat plate held perpendicular to the free stream flow. In this position the velocity profile is always centred at the middle of the flat plate, where it is minimal, while the turbulence intensity increases as we move away from the surface of the flat plate. The central portion of the flat plate creates a hindrance in the path of free stream flow, which decreases the air velocity. As we move outside of the flat plate, the velocity increases and becomes similar to the velocity at the entrance of the wind tunnel. The turbulence intensity is obviously at its maximum in the middle part of the flat plate but as we move away, the turbulence intensity decreases. When moving farther from the surface of the flat plate the turbulence intensity is increased as long as the flow remains affected by the proximity of the stagnation point. Fig.IV- 4 (c-d) shows little asymmetry in the flow profile, which reflects the sensitivity of the boundary layer flow to the trailing edge of the flat plate. Hence, high accuracy manufacturing is required in these conditions.

All our results showed that we observe the development of a boundary layer on top of the aluminium plate. This boundary layer could not be considered as the classical laminar boundary layer on a flat plate. Even if the upstream edge of the plate was thin (3 mm in thickness) it generated vortices which increased turbulence near the plate wall. Actually turbulence intensities up to 30-40% were measured in the wind tunnel above the plate which revealed the development of those turbulent vortices. In this case it was shown in literature (Ghisalberti and Kondjoyan 2002) that close to the wall the velocity profile was similar to that of a classical laminar boundary layer, even if the velocity gradient increased with turbulence, while the contact region between the free stream and the boundary layer became less distinct similarly to the outer region of a turbulent boundary but without any logarithmic behaviour of the velocity profile. It was also shown in literature that the global boundary layer thickness including the outer turbulent part was a little bit increased compared to thickness of a classical laminar boundary layer. This thickening of the boundary layer due to free stream turbulence was always very small (10% to 20%). Boundary layer thickness was measured in our study for different air flow velocities by considering that the end of the boundary layer was reached when the turbulence intensity was the same as in the upstream flow. We have calculated the boundary layer thickness using Blasius' solution ($\delta \cong 4.64\sqrt{\upsilon L/U}$ (Bird et al. 2002); see Table IV-1 for air properties), and obtained results close to the ones observed experimentally (3-9%). The plots are given in the figs.IV-5 (a-b) for comparison with the Blasius' solution

and its relative error with the measured one (Tiwari et al. 2010, Fontaine and Tiwari 2010).

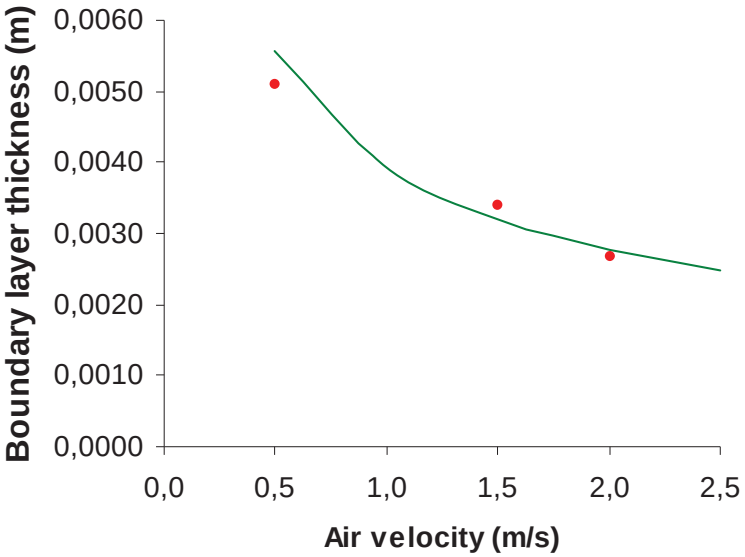

(a)

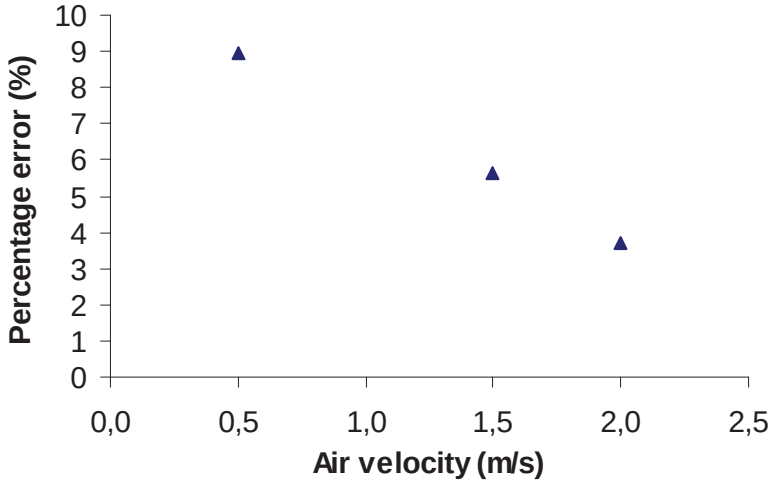

(b)

Fig.IV-5 (a-b): A comparative plots of boundary layer thickness calculated using Blasius solution (continuous line) and observed experimentally (square points) (b) its relative percentage error.

Table IV-1: Values of parameters used in calculations and taken at the time of the experiment.

Parameters	**Range**
Atmospheric pressure, mbar	920-924
Dew point temperature, °C	1.2-6.6
Density of air, kg/m^3	1.202
Kinematic viscosity, m^2/s	1.525 x 10^{-5}

4.4.1.2 Plate with all the accessories

On mounting all the accessories for cooling the aluminium flat plate gave the external dimensions of approximately 7 cm in thickness and 7.5 cm in width facing the flow with plate and Peltier element. The dimensions of the heat sink were 8.3 x 7.5 cm^2 on which the Peltier element and aluminium plate were mounted. The front face of this unit sufficiently rebound the air flow, which causes a generation of turbulence on the surface of the horizontal flat plate. Measurement of velocity and turbulence at similar points as earlier experiments on the surface of the plate has been carried out from 1 mm height to the end of the boundary layer, at each 2 and 4 mm increasing height.

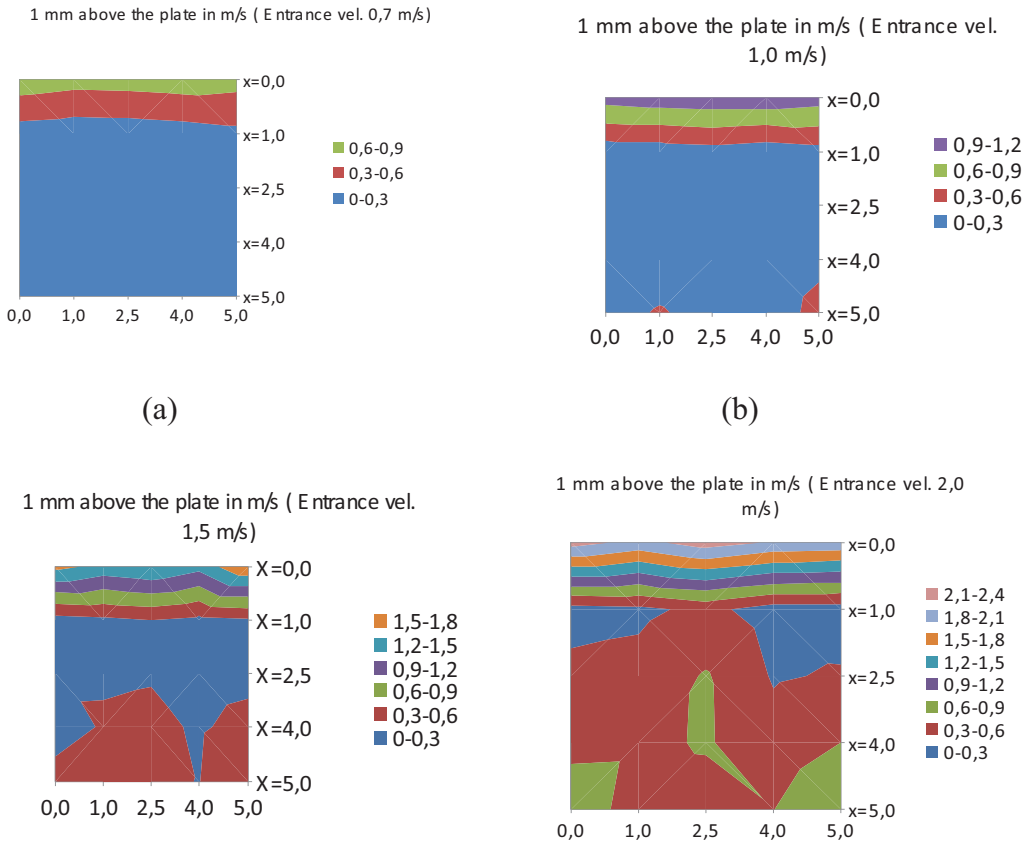

Fig.IV-6 (a-d): A comparative surface plots of velocity profile (m/s) on a horizontal flat plate at 1 mm height for four different entrance velocities.

The surface plots of velocity profile on the plate surface at minimum height above the plate i.e. 1 mm is shown in fig.IV-6 (a-d) for 0.7, 1.0, 1.5, and 2.0 m/s entrance velocities. It can be easily observed in the plots that the velocity at the flow facing corner of the plate is maximum similar to entrance velocity, and it has several variation bands within 1 cm at X-axis towards the direction of the flow. For low velocities till 1.0 m/s, over the backside of the plate, almost 80 % of the surface has equal and minimum velocity variations. On increasing the velocity the variations have been increased, which can be observed from figs.IV-6 (c-d), these variations started from 1.0 m/s, and can be easily seen as a very small trailing spots of the velocity range 0.3 - 0.6 m/s in fig.IV-6 (b).

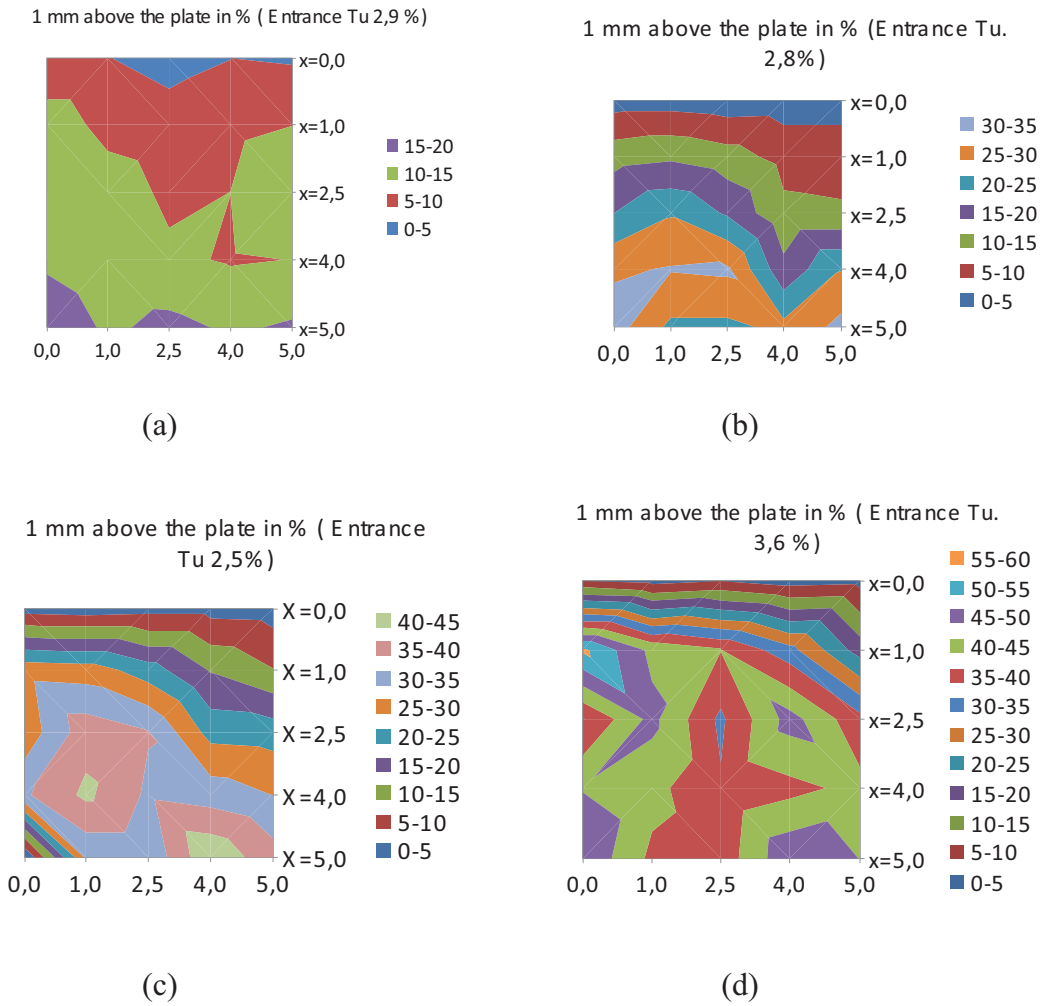

Fig.IV-7(a-d): A comparative surface plots of turbulence intensity (%) on a horizontal flat plate at 1 mm height for four different entrance velocities.

Figs.IV-7 (a-d) represents the turbulent intensity for the same plots as it was given in figs.IV-6 (a-d). From the observation of the plots, one can observe the variations in the

turbulence intensity with increasing velocity. On increasing the velocity in a step of 0.5 m/s, the turbulence intensity was increased by 10-15 %. The maximum value of turbulence intensity for the velocity of 0.7 m/s is 18.8%, for 1.0 m/s is 32.5%, for 1.5 m/s is 44.0 %, and for 2.0 m/s is 56.1 %. If we compare these results with our previous results with a plate only, the symmetric nature of the flow is absent very near to the flat plate surface. Further experiments a little farther away from the surface of the flat horizontal plate showed that the flow behaviour was slightly symmetric.

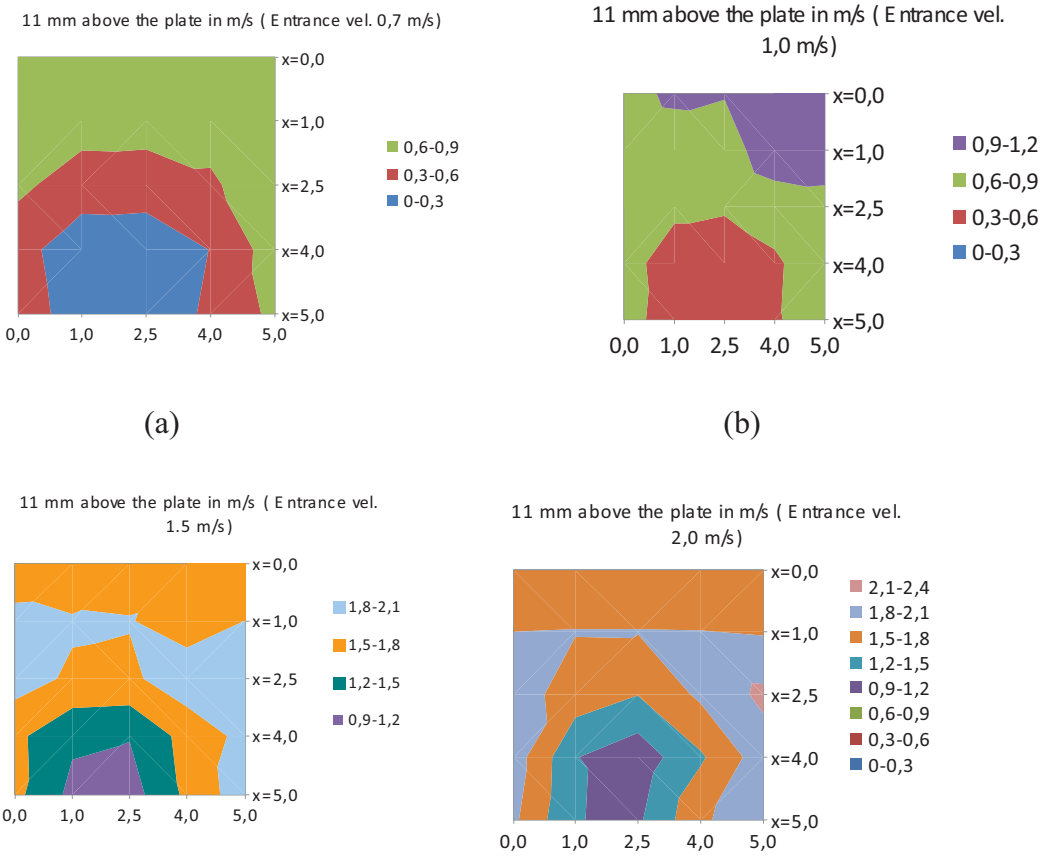

Fig.IV-8(a-d): A comparative surface plots of velocity profile (m/s) on a horizontal flat plate at 11 mm height for four different entrance velocities (i.e. 0.7, 1.0, 1.5, 2.0 m/s.

Figs.IV-8 (a-d) and figs.IV-9 (a-d) are the similar plots for the same velocity range as described above but at a 11 mm height from the surface of the plate. One can observe the symmetrical nature of the velocity profile and turbulence intensity at this height, which was absent at lower heights. The experiments have been conducted up to the plane of 24 mm height with a 2 mm gap between each measurement plane from 1 mm above the plate surface for a minimum velocity of 0.7 m/s, and we have found little less variations in velocity at this plane, but the turbulence intensity was only less than 5 % nearly half of the plate (fig.IV-9(a), but at the same velocity for 1 mm plane, the turbulence intensity was varied from minimum to 15%, which shows the decreasing nature of the turbulence on moving upwards at this velocity.

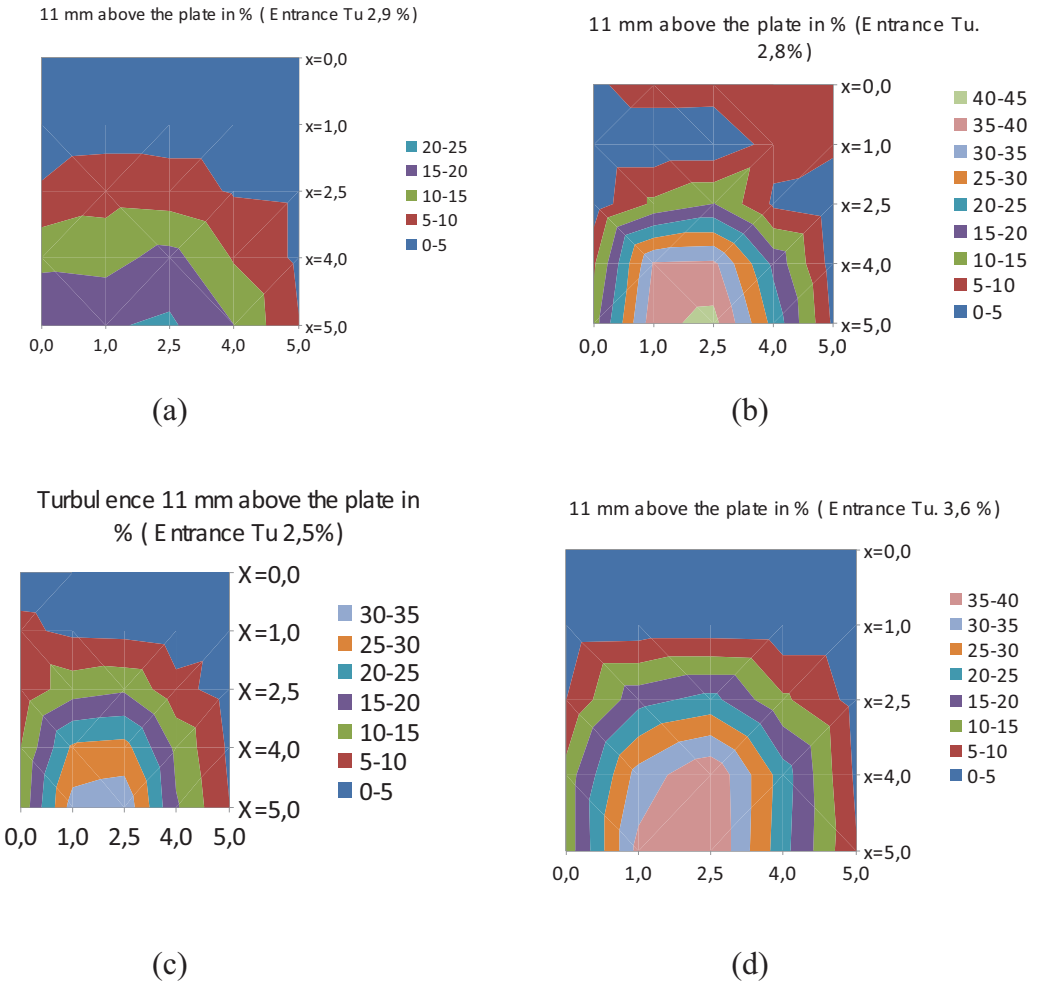

Fig.IV-9 (a-d): A comparative surface plots of turbulence intensity (%) on a horizontal flat plate at 11 mm height for four different entrance velocities.

Similar measurements have been taken for other velocities as well, and the symmetrical nature of turbulence intensity on the back side of the plate has been seen. The boundary layer thickness for each velocity range has also been measured, and it shows variations according to the velocity value. Fig.IV-10 (a) shows the measurement of velocity at a particular point i.e. last middle point on the plate (X = 5.0 cm, Y = 2.5 cm, Z = 0.1 cm to 11.5 cm) with entrance velocities of 1.0, 1.5, 2.0, 2.5, 3.0 m/s. The plot describes the nature of the boundary layer thickness, the trend inside and outside of boundary layer, and also the variation of velocity from very close to the plate surface to free stream flow of the wind tunnel.

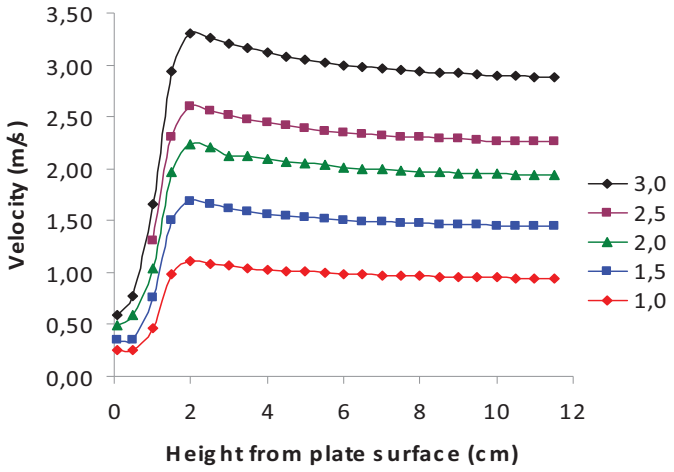

(a)

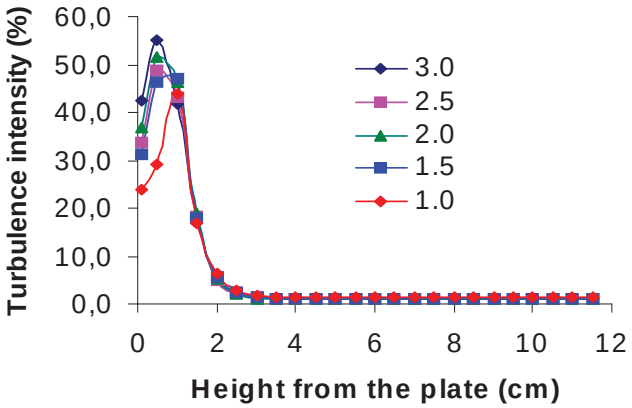

(b)

Fig.IV-10 (a-b): Plots of velocity and turbulence intensity versus height (starting at 0.1 cm, very near to the wall surface, the values are erroneous) above the plate for 1.0, 1.5, 2.0 2.5, and 3.0 m/s entrance velocity.

Very near to the plate (i.e. 1 mm above the plate or just above) the velocity is very low for all ranges, when moving away from the plate, it increases till a maximum value at a

certain height, and then it decreases very slowly and becomes stable. Moreover, this maximum value, which we have obtained at the boundary layer, is slightly more than the average entrance velocity. This reflects a “vena contracta” effect, as the obstacle reduces the cross section of the mean flow. Fig.IV-10 (b) shows the behaviour of turbulence intensity at the same points as described in fig.IV-10 (a) for velocity. The turbulence is the maximum inside the boundary layer; moreover it is maximum till 1 cm height above the plate surface, after that it decreases exponentially and becomes zero. But the maximum value of velocity is 2 cm above the plate or very close to it.

4.4.2 Wet conditions

The measurements in wet conditions have been carried first to find out whether the growth of the local condensate drops grew at the similar region or location, and second to see if the coalescence of the drops process for the formation of big drops affects the velocity profile and turbulence intensity on the plate surface.

Fig.IV-11 (a-d) shows the surface plots of the velocity profiles and turbulence intensities on the surface of a condensing unit after a collection of 2.0 g of condensate on the surface of the active plate within entrance velocity of 2.5 m/s.

A visual observation of the condensate plate shows that the drops start growing in a similar way, but when coalescence proceeds the global growth do not behave always in the same way. Sometimes, it coalesces with left drops sometimes with right ones, and then produces a few big drops on the surface of the plate, which are not at the same location. It is difficult to define precisely the mechanism and the prediction of the formation of big drops at this level. But the localization of these big drops on the surface of the plate determines clearly the flow profile on the surface. Observation of fig.IV-11(a, c) shows that the flow processes a symmetrical nature, but it was disturbed by the obstructions created by these big drops on the surface. It was experienced that the formation of big drops found maximum at two regions around the leading edge and towards the rear part of the flat plate surface.

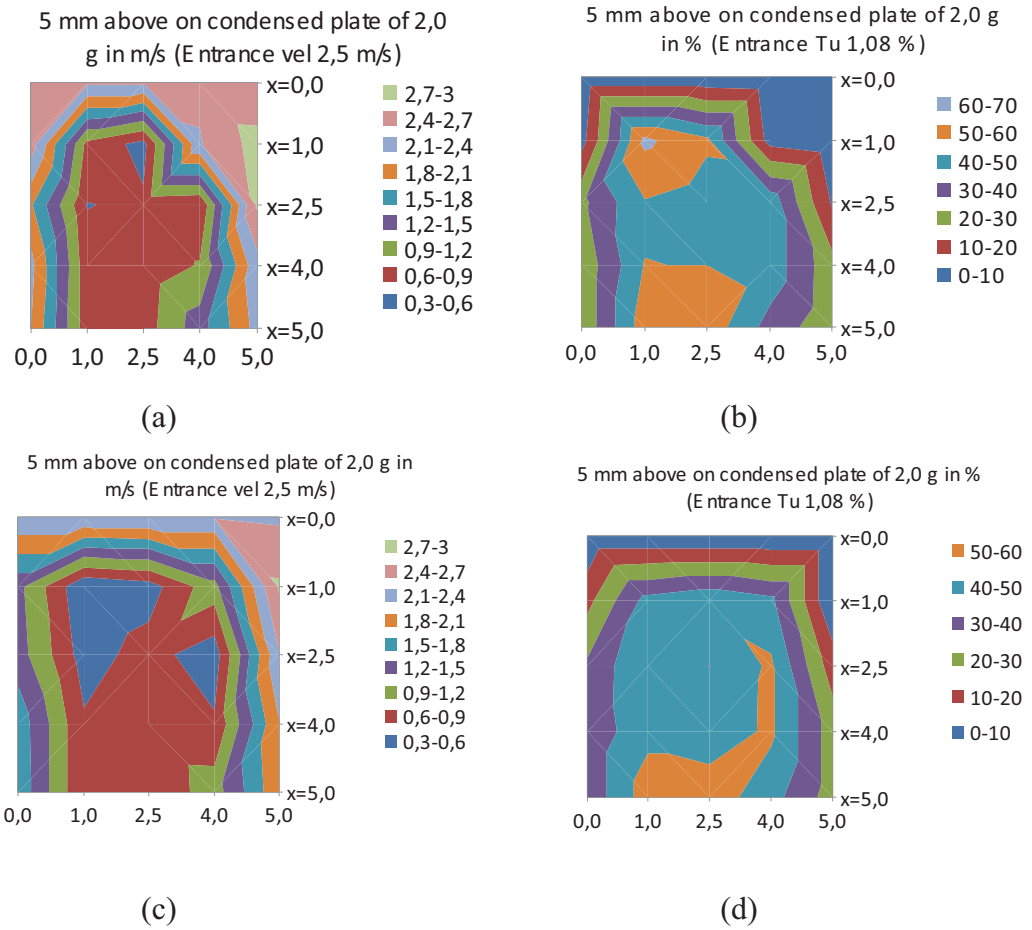

Fig.IV-11 (a-d): A comparative surface plots of (a, c) velocity profile (m/s) and (b, d) turbulence intensity (%) on a horizontal flat plate at 5 mm height during condensation, after a constant value 2.0 g of condensate collected on the surface of the plate for 2.5 m/s velocity in two different experiments - (a-b) CEI-38, and (c-d) CEI-39.

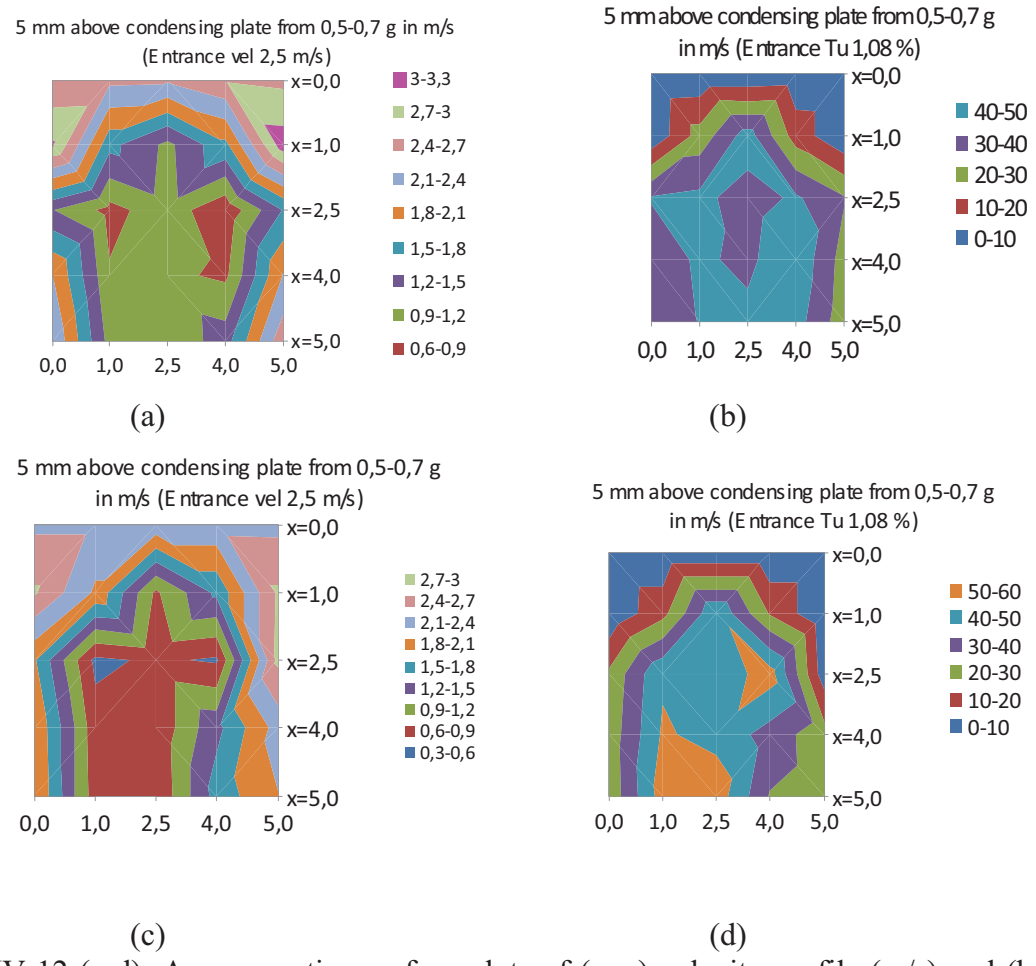

Fig.IV-12 (a-d): A comparative surface plots of (a, c) velocity profile (m/s) and (b, d) turbulence intensity (%) on a horizontal flat plate at 5 mm height during condensation on increasing weight (from 0.5 g to 0.7 g) of condensate on the surface of the plate for 2.5 m/s velocity in two different experiments- (a-b) CEI-37, and (c-d) CEI-39.

Fig.IV-12 (a-d) gives an idea of the growth of the drops for two different experiments in similar weather conditions performed on two different days at the same mean velocity. The velocity profile and the turbulence intensity were measured at 5 mm above the surface during the condensation process, with 0.5 g of condensate on the surface and it was performed till the collection of 0.7 g of water on the plate surface. One can easily observe from fig.IV-12(a, c) the existence of low velocity zones in the middle of the plate, that zone is shorten at the right side of the surface plot in fig.IV-12 (c), but is quite visible in fig.IV-12 (a). The turbulence intensity plot also verifies the changes in the middle part of the plate in comparison to the flow facing side of the plate, which looks similar.

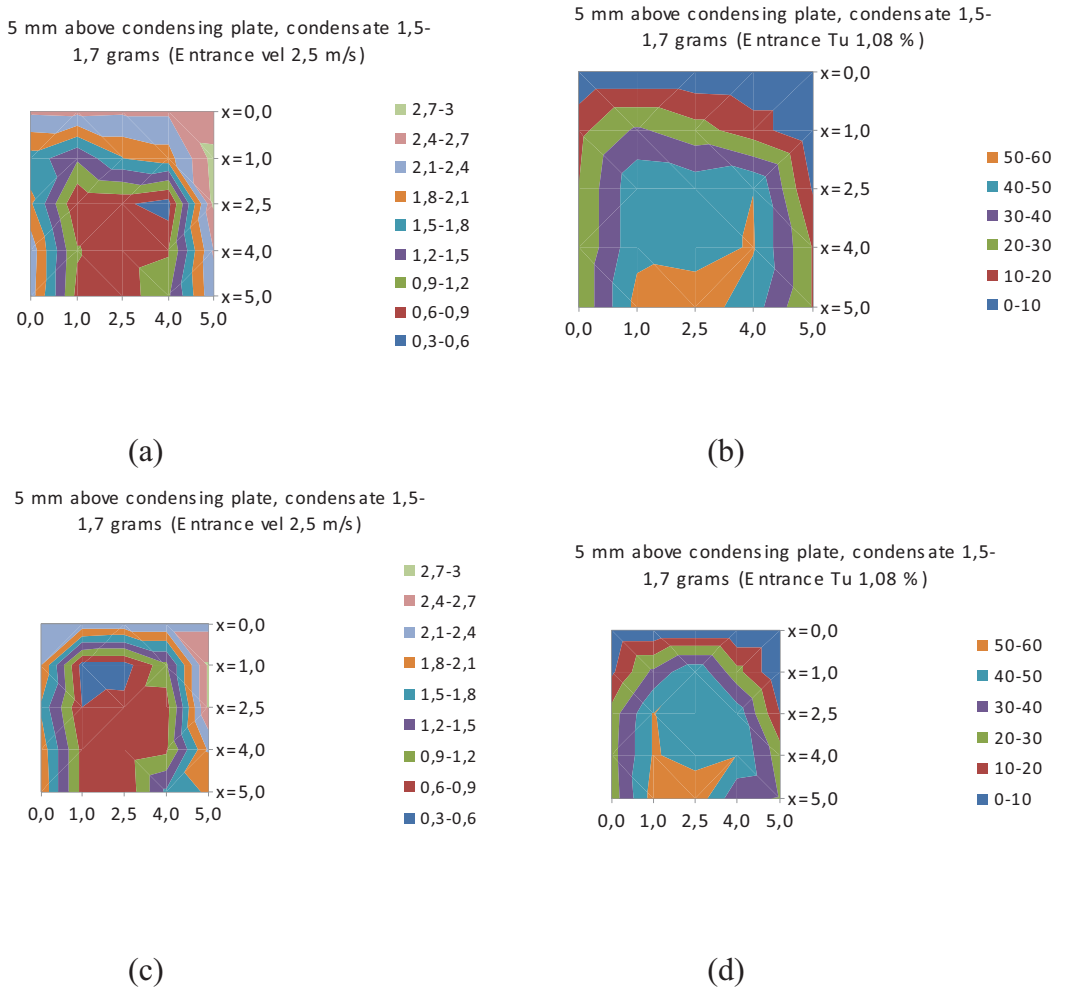

Fig.IV-13 (a-d): A comparative surface plots of (a, c) velocity profile (m/s) and (b, d) turbulence intensity (%) on a horizontal flat plate at 5 mm height during condensation on increasing weight (from 1.5 g to 1.7 g) of condensate on the surface of the plate for 2.5 m/s velocity in two different experiments- (a-b) CEI-38, and (c-d) CEI-39.

The experiment has been repeated with more condensate up to 1 g more on the plate to know if this variation of coalescence site continues to change or not with bigger drops, it has been observed that after the collection of even more condensate on the plate the flow profile is continuously affected by the growth of bigger drops and its movement by coalescence. Fig.IV-13 (a-d) describes the behaviour of velocity profile and the turbulence intensity in two different experiments with similar conditions, to reproduce the same profile, it can be seen from the figure that flow has similar values of velocity and turbulence on the same position but a few positions have been changed. The photograph of the condensed plate presented in the fig.IV-14 (a-b) gives an overview of the real situation on the surface of the plate.

(a)

(b)

Fig.IV-14 (a-b): Photographs of condensing horizontal flat plate with a condensate (a) 2.0 g (b) 2.1 g of condensate on the surface of the plate in flow of 2.5 m/s velocity in two different experiments- (a) CEI-38, and (b) CEI-39.

Fig.IV-15 shows the variation of the velocity from inside the boundary layer to the free flow stream at the centre of the trailing edge. The figure shows a flow of similar nature with a little variation in the velocity, with the same entrance velocity in both experiments. Usually, it was observed that the thickness of the film condensate layer was in the range 1 to 3 mm. Fig.IV-14 already gives an idea of the film on the surface of the plate, which was born by the coalescence of drops in different ways, and fig. IV-13 shows that the flow profile very close to the surface, present little differences proven by the visible observation of the condensate.

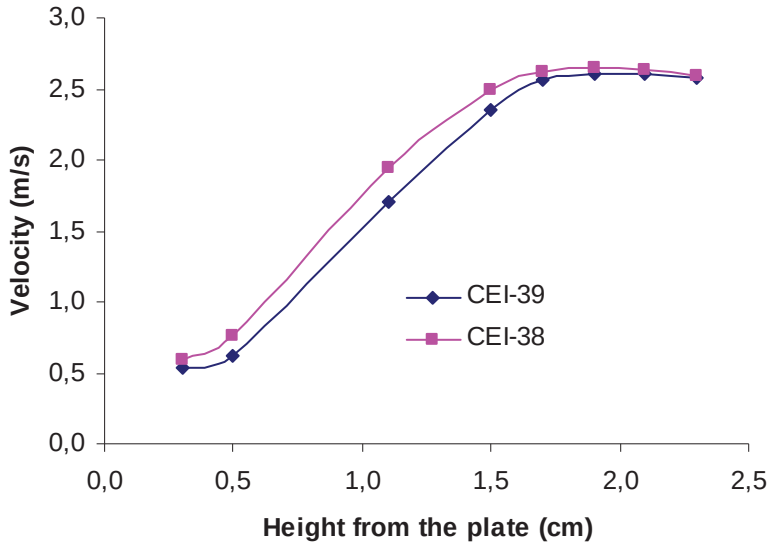

Fig.IV-15: Comparative plots of two experiments (CEI-38, CEI-39) showing variation of velocity at last middle point of the plate (i.e. X = 5.0 cm, Y = 2.5 cm, Z = 0.3 – 2.3 cm) from inside the boundary layer to free flow stream.

4.5 Flow about blunt-faced flat plate

The numerical and experimental studies of blunt-faced flat plates, placed in a uniform stream, have already been discussed by several workers (Ota and Kon 1974, Hwang et al 1996, 2001, Velayati & Yaghoubi 2005, Marty et al 2008). Most of the numerical studies dealt with two-dimensional flow structures, a semi-infinite flat plate of finite thickness, which kept in a uniform parallel stream of approaching flow to the plate surface (Hwang et al 1996). The plate which we have used first in our experiments (without cooling arrangement) had an aspect ratio (Length (*L*)/ thickness (*e*)) L/e=17, with a conical flow structure from the leading edge to the rear of the plate.

The structure used for the condensation of humid air had a much lower aspect ratio. The velocity profiles are described in section 4.3.1.1.2. We have also performed very few experiments for the visual observation of the flow, by using a very light weight small piece of cork on the surface of the water condensate, when the surface was covered by film of water. The air velocity inside the wind tunnel varied from very low velocity less than 0.5 m/s to more than 4.0 m/s in this position. The motion of this piece of cork was filmed. It was observed that as the water flow moves from the leading edge to the rear part of the plate, it

circulated from the outer side to the centre part of the plate and again returned back to its previous path and re-circulated. Similarly on the other half part of the plate, the cork repeated this motion describing oval shapes. The velocity profile plotted at different heights above the flat plate showed that very close to the plate surface and around 1.0 cm from the leading edge, the velocity was always smaller near the centre of the plate at the same height. As only one component hot-wire sensor were used, we do not have information regarding the direction of the flow at a particular point. Thus, the visual observation experiments showed that it was not only a conjecture but a proven re-circulating flow around this area. It arose from the separation of the boundary layer and, its subsequent reattachment occurred due to the decrease in velocity caused by a positive pressure gradient on the front surface.

As specified by Velayati & Yaghoubi (2005), the excess of pressure in the stream-wise path and adverse pressure towards the side surfaces cause the flow to separate from the leading edge, and after a distance there is a possibility to reattach to the plate surface, but in this case the size of the device as the horizontal flat surface was 8.3 cm long, and the actual size of the condensing unit was just 5.0 cm upstream. Perhaps it could reattach towards the rear edge of the active plate or beyond the surface of the heat sink, where we did not perform measurements.

Fig.IV-16 (a, b, c, d, e, f) represents one of our velocity measurements for the mean entrance velocity 2.5 m/s, at different heights from the surface of the condensation unit. The measurements were taken at 25 points on each plane of particular height. Normally, height measurements were taken every 2 to 5 mm, and few of them are given here in fig.IV-16. As seen on the figure the flow close to the plate surface, 0.1 cm and 0.3 cm height from plate surface, is much stringer on one side (x, 0), which was may be, because of the sponge alignment along the vertical surface of the Peltier element or because of the imperfection in cutting or machining the edge of the square shape flat plate.

Further up (0.7 cm and 0.9 cm) the plots IV-16 c, d show very low velocity zone at around 4.0 cm from the leading edge of the plate, which might reflect a re-circulating zone and then the velocity increases, which could indicate a reattachment region as described by the earlier workers for a blunt-faced flat plate (Hwang et al 1996, Velayati & Yaghoubi 2005) and discussed here above. At 1.9 cm and 2.1 cm (fig.IV-16 (e, f)) the velocity profile seems more uniform and reaches the mean entrance velocity. Since, the velocity measurements

consider only one component, it is difficult to conclude on a re-circulating flow and on its direction, but after the visualization of the floating cork experiment, it is fair to assume that there is a circulating effect before the centre part of the blunt-faced structure.

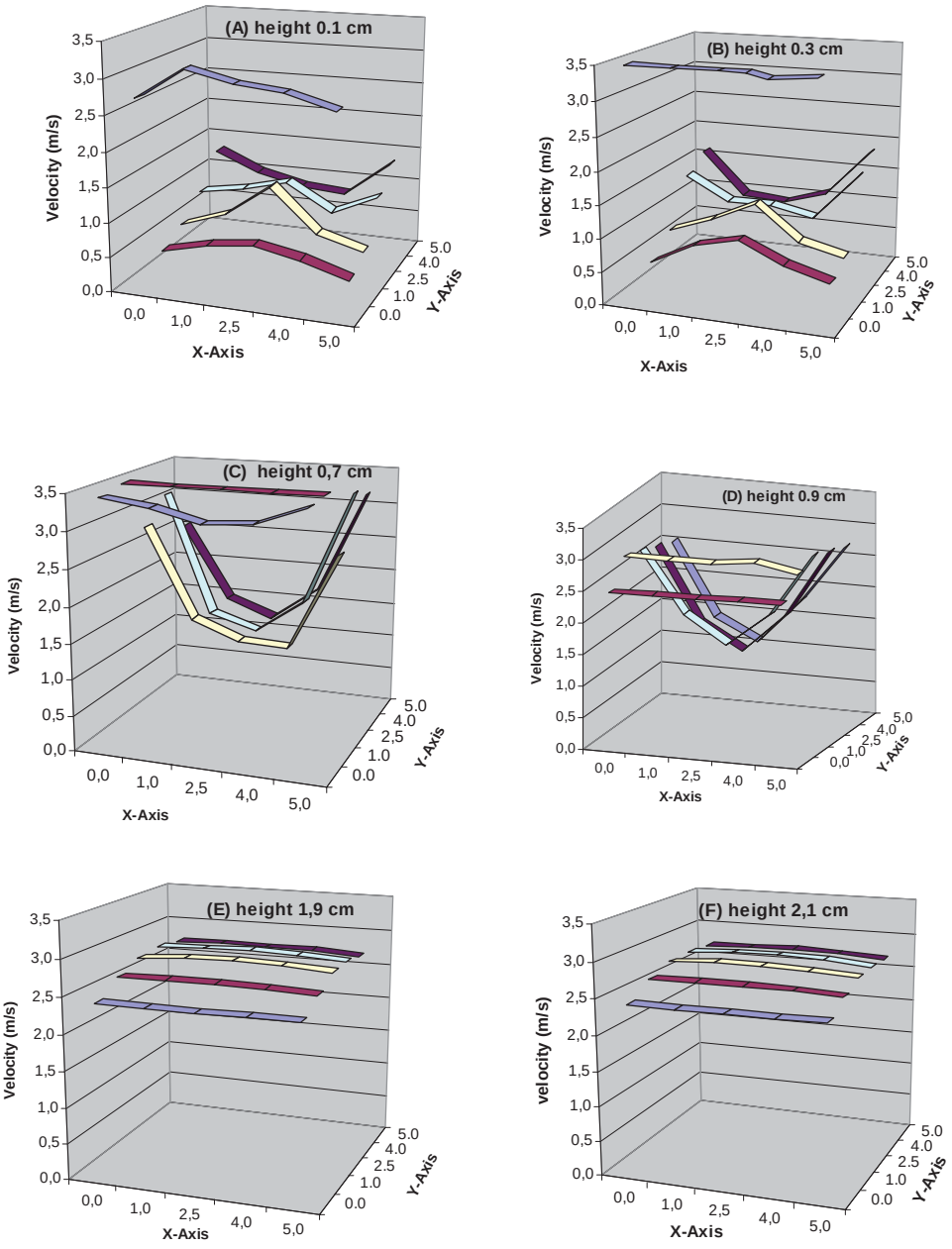

Fig.IV-16 (a, b, c, d, e, f): 3D curves of the velocity profile at fan frequency 32.1 Hz and mean entrance velocity 2.5 m/s at different heights from the surface of the plates. X and Y – Axis representing the plate cross section on which the velocity measurements have been taken. Z- Axis as velocity (m/s).

The experimental device used in here (Fig.II-5 (b)) has a complex geometry, as opposed to a classical blunt bodies and it is difficult to choose the thickness of the blunt face, which has a maximum height of 6.6 cm including a 2.5 cm high part composed of dense fins (heat sink), and more than 6.0 cm^2 open area without any obstacle, below this part and above the connecting rod. To study the reattachment phenomenon of the blunt-faced flow, the earlier workers (Chen and Chieu 1997, Ota and Itasaka 1976, Hwang et al. 1996, Marty et al. 2008) considered the evolution of the pressure along the plate as an indicator, and they have suggested that a sudden increase in the pressure appeared between $2x/e = 6$ and 13 (where x is the axial coordinate along the plate length and e the thickness of the plate). This increase in pressure will affect the heat and mass transfer as a consequence of the flow of the external fluid, which is projected towards the surface through the boundary layer around the reattachment area by the recirculation phenomenon.

4.6 Conclusion

The above experimental discussions presented an experimental facility that is needed to evaluate accurately the mass transfer coefficients of condensation on small obstacles with a precise control and measurements of the velocity profiles and turbulence intensity around such obstructions. It involves a climatic wind tunnel facility; it has been tested with a flat plate in dry and wet conditions. At low turbulence intensity the average velocity profile inside the boundary layer can be roughly approximated by the Blasius' solution even if the boundary layer is 5-10 % thicker and if there is already a presence of turbulent fluctuations inside that layer. But for moderate turbulence intensity, the velocity boundary layer thickens a lot with the free stream velocity. The understanding of the coalescence and growth of the condensate drops during the wet condition is important, because it affects the velocity profile and turbulence intensity very close to the surface of the plate. Since, the evaporation of these condensate drops different in shape and size, takes diverse timings to clear the surface on which it appears. In the literature it is also termed as surface wetness or leaf wetness in a plant canopy studies to describe the affect of pathogens in plants because the predominant plant organ is a leaf and also most pathogens infect the leaves. The size and shape of drops on leaf surfaces strongly affect their persistence (Brain and Butler 1985). Surface wetness has been used by several authors in the past when discussing leaf wetness (Deshpande *et al.* 1995, Huber and Gillespie 1992). The mathematical model for wheat and maize for maximum wetness duration for water drops on leaves in the field and drop size distribution have been

discussed in detail by Brain and Butler (1985).

The geometry used for the condensation experiments was a blunt-faced flat plate, and the flow envisaged on the surface of the flat plate, describes the velocity measurements considering only one component, it is difficult to conclude on a re-circulating flow and on its direction, but after the visualization of the floating cork experiment. It is fair to assume that there is a circulating effect before the centre part of the blunt-faced structure. This kind of study will help for the validation of a low *Re* turbulence model used for CFD simulations to predict the flow in a space environment (greenhouse or planetary outpost).

Chapter V

Condensation experiments in an open environment

5.1 Introduction

To initiate the study on the mass flux by condensation of humid air and also to verify the concept, the experimental device has been primarily tested inside a room with no air-conditioning system, i.e. where the ambient environment changed according to the external weather conditions. Thus, the temperature, hygrometry and hydrodynamic conditions were uncontrolled. In this phase of work the goal was first to characterize each stage of the design, to select the substrate (material, size, thickness, and preparation), heat sink (material, size, and suitability for use in the wind tunnel and outside), and to calibrate the measurements of all the various sensors. The choice of the plate material, size, thickness and other parameters are described in detail in the chapter III of this thesis. A photograph of the experimental arrangement is given in fig.V-1.

For these experiments the condensing unit was directly placed on a balance (Ohaus Navigator N24120, precision of ±0.01 g). A small fan of the size of the heat sink (12 V input voltage) was used to improve heat dissipation and to induce a non laminar flow of humid air above the plate. Normally, we have performed 3 to 8 h experiments for the collection of sufficient amount of condensate on the surface of the small flat plate, and this is the time, which allows the condensation process to give measurable quantity of water condensate for further analysis, which can be weighed accurately on the balance. A hotwire sensor (Testo) has been used to measure the air velocity near the surface of the plate and, also the ambient temperature. The relative humidity and ambient temperature of the room were determined by a dual channel electronic sensor (Testo 175-H2 and 175-S2).

5.2 Initial condensation experiments in ambient conditions

The average air velocity of the flow induced mainly by the fan was almost constant during all the experiments. More than 15 experiments were carried out with three different sizes of the plates. Each experiment was performed in different ambient atmospheric conditions, which depended on the weather of the day.

Fig.V-1: Photograph of the experimental arrangement in LGCB.

For the condensation experiments, we have used a 3 mm thick plate, the measurements of the temperature distribution on the surface of this flat plate and on the surface of the Peltier element only were carried out in the ambient air and they showed that the top surface temperature was more or less homogeneous for a 3 mm thick plate (variation of less than 1°C for a plate of 5 x 5 cm^2), in comparison to the plates of smaller thickness, which has already been discussed in detail in chapter II.

Tables 1 A and 1 B give the details of the experiments carried out in varying weather conditions. These condensation experiments were performed for the air velocity range of 1.0-1.2 m/s over the surface of the square flat plates of three dimensions 5 x 5 cm^2, 4 x 4 cm^2, and 3 x 3 cm^2. The duration of the experiments was varied from 3 h to over 9 h. The maximum amount of condensate collected was 4.8 g on the 5 x 5 cm^2 plate and the minimum 0.8 g. The bold face values in the controller temperature column shows that the controller temperature was below the surface of the plate varied during the experiments in order to keep the temperature difference stable between the dew point and the active plate. The Reynolds number $\mathrm{Re} = (\rho_\infty v L) / \mu_\infty$ for these studies was in the range 3700-4000, 3100-3200, and 2300-2400 respectively for 5 x 5 cm^2, 4 x 4 cm^2, and 3 x 3 cm^2 plates, where L is the length of the plate and the Schmidt number $Sc = \mu_\infty / (\rho_s D)$ was 0.6.

Table V - 1A Condensation Experimentation (LGCB) - (approx. wind velocity 1.0-1.2 m/s)

Peltier Element and Plate size	Plate Thickness	Amount of cond collected	Data Acquisition time	Ambient Temp Range (T_a)	Dew Point (T_d)	Controller temp (T_c)	Surface temp (T_s)	Temp Diff (T_d-T_s)	Temp Diff (T_a-T_s)	Relative Humidity	Average Partial P diff P(T_a)-P(T_s)	Exp no.	Date Performed
1	2	3 g	4 h-min	5 mean(°C)	6 mean(°C)	7 °C	8 °C	9 mean(°C)	10 mean(°C)	11 mean(%)	12	13	14
50 x 50 Peltier		0,8	5-22	**24,1**	**12,8**	11,4	11,9	**0,8**	**12,7**	**47,8**	**0,0355**	**CEL-12**	03/09/2009
50 x 50 Plate	3 mm	1,3	3-00	**24,1**	**11,9**	10,0	10,5	**1,4**	**14,1**	**45,3**	**0,0945**	**CEL-13**	04/09/2009
		1,5	5-17	**27,2**	**15,0**	13,5	14,5	**1,0**	**13,7**	**46,1**	**0,0526**	**CEL-5**	13/08/2009
		1,8	3-08	**26,7**	**17,7**	15,0	15,5	**2,2**	**11,7**	**56,0**	**0,1891**	**CEL-3**	07/08/2009
		1,9	9-23	**24,6**	**8,3**	**6,5**	6,9	**1,3**	**18,1**	**34,1**	**0,0457**	**CEL-14**	07/09/2009
		2,1	7-54	**25,9**	**14,5**	12,6	13,1	**1,4**	**13,3**	**47,6**	**0,0725**	**CEL-11**	02/09/2009
		2,6	9-13	**24,4**	**9,2**	**6,7**	7,2	**1,9**	**17,7**	**37,2**	**0,1213**	**CEL-15**	08/09/2009
		1,8	4-54	**25,7**	**14,8**	12,5	13,0	**2,3**	**13,2**	**49,1**	**0,1764**	**CEL-9**	26/08/2009
		2,7	7-30	**24,5**	**10,4**	8,0	8,5	**1,9**	**16,5**	**41,3**	**0,1618**	**CEL-16**	09/09/2009
		2,7	5-52	**26,5**	**17,7**	15,0	15,5	**2,2**	**11,5**	**56,7**	**0,2088**	**CEL-4**	08/08/2009
		3,1	4-44	**29,4**	**17,6**	14,0	14,5	**3,0**	**15,4**	**46,2**	**0,2484**	**CEL-7**	18/08/2009
		4,0	8-17	**26,9**	**14,1**	10,0	10,5	**3,6**	**16,9**	**42,8**	**0,2497**	**CEL-10**	27/08/2009
		4,8	8-32	**29,8**	**15,1**	11,0	11,5	**3,6**	**18,8**	**38,0**	**0,2381**	**CEL-6**	17/08/2009
40 x 40 Peltier		0,9	6-38	**21,6**	**2,0**	-3,0	-2,5	**4,5**	**24,6**	**24,9**	**0,1371**	**CEL-20**	19/10/2009
40 x 40 Plate	3 mm	1,3	6-23	**22,5**	**7,6**	**2,7**	3,2	**4,4**	**19,8**	**37,1**	**0,2440**	**CEL-23**	22/10/2009
		1,6	8-26	**21,1**	**6,9**	2,0	2,5	**4,4**	**19,1**	**38,6**	**0,2353**	**CEL-21**	20/10/2009
		2,1	9-05	**21,4**	**8,7**	**3,7**	4,2	**4,5**	**17,7**	**43,9**	**0,2970**	**CEL-22**	21/10/2009
30 x 30 Peltier		0,9	8-16	**20,2**	**0,8**	-4,0	-3,5	**4,3**	**25,2**	**27,3**	**0,1770**	**CEL-18**	15/10/2009
30 x 30 Plate	3 mm	1,0	6-09	**21,2**	**5,8**	**2,1**	2,6	**3,2**	**-2,1**	**36,7**	**0,1846**	**CEL-17**	14/10/2009

Table V - 1B		Linear Curve Fit		Exp average rate of condensation				Average values of theoretical calculation					
Exp no.	Date Performed	Slope	Coffs. of Regression	(Tot wt / Tot time)	Mass flux	$((m_2-m_1)/(t_2-t_1)$	Mass flux	Rate of condensation	Mass flux	Diffusivity of water vapour in air	Schmidt number at surface	Reynolds number	Sherwood number
13	14	15 (g/h)	16 R^2	17 (g/h)	18 ($Kgm^{-2}s^{-1}$)	19 (g/h)	20 ($Kgm^{-2}s^{-1}$)	21 (g/h)	22 ($Kgm^{-2}s^{-1}$)	23 m^2/s	24 Sc	25 Re	26 Sh
CEL-12	03/09/2009	0,0709	0,6889	0,3945	4,38E-05	0,1977	2,20E-05	0,0406	4,51E-06	2,34E-05	0,6144	3855,07	35,35
CEL-13	04/09/2009	0,4109	0,9815	0,3679	4,09E-05	0,5014	5,57E-05	0,1075	1,19E-05	2,32E-05	0,6139	3855,06	35,32
CEL-5	13/08/2009	0,2719	0,9836	0,3771	4,19E-05	0,2630	2,92E-05	0,0603	6,70E-06	2,38E-05	0,6150	3780,82	35,07
CEL-3	07/08/2009	0,5398	0,9991	0,5221	5,80E-05	0,4828	5,36E-05	0,2181	2,42E-05	2,40E-05	0,6153	3794,50	35,17
CEL-14	07/09/2009	0,1691	0,9103	0,3024	3,36E-05	0,2010	2,23E-05	0,0511	5,68E-06	2,27E-05	0,6125	3844,82	35,18
CEL-11	02/09/2009	0,2136	0,8189	0,2046	2,27E-05	0,3173	3,53E-05	0,1005	1,12E-05	2,36E-05	0,6147	3814,88	35,20
CEL-15	08/09/2009	0,2832	0,9343	0,4057	4,51E-05	0,3182	3,54E-05	0,1361	1,51E-05	2,28E-05	0,6126	3848,21	35,20
CEL-9	26/08/2009	0,3736	0,9962	0,4292	4,77E-05	0,4052	4,50E-05	0,2239	2,49E-05	2,35E-05	0,6146	3944,13	35,78
CEL-16	09/09/2009	0,3248	0,9717	0,5081	5,65E-05	0,3648	4,05E-05	0,1824	2,03E-05	2,30E-05	0,6132	3846,00	35,23
CEL-4	08/08/2009	0,4766	0,9616	0,5967	6,63E-05	0,4240	4,71E-05	0,2410	2,68E-05	2,40E-05	0,6153	3797,46	35,19
CEL-7	18/08/2009	0,6624	0,9851	0,7977	8,86E-05	0,6888	7,65E-05	0,2839	3,15E-05	2,38E-05	0,6151	3736,39	34,87
CEL-10	27/08/2009	0,4892	0,9977	0,4424	4,92E-05	0,4771	5,30E-05	0,2818	3,13E-05	2,32E-05	0,6139	3793,68	35,03
CEL-6	17/08/2009	0,6178	0,9570	0,6659	7,40E-05	0,5349	5,94E-05	0,2676	2,97E-05	2,34E-05	0,6143	3728,15	34,76
CEL-20	19/10/2009	0,1318	0,9936	0,1527	1,70E-05	0,1364	2,37E-05	0,1069	1,86E-05	2,14E-05	0,6069	3130,84	31,55
CEL-23	22/10/2009	0,2142	0,9902	0,2247	2,50E-05	0,2105	3,65E-05	0,1965	3,41E-05	2,22E-05	0,6106	3113,77	31,58
CEL-21	20/10/2009	0,1829	0,9894	0,2122	2,36E-05	0,1826	3,17E-05	0,1874	3,25E-05	2,21E-05	0,6102	3139,85	31,70
CEL-22	21/10/2009	0,2374	0,9883	0,2671	2,97E-05	0,2300	3,99E-05	0,2379	4,13E-05	2,23E-05	0,6112	3134,53	31,71
CEL-18	15/10/2009	0,1222	0,9192	0,1117	1,24E-05	0,1245	3,43E-05	0,0894	2,76E-05	2,12E-05	0,6061	2370,40	27,44
CEL-17	14/10/2009	0,1658	0,9782	0,1489	1,65E-05	0,1619	5,00E-05	0,0994	3,07E-05	2,21E-05	0,6102	2353,65	27,45

The description of columns given in the Table V-1A and 1B are:

1. Size of the used the Peltier element and the aluminium plate (mm)
2. Thickness of the plate (mm)
3. The total weight of the condensate collected on the plate during the experiment (g)
4. The total condensing time on the plate to collect above amount (h-min)
5. Ambient temperature far from the condensing plate (°C)
6. Dew point (°C)
7. Temperature below the surface of the plate set by the Controller (°C)
8. Surface temperature taken as temperature set on the controller plus 5 °C.
9. Temperature difference between dewpoint (T_d) and surface temperature (T_s)
10. Temperature difference between ambient temp and surface temp (°C)
11. Relative humidity
12. Average of difference in partial pressure at ambient temp and surface temp
13. Condensation Experiment reference no performed in the laboratory
14. Date performed
15. Gradient of the plots between amounts of condensate versus total time of exp
16. Coefficient of regression for linear data fit.
17. Total weight of condensate collected on the plate divided by total time of exp
18. Mass flux calculated by column 17
19. Difference in mass between two consecutive readings divided by time difference for same period
20. Mass flux computed by the data of column 19
21. Rate of condensation calculated theoretically
22. Theoretical calculation of mass flux
23. Diffusivity of water vapour in air (m^2/s)
24. Schmidt number at surface temperature (*Sc*)
25. Reynolds number (*Re*)
26. Sherwood number (*Sh*)

5.3 Results and Discussion

Fig.V-2 (a-b) and fig.V-3 (a-b) shows the plots of condensation experiments carried out on two different days with variable hygrometric and hydrodynamic atmospheric conditions. These experiments were performed with a 5 × 5 cm^2 flat plate in horizontal

position for temperature differences, $\Delta T_s = T_d - T_s$ (between the surface temperature (T_s) and the dewpoint (T_d)) of approximately 1.5 °C. The variation in relative humidity was from 2 to 15% and in ambient temperature less than 10% according to the local weather conditions during day time, sometimes both relative humidity and temperature were increased or decreased simultaneously, other times one increased and the other decreased, which created a difference in dewpoint temperature by less than 1°C up or down during the experiment. However, it was important to maintain the temperature of the active surface sufficiently below the dewpoint temperature for the condensation of water vapour in air to proceed (Fontaine and Tiwari 2010).

It is observed from fig.V-2 (a) (from Exp no CEL-5) that the amount of condensate increases with time and the temperature difference (ΔT) between the dewpoint and the temperature set on the controller varies from 1.2 °C to 1.8 °C during the experiment. The surface temperature (T_s) The ambient temperature was increased by 8% and the relative humidity decreased by almost 15% during the 5 h experiment, which provided a decrement in the initial dewpoint value by 0.5 °C. The amount of condensate collected during this time was 1.5 g with an average rate of condensation of 0.26 g/h. Fig.V-2 (b) (from Exp no CEL-14) shows another experiment with similar weather conditions, in which the temperature difference (ΔT) first decreased then went up by 0.7 °C and then again decreased by 0.8 °C, it is because the ambient temperature went up 5%, but the relative humidity was slightly increased and again decreased by 5%. The dewpoint decreased during 1 h and then increased; still the temperature difference remained below 1 °C during 5 h experiment, which resulted in a collection of 1.4 g of condensate with an average mass rate of 6.62×10^{-5} kg m^{-2} s^{-1}.

Fig.V-3 (a, b) shows the mass flux and temperature difference as a function of the total time of the experiments. Fig.V-3 (a) indicates that the rate of condensation follows the trend of the temperature difference except after 4 h, where the measured rate of condensation decreased even though the temperature difference increased. Fig.V-3 (b) shows that the rate of condensation has more or less a similar behavior as the temperature difference ΔT. As the temperature difference starts decreasing, the condensation rate decreases significantly, because of the low temperature difference and the reduced active surface area left on the surface of the plate as the condensate/air interface may not be cold enough to induce condensation.

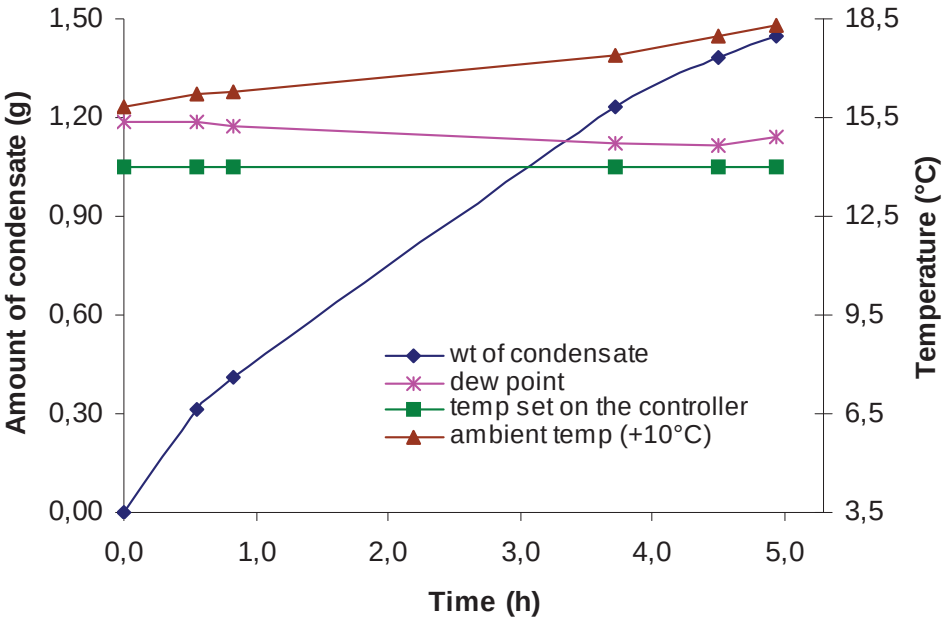

(a)

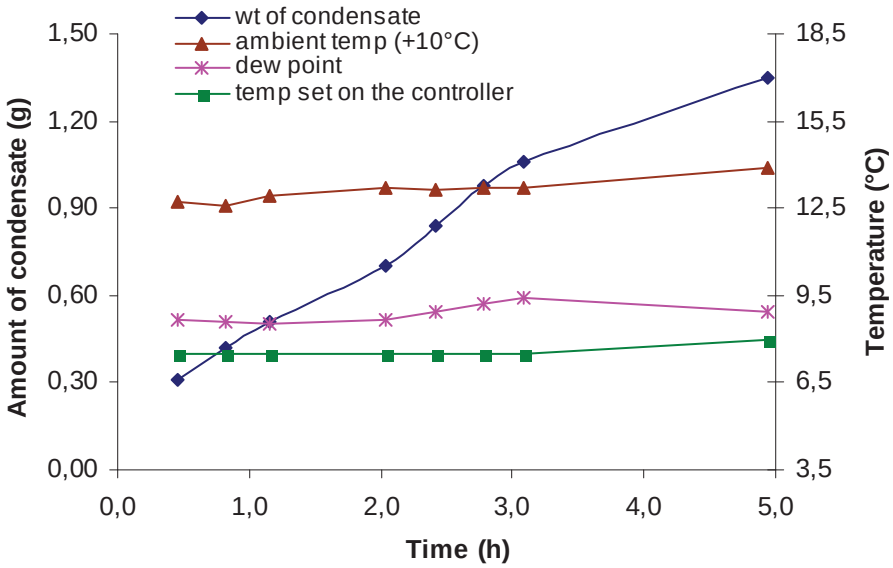

(b)

Fig.V-2(a-b): Amount of condensate and temperature as a function of time. The value of ambient temperature is also given in the graph after reducing 10 °C to fit in scale (Ambient Temperature = T (in Plot) + 10 °C).

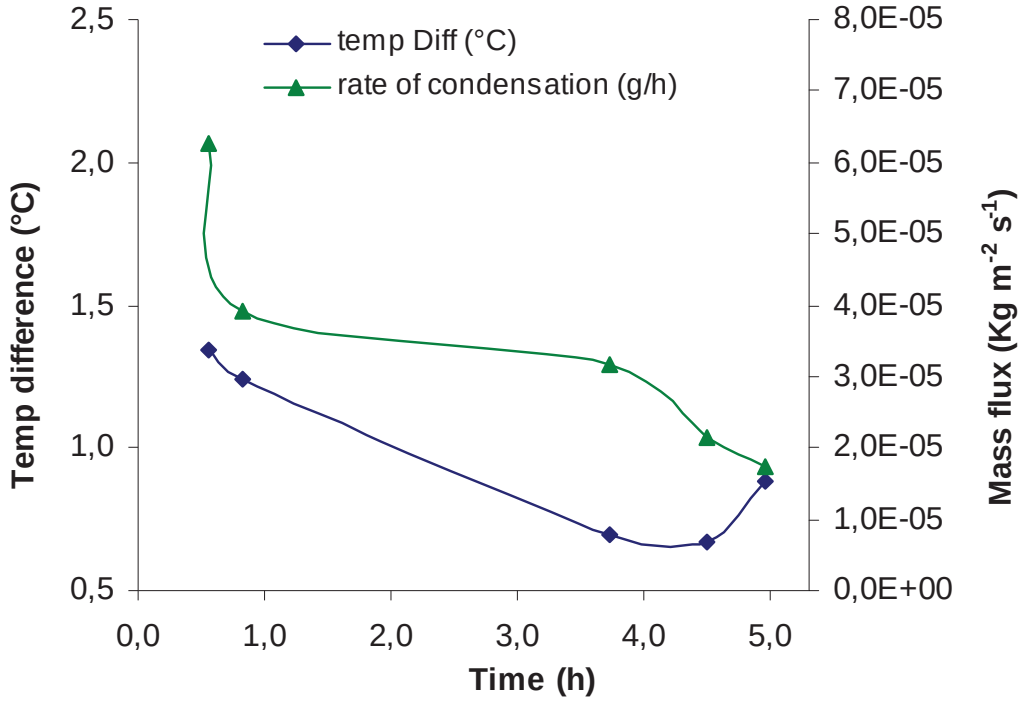

(a)

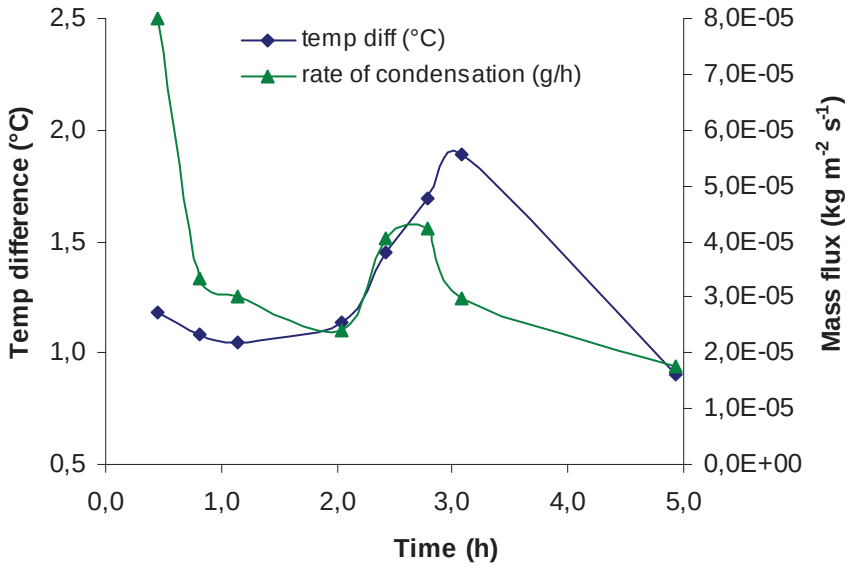

(b)

Fig.V-3(a-b): The temperature difference and mass flux as a function of total time.

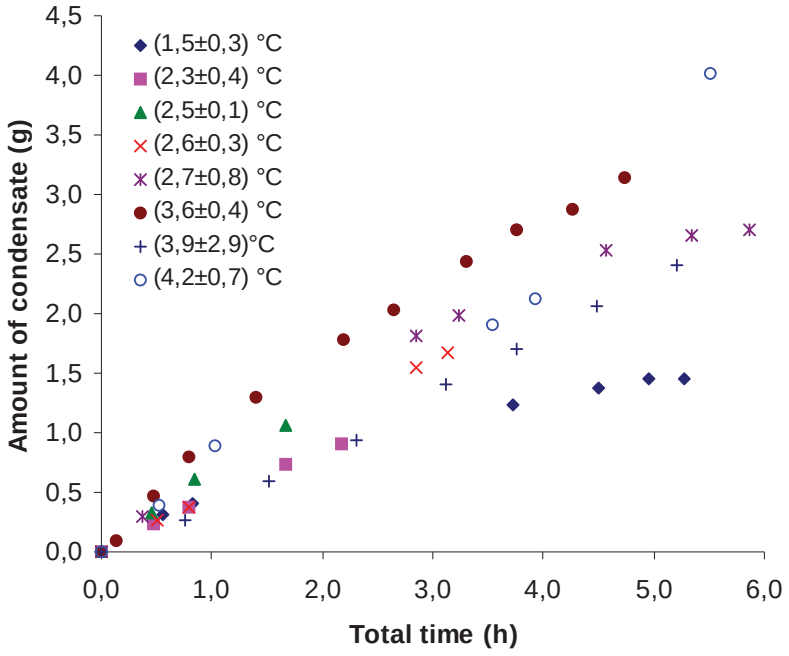

(a)

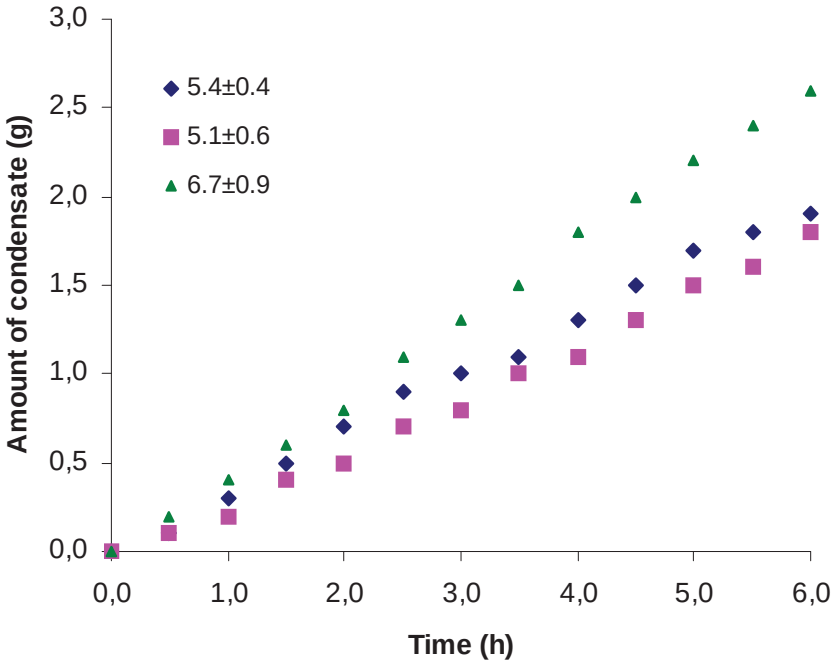

(b)

Fig.V-4: (a) Amount of condensate as a function of total time of experiment for 8 experiments in open environment (b) inside the wind tunnel for 3 experiments at given temperature differences

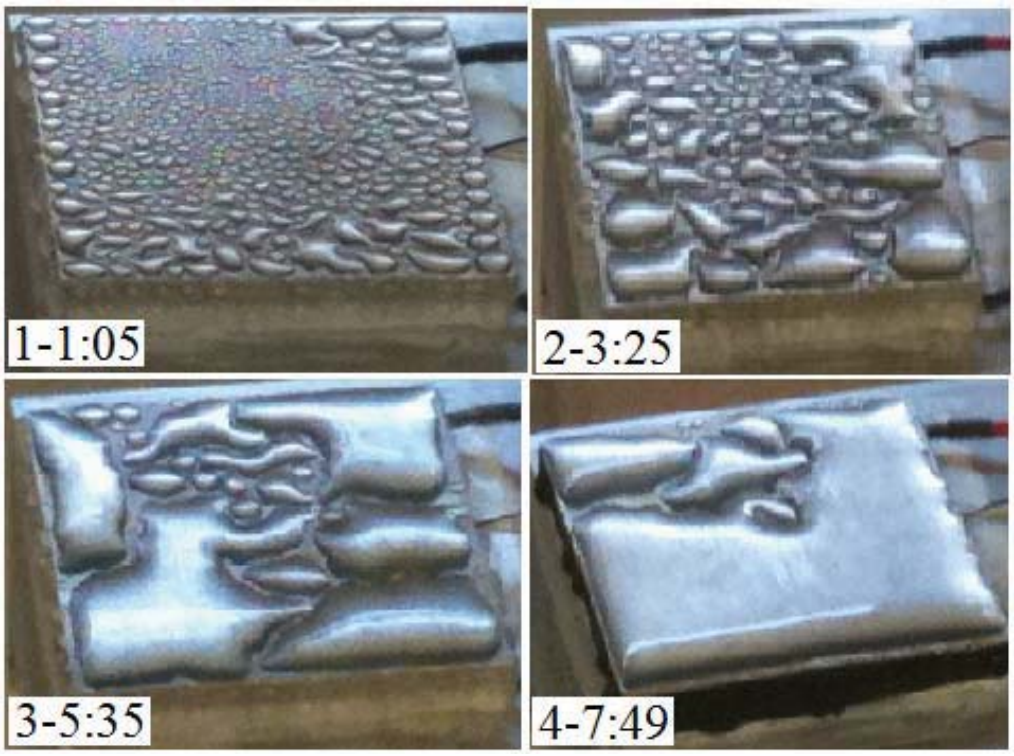

Fig.V-5(1-4): Photographs of the flat plate with condensation on it at different duration of time (in hours) from starting point of condensation.

Fig.V-4 (a-b) has been given here for the comparison purpose to show how the amount of collected condensate is significantly affected by a variation in different environmental parameters. Fig.V-4 (a) shows the variation of the amount of condensate versus time for several average temperature differences ΔT in an open environment. The trends are affected by the hygrometric conditions, which are not completely stable. Fig.V-4 (b) indicates more regular variations inside the controlled wind tunnel for three different experiments of dissimilar temperature differences, which indicates that on increasing the temperature difference, the rate of collection of condensate also increases accordingly. However, the main behavior indicates the sensitivity of the slope and, thus, of the mass flux to the temperature difference as expected. The evolution in time in open air is also influenced by the active area which decreases with time as condensation covers more and more the flat plate and after long duration we can observe some type of saturation which could be related to the fact that most of the plate surface is covered with water. It is also worth noting that the shape of the condensate is also strongly influenced by the physico-chemical properties of the aluminium plate (contact angle, etc.). Initially drop-wise condensation is induced (Fig.V-5 (1)), but after a few hours (Fig.V-5 (3)), a large part of the plate is covered by mainly 4-5 big drops of water

which can flow out of the plate or be thrown out by the air flow. These complex phenomena greatly affect the heat-mass transfer at the surface of the plate. Some evaporation may also proceed at the condensate / air, because of the forced flow.

Long duration experiments were also conducted for more than 9 h to know the effect of condensation on the plate for extended time. But for the long duration the parameters like ambient temperature and relative humidity varied much and it affected the dew point a lot. To keep the temperature difference stable on the active surface of the plate, sometimes it is necessary to change the regulator temperature setting during the experiment, which affects the rate of condensation as well. Figure V-6 (a-b) (exp no CEL-15 in Table 1A, 1B) given here is such an experiment.

In fig.V-6 (a), the temperature difference was chosen over 2°C between the dewpoint and the temperature set by the controller. Due to increases in the relative humidity and ambient temperature the dewpoint temperature increased and the difference increased as well and up to more than 3 °C within 3 h of the experiment. After 3 h the temperature difference went above 3.6 °C, then, I have increased the controller temperature to keep the difference between 2 °C and 3 °C. And after 4 h the relative humidity started decreasing, but the ambient temperature was continuously increased from the beginning, due to this the difference in dewpoint temperature gradually increased till almost after 4 h and then started to decrease. It affected the rate of condensation as it was increasing at the beginning, with a growth rate almost stable but slightly increased because of the increment in the temperature difference. The dew point started to decrease rapidly after 6 h 30 min and the rate of condensation decreased and went down, finally after 9 h of experiment the amount of condensate collected was 2.6 g.

Fig.V-6 (b), gives the variation of the mass flux and temperature difference between the dewpoint and temperature set on the controller with the total time of experiment. In the figure, theoretical and experimental mass flux values have been compared. For the calculation of mass flux, the diffusion coefficients were calculated by using the binary diffusion coefficient of water vapour in air from the kinetic theory of gases (Hirschfelder 1952). The mass flux of water vapour in air was calculated by using the formula (Asano 2006):

$$N_{WV} = \frac{Sh\rho_s D(\omega_\infty - \omega_s)}{L(1-\omega_s)}$$

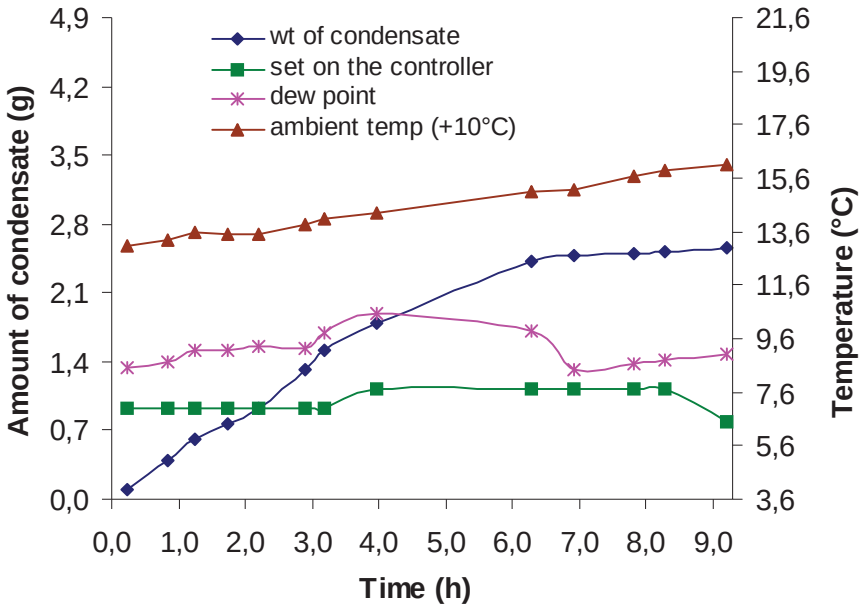

(a)

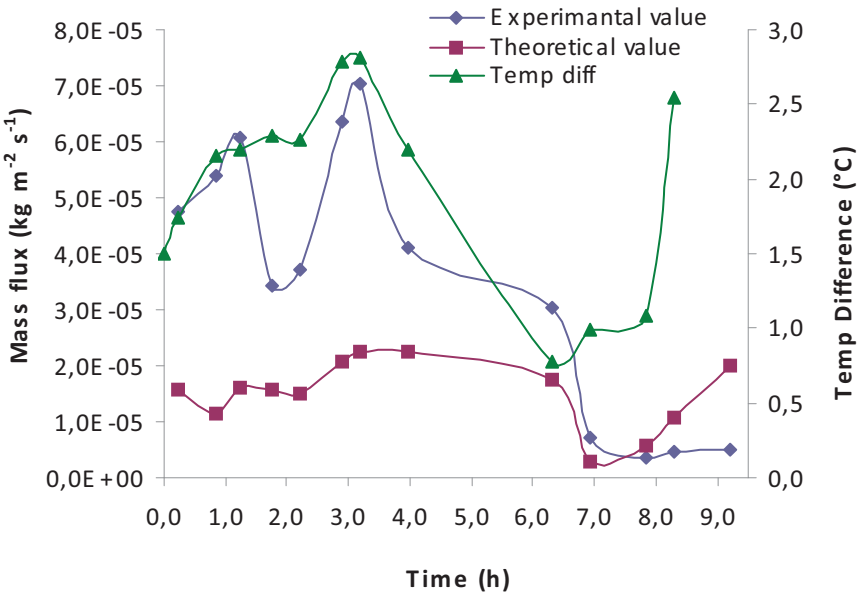

(b)

Fig.V-6 (a-b): a) Amount of condensate and temperature as a function of time. The value of ambient temperature is also given in the graph after reducing 10°C to fit in scale b) Mass flux and temperature difference as a function of time.

where the average Sherwood number is computed from, $Sh(1-\omega_s) = 0.664\,\mathrm{Re}^{\frac{1}{2}}\,Sc^{\frac{1}{3}}$ and the Reynolds number (Re) and the Schmidt number (*Sc*) are standard dimensionless numbers, where the Sherwood number is expressed with mass fraction and not with concentration. That specific relation proposed by Asano (2006) is deduced from the analogy with heat transfer measurement.

From the observation of plot V-6 (b), we can say that the rate of condensation was not stable with time. The figure shows that the experimental value of the mass flux was varied more or less according to the temperature difference, but the theoretical value shows smaller variations. It varied only for large variations of temperature difference. After 6 h and 30 min of experiment, when the temperature difference went down below 2 °C, the mass flux decreased too, however as the temperature difference started increasing again, the rate of theoretical mass flux responded and went up quickly in comparison to experimental value of mass flux, which was stable. That behavior is opposite to the initial one where the experimental mass flux responds promptly and significantly with the temperature difference. That effect could be caused by the amount of condensate collected on the active condensing surface which behaves as a resistance to the response of this temperature difference. Within the first hour of the experiment the theoretical value shows a decreasing nature, this is because of the temporary decrease of relative humidity, almost 5% in the ambient environment within the same period of time. It is worth noting that the rate of condensation is proportional to the active surface and that this area decreases with time as condensation develops. Moreover, some evaporation takes place at the water / air interface. The theoretical value of the mass flux has fewer variations during the whole experiment because the effect of the condensate collected on the surface was not considered in the theory.

The temperature difference and the relative humidity both have an effect on the condensation mass flux but with a different rate. In fig.V-7 (a-b) the experimental and theoretical values of the average mass flux are given as a function of the difference in average partial pressures of water vapour in humid air at ambient temperature and liquid/air interface temperature (in these experiments the interface temperature has been taken as the temperature set on the controller plus 0.5 °C) for 12 experiments with the 5 x 5 cm^2 plate and 4 experiments with the 4 x 4 cm^2 plate. The experimental values are more dispersed in comparison to the theoretical ones, which could be due to the varying open air conditions.

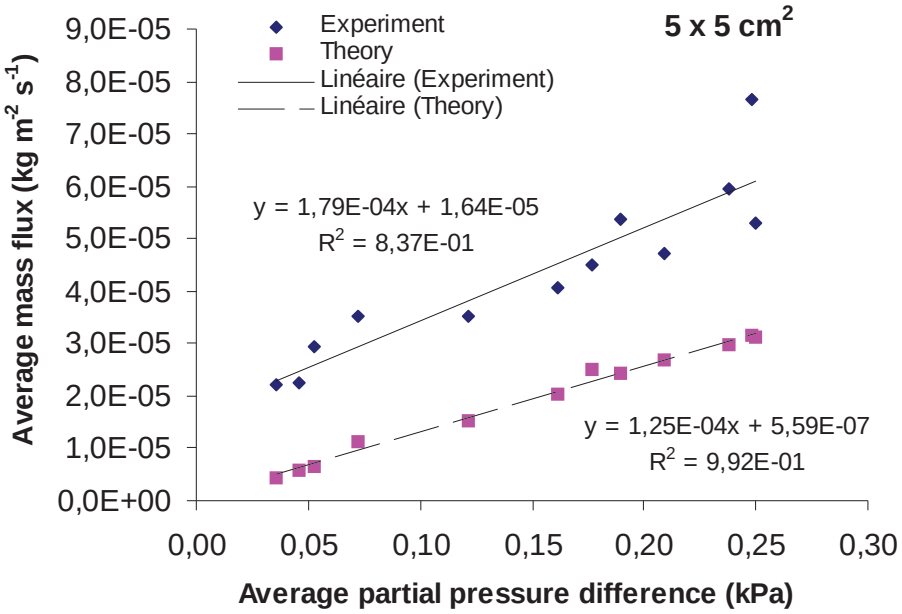

(a)

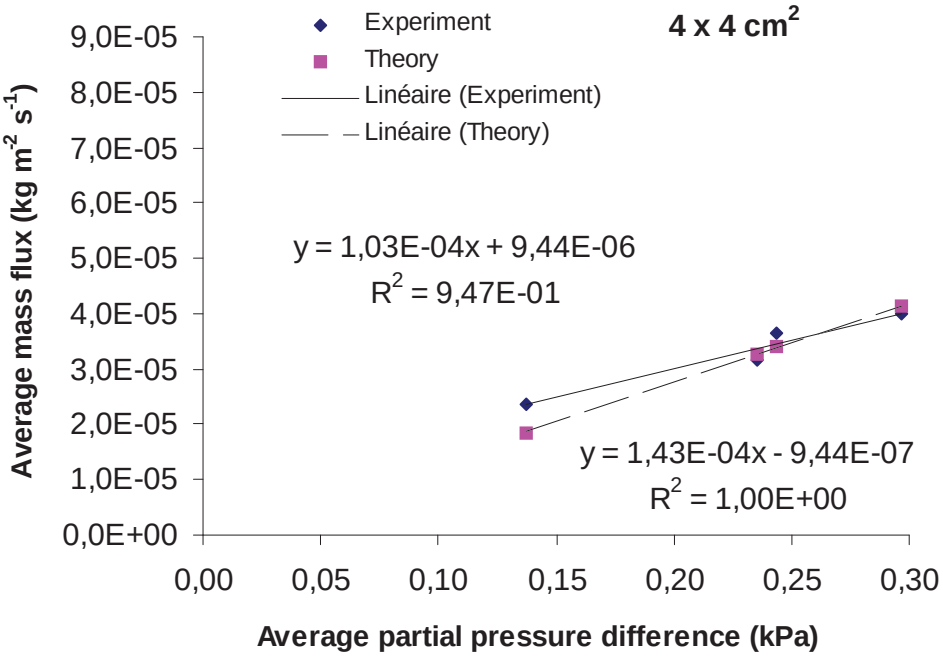

(b)

Fig.V-7 (a-b): Average mass flux as a function of average partial pressure difference at ambient temperature and interface temperature for the plate sizes a) 5 x 5 cm^2 and b) 4 x 4 cm^2 for experimental data shown in Table V-1A, 1B.

The gradient of the average mass flux per unit difference in average partial pressure for the plate 5 x 5 cm^2 is 1.79 x 10^{-4} and for plate 4 x 4 cm^2, it is 1.03 x 10^{-4}. Table V-1A and 1B shows that the experiments were performed for temperature differences above 4 °C with the smaller plate and temperature difference below 6 °C with the 5 x 5 cm^2 plate. This temperature difference on the plate surface plays a key role for mass flux studies, which will be discussed in detail, later on, with the data of controlled wind tunnel experiments.

5.4 Conclusion

The above experimental findings show that the use of a wind tunnel is needed for the precise characterization of mass transfer by condensation of air on surfaces. Also the concept based on thermoelectric cooling and weighing the growing mass of condensation to study mass transfer is validated. Indeed, we have performed experiments in a closed wind tunnel, in which, it is possible to control the psychometric parameters (relative humidity, temperature). This will be discussed in the next chapter.

Chapter VI

Condensation experiments in a controlled wind tunnel environment

6.1 Introduction

Substantially, the physical parameters of the local climate are interdependent and an effort to regulate one of them will affect the others. In an open atmosphere, the local environment is controlled by its position on the Earth surface and time automatically by nature in the form of seasons. To generate a model of fully controlled regulated environments is one of the current challenges, which could regulate all the modes of natural atmospheres. It can be possible to manipulate and regulate its few parameters, in a confined space. We have used a closed circuit wind tunnel for the control of the hygrometric conditions and the hydrodynamics of the air considered at room temperature.

Theoretical and experimental studies of fluid flow and heat transfer from horizontal thin parallel surfaces have been reported in detail in the literature (Collier 1996, Incropera and DeWitt 1990), also the mass transfer analogy has previously been discussed. Most of the first hand experimental studies on mass transfer have been based on the naphthalene sublimation technique (Goldstein and Cho 1995, Hwang et al. 1996). The naphthalene sublimation technique has been used for the specific measurements of the mass transfer, and the full entailments have been documented (Goldstein and Cho, 1995). Sun (2001) did numerical simulation for a similar range of velocities as 0.4 to 7.0 m/s, to study the mass transfer coefficients for kiln stacks by using naphthalene sublimation technique, and discussed the formation of re-circulating eddies near the edges and at different locations, and showed a good agreement with previous experimental workers. In recent years the flow around blunt-faced bodies, placed in a uniform fluid flow, has been extensively studied. A perusal of the pertinent published literature on mass transfer studies by condensation of humid air reveals that the studies on mass transfer phenomena of this configuration are limited.

The present chapter aims to depict the variation of the local mass transfer coefficient during the condensation of water vapour from humid air on a blunt-faced solid surface of the flat plate. The flow was weakly turbulent, a mean velocity of 0.5-3.0 m/s on the horizontal surface of the flat plate, and the Reynolds number was in the range (3-10) $\times 10^3$. Direct measurements of the mass flux were deduced from the weight of the amount of condensate by assuming that the active surface was isothermal. This is equivalent to the constant temperature surface in case of heat transfer experiments. We will discuss here the results for condensation experiments obtained for each velocity measurements and compare the results to theoretical ones.

6.2 Experimental characteristics

6.2.1 Mean velocity control

To plan an experiment in the wind tunnel, the first step is to set a frequency for the fan that drives the flow, which has already been calibrated for chosen velocity (Tiwari and Fontaine 2009), and then leave it running for a few hours, sometimes overnight to homogenize the internal physical parameters of the closed circuit wind tunnel. The condensation experiments have been carried out for five values of the mean entrance velocity i.e. 1.0, 1.5, 2.0, 2.5, and 3.0 m/s inside the wind tunnel, which are dependent on the fan frequency of the wind tunnel as 15.6, 21.5, 27.6, 32.1, 40.0 Hz successively.

6.2.2 Environmental conditions

More than 70 condensation experiments were performed on the horizontal position of the flat plate for the above - mentioned velocities. The temperature and hygrometry of the wind tunnel were controlled well enough, except if there was a very large variation in the exterior ambient weather conditions (humidity or temperature), a noticeable variation in internal parameters has been seen accordingly. The experimental setup of the wind tunnel was situated at INRA, Theix: 45°45’51”N 3°6’1” E, and a height of 852 m from sea level. It was possible to slightly regulate the inside parameters, as temperature could be increased but not decreased, and relative humidity could be decreased by a few percent, and increased as well. The global air volume of the closed loop was about 50 m^3.

6.2.3 Mass condensate measurement

As already discussed in chapter II, the condensing unit including the temperature controller and all accessories were placed on the balance before condensation started. The weight of the condensing unit with all the supporting devices (such as stand, wires, heat sink, and all screws to tighten up the stand, shown in the schematic figure II-5) was approximately 7.2 kg, and with the addition of the temperature controller the balance indicated a weight of approximately 11.8 kg before the fan was turned on. It was proven during calibration process that the air flowing intensity had no influence on the weighing process once stability was reached. The least count of the balance was 0.1 g with a maximum balance limit of 30 kg. The photographs of the arrangement inside the test chamber of the wind tunnel (1), outside but above the balance (2) are shown in fig.VI-1. As it is shown in the photograph the front face of the condensing unit was 7.5 cm wide and 6.7 cm high (or thickness). In this way, the flow of

air was used to cool down the fins of the heat sink and dissipate the heat produced by the thermoelectric elements

Fig.VI-1: Closure view photograph of the experimental arrangement (1) inside the wind tunnel, and (2) below the test chamber, temperature controller with electronic weight balance.

The controller temperature was chosen relatively to the dewpoint temperature. The value of ΔT_c was selected such that, a sufficient amount of condensate could be produced at the end of the experiment. Once the process of condensation had started it was continued regularly till the end of the experiment without interruption apparently. The electronic balance showed an increase in weight, and this weight of condensate was recorded every 30 minutes,

which has been plotted with respect to time, with the temperature set on the controller, the ambient temperature and the dewpoint as secondary axis (such as fig.VI-4). Also the rate of condensation in grams per hour has been calculated in two ways:

$$\text{(i.) Mean rate of condensation (g/h)} = \frac{\text{Total weight on balance (g)}}{\text{Total time (h)}}$$

$$\text{(ii) Rate of condensation (g/h)} = \frac{\text{Increment in mass } (m_2 - m_1)\text{(g)}}{\text{Time taken for increment in that mass } (t_2 - t_1)\text{ (h)}}$$

And then the mass flux in $kg.m^{-2}.s^{-1}$ was calculated using the total area of the condensing surface i.e. 5×5 cm^2.

6.3 Experiments with a mean entrance velocity 1.0 m/s (15.6 Hz fan frequency)

24 condensation experiments were performed for the mean entrance velocity of 1.0 m/s and fan frequency of 15.6 Hz (Fontaine and Tiwari 2010). All the experiments were carried out on a square aluminium flat plate of dimension 5 x 5 cm^2 with a thickness of 3 mm, which was used as an active surface for the condensation. Out of the 24 experiments seven lasted more than 7 hours and 30 minutes, 10 experiments 7 h 30 min, 6 experiments 6 h 30 min and 7 h and one 3 h 30 min. The details of the experimental average values are given in the Table VI-1A and VI-1B.

The experiments started by setting a value of temperature to the controller, below the dew point, and within less than 2 minutes the temperature measured by the thermistor inserted inside the aluminium plate surface below the surface in contact with the flow of air, reached a constant value. The goal is to keep the surface of the aluminium flat plate nearly homogeneous, within less than 1°C of temperature gradient from corners to middle part of the flat plate. The condensation started as the temperature of the plate went below the dew point. After a few minutes of condensation, the first signs of visible drops of condensate (very small in size) appeared on the surface of the plate, the localization of the drops on the surface was scattered, and the size of the drops seemed not homogeneous. The time of appearance of the initial visible drops was dependent on the temperature difference ($\Delta T_c = T_d - T_c$) between dewpoint and the controller temperature. The concentration of condensate drops at the corners of the plate was dense and the drops there were bigger in size at the early stages (fig.VI-2).

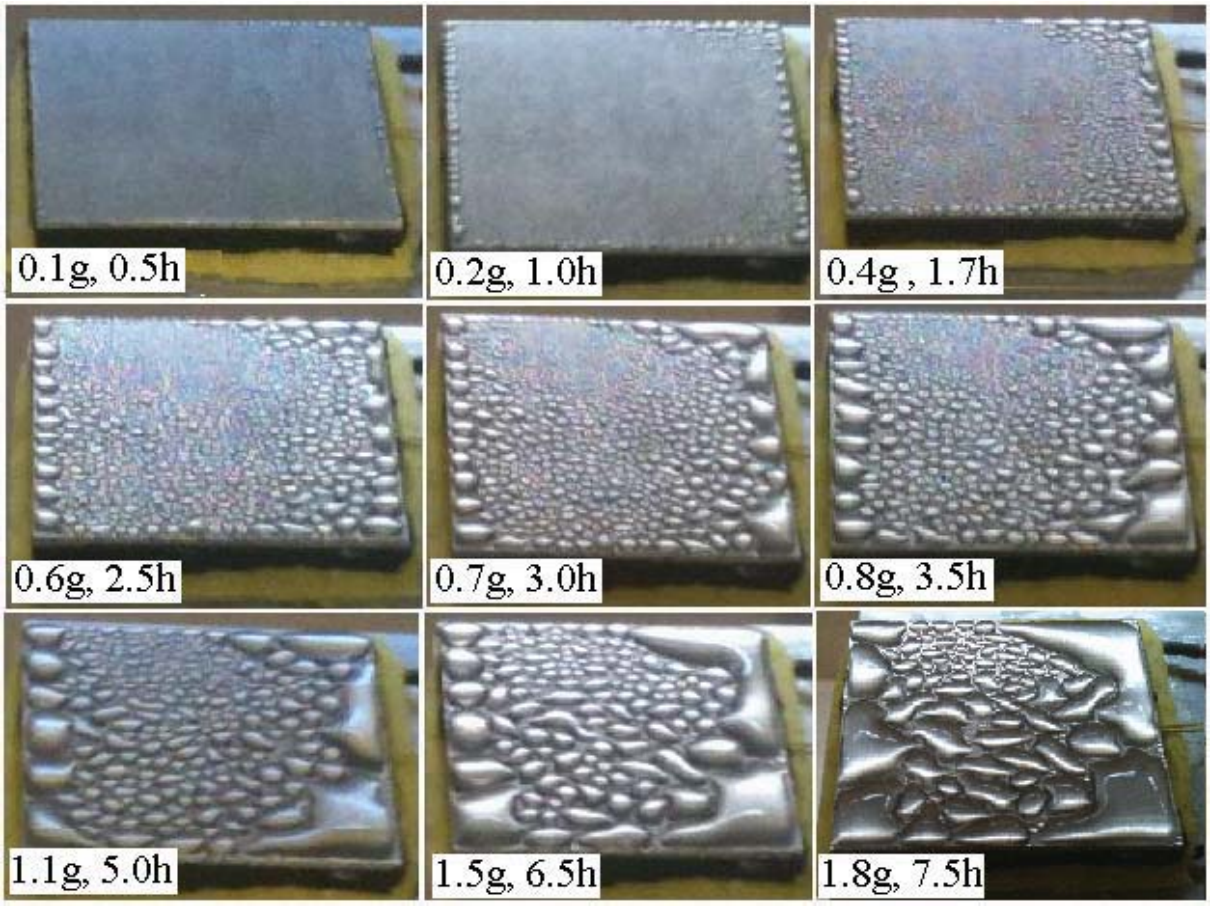

Fig.VI-2: Photographs of the flat plate during condensation at different times, showing how the drops develop and their localization. The corresponding weight of condensate is indicated.

The discontinuous appearance of condensate drops on the surface of the plate continued with respect to time, and the growth of mass on the balance has been recorded every 30 minutes of condensation till the end of the experiment. After performing more than 20 experiments, the data acquisition was changed from every 30 minutes to every 0.1 g mass raise of condensate, because of the least count of the electronic balance. Sometimes, after 30 minutes the balance fluctuated between two values. The 0.1 g mass increase method was more accurate in recording and it also lead to more continuous growth rate in the plots. The growth of small drops into big drops goes through coalescence phases of small drops, it can be easily observed from fig.VI-2. For similar atmospheric conditions the coalescence of drops was not always similar, and has shown a little influence of the turbulence of the velocity profile on the surface of the plate within the boundary layer.

Most of the experiments for these mean velocity range (0.5 – 3.0 ms^{-1}) were carried out for more than 7 h and 30 minutes. Moreover, it appeared that after the first hour a small number of drops of the condensate fell down on the surface of the heat sink or inside the

tunnel surface because of gravity and a condensation on the slice (vertical) of the plate, which reproduced periodically in time till the end of the experiment, and it caused a loss of total condensate weight. This is shown in fig.VI-3; drops appear, become big in size and then wipe off the surface due to gravity, and fall down on the lower surface, and usually those drops originated from the vertical slice of the plate. As a result, to reduce significantly the condensation on those vertical sides, a very thin layer of plastic tape has been applied first, and the a square shaped 3 mm thick and 3 mm wide sponge has been wrapped around the vertical surface of the Peltier element below the plate, so that the falling drops could be soaked by the sponge and thus the loss of condensate from the condensing unit could be prevented. Three/four experiments were performed to optimize the thickness, wideness and the localisation of the sponge. The primary aim of that optimization of the sponge layer was to minimize the disturbance caused to the velocity profile on the surface of the horizontal plate. The experiments carried out after CEI-11 used this optimized sponge position.

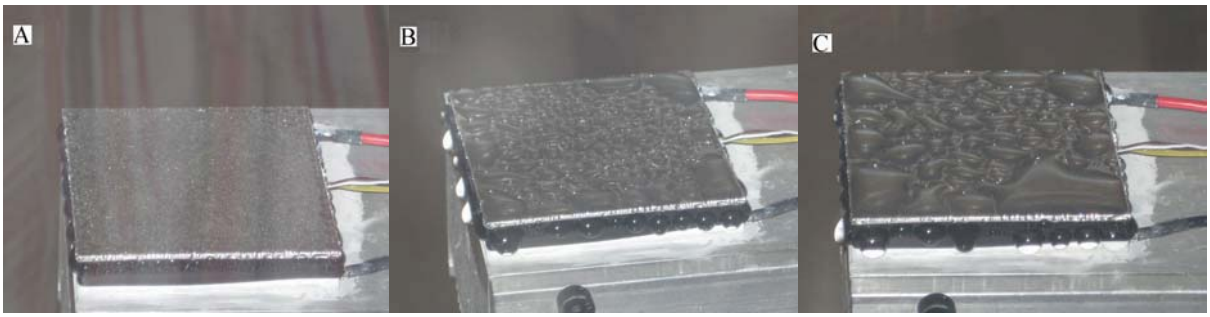

Fig.VI-3: Photographs of flat plate showing the falling drops of condensate before applying sponge from the vertical surface of the plate (a) after 40 min of the exp (b) after 5 h and (c) after 7 h 30 min of the condensation exp (CEI-7).

The experiments were performed for several temperature differences ($\Delta T_c = T_d - T_c$) between the dewpoint (T_d) and the temperature set on the controller (T_c). Usually, each experiment lasted one day, and the local daily weather conditions outside the wind tunnel affected the ambient temperature and relative humidity inside it, and sometimes it caused a variation in dewpoint as well. In these experiments, condensation on the plate and evaporation in the air flow caused by forced convection were simultaneous processes, and the amount of condensate collected on the surface of the flat plate was the net rate between these two opposite processes. On increasing the difference of temperature between the ambient temperature (T_a) and the controller temperature (T_c), and if the humidity level remains constant the rate of condensation will augment, and the rate of evaporation as well.

6.3.1 Analysis of the evolution of the condensation rate versus time

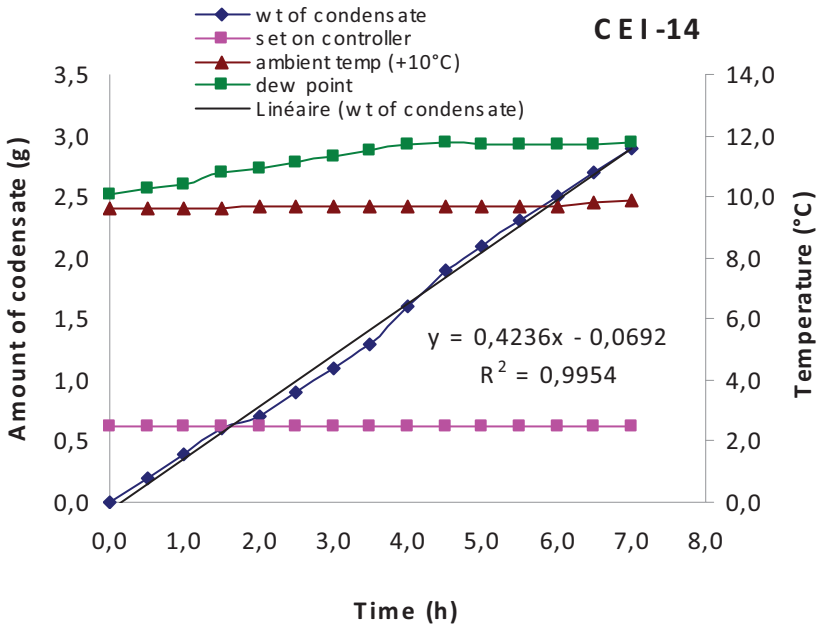

Fig.VI-4: Plot of amount of condensate and secondary Y-axis as temperature ambient (-10°C), dewpoint, and set on controller with respect to time.

Similar plots were drawn for each experiment with linear least square data fits to deduce the gradient of mass with respect to time. For example, the experiment CEI-14 (fig.VI-4) gives a gradient of linear square data fit as 0.4236, and the average of the rate of condensation calculated by the 2nd method is 0.4143 g/h, and 0.3968 g/h with the 1st method. The 2nd method seems more accurate because the experimental conditions were not constant during the whole time, it presents variations, as one can observe from figure VI-4 that the ambient temperature was almost constant but the dew point increased due to an increase in the relative humidity. The increasing tendency in the dewpoint only lasted 4 h, and then became constant. This variation in an environmental parameter affected the rate of condensation for that particular time, which is better taken care of in the 2nd method, as the 1st method only produces the global data. This type of calculations has been done for all the experiments.

The Reynolds number for 1.0 m/s mean velocity is in the range of 3100-3300, and several experiments were performed by changing the temperature difference ($\Delta T_c = T_d - T_c$) from 3.3 to 9.6 °C. The relative humidity varied from 43% to 63%, and the ambient temperature was in the range of 17-25 °C but more than 90% experiments were carried out within the temperature range of 19-24 °C.

Table VI - 1A Condensation Experimentation (Mean wind velocity-1,0 m/s)

	Peltier Element and Plate size, Thickness	Atm. Pressure	Amount of cond collected	Data Aquisition time	Ambient Temp Range (T_a)	Dew Point (T_d)	Controller (T_C)	Surface temp (T_s)	Temp Diff (T_d-T_s)	Temp Diff (T_a-T_s)	Relative humidity	Average partial $P(T_a)$-$P(T_s)$	Exp no.	Date Performed
		Millibar	g	h-min	mean (°C)	mean (°C)	mean (°C)	mean (°C)	mean (°C)	mean (°C)	Mean (%)	kPa		
	1	2	3	4	5	6	7	8	9	10	11	12	13	14
1	**50x50 Peltier**	928	0,6	7-30	21,9	8,3	4,6	7,5	0,8	14,4	42,6	0,0830	**CEI-22**	06/10/2010
2	**50x50 Plate**	928	0,8	3-30	18,9	7,2	0,9	3,9	3,3	15,0	49,2	0,2738	**CEI-13**	15/09/2010
3		925	1,0	7-08	23,7	12,1	9,0	11,5	0,7	12,2	54,6	0,1411	**CEI-4**	08/07/2010
4	3 mm	929	1,1	7-30	22,3	10,0	5,7	8,5	1,5	13,8	48,0	0,1925	**CEI-23**	07/10/2010
5	Fan Freq.	928	1,2	7-30	19,5	5,8	0,5	3,7	2,2	15,9	43,8	0,2111	**CEI-19**	01/10/2010
6	15,6 Hz	928	1,3	7-50	21,7	10,8	7,0	10,0	1,3	11,7	55,3	0,2523	**CEI-6**	04/08/2010
7		928	1,3	6-30	17,4	6,0	-0,2	2,7	3,4	14,6	49,3	0,2418	**CEI-16**	28/09/2010
8		924	1,4	7-30	19,4	9,2	4,0	6,6	2,6	12,8	52,6	0,2196	**CEI-18**	30/09/2010
9		915	1,6	6-30	19,3	7,2	0,9	3,9	3,3	15,3	48,2	0,2726	**CEI-15**	17/09/2010
10		916	1,6	7-30	18,6	8,1	2,4	5,1	3,0	13,5	52,2	0,2484	**CEI-17**	29/09/2010
11		915	1,8	7-30	20,0	7,9	1,5	4,3	3,6	15,7	49,1	0,3252	**CEI-11**	08/09/2010
12		921	2,1	7-30	19,6	9,4	2,5	5,3	4,1	14,3	53,6	0,3278	**CEI-12**	09/09/2010
13		926	2,3	7-50	23,2	14,3	9,0	11,4	2,9	11,8	57,2	0,2814	**CEI-1**	30/06/2010
14		921	2,3	7-50	23,6	13,2	8,0	10,6	2,6	13,0	56,9	0,3900	**CEI-2**	01/07/2010
15		926	2,3	7-50	21,2	8,0	1,4	4,7	3,4	16,5	44,8	0,2897	**CEI-8**	06/08/2010
16		926	2,4	7-40	22,1	9,7	3,0	6,1	3,6	16,0	48,0	0,3407	**CEI-7**	05/08/2010
17		924	2,4	6-30	20,8	11,1	3,4	6,3	4,8	14,5	54,8	0,3986	**CEI-20**	04/10/2010
18		924	2,5	7-30	21,1	8,9	0,3	3,8	5,1	17,3	49,6	0,4516	**CEI-21**	05/10/2010
19		924	2,6	7-00	21,3	10,3	2,9	6,0	4,4	15,3	55,3	0,4900	**CEI-9**	06/09/2010
20		907	2,6	7-30	21,4	13,1	6,5	9,0	4,1	12,4	60,9	0,4137	**CEI-10**	07/09/2010
21		916	2,9	7-00	20,2	11,2	2,4	5,4	5,9	14,9	57,5	0,4780	**CEI-14**	16/09/2010
22		918	3,2	7-50	24,7	14,4	8,0	10,8	3,6	13,9	52,7	0,3502	**CEI-3**	02/07/2010
23		922	3,2	7-30	22,2	10,9	1,1	4,6	6,3	17,5	50,7	0,5109	**CEI-24**	08/10/2010
24		921	3,4	7-50	22,3	14,4	7,0	9,6	4,9	12,7	63,0	0,5087	**CEI-5**	02/08/2010

Table VI - 1B				Exp average rate of condensation				Average values of theoretical calculation					
Exp no.	Date Performed	Slope	R^2	(Tot wt / Tot time)	Mass flux	$((m_2-m_1)/(t_2-t_1)$	Mass flux	Rate of condensation	Mass flux	Difusivity of water vapour in air	Schmidt number at surface	Reynolds number	Sherwood number
		g/h		g/h	(Kg $m^{-2}s^{-1}$)		(Kg $m^{-2}s^{-1}$)	g/h	(Kg $m^{-2}s^{-1}$)	m^2/s	Sc	Re	Sh_1
13	14	15	16	17	18	19	20	21	22	23	24	25	26
CEI-22	06/10/2010	0,0876	0,9638	0,0694	7,71E-06	0,0800	8,89E-06	0,0941	1,05E-05	2,52E-05	0,6156	3226,41	32,31
CEI-13	15/09/2010	0,2160	0,9880	0,2741	3,05E-05	0,2286	2,54E-05	0,3087	3,43E-05	2,44E-05	0,6137	3340,67	32,79
CEI-4	08/07/2010	0,1467	0,9320	0,1047	1,16E-05	0,1398	1,55E-05	0,1591	1,77E-05	2,56E-05	0,6182	3158,83	32,05
CEI-23	07/10/2010	0,1524	0,9877	0,1210	1,34E-05	0,1467	1,63E-05	0,2177	2,42E-05	2,53E-05	0,6165	3211,70	32,27
CEI-19	01/10/2010	0,1571	0,9937	0,1523	1,69E-05	0,1600	1,78E-05	0,2382	2,65E-05	2,44E-05	0,6134	3338,47	32,77
CEI-6	04/08/2010	0,1515	0,9539	0,1216	1,35E-05	0,1597	1,77E-05	0,2873	3,19E-05	2,52E-05	0,6118	3240,95	32,35
CEI-16	28/09/2010	0,2000	1,0000	0,2000	2,22E-05	0,2000	2,22E-05	0,2726	3,03E-05	2,42E-05	0,6128	3369,17	32,90
CEI-18	30/09/2010	0,1956	0,9976	0,1991	2,21E-05	0,1867	2,07E-05	0,2479	2,75E-05	2,49E-05	0,6154	3266,22	32,49
CEI-15	17/09/2010	0,2162	0,9834	0,2776	3,08E-05	0,2133	2,37E-05	0,3073	3,41E-05	2,44E-05	0,6137	3338,86	32,78
CEI-17	29/09/2010	0,2082	0,9968	0,2309	2,57E-05	0,2133	2,37E-05	0,2804	3,12E-05	2,46E-05	0,6144	3302,99	32,64
CEI-11	08/09/2010	0,2300	0,9954	0,2291	2,55E-05	0,2400	2,67E-05	0,3689	4,08E-05	2,48E-05	0,6141	3289,57	32,56
CEI-12	09/09/2010	0,2791	0,9951	0,2850	3,17E-05	0,2800	3,11E-05	0,3706	4,11E-05	2,48E-05	0,6148	3285,10	32,56
CEI-1	30/06/2010	0,2997	0,9893	0,3142	3,49E-05	0,2938	3,26E-05	0,3175	3,53E-05	2,55E-05	0,6183	3167,89	32,12
CEI-2	01/07/2010	0,3040	0,9980	0,2739	3,04E-05	0,2938	3,07E-05	0,4398	4,89E-05	2,54E-05	0,6182	3184,61	32,20
CEI-8	06/08/2010	0,2962	0,9924	0,3101	3,45E-05	0,2938	3,26E-05	0,3270	3,63E-05	2,46E-05	0,6143	3312,98	32,68
CEI-7	05/08/2010	0,3231	0,9905	0,3579	3,98E-05	0,3250	3,61E-05	0,3837	4,26E-05	2,47E-05	0,6153	3291,44	32,61
CEI-20	04/10/2010	0,3640	0,9913	0,4162	4,62E-05	0,3692	4,10E-05	0,4542	5,05E-05	2,53E-05	0,6157	3210,80	32,22
CEI-21	05/10/2010	0,3124	0,9852	0,3110	3,46E-05	0,3333	3,70E-05	0,5119	5,69E-05	2,46E-05	0,6141	3303,46	32,62
CEI-9	06/09/2010	0,3400	0,9900	0,3736	4,15E-05	0,3714	4,13E-05	0,5558	6,18E-05	2,50E-05	0,6156	3246,48	32,38
CEI-10	07/09/2010	0,3353	0,9913	0,3938	4,38E-05	0,3467	3,85E-05	0,4694	5,22E-05	2,55E-05	0,6173	3179,88	32,13
CEI-14	16/09/2010	0,4236	0,9954	0,3968	4,41E-05	0,4143	4,60E-05	0,5404	6,00E-05	2,48E-05	0,6152	3282,74	32,55
CEI-3	02/07/2010	0,4186	0,9963	0,4223	4,69E-05	0,4062	4,25E-05	0,3956	4,40E-05	2,55E-05	0,6182	3170,01	32,13
CEI-24	08/10/2010	0,4229	0,9936	0,4176	4,64E-05	0,4339	4,82E-05	0,5776	6,42E-05	2,46E-05	0,6148	3299,49	32,62
CEI-5	02/08/2010	0,4427	0,9982	0,3806	4,23E-05	0,4126	4,58E-05	0,5734	6,37E-05	2,52E-05	0,6179	3207,20	32,29

Usually, the temperature of the controller was fixed for each experiment at the beginning and stayed unchanged throughout the experiment. Only for a few experiments it was modified during the experiment like when a large variation of the dewpoint occurred. The value of the atmospheric pressure outside the wind tunnel for all the experiments at 1.0 m/s was in the range of 907-929 millibar, however, during the course of an experiment the atmospheric pressure was almost constant, and its value was recorded at the beginning and then at the end of the experiment.

The Table VI-1A and Table VI-1B give the average values of the experimental and calculated data for each experiment. Normally, the physical parameters were regulated inside the wind tunnel, but if there were a large variation in any parameter, like in figure VI-5(a) the dew point first decreased slowly for one and a half hour then decreased little faster till six hours of the experiment, and then became almost stable up to the end. The variation in the dewpoint reflected fluctuations in the relative humidity, which started at 52% and finished at 45%, while the tunnel temperature was nearly stable (variation of 0.3 °C in 7 h 30 minutes). The value of the controller temperature was fixed at 1.0 °C for the whole duration of the experiment. It can be easily observed from figure VI-5 (a) that the amount of condensate follows four trends i) 0.4 g/h till 1 h ii) 0.2 g/h till 5 h, and iii) 0.1 g/h up to 6 h 30 min iv) saturation afterword's. In air-conditioned conditions, this experiment is the only one that seemed to tend towards a saturation phase, although the condensate distribution is still very heterogeneous and such a saturation effect does not appear. The average value of the rate of condensation was 0.22 g/h for the experiment. The temperature difference ΔT_c (T_d-T_c) went down continuously from 7.7 °C to 5.2 °C, and the global average was 6.2 °C. Then for long duration experiments, local variations in hygrometry affect the global value as well.

In figure VI-5(b) CEI-21, the dewpoint decreased first for a few hours (~1.5 °C) and increased at a similar rate for 3 h and slower afterword's. This fluctuation in the dewpoint affected the rate of condensation, and the curve of the amount of condensate shows also three different trends: i) 0.4 g/h for the first hour, ii) 0.2 g/h for the next 2 h 30 min iii) again gave 0.4 g/h up to 5 h 30 min, and then iv) 0.34 g/h between 6^{th} and 7^{th} hours. Globally the value of rate of condensation was 0.31 g/h. During this period the ambient temperature increased by less than 1 °C, and the relative humidity varied from 48% to 51%. The temperature difference ΔT_c imposed for this experiment was 7.8 °C at the beginning and 9.7 °C at the end, there was an increase of almost 2 °C.

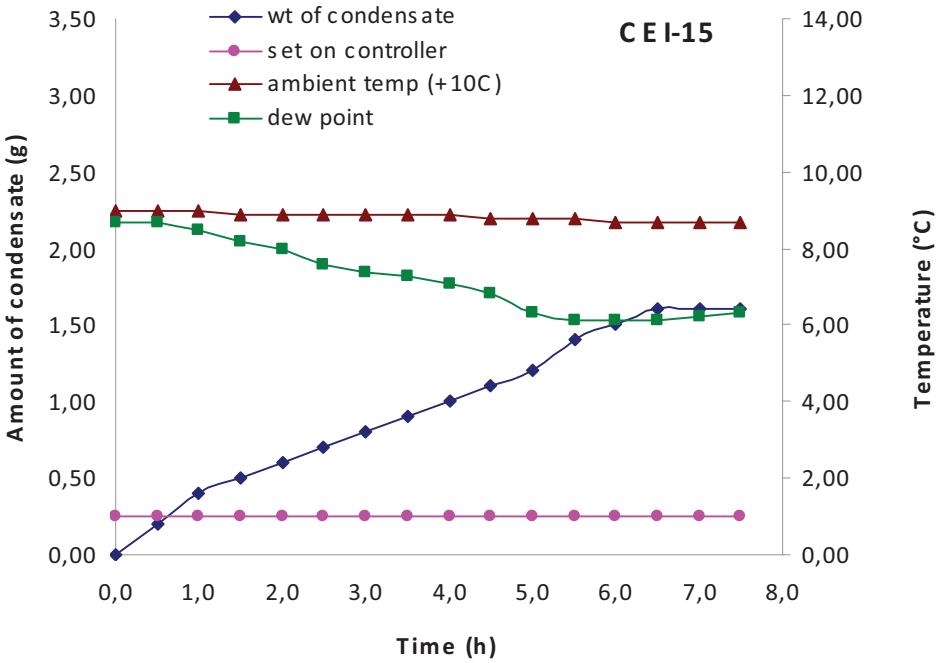

(a)

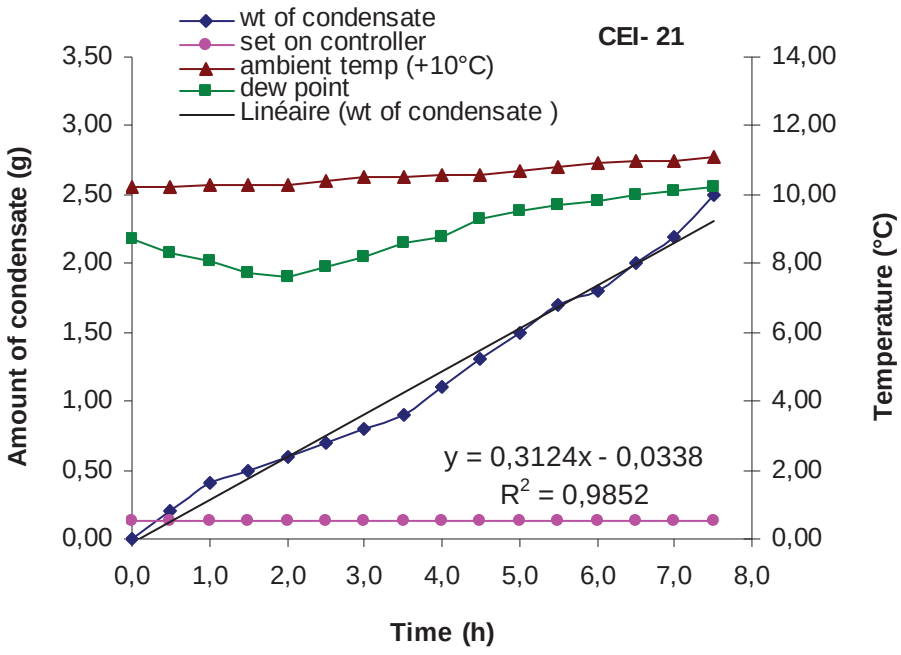

(b)

Fig.VI-5: (a, b) Plot of the amount of condensate and secondary Y-axis as temperatures ambient (-10°C), dewpoint, and set on controller, as a function of time.

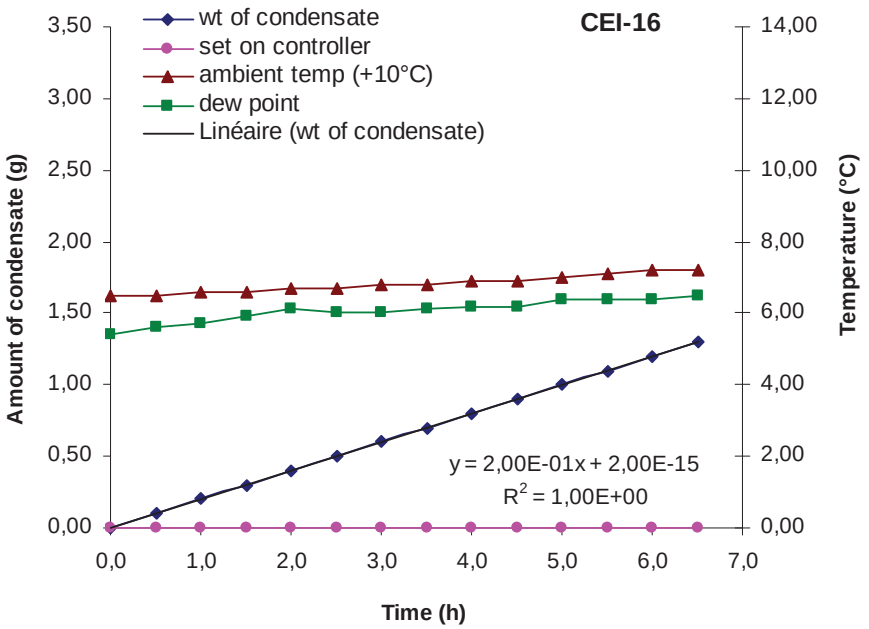

(a)

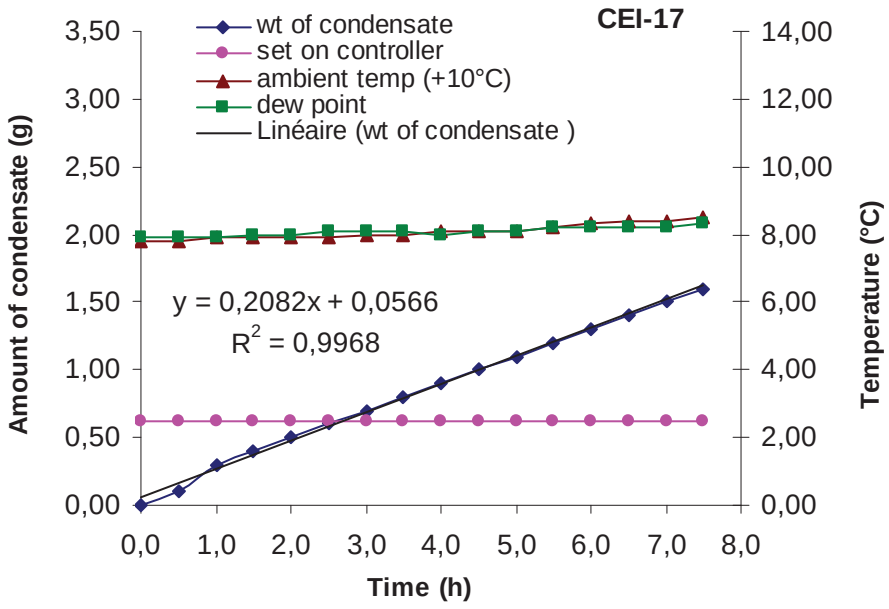

(b)

Fig.VI-6 (a, b): Plot of the amount of condensate and secondary Y-axis as temperatures ambient (-10°C), dewpoint, and set on controller, as a function of time.

From the above observations it is seen that the global condensation rate goes up by 50%. When the temperature difference ΔT_c is increased by 50%, however the "local" trends (obtained for at least 1h) do not overcome 0.4 g/h. When the variation in the dewpoint during the total time of the experiment was low, a single trend of rate of condensation could be achieved. Figure VI-6 (a) (experiment CEI-16) relates a 6.5 h experiment, in which the dewpoint variation was less than 1°C and temperature difference (ΔT_c) as well (it started at 5.6 °C, went up to 6.0°C for 3 h and reached 6.5°C at the end). The total amount of condensate collected was 1.3 g with the rate of 0.2 g/h. The ambient temperature was almost constant with a variation of 0.7 °C and the variation in the relative humidity was below 1%.

Figure VI-6(b) shows an experiment with even less dewpoint variation (0.4 °C) in 7 h 30 min. At the beginning of the experiment, the chosen ΔT_c was 5.4 °C and at the end it was 5.8 °C. These nearly stable conditions induced a constant rate of condensation of 0.2 g/h. The other parameters like the ambient temperature and the relative humidity have variations below 1%, were also steady. However, it was not very easy to get such "quiet" experimental conditions for long duration in which the environmental parameters have less than 1% variations. The ambient temperature was plotted in those figures after subtracting 10 °C to fit in the scale.

6.3.2 Analysis of the condensation rate versus the temperature difference (ΔT_c)

As shown here above, the temperature difference (ΔT_c) chosen for the condensation experiments has obviously a significant effect on the rate of condensation. Usually, each experiment was planned on the basis of this temperature difference (ΔT_c), which was imposed to the flat plate with the help of the temperature controller. Figure VI-7 (a, b), shows the effect of the temperature difference (ΔT_c) on the condensation rate. It gives an idea on the relationship between the rate of condensation and the temperature difference imposed on the active condensing surface. These are the data of the first three experiments carried out on three different days for a mean entrance velocity of 1.0 m/s. The first two experiments started with the same ΔT_c equals 4.7 °C.

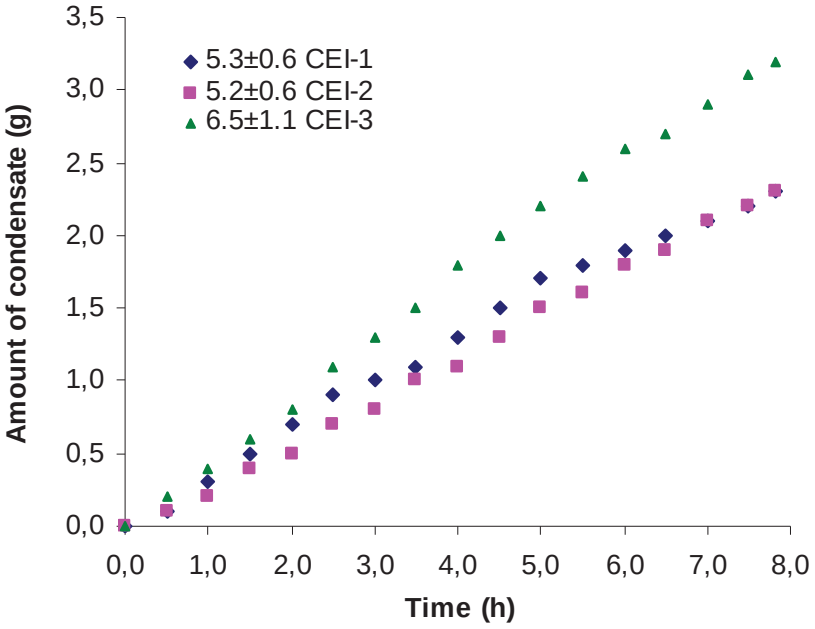

(a)

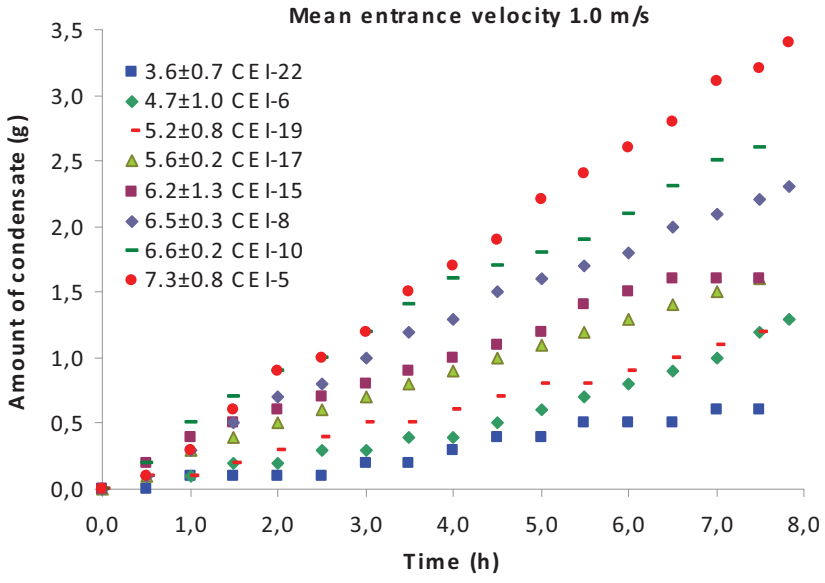

(b)

Fig.VI-7 (a, b): Amount of condensate as a function of time for different average temperature differences (ΔT_c), for 1.0 m/s mean entrance velocity.

On the day of CEI-1, the dew point increased for 3 h and ΔT_c went up to 5.7 °C, then

stabilized for 1 hour, and then decreased down to 4.6 °C. After 7 h 50 minutes, 2.3 g of condensate were collected on the plate, with an average ΔT_c value of 5.3 °C, and an average fluctuation of ±0.6 °C. The experiment CEI-2 has also collected 2.3 g in 7 h 50 min, furthermore ΔT_c started at 4.7 °C, as for CEI-1, but the dewpoint slightly decreased first, it became 4.6 °C within 30 min and stayed like this till 1 h 30 min, then increased up to 5.7 °C in 3 h (total time was 4 h 30 min) stayed constant for 1 h 30 min and went slightly down to 5.5 °C at the end of the experiment. The global average value of ΔT_c was 5.2 °C (±0.6°C). Consequently, figure VI-7(a) shows that the rates of condensate curves were not completely similar in the middle. While for CEI-3, the experiment started with a ΔT_c of 5.9 °C almost 1.2 °C more as compared to the first two experiments, ΔT_c was increased continuously up to 7.6 °C within 4 h, then ΔT_c decreased down to 5.4 °C at the end (7 h 50 min); finally, 3.2 g of water condensate were collected. The average of ΔT_c was 6.5 °C ±1.1°C. Figure VI-7 (b) represents the outcomes for several average ΔT_c values. All condensation rates reflect linear growths with time, whose slope increases with ΔT_c, as it generates the driving force through the partial pressure gradient.

To keep the temperature difference (ΔT_c) stable and to compensate the large fluctuations in dewpoint during an experiment, the setting of the controller temperature was sometimes changed during the experiment. However, such an action was intricate as the controller was on the balance and thus, the risk of destabilizing the mass weighing was high. The plots given in figure VI-8 (a-c) are the similar plots as the ones detailed above, but in these experiments ΔT_c was modified manually during condensation. Figure VI-8(a) is one of the lowest temperature difference (ΔT_c) experiments, in which during 7 h 30 min only 0.6 g of water condensate was collected. During the experiment the dewpoint went up from 8.4 °C to 9.3 °C (3 h 30 min) and then went down to 7.2 °C and again increased to 7.4 °C. The controller temperature was fixed at 5.0 °C at the beginning, and after 5 h when ΔT_c had decreased below 3.0 °C, I setted the controller temperature to 4.0 °C to keep the ΔT_c above 3.0°C. The curve shown in the plot VI-8 (a) reflected those effects, and it has to be noticed that condensation started from the beginning, the least count of the balance (0.1 g) was not reached for the balance to detect the mass increase. After 7 h 30 min the average rate of condensation was 0.08 g/h. As at the early stage when ΔT_c was weak due to an increase in dewpoint, the increase in mass was not indicated by the curve either.

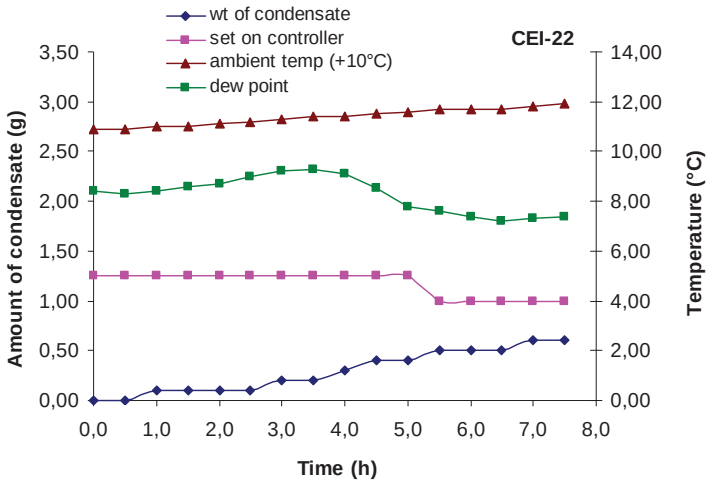

(a)

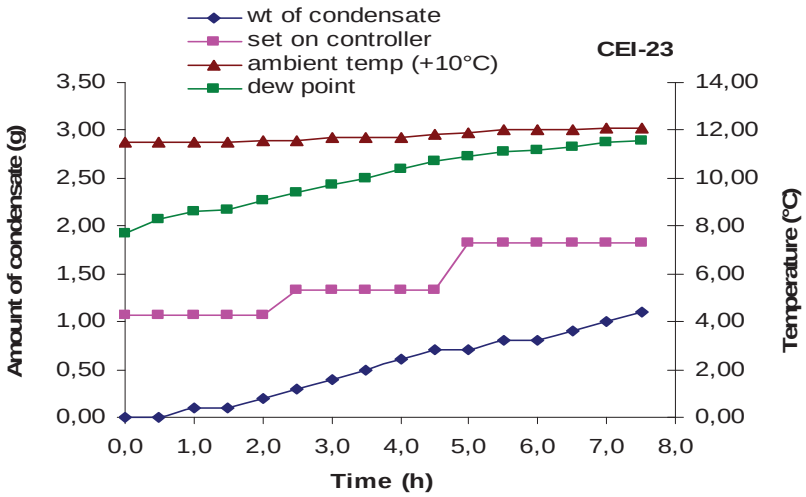

(b)

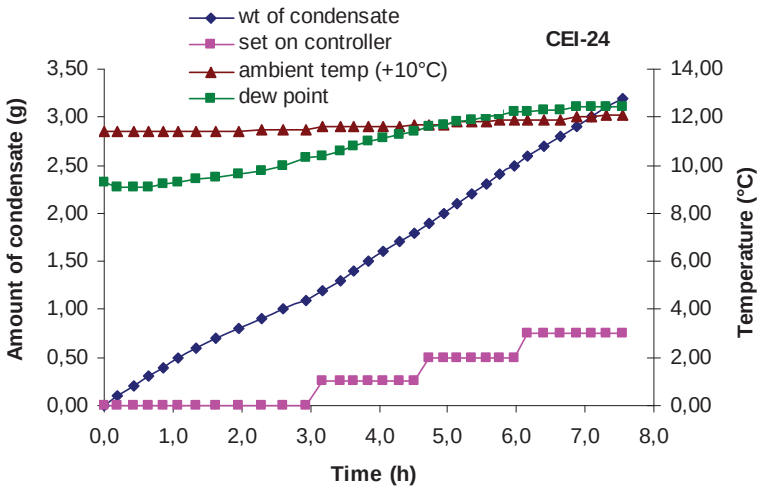

(c)

Fig.VI-8 (a, b, c): Amount of condensate and temperature as a function of time.

In CEI-23 (Fig.VI-8 (b)), the goal was to operate with a ΔT_c around 4 °C. The dewpoint increased continuously from 7.7 °C to 12.5 °C after 7 h 30 min, which caused a raise in relative humidity of more than 10%. The controller temperature was set at 4.3 °C, I have increased it by 1.0°C after 2 h, and again by 2.0 °C after 2 h 30 min to keep ΔT_c below 4.5 °C. At the end of the experiment 1.1 g of water condensate was collected, and the average ΔT_c for the total time was 4.3 °C. Again condensation started at the beginning and an average of 0.15 g/h was obtained after completion.

After this experiment, it was decided to modify the mass data acquisition: I stopped taking the reading of the weight balance every 30 minutes, I started to note down the time every 0.1 g increase on the electronic balance. Figure VI-8 (c) shows one of the highest ΔTc considered. The amount of condensate curve is smooth even though the variation in the controller setting changed three times during the experiment to compensate the continuous increase in dewpoint, except at the very beginning, from 9.3 °C up to 12.4 °C at the end. After 7 h 33 min 3.2 g of water condensate were collected. The average ΔT_c set on the controller was 9.6 °C, as the controller setting was increased three times to keep this value within 9-10 °C. An average mass rate of 0.43 g/h was reached. That result confirmed the previous conclusions, as the average condensation rate increases directly with ΔT_c and vice-versa.

6.4 Influence of the mean entrance velocity

Similar measurements have been done for other velocities as well and comparable observations have been made. The number of experiments performed was lower than for the average velocity of 1.0 m/s, because both the experimental and analysing techniques had already been optimised.

6.4.1 Experiments with a mean entrance velocity of 1.5 m/s (21.5 Hz fan frequency)

There were 9 condensation experiments performed for a 21.5 Hz fan frequency, which was generally for 1.5 m/s mean entrance velocity at the centre of the test chamber. These experiments were conducted with 3.1 °C to 8.2 °C temperature differences (ΔT_c), and collected a minimum of 0.7 g of water condensate in 7 h 8 min, and a maximum of 3.0 g in 7 h 36 min. The experimental and calculated data are shown in Table VI-2 A-B.

6.4.2 Experiments with a mean entrance velocity of 2.0 m/s (27.6 Hz fan frequency)

10 condensation experiments were carried out for the fan frequency 27.6 Hz, which corresponds to a mean entrance velocity of 2.0 m/s. The experiments were conducted for a temperature differences (ΔT_c) between 6.6 °C and 10.1 °C. The details are given in Table VI-3 A-B. These are the experiments in which highest ΔT_c ranges were used.

6.4.3 Experiment with a mean entrance velocity of 2.5 m/s (32.1 Hz fan frequency)

Nine condensation experiments were conducted for this mean entrance velocity and fan frequency of 32.1 Hz, and the details of the data are shown in Table VI-4 A-B. The range of temperature difference (ΔT_c) chosen was [4.5 °C, 9.0 °C]. The minimum condensate produced was 0.9 g in 3 h 33 min, and the maximum was 4.2 g in 7 h 10 min.

6.4.4 Experiment with a mean entrance velocity of 3.0 m/s (40.0 Hz fan frequency)

Twelve experiments were executed using a 40 Hz fan frequency that corresponds about to 3.0 m/s for the mean entrance velocity. This is the highest frequency, which we have used for the condensation experiments. The experimental details and the parameters calculated theoretically are given in Table VI-5 AB. The temperature difference (ΔT_c) imposed on the flat plate by the temperature controller was between 4.8 °C and 8.6 °C.

6.5 Theoretical calculations and discussion

The theoretical calculations have been done for each experiment using the local weather conditions of the specific experiment. The physical parameters of the environmental air (the term ‘air’ used herein describe ‘humid air’) such as partial vapour pressure of water vapour in air, saturation partial vapour pressure of water vapour in air, viscosity of air, density of air, mass fraction of water vapour in air, and diffusivity of water vapour in air have been calculated at different temperatures. The definitions and correlations of temperature dependence on these physical parameters have already been described in chapter II. To calculate the above properties theoretically, the experimental data like relative humidity, ambient temperature, atmospheric pressure and controller temperature have been recorded and used. The density, viscosity, and diffusivity of water vapour in air have been considered as

temperature dependent. Normally, near ambient conditions (i.e. 22 °C), the influence of water vapour on the density of air is less than 2%, and when the temperature change reaches approximately 20 °C, the change in density of dry air is about 7% (Balasubramaniam et al. 2006) which is not the case in these current experiments. The minimum ambient temperature recorded was 16.6 °C and the maximum was 25.8 °C, with a maximum variation during one day of 3.5 °C inside the wind tunnel. Usually, during the experiments, the ambient temperature had variations below 1.5 °C for total time of one experiment. These properties were basically calculated at two temperatures, one was at the ambient temperature (T_a) and another one at the surface temperature (T_s). The ambient temperature has been taken from the sensor of the wind tunnel, which gave the global temperature of the free flow inside the closed circuit wind tunnel. The surface temperature was calculated with theoretical models using the controller temperature (T_c), which was the temperature given by a thermistor inserted just below (approximately 1 mm) the surface of the active condensing plate (temperature measurement by contact), and the temperature of the free flow inside the wind tunnel. Although, the measurement of the surface temperature remained more or less unknown and even more when condensation develops, several surface temperature measurement experiments were performed during the calibration process, and they showed a gradient of temperature less than 1°C. The accurate knowledge of the surface temperature on the air/water and air/plate interfaces in heat and mass transfer experimental problems would improve the understanding of the results.

6.5.1 Surface temperature estimation

The calculation of the condensation mass flux involves the partial pressure gradient at the interface liquid/air or metal/air where condensation proceeds, the area of the interface and the correlated mass transfer coefficient. Here the area is not known and the goal is to determine the $k_L.A$ coefficient. The partial pressure of the air is deduced from the ambient temperature and the relative humidity, whereas neither the pressure nor the temperatures are known. Moreover, the only accurate data available is T_c which is the temperature measured by the contact 1 mm below the metal/air surface at the centre of the plate. Modelling could have given some insights about the thermal gradient in the plate (thickness) and on its surface, and within the volumes (drops, masses) of condensate. But this is a 3D transient problem that involve change of phase (mass transfer coefficient again), and turbulent flow modelling.

Consequently, the knowledge of the surface temperature of the active condensing flat

plate became an important task for the estimation of the mass transfer coefficient relative to condensation by humid air. The mean values of the controller temperature (T_c) and the ambient temperature (T_a) have been used in theoretical calculations. Also, the temperature set on the controller was proven to be slightly smaller than just above at the interface with the air (chapter III) and that some discrepancy was present over the flat plate (about 1 °C) in dry air, which means that such in-homogeneity was probably reinforced by the heterogeneous mass transfer that develop on the plate. The use of a surface sensor was not convincing because of the presence of forced convection (see chapter III). It encouraged us to do some assumptions for the surface temperature, which was above the controller temperature, and below the ambient temperature. For the positive rate of condensation on the active plate, $\Delta T_s = T_d - T_s$ should be positive, we have tested the following relations to predict the surface temperature

$$T_s = \frac{T_c + T_a}{2} = T_c + 0.5(T_a - T_c) \qquad \text{(VI-1)}$$

$$T_s = \frac{3 * T_c + T_a}{4} = T_c + 0.25(T_a - T_c) \qquad \text{(VI-2)}$$

$$T_s = \frac{5 * T_c + T_a}{6} = T_c + 0.16(T_a - T_c) \qquad \text{(VI-3)}$$

T_s calculated by eq.(VI-1), led to sometimes negative temperature difference (ΔT_s), when a positive rate of condensation was observed in the experiments. The eq.(VI-2) induced for a few experiments a similar effect, which showed a bad assumption. That effect was not reached with eq.(3), the estimated T_s resulted in positive ΔT_s for every experiment with a positive rate of condensation.

Incropera and DeWitt (1990) have suggested for the evaluation of all the liquid properties in the Nusselt analysis (vertical filmwise condensation), to consider the film temperature as $T_f = (T_{sat} + T_s)/2$, where T_{sat} is the saturation temperature and T_s is the surface temperature. On using this hypothesis and taking $T_{sat} = T_d$, $T_s = T_c$, we have calculated the surface temperature as $T_s = (T_d + T_c) / 2$, and found that this value is approximately (±1.0 °C) equal to the calculated one by eq. (VI-3), because in our experiments, we have only measured T_c, T_d, and T_a, and not T_s or T_{sat}.

For the evaluation of the Nusselt number in heat transfer problems, Minkowycz and

Sparrow (1966) proposed the use of a reference temperature based on their detailed numerical calculations, defined by the equation $T_{ref} = T_c + 0.31(T_a - T_c)$ for a vertical configuration. Also, it is reported that for heat transfer coefficient estimation the Nusselt model gave a good agreement with their results of numerical calculations taking into account the effect of variable physical properties at the reference temperature by means of this equation. The surface temperatures given in the Tables VI-1A to VI-6A at column 8 were calculated by using equation (3). We have also considered two "limit" cases to calculate T_s

$$T_s = T_c + 1.0 \qquad \text{(VI-4)}$$

And $$T_s = T_d \qquad \text{(VI-5)}$$

These are the extreme cases for the surface temperature because eq. (VI-4) gives an approximate of the minimum possible surface temperature according to our surface temperature studies, and eq. (VI-5) gives a maximum possible temperature for condensation to start, as the condensation can only occur when $T_s < T_d$.

The dropwise condensation was attained on the surface of the flat plate, with various visual drop sizes. For long duration experiments, condensation continued on the surface as well as on the barren areas. The coalescence process pushes the small drops to be absorbed by bigger drops, and the emergence of new drops continued on swiped of regions. It results in the appearance of very different size drops on the surface of the flat plate (Beysens, 2006). The temperature gradient within the water droplets and their variable size were one of the difficulties in predicting the active surface area for condensation and its surface temperature.

6.5.2 Calculation of the Sherwood number (*Sh*)

The effect of the temperature dependence has been considered in the numerical calculations for the physical properties of humid air, and the surface temperature T_s has been considered as a reference temperature using eq.(VI-3), calculated with the measured variable ambient temperature and the controller temperature. These physical properties have been used to calculate the Sherwood number for different concepts. The theory for laminar and turbulent flows over a horizontal thin finite flat plate has been well developed, and the formulations for heat and mass transfer coefficients are discussed in the literature (Incropera and DeWitt 1990, Asano 2006, Collier 1996).

The discussions concerned the problem of computing the mass transfer rates in an

external flow, where a boundary layer develops freely, and there is a region of the flow outside the boundary layer, where there is negligible variation in velocity, temperature and concentration. For a low speed forced convection flow, where the relative motion between the surface and the fluid was maintained by a fan in the wind tunnel, the convection coefficients for different geometries are extensively described in Incropera and DeWitt (1990) and also, the mass transfer, local and average Sherwood numbers given as a function of a characteristic length (L), Reynolds number (Re), and Schmidt number (Sc)

$$Sh_L = f(L, \mathrm{Re}, Sc) \qquad \text{(VI-6)}$$

$$\overline{Sh} = f(\mathrm{Re}, Sc) \qquad \text{(VI-7)}$$

with the analogy of heat and mass transfer, to obtain the correlations for the mass transfer convection coefficient, it is given as

$$\overline{Sh}_L = K * \mathrm{Re}_L^m * Sc^n \qquad \text{(VI-8)}$$

where as, according to the geometry and the flow conditions, the values of K, m, n are the same for different studies.

For a flat plate in a parallel flow (laminar)

$$\overline{Sh_L} = 0.664\,\mathrm{Re}_L^{1/2}\, Sc^{1/3} \qquad 0.6 \le Sc \le 50 \qquad \text{(VI-9)}$$

For turbulent flow, the local Sherwood number

$$Sh_L = 0.0296\,\mathrm{Re}_L^{4/5}\, Sc^{1/3} \qquad 0.6 \le Sc \le 300 \qquad \text{(VI-10)}$$

And if it is a mixed type of flow, with a mixed boundary layer laminar/ turbulent, the leading edge has a laminar boundary and approaching the rear edge it is turbulent, then

$$\overline{Sh_L} = 0.037\,\mathrm{Re}_L^{4/5}\, Sc^{1/3} \qquad \text{(VI-11)}$$

Also, if we consider the definition of the Sherwood number (Asano, 2006) (already described in detail in Chapter-II)

$$Sh = \frac{N_A}{\rho D(\omega_\infty - \omega_s)/L} \qquad \text{(VI-12)}$$

Here we have taken N_A as the experimental mass flux in $kg.m^{-2}.s^{-1}$, ρ the density (kg/m^3), D the diffusivity of water vapour in air (m^2/s), the difference in mass fraction at free stream temperature and at the surface temperature, and L the characteristic length of the flat plate (0.05 m).

In the plots the Sherwood numbers referred to as Sh_1, Sh_2 and Sh_3, correspond to eq. (VI-9), (VI-11), and (VI-12), respectively. They were calculated with the local physical parameters taken at the time of the experiments, all the fluid properties were normally calculated at the surface temperature.

6.5.3 Partial pressure difference (ΔP) estimation

To describe the condensation of water vapour of humid air on the surface of the flat plate, it has been considered that, due to the difference in temperature between the free stream flow and the condensation interface, which is below the dew point temperature, the water vapour diffused through the free stream towards the surface of the plate, and a binary diffusion system has been (air/water) considered. Due to the difference in temperature, where one point is lower than the saturation temperature, there is a difference in partial pressure between the free stream flow and the interface, and the mass flux is considered as

$$N_A \equiv C * \left[P(T_a) - P(T_s) \right] \qquad \text{(VI-13)}$$

Where C is a constant, and P denotes partial pressure. In each experiment, for every time interval, we have calculated the partial pressure at ambient temperature (T_a) and the saturation vapour pressure at the surface temperature (T_s). The dependence of the mass flux on the proportionality of this partial pressure difference will be discussed hereafter.

6.5.4 Velocity boundary layer and temperature profile

We have used the variation of the velocity versus height above the surface of the horizontal plate to obtain a rough estimate of the temperature profile, on considering that this function should be similar in nature as $P_r^{1/3} \approx 1$ for the air at about 20 °C. If we consider z as the height from the surface of the flat plate, then

for the dimensionless velocity

$$f(z) = \frac{U_z - U_\infty}{U_s - U_\infty} \quad (U_z \text{ is the boundary layer velocity}) \qquad \text{(VI-14)}$$

for the dimensionless temperature

$$f'(z) = \frac{T_z - T_\infty}{T_c - T_\infty} \quad (\text{In this case, } T_\infty = T_a) \qquad \text{(VI-15)}$$

If we consider $f'(z) \cong f(z)$, then

$$T_z = (T_c - T_\infty) \times f(z) + T_a \qquad \text{(VI-16)}$$

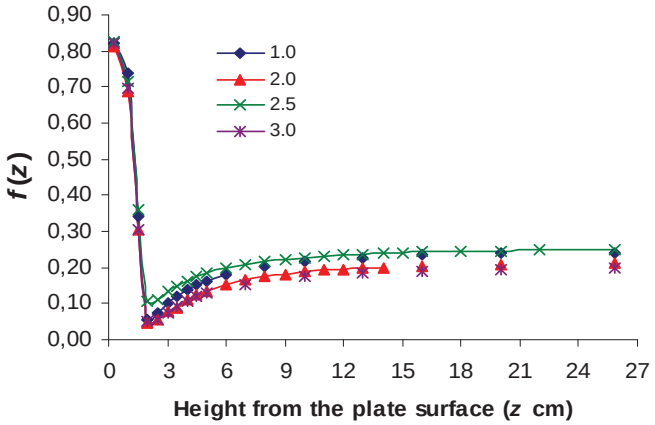

(a)

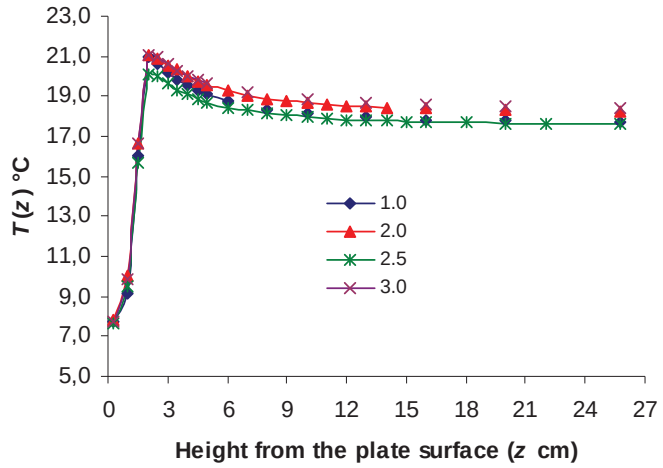

(b)

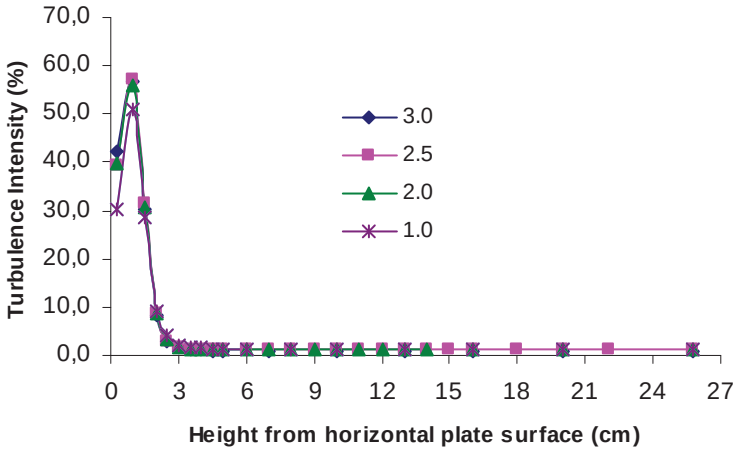

(c)

Fig.VI-9(a, b, c): (a) Velocity function *f*(z) versus height from the surface of the flat plate; (b) estimated temperature using eq. (VI-16) as a function of height from the surface of the plate (c) turbulence intensity versus height from the plate surface.

The velocity profile has already been described in detail in chapter IV, here we have considered the velocity from the surface of the plate up to outside the boundary layer, i.e. from 0.3 cm near the plate till 25.8 cm above the plate surface (at the point X = 5.0, Y = 2.5, where X is in the down stream flow direction), the flat plate surface was at 40 cm below the upper surface of the wind tunnel (similar measurements as the one given in fig.IV-10 (a, b)). The function $f(z)$ has been calculated and plotted in fig.VI-9 (a). Using this function the temperature has been calculated, as a function of the height (z) for each experiment with the corresponding velocity function (eq. VI-16), and this temperature has been plotted in fig.VI-9 (b) for the data of one experiment (CEI-22, $U_\infty \approx 1.0$ m/s). As it can be seen from fig.VI-9 (b & c) the effect of turbulence appears up to about 7 cm above the surface of the horizontal plate, and beyond that the turbulence is less than 1% as it can be read in fig.VI-9(c). The maximum turbulence intensity is below a height of 2.5-3.0 cm, and then up to the height of about 7 cm it is between 1-3%, which indicates that the limit of the boundary layer was near a 7 cm height above the middle point of the trailing edge of the plate. Thus a 7 cm thick vortex seems to have developed above the plate; such a thickness is caused by the blunt shape of the condensing unit.

Similar plots have been drawn for each experiment, and an interesting phenomenon was found, as the temperature calculated with this function at a 0.3 cm height is similar to the surface temperature $T_{s,}$ calculated by eq. (VI-3). The value given by eq. (VI-3) is little lower, and the difference is in the range of 0.1-0.5 °C, more than 85% experiments show a difference of 0.2 °C.

Table VI - 2A Condensation Experimentation (Mean wind vel.- 1.5 m/s)

	Peltier Element, Plate size, and Thickness	Atm. Pressure	Amount of cond collected	Data Aquisition time	Ambient Temp Range (T_a)	Dew Point (T_d)	Controller (T_c)	Surface temp (T_s)	Temp Diff (T_d-T_s)	Temp Diff (T_a-T_s)	Relative Humidity	Av $P(T_a)$-$P(T_s)$	Exp no.	Date Performed
		Millibar	g	h-min	mean (°C)	mean (°C)	mean (°C)	mean (°C)	mean (°C)	mean (°C)	mean (%)	kPa		
	1	2	3	4	5	6	7	8	9	10	11	12	15	16
1	**50x50 Peltier**	923	0,7	7-08	19,6	3,5	0,2	3,5	0,1	16,2	38,4	0,0938	**CEI-30**	16/11/2010
2	**50 x 50 Plate**	924	0,8	5-07	20,5	4,8	0,6	3,9	0,9	16,5	38,8	0,1272	**CEI-25**	02/11/2010
3	**Fan freq.**	916	1,4	6-31	18,7	3,5	-2,2	1,3	2,2	17,4	39,1	0,1780	**CEI-32**	18/11/2010
4	**3 mm**	929	1,6	4-50	20,4	7,3	-0,2	3,3	4,0	17,2	41,3	0,2222	**CEI-57**	13/05/2011
5	**21,5 Hz**	909	1,9	6-04	18,4	4,2	-2,2	1,2	3,0	17,2	44,6	0,2806	**CEI-34**	22/11/2010
6		929	1,9	4-19	20,6	8,0	-0,2	3,3	4,7	17,3	46,3	0,3596	**CEI-58**	13/05/2011
7		925	2,0	7-44	21,9	9,0	3,5	6,6	2,4	15,3	44,9	0,2083	**CEI-26**	03/11/2010
8		934	2,8	7-28	22,9	10,7	3,8	7,0	3,7	15,9	47,5	0,3279	**CEI-27**	04/11/2010
9		935	3,0	7-36	23,6	10,4	3,2	6,6	3,8	17,0	45,8	0,3662	**CEI-28**	05/11/2010

Table VI - 2B		Curve fitting		Exp average rate of condensation				Average values of theoretical calculation					
Exp no.	Date Performed	Slope	R^2	(Tot wt / Tot time)	Mass flux	$((m_2-m_1)/(t_2-t_1))$	Mass flux	Rate of condensation	Mass flux	Diffusivity of water vapour in air	Schmidt number	Reynolds number	Sherwood number
		g/h		g/h	Kg $m^{-2}s^{-1}$	g/h	Kg $m^{-2}s^{-1}$	g/h	Kg $m^{-2}s^{-1}$	m^2/s	Sc	Re	Sh_1
15	16	13	14	17	18	19	20	21	22	23	24	25	26
CEI-30	16/11/2010	0,1060	0,980	0,1025	1,14E-05	0,1101	1,22E-05	0,1298	1,44E-05	2,44E-05	0,6129	5013,7	40,12
CEI-25	02/11/2010	0,1590	0,997	0,1496	1,66E-05	0,1612	1,79E-05	0,1664	1,95E-05	2,45E-05	0,6134	4999,8	40,11
CEI-32	18/11/2010	0,2078	0,983	0,2674	2,97E-05	0,2398	2,66E-05	0,2472	2,75E-05	2,42E-05	0,6116	5057,8	40,27
CEI-57	13/05/2011	0,3370	0,999	0,3196	3,55E-05	0,3412	3,79E-05	0,3064	3,40E-05	2,42E-05	0,6131	5051,6	40,30
CEI-34	22/11/2010	0,3068	0,975	0,4196	4,66E-05	0,3578	3,98E-05	0,3911	4,35E-05	2,44E-05	0,6118	5018,8	40,12
CEI-58	13/05/2011	0,4271	0,995	0,4987	5,54E-05	0,4603	5,11E-05	0,4890	5,43E-05	2,42E-05	0,6135	5047,6	40,29
CEI-26	03/11/2010	0,2603	0,998	0,2693	2,99E-05	0,2643	2,94E-05	0,2879	3,20E-05	2,48E-05	0,6153	4906,8	39,82
CEI-27	04/11/2010	0,3730	1,000	0,3718	4,13E-05	0,3900	4,33E-05	0,4510	5,01E-05	2,47E-05	0,6158	4936,9	39,96
CEI-28	05/11/2010	0,3845	0,997	0,4421	4,91E-05	0,4136	4,60E-05	0,5032	5,59E-05	2,46E-05	0,6157	4955,5	40,03

Table VI - 3A Condensation Experimentation (Mean wind vel.- 2.0 m/s)

	Peltier Element, Plate size, and Thickness	Atm. Pressure	Amount of cond collected	Data Aquisition time	Ambient Temp Range (T_a)	Dew Point (T_d)	Controller (T_c)	Surface temp (T_s)	Temp Diff (T_d-T_s)	Temp Diff (T_a-T_s)	Relative humidity	Av P(T_a)-P(T_s)	Exp no.	Date Performed
		Millibar	g	h-min	mean (°C)	mean (°C)	mean (°C)	mean (°C)	mean (°C)	mean (°C)	mean (%)	kPa		
	1	2	3	4	5	6	7	8	9	10	11	12	15	16
1	**50 x50 Peltier**	906	1,6	3	18,4	6,8	-2,2	1,2	5,6	17,2	51,2	0,4191	**CEI-35**	07/12/2010
2	**50 x 50 Plate**	929	1,8	6-03	23,5	4,7	-2,2	2,1	2,6	21,4	32,9	0,2391	**CEI-47**	04/04/2011
3	**Fan freq.**	907	2,0	5	21,4	6,7	-0,2	3,4	3,3	17,9	42,4	0,2982	**CEI-36**	08/12/2010
4	**3 mm**	931	2,8	7-33	22,9	7,1	-0,2	3,7	3,5	19,2	37,3	0,2438	**CEI-46**	01/04/2011
5	**27,6 Hz**	929	2,9	5-16	21,1	9,2	1,0	4,2	5,0	16,9	46,4	0,3402	**CEI-51**	09/05/2011
6		929	3,0	4-59	23,2	9,8	1,0	4,6	5,2	18,6	43,9	0,4018	**CEI-53**	10/05/2011
7		929	3,1	4-56	22,6	10,8	2,0	5,3	5,5	17,3	47,1	0,3985	**CEI-52**	10/05/2011
8		929	3,1	4-52	21,1	10,5	2,0	5,1	5,4	16,0	54,7	0,4926	**CEI-55**	12/05/2011
9		929	3,3	4-30	22,9	11,6	2,0	5,4	6,3	17,6	47,8	0,4345	**CEI-54**	11/05/2011
10		929	3,6	4-18	21,6	12,1	2,0	5,2	6,9	16,4	54,7	0,5265	**CEI-56**	12/05/2011

Table VI - 3B		Curve fitting		Exp average rate of cond				Average values of theoretical calculation					
Exp no.	Date Performed	Slope	R^2	(Tot wt / Tot time)	Mass flux	$((m_2-m_1)/(t_2-t_1))$	Mass flux	Rate of condensation	Mass flux	Diffusivity of water vapour in air	Schmidt number	Reynolds number	Sherwood number
		g/h		g/h	Kg $m^{-2}s^{-1}$	g/h	Kg $m^{-2}s^{-1}$	g/h	Kg $m^{-2}s^{-1}$	m^2/s	Sc	Re	Sh_1
15	16	13	14	17	18	19	20	21	22	23	24	25	26
CEI-35	07/12/2010	0,5430	0,996	0,5564	6,18E-05	0,5493	6,10E-05	0,6756	7,51E-05	2,45E-05	0,612	6666	46,24
CEI-47	04/04/2011	0,3050	0,997	0,2946	3,27E-05	0,3040	3,38E-05	0,3807	4,23E-05	2,40E-05	0,612	6795	46,70
CEI-36	08/12/2010	0,3970	0,999	0,4146	4,61E-05	0,4091	4,55E-05	0,4850	5,39E-05	2,48E-05	0,613	6565	45,96
CEI-46	01/04/2011	0,3780	0,999	0,3628	4,03E-05	0,3800	4,22E-05	0,3877	4,31E-05	2,42E-05	0,613	6729	46,53
CEI-51	09/05/2011	0,5540	0,999	0,5210	5,79E-05	0,5666	6,30E-05	0,5416	6,02E-05	2,44E-05	0,614	6683	46,39
CEI-53	10/05/2011	0,5820	0,993	0,7379	8,20E-05	0,6293	6,99E-05	0,6396	7,11E-05	2,44E-05	0,614	6664	46,34
CEI-52	10/05/2011	0,6360	0,995	0,6919	7,69E-05	0,6444	7,10E-05	0,6344	7,05E-05	2,45E-05	0,615	6627	46,24
CEI-55	12/05/2011	0,6190	0,998	0,6666	7,41E-05	0,6665	7,34E-05	0,7841	8,71E-05	2,45E-05	0,615	6636	46,27
CEI-54	11/05/2011	0,7390	0,999	0,7621	8,47E-05	0,7395	8,22E-05	0,6895	7,69E-05	2,45E-05	0,615	6623	46,23
CEI-56	12/05/2011	0,8350	0,999	0,8445	9,38E-05	0,8466	9,41E-05	0,8379	9,31E-05	2,45E-05	0,615	6631	46,26

Table VI - 4A Condensation Experimentation (Mean wind vel.- 2.5 m/s)

	Peltier Element, Plate size, and Thickness	Atm. Pressure	Amount of cond collected	Data Aquisition time	Ambient Temp Range (T_a)	Dew Point (T_d)	Controller (T_c)	Surface temp (T_s)	Temp Diff (T_d-T_s)	Temp Diff (T_a-T_s)	Relative Humidity	Av $P(T_a)$-$P(T_s)$	Exp no.	Date Performed
		Millibar	g	h-min	mean (°C)	mean (°C)	mean (°C)	mean (°C)	mean (°C)	mean (°C)	mean (%)			
	1	2	3	4	5	6	7	8	9	10	11	12	15	16
1	**50x50 Peltier**	911	0,9	3-33	17,5	2,4	-2,2	1,1	1,4	16,5		0,1463	**CEI-37**	21/12/2010
2	**50 x 50 Plate**	925	1,3	6-05	21,6	4,5	0,0	3,45	1,1	18,2	35,0	0,1503	**CEI-67**	27/05/2011
3	**Fan freq.**	905	2,0	4-36	19,9	5,6	-2,2	1,5	4,2	18,4		0,2569	**CEI-38**	22/12/2010
4	**32,1 Hz**	901	2,0	4-34	21,5	6,0	-1,0	2,6	3,4	18,9		0,2960	**CEI-39**	23/12/2010
5	3 mm	921	2,0	5-39	24,0	5,7	-1,0	3,0	2,7	21,0	32,1	0,2038	**CEI-43**	29/03/2011
6		921	2,1	6-39	22,2	5,3	-1,0	2,7	2,6	19,5	34,8	0,1919	**CEI-44**	30/03/2011
7		925	2,2	4-01	23,5	8,1	0,0	3,8	4,3	19,7	39,4	0,3411	**CEI-66**	26/05/2011
8		926	4,2	7-10	22,3	8,8	0,0	3,6	5,2	18,7	42,8	0,3654	**CEI-45**	31/03/2011
9		920	3,4	5-02	19,9	12,5	3,5	6,2	6,3	13,8	62,5	0,5162	**CEI-68**	25/07/2011

Table VI-4B		Curve fitting		Exp average rate of cond				Average values of theoretical calculation					
Exp no.	Date Performed	Slope	R^2	(Tot wt / Tot time)	Mass flux	$((m_2-m_1)/(t_2-t_1))$	Mass flux	Rate of condensation	Mass flux	Diffusivity of water vapour in air	Schmidt number	Reynolds number	Sherwood number
		g/h		g/h	Kg $m^{-2}s^{-1}$	g/h	Kg $m^{-2}s^{-1}$	g/h	Kg $m^{-2}s^{-1}$	m^2/s	Sc	Re	Sh_1
15	16	13	14	17	18	19	20	21	22	23	24	25	26
CEI-37	21/12/2010	0,2540	0,999	0,2550	2,83E-05	0,2558	2,84E-05	0,2630	2,92E-05	2,43E-05	0,611	8397	51,88
CEI-67	27/05/2011	0,2087	0,996	0,2013	2,24E-05	0,2200	2,44E-05	0,2681	2,98E-05	2,44E-05	0,613	8373	51,89
CEI-38	22/12/2010	0,4480	0,998	0,4263	4,74E-05	0,4504	5,00E-05	0,4634	5,15E-05	2,46E-05	0,612	8313	51,64
CEI-39	23/12/2010	0,4280	0,994	0,4659	5,18E-05	0,4716	5,24E-05	0,5371	5,97E-05	2,49E-05	0,613	8204	51,35
CEI-43	29/03/2011	0,3590	0,999	0,3333	3,70E-05	0,3597	4,00E-05	0,3643	4,05E-05	2,44E-05	0,613	8362	51,84
CEI-44	30/03/2011	0,3130	0,997	0,3256	3,62E-05	0,3250	3,61E-05	0,3431	3,81E-05	2,43E-05	0,613	8376	51,89
CEI-66	26/05/2011	0,5440	0,998	0,5414	6,02E-05	0,5503	6,11E-05	0,6085	6,76E-05	2,44E-05	0,614	8347	51,83
CEI-45	31/03/2011	0,5920	0,999	0,5661	6,29E-05	0,5933	6,59E-05	0,6514	7,24E-05	2,43E-05	0,614	8368	51,89
CEI-68	25/07/2011	0,6575	0,992	0,6105	6,78E-05	0,7050	7,83E-05	0,9232	1,03E-04	2,49E-05	0,616	8147	51,31

Table VI - 5A Condensation Experimentation (Mean wind vel.- 3.0 m/s)

	Peltier Element, Plate size, and Thickness	Atm. Pressure	Amount of cond collected	Data Aquisition time	Ambient Temp Range (T_a)	Dew Point (T_d)	Controller (T_c)	Surface temp (T_s)	Temp Diff (T_d-T_s)	Temp Diff (T_a-T_s)	Relative humidity	Av P(T_a)-P(T_s)	Exp no.	Date Performed
		Millibar	g	h-min	mean (°C)	mean (°C)	mean (°C)	mean (°C)	mean (°C)	mean (°C)	mean (%)	kPa		
	1	2	3	4	5	6	7	8	9	10	11	12	13	14
1	**50x50 Peltier**	925	0,7	2-19	23,2	1,8	-3,0	1,2	**0,6**	22,1	23,1	0,0183	**CEI-41**	11/02/2011
2	**50 x 50 Plate**	926	1,2	5-32	23,7	1,8	-3,0	1,3	**0,6**	22,4	21,0	0,0073	**CEI-40**	10/02/2011
3	**Fan freq.**	930	1,8	4-32	18,7	5,4	-1,0	2,1	3,3	16,6	44,2	0,2418	**CEI-59**	16/05/2011
4		932	2,0	4-06	21,2	6,3	0,0	3,4	2,9	17,8	39,1	0,2116	**CEI-60**	16/05/2011
5	3 mm	930	2,0	4-43	22,3	6,5	0,0	3,6	2,9	18,6	37,1	0,2293	**CEI-61**	17/05/2011
6	**40,0 Hz**	930	2,1	3-50	23,5	6,9	0,0	3,8	3,1	19,7	35,4	0,2279	**CEI-62**	17/05/2011
7		919	2,5	5-56	22,5	5,7	-1,0	2,8	**2,8**	19,7	35,3	0,2200	**CEI-42**	28/03/2011
8		925	2,8	4-14	24,1	8,3	0,0	3,9	4,4	20,2	36,8	0,3032	**CEI-63**	18/05/2011
9		930	3,0	3-54	22,0	9,4	1,0	4,4	5,0	17,6	46,7	0,4047	**CEI-64**	24/05/2011
10		924	3,1	4-07	21,7	10,6	2,0	5,2	5,4	16,5	52,3	0,4792	**CEI-70**	27/07/2011
11		932	3,6	5-22	25,2	8,6	0,0	4,1	4,6	21,1	35,7	0,3368	**CEI-65**	25/05/2011
12		920	3,6	4-08	21,0	12,6	4,5	7,2	5,4	13,8	60,3	0,4838	**CEI-69**	26/07/2011

Table VI-5B		Curve fitting		Exp average rate of condensation				Average values of theoretical calculation					
Exp no.	Date Performed	Slope	R^2	(Tot wt / Tot time)	Mass flux	$((m_2-m_1)/(t_2-t_1))$	Mass flux	Rate of condensation	Mass flux	Diffusivity of water vapour in air	Schmidt number	Reynolds number	Sherwood number
		g/h		g/h	Kg $m^{-2}s^{-1}$	g/h	Kg $m^{-2}s^{-1}$	g/h	Kg $m^{-2}s^{-1}$	m^2/s	Sc	Re	Sh_1
13	14	15	16	17	18	19	20	21	22	23	24	25	26
CEI-41	11/02/2011	0,3000	0,990	0,3355	3,73E-05	0,2940	3,27E-05	0,0332	3,69E-06	2,40E-05	0,611	8809,81	53,13
CEI-40	10/02/2011	0,2120	0,998	0,2399	2,67E-05	0,2253	2,50E-05	0,0132	1,47E-06	2,40E-05	0,611	8801,47	53,10
CEI-59	16/05/2011	0,4020	0,999	0,3839	4,27E-05	0,4001	4,45E-05	0,4711	5,23E-05	2,40E-05	0,6123	10202,10	57,23
CEI-60	16/05/2011	0,4850	0,997	0,5655	6,28E-05	0,5042	5,60E-05	0,4118	4,58E-05	2,42E-05	0,6132	10125,85	57,06
CEI-61	17/05/2011	0,4230	0,997	0,4160	4,62E-05	0,4300	4,78E-05	0,4468	4,96E-05	2,42E-05	0,6134	10085,88	56,96
CEI-62	17/05/2011	0,5430	0,992	0,6242	6,94E-05	0,5664	6,29E-05	0,4440	4,93E-05	2,43E-05	0,6135	10074,81	56,94
CEI-42	28/03/2011	0,4310	0,998	0,3913	4,35E-05	0,4443	4,94E-05	0,4313	4,79E-05	2,44E-05	0,6123	10019,82	56,77
CEI-63	18/05/2011	0,6570	0,999	0,6422	7,14E-05	0,6696	7,44E-05	0,5924	6,58E-05	2,44E-05	0,6137	10009,54	56,76
CEI-64	24/05/2011	0,7553	0,997	0,8601	9,56E-05	0,7860	8,73E-05	0,7886	8,76E-05	2,44E-05	0,6143	10021,48	56,83
CEI-70	27/07/2011	0,7352	0,993	0,7880	8,76E-05	0,7563	8,40E-05	0,9369	1,04E-04	2,46E-05	0,6151	9893,99	56,51
CEI-65	25/05/2011	0,6526	1,000	0,6959	7,73E-05	0,6797	7,55E-05	0,6555	7,28E-05	2,43E-05	0,6139	10070,46	56,94
CEI-69	26/07/2011	0,8550	0,995	1,0020	1,11E-04	0,8984	9,98E-05	0,9482	1,05E-04	2,51E-05	0,6164	9704,73	56,06

6.6 Discussion

6.6.1 Experimental measurements of the rate of condensation at 1.0 m/s

The data given in the tables VI- 1 to 5 correspond to 5 different velocities basically; all experiments have been performed with the same substrate of 25 cm^2. In fact, the active condensing area might have been slightly larger because of the additional condensation that occurred on the 3 mm vertical slice (sides) of the plate. Usually, all the four sides were partially covered by the sponge, and this surface was also covered by a very thin layer of plastic tape to prevent condensation on this side, even though a few condensate drops were seen on this surface during the experiment. This condensing area is not included in the calculations. The rate of condensation without including the active area of condensation is given in the figure VI-10 (a, b, c) as a function of the temperature difference (a) (ΔT_c) and (b, c) ($\Delta T_s = T_d - T_s$) between dew point and surface temperature calculated by eq.(VI-3) for comparison. In all plots the average rate of condensation has been calculated by two methods: (i) (Total wt / Total time) - cumulative weight of condensate divided by the total time in collecting that weight; (ii) taking the average of all data points for one experiment obtained as $(m_2-m_1)/(t_2-t_1)$ increase in the weight of condensate in each step (every 30 min or every 0.1g increase) divided by the time taken in that step. After the observation of the fig.VI-10 (a, b), it was found that the regression coefficients for the rate of condensation using (ii) method in both plots were better. Similar results have been found for the majority of the data, and finally the assumption (ii) was chosen for further discussion. Fig.VI-10 (c) is for a 3.0 m/s flow field and the mode of data taken was in every 0.1 g increase on the balance. For this velocity the least square fit has given better regression coefficients with the (ii) method. It has been already discussed that the latter one gives a better fitting, as it included the effect of local changes in environment, and its effect on the rate of condensation. It is noteworthy that the condensation rate increased significantly (x 2.2) when the average velocity increased by a ratio of 3. The variation in data points for a similar ΔT_s indicates the variation in relative humidity, which was not constant for all the experiments. The variation in ambient temperature and relative humidity during the experimental time was not similar for different day experiments, which causes the data points to be scattered. The temperature range for all the experiments at 1.0 m/s was 17 - 25 °C, but the maximum variation for one day experiments was not more than 2.5 °C. The range of relative humidity was 41-65 %, and the maximum variation in one day was less than 13 % and the minimum variation was less than 1%.

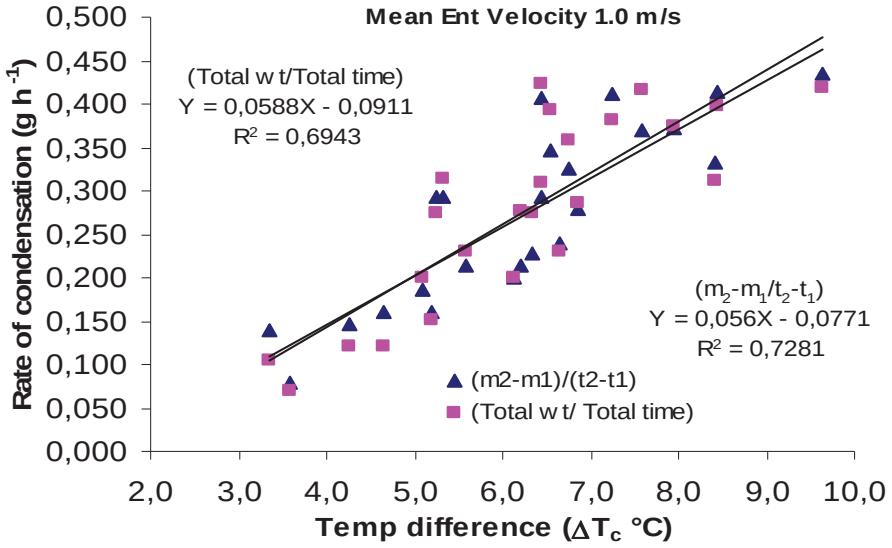

(a)

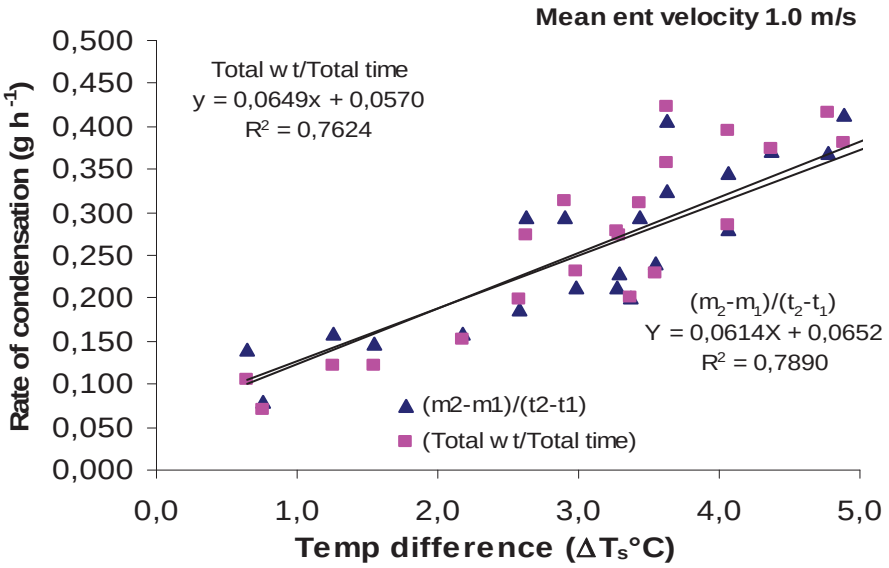

(b)

Fig.VI-10: Rate of condensation (g/h) for a mean entrance velocity of 1.0 m/s as a function of (a) temperature difference (ΔT_c °C) (b) temperature difference (ΔT_s °C).

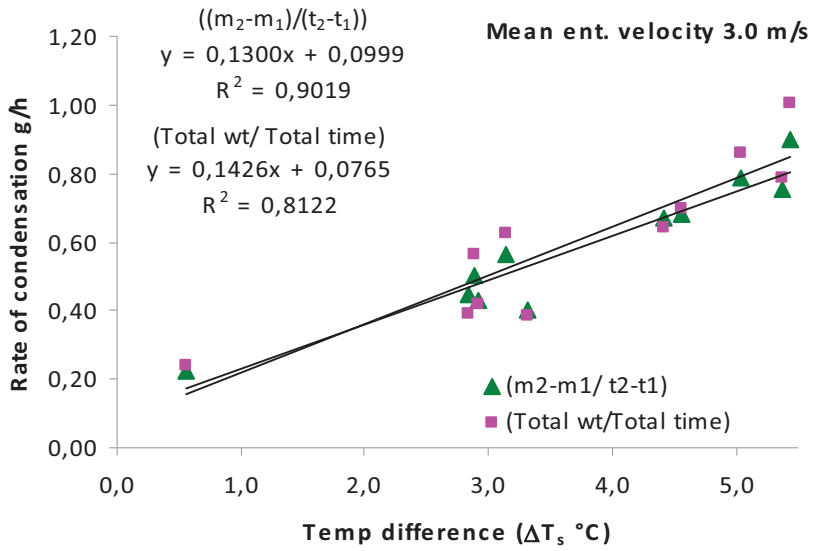

(c)

Fig.VI-10: (c) Rate of condensation (g/h) for a mean entrance velocity of 3.0 m/s as a function of temperature difference (ΔT_s °C).

If the temperature difference (ΔT_c) were constant, and the relative humidity and the ambient temperature had less than 3% variation, the rate of condensate would be similar, also it would give a similar average value of rate of condensation. For example – the experiment CEI-1, CEI-2 and CEI-8 have the same average rate of condensation value of 0.2938 g/h, the experiment CEI-1 and CEI-2 had averages of ΔT_c, equal to 5.2 °C and 5.3 °C, and averages of relative humidity of 57.2 % and 56.9% respectively, which is almost same. But in the experiment CEI-8, the average ΔT_c was 6.5 °C and the average relative humidity was 44.8%, which is almost 10% less than CEI-1 and CEI-2. The variation in relative humidity was more than 20%, which was compensated by the increment in the ΔT_c average by increasing it by more than 1.2°C, and this was 20% more than CEI-1 and CEI-2. The detailed data are shown in Table VI-1 A, B. Thus, as we are only comparing average mass rates a variation in relative humidity could be compensated by an opposite variation in ΔT_c, but it is necessary that all other parameters should be stable. The parameters like temperature difference imposed on the plate, dewpoint, relative humidity, ambient temperature, and the air velocity have shown direct influence on the rate of condensate.

Due to the continuous condensation process on the plate surface, the condensation interface evolved from the initial solid/air interface to a partial liquid/air interface, owing to

the developing dropwise condensation on the active surface. Also, the distribution of the condensate drops on the plate surface was heterogeneous as a result of nucleation, and the drop sizes were uneven because of the continuous coalescence process. Thus, the new condensation interface formed was at a temperature different from the controller temperature. So that, the empirical relations given in eqs.(VI-1 to 5) have been used to predict the surface temperature, and the difference ΔT_s used in fig.VI-10 (b) and VI-10 (c) as X-axis.

6.6.2 Comparison with theoretical results at 1.0 m s^{-1}

Fig.VI-10 gives a comparison of the experimental rate of condensation and theoretical ones versus the temperature difference ΔT_c. For the evaluation of the theoretical rates, the surface temperature was estimated with eq. VI-1 to VI-5. The fitting of the theoretical values calculated using equation (VI-3) correspond to the plot marked as 'Theory 1'. The other two cases marked as 'Theory 2' and 'Theory 3' are the extreme cases of condensation with eq. (VI-5) and eq. (VI-4) respectively, one considers the maximum temperature possible for condensation to occur, and the other one was the maximum temperature difference possible created in the particular experiment.

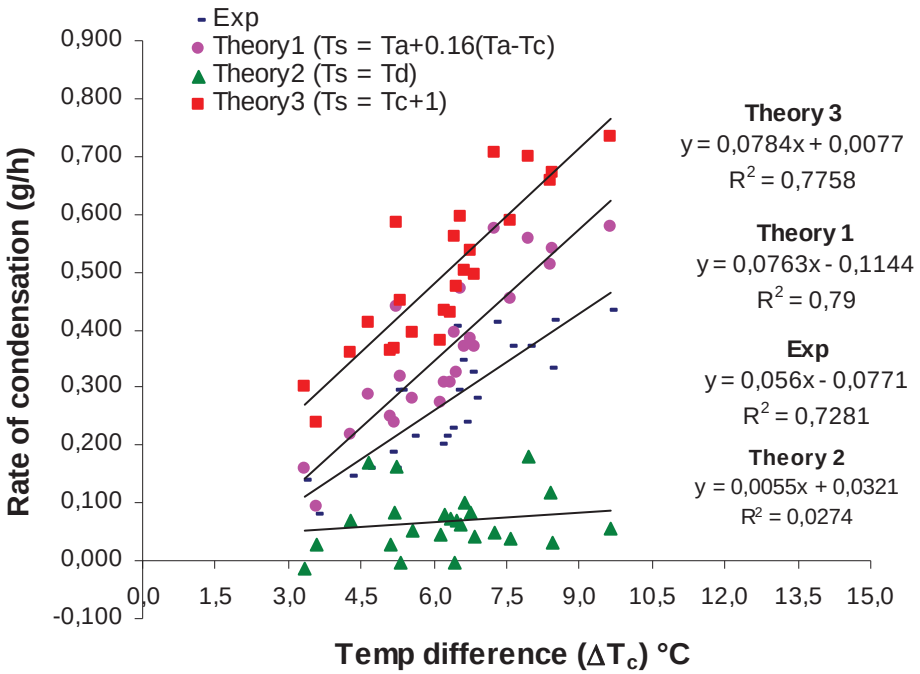

Fig.VI-11: Rate of condensation as a function of temperature difference (ΔT_c °C). The theoretical values calculated using the surface temperature formula given as eqs (VI-3, 4, 5).

The ‘Theory 2’ has some negative values for the rate of condensation, however during the experimental observations, they were positive as seen on the figure. Comparisons have also been made using eqs. VI-1, VI-2, and the assumption proposed by Minkowycz and Sparrow (1966) which concerned a vertical case, but the surface temperature given by eqs VI-1 was far away for most of the cases even more than the dewpoint temperature, and the surface temperature recommended by eqs VI-2 gave negative temperature difference ΔT_s in a few cases, where the experimental data gave positive rates of condensation. However, eq-VI-3 generates better results in comparison to others, ΔT_s was positive in all condensation cases.

The rate of condensation is also plotted versus the temperature difference ΔT_s for all the three cases which have already been discussed in figure VI-10 with ΔT_c, they are given here separately as figure VI-12 (a, b, c).

All figures VI-11, VI-12 (a, b, c) present the same experimental data, only the calculated temperature difference (ΔT_s) data have been changed, according to the model used, which induced variations in the estimation of the surface temperature ΔT_s. The linear curve fittings show approaching gradients between the experimental and the theoretical results (fig.VI-12 (a)), and more discrepancy with the other two models (fig.VI-12 (b, c). This is also indicated by the values of the coefficients of regression given in these plots. It can also be observed from these figures that the range of temperature difference data for 1.0 m/s vary: i) ΔT_c exp 3.6 °C to 9.6°C; ii) ΔT_s theory 1, 0.7 °C to 6.3 °C; iii) ΔT_s theory 2, 5.8 °C to 14.4°C; and iv) ΔT_s theory 3, 2.2 °C to 8.8 °C. This influence is notable on the plots and also its effect on the rate of condensation.

Furthermore, the analysis has been done with the difference in partial pressure of water vapour in humid air at the temperatures of the free stream flow and at the assumed surface temperature (T_s), on which condensation was considered. Mathematically, partial pressure was calculated using both temperature and relative humidity.

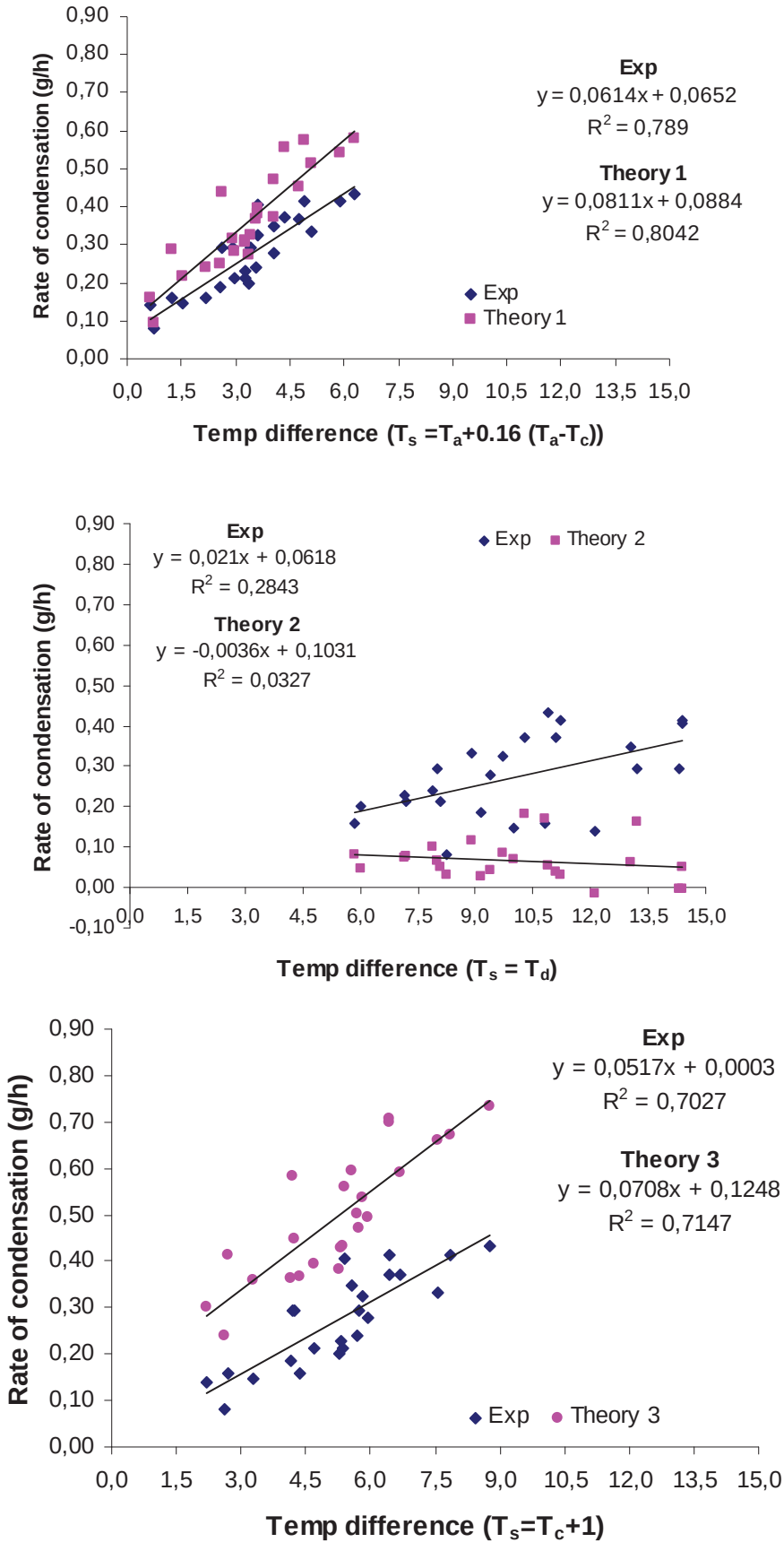

Fig.VI-12: Rate of condensation as a function of temp difference (ΔT_s) for 1.0 m/s velocity.

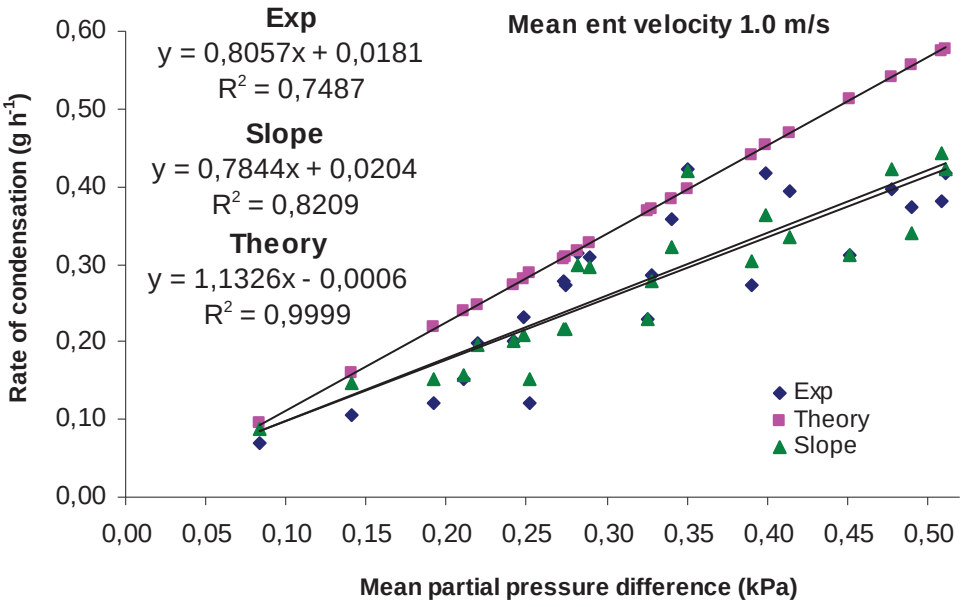

Fig.VI-13: Rate of condensation as a function of average difference in partial pressure of water vapour in humid air at ambient temperature and surface temperature.

Fig.VI-13 shows the variation of the rate of condensation as a function of the algebraic average of partial pressure difference between free stream partial pressure and partial pressure at the surface temperature. Each point in the rate of condensation curve correspond to an experiment of 6 h to 8 h. The experimental value is the algebraic average of the data points as described earlier taken with the method (m_2-m_1/t_2-t_1), the 'slope' corresponds to the gradient of the curves plotted for the increase in weight with time for each experiment, and the theory points correspond to the arithmetic mean of points calculated using the environmental data recorded at the time of experiment. The theoretical data shows the best fit, the 'slope' gives slightly better coefficients of regression in comparison to the algebraic average (exp), where some scattered data are obtained. Most of the scattering in data can be justified by the experimental conditions. Indeed, only average rates are presented and temperature difference (ΔT_c /ΔT_s) omitting the hygrometric conditions of the experiment and that those conditions at times varied during the experiment. The global experimental set up did not allow us to be more precise and to conduct experiments at a specific ambient temperature coupled with a specific relative humidity over 7 hours.

The partial pressure difference created at the solid / air or liquid / air interface was the

driving force for the diffusion of water vapour at the condensing surface of the flat plate. This difference in partial pressure at the interface was caused by the difference in temperature, a temperature below the dewpoint at the interface caused the saturation to occur. The dependence of the mass flux on the temperature difference, measured as ΔT_c or ΔT_s, and on the mean velocity of the air inside the wind tunnel is established. From the above discussion, it is obvious that the choice of ΔT_s, in lieu of ΔT_c, gives a better representation of the phenomenon.

6.6.3 Mass flux evaluation at 1.0 m/s

The dependence of the mass flux as a function of the mean difference in partial pressure, and on ΔT_s are given in figure VI-14 (a, b) for the 1.0 m/s velocity with the same mass flux data. The data are more scattered when ΔT_s is considered (fig.VI-14 (b)), also the regression coefficients for both theoretical and experimental results give smoother trends as given in figure VI-14 (a). The mass flux depends on several factors, which are interdependent; one of the key factors is the relative humidity, and in a plot showing the variation of mass flux with respect to ΔT_s like VI-14 (b), a fluctuation or variation in relative humidity will induce some deviation, as they were not included in the plot. As already mentioned, RH should be kept constant to avoid any deviation. As a matter of fact, a long variation in RH would act as a spurious mode, as the global problem is multi-parametric and the bi-dimensional plots given herein can only deal with 1 to 3 parameters only.

It has been observed that, for the same temperature difference imposed on the active plate, if the relative humidity varies by more than 5 % then the mass flux will be significantly affected. However, the temperature difference has a considerable effect on the mass flux also; theoretically keeping all other parameters constant, on increase of 1 °C in the temperature difference will cause a more than 20 % increase in the mass flux value. Also, an increase of 1% in relative humidity will cause an almost 9 % increase in the average mass flux, while keeping constant all the other parameters.

6.6.4 Influence of the flow intensity on the condensation mass flux

An increase in the air flow intensity is seen on figure VI-15 (a, b), though the mass flux as a function of ΔT_s and the mean partial pressure difference for the mean entrance velocity 1.5 m/s. It shows similar effects and again comparative better data fit for partial

pressure difference as compared to ΔT_s.

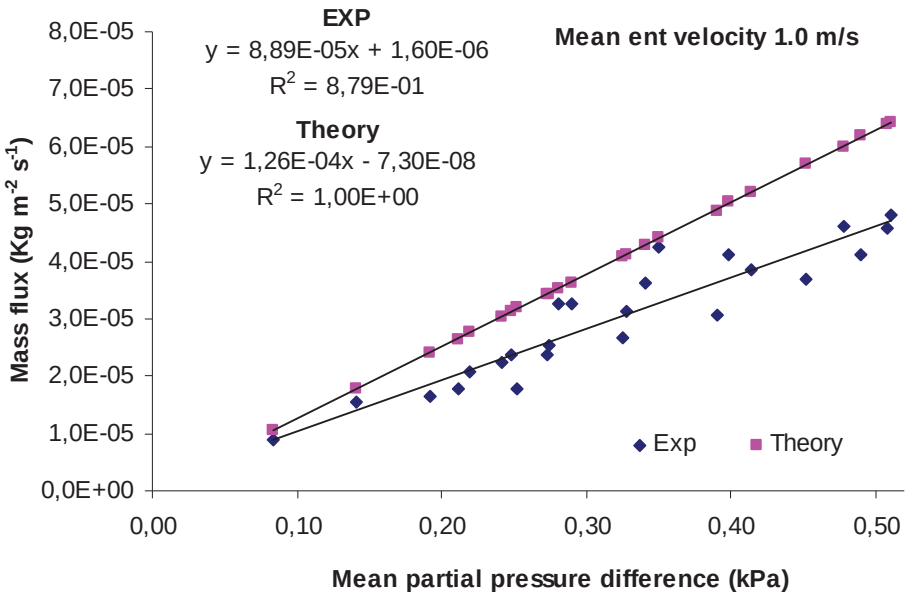

(a)

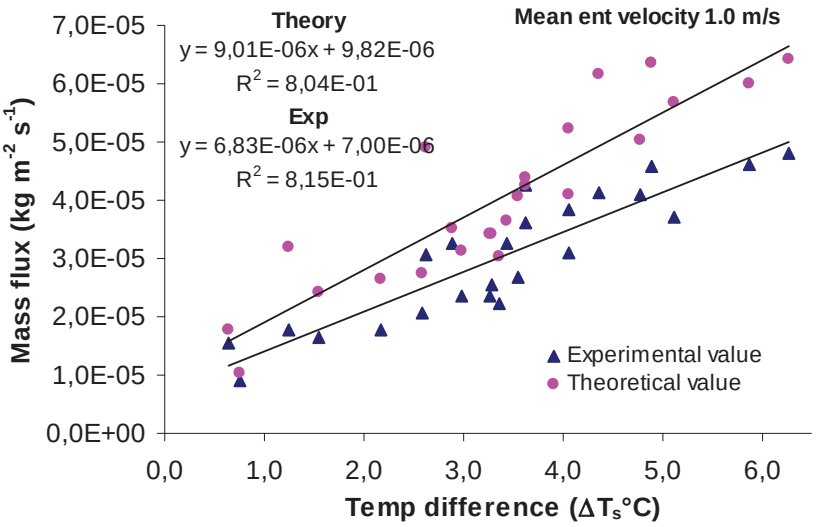

(b)

Fig.VI-14: Mass flux for mean entrance velocity 1.0 m/s a) as a function of the mean partial pressure difference, and b) of the temperature difference (ΔT_s).

The theoretical data in the figure VI-15(b) mass flux versus ΔP plot shows 100% linearity, and 95% for the experimental one. The gradient of mass flux with partial pressure difference amounts to 1.29×10^{-4} in the experiments and 1.52×10^{-4} for the theory, also the corresponding values of the gradient with ΔT_s are 8.42×10^{-6} for the experiments, and 8.89×10^{-6} for the theory. When increasing the flow intensity further similar results have been found; the gradient of mass flux with temperature difference is always lower than with partial

pressure difference; also the theoretical values are always higher than the experimental ones.

In addition, it has been found that, for the velocity range, which we have used in this thesis, the regression coefficients of the mass flux with partial pressure difference reached nearly 100% fit for the theory, and a little bit less for the experiments. In opposition, the regression coefficients for ΔT_s plots were most of the time higher for the experimental data than for the theoretical data. For 1.0 m/s (fig.VI-14 (a, b)) more data were available, but these data cover more variations in physical environmental conditions: (ΔT_c) was in the range 3.4°C - 9.8 °C, while the relative humidity was in 43-63 % for total of 24 data points. For 1.5 m/s, ΔT_c was in 3.3 °C -8.2 °C ΔT_c RH in 38-48%, with a total of 9 data points only.

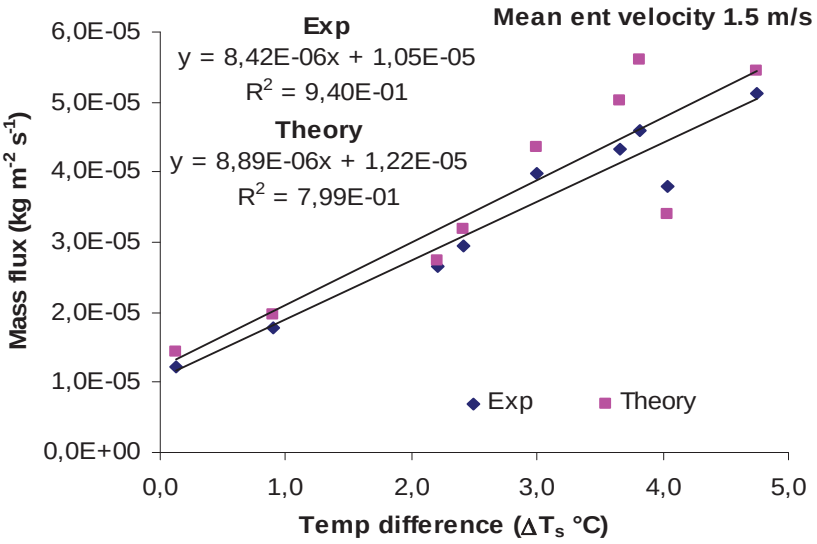

(a)

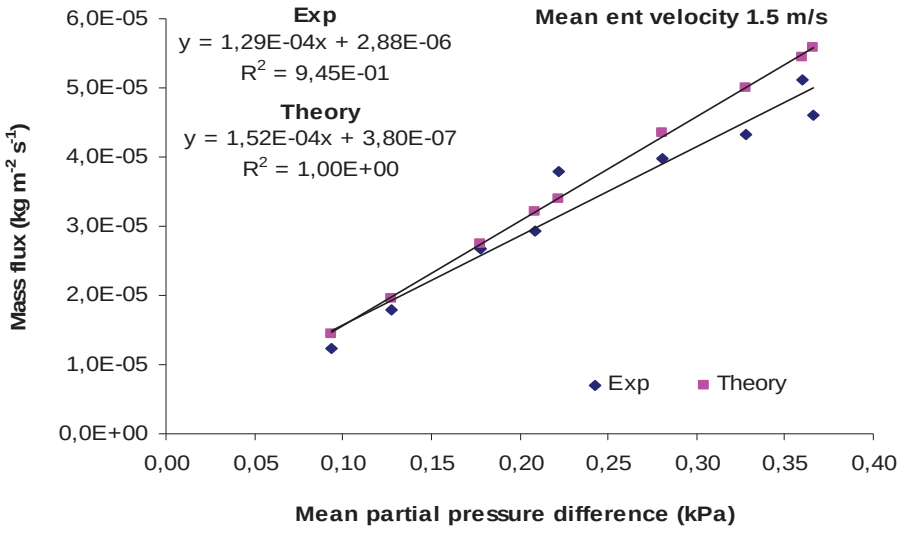

(b)

Fig.VI-15: Mass flux as function of (a) ΔT_s (°C), and (b) mean partial pressure difference (kPa) for a mean entrance velocity 1.5 m/s.

The linearized mass flux trends versus the partial pressure difference or the temperature difference were plotted for each mean entrance velocity, with the experimental (fig.VI-16(a), & VI-17(a)) and the theoretical data (fig.VI-16(b) & VI-16(b)).

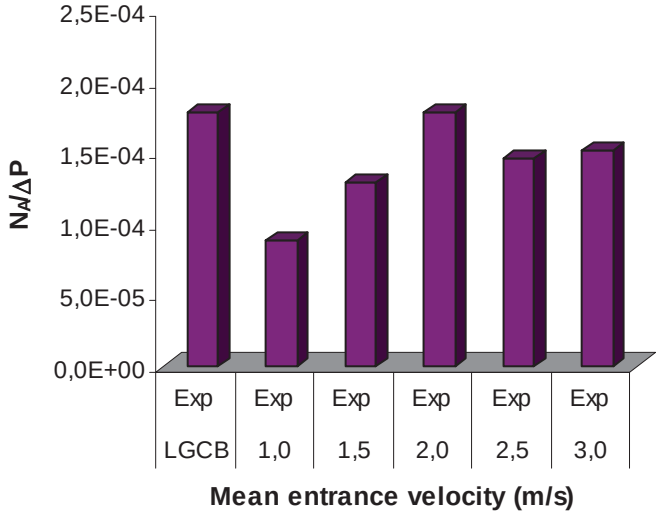

(a)

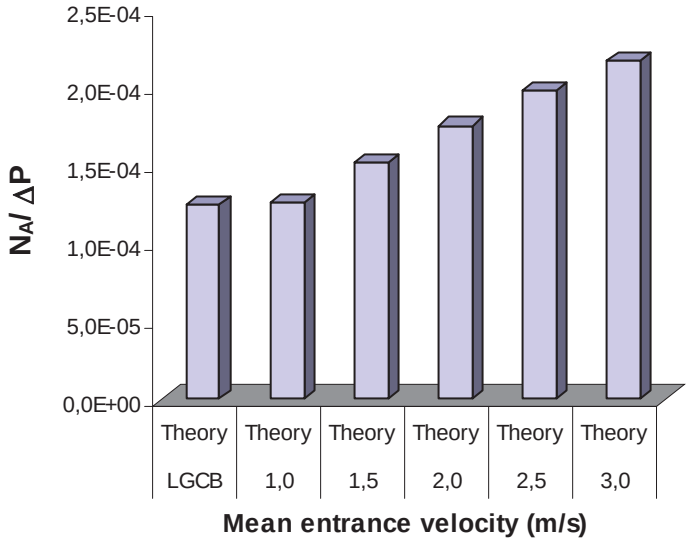

(b)

Fig.VI-16(a,b): Plots of $N_A/\Delta P$ as a function of the mean entrance velocity, for (a) the experimental data, and (b) the theoretical data. All the experimental data are shown in here including the experiments performed in unregulated open environment marked as LGCB.

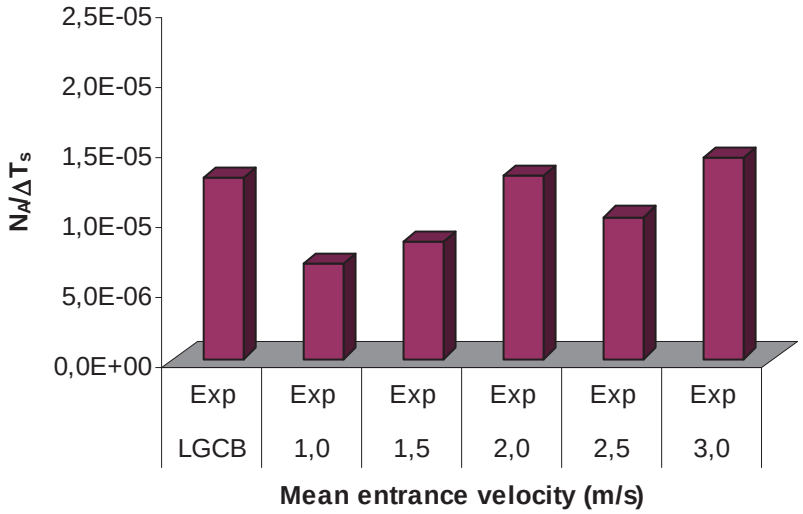

(a)

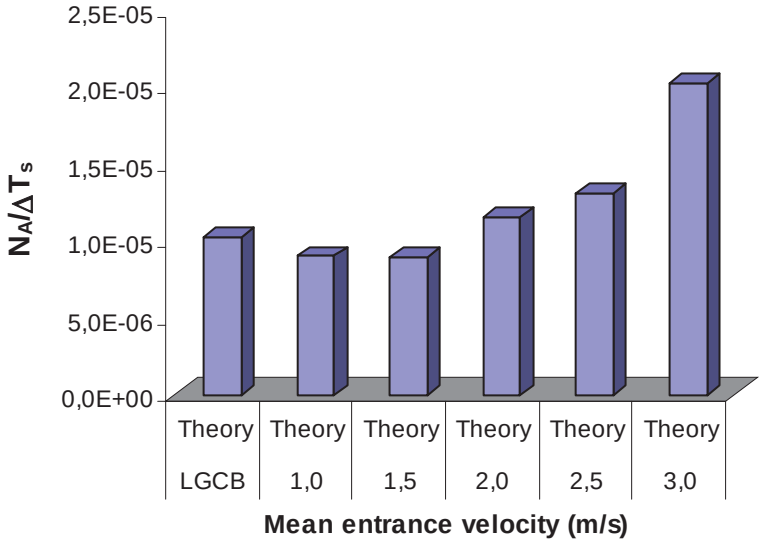

(b)

Fig.VI-17(a,b): Plots of $N_A/\Delta T_s$ as function of the mean entrance velocity for (a) the experimental data, and (b) the theoretical data. All the experimental data are shown in here including the experiments performed in unregulated open environment marked as LGCB.

On increasing the mean entrance velocity inside the wind tunnel, the mass flux has a tendency to increase but not according to a linear variation. The histogram shown in the figure VI-16 (a) corresponds to the variation of the mass flux (N_A) with respect to the mean partial pressure difference as a function of velocity for the experimental data, and VI-16 (b) for the calculated data, and similar histogram plots were given in Figure VI-17 (a, b) for ($N_A/\Delta T_s$). In these plots all the experimental data have been used, and an extra bar, marked 'LGCB', was added, which represents the data recorded in an unregulated environment of the lab under the air flow measured during these experiments, the measured velocity near the condensing plate was very roughly 1.2 m/s, and the other conditions are discussed in chapter V. These "LGCB" values of $N_A/\Delta T_s$ and $N_A/\Delta P$ are not clearly understood as the plots correspond to a mean entrance velocity of 2.0 m/s for the experimental data, and 1.0-1.8 m/s for the theoretical data, as compared to data obtained in the wind tunnel, even if slower velocities were measured. In the open environment some other parameters might have played a role as well, such as cross ventilation and local variations in temperature and RH. The temperature difference ΔT_c chosen for these experiments were in the range 1.2 °C to 4.1 °C, which was quite low in comparison to the regulated environment of the wind tunnel. In fig.VI-16 (a) and VI-17 (a) with the experimental data, the mass flux coefficients for the 2.0 m/s mean entrance velocity have higher values in comparison to the other velocities. It is because of the higher temperature differences chosen during these condensation experiments and durations of a few experiments, the physical environmental parameters have recorded large variations for this velocity. On removing a few scattered experimental data, and also eliminating the open environment experimental data, more regular plots were obtained, see fig.VI-18 (a, b) and VI-19 (a, b) for both cases of mean partial pressure difference and mean temperature difference. Fig.VI-18 (a, b), and VI-19 (a, b) establish clearly the raise in the mass transfer coefficients on increasing the velocity inside the wind tunnel. Nevertheless, during these measurements the range of the average physical parameters was not the same. For each velocity, the relative humidity (RH %) and the temperature difference (ΔT_c °C) charts are given as Table VI-6 A, and VI-6 B to give an idea of these two important parameters involved in the summarized data, which are given in the plots VI-16 to VI-19 as well.

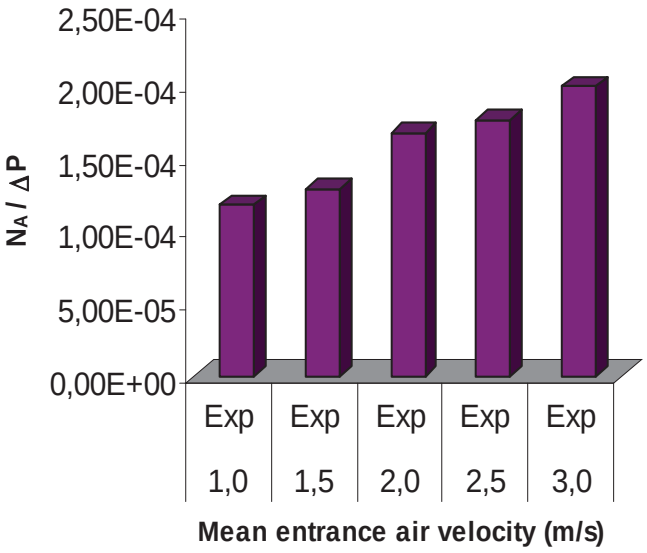

(a)

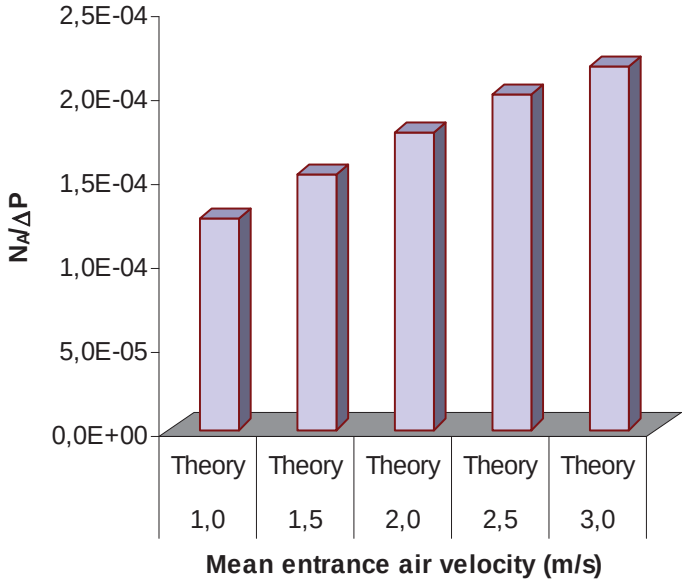

(b)

Fig.VI-18(a, b): Plots of $N_A/\Delta P$ as a function of the mean entrance velocity for the (a) the experimental data, and (b) the theoretical data. Scattered experimental data have been removed including the experiments performed in unregulated open environment to reduce the discrepancy.

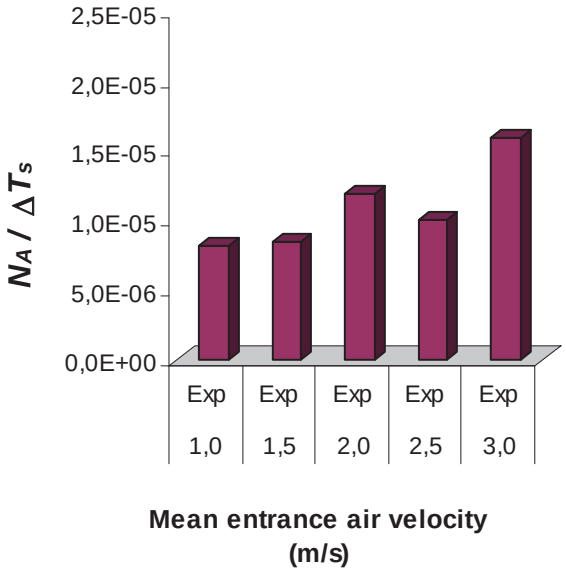

(a)

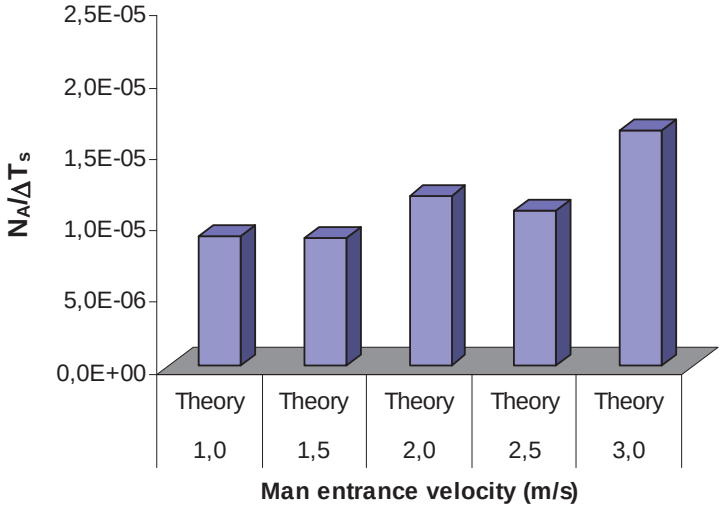

(b)

Fig.VI-19 (a, b): Plots of $N_A/\Delta T_s$ as a function of the mean entrance velocity with (a) the experimental data, and (b) the theoretical data. Scattered experimental data have been removed including the experiments performed in unregulated open environment to reduce the discrepancy.

As been in the table VI-6 B mainly large ΔT_c were used for the velocity of 2.0 m/s (7-10 °C), and at the same time RH was 33-57 %, whereas for 2.5 m/s and 3.0 m/s most of the experiments were carried out below 45% of RH, and the range of ΔT_c were at least 1°C lower in average. As previously discussed these environmental conditions were dependent on the weather of the day.

Table VI-6A Relative Humidity Chart

Mean ent Vel. (m/s)	Relative Humidity (RH %)							Total Range
	30-35	35-40	40-45	45-50	50-55	55-60	60-65	
LGCB	**1** 34.1	**2** 37.2-38.0	**3** 41.3-45.3	**5** 47.6-49.1	**2** 50.8-54.5	**2** 56.0-56.7		**15** 34.1-56.7
1.0			**3** 42.6-44.8	**7** 48.0-49.6	**9** 50.7-55.3	**3** 56.9-57.2	**2** 60.9-63.0	**24** 42.6-63.0
1.5		**3** 38.4-39.1	**3** 41.3-44.9	**3** 45.8-47.5				**9** 38.4-47.5
2.0	**1** 32.9	**1** 37.3	**2** 42.4-43.9	**3** 46.4-47.8	**3** 51.2-54.7			**10** 32.9-54.7
2.5	**3** 32.1-35.0	**4** 39.4-40.4	**1** 42.8				**1** 62.5	**9** 32.1-62.5
3.0	**2** 35.3-35.4	**4** 35.7-39.1	**1** 44.2	**1** 46.7	**1** 52.3	**1** 60.3		**10** 35.3-46.7
Total	**7**	**14**	**13**	**19**	**15**	**6**	**3**	**77**

Table VI-6B Temperature Difference chart

Mean ent Vel. (m/s)	Temperature difference (°C)									Total Range
	1.0-2.0	2.0-3.0	3.0-4.0	4.0-5.0	5.0-6.0	6.0-7.0	7.0-8.0	8.0-9.0	9.0-10.0	
LGCB	**9** 1.2-2.4	**3** 2.5-2.7	**3** 3.6-4.1							**15** 1.2-4.1
1.0			**4** 3.1-4.3	**4** 5.2-5.4	**5** 5.7-6.4	**7** 6.6-7.4	**1** 7.7	**2** 8.6-8.8	**1** 9.8	**24** 3.1-9.8
1.5			**2** 3.3-4.2		**3** 5.5-6.4	**2** 6.8-7.2	**2** 7.5-8.2			**9** 3.3-8.2
2.0						**3** 6.9-7.3	**1** 8.2	**4** 8.5-9.1	**2** 9.6-10.1	**10** 6.9-10.1
2.5				**2** 4.5-4.6	**1** 6.3	**2** 6.7-7.0	**2** 7.8-8.1	**2** 8.8-9.0		**9** 4.5-8.8
3.0					2 6.3-6.4	3 6.5-6.9	3 8.1-8.4	2 8.6-8.6		**10** 6.3-8.6
Total	**9**	**3**	**9**	**6**	**11**	**17**	**9**	**10**	**3**	**77**

The Sherwood numbers calculated using equations VI-9, VI-11, and VI-12 are plotted as a function of the Reynolds number given in figure VI-20, shown as Sh_1, Sh_2 and Sh_3, respectively, for the above mentioned equations. Power series data fit was performed, and it resulted in the value of m (mentioned in the eq. VI-8 as a power of Re) as 0.498, 0.786, and 0.616 for the above three definitions, which are approximately equal to the fractions 1/2, 4/5,

and 2/3 respectively. The experimental value of Sh_3, given in the plot VI-20 was obtained when including all experimental data without any kind of selection. The experimental value of Sherwood number represents the dependence of results very near to the $Re^{2/3}$, which was already predicted on an early study from Ota and Kon (1974) for blunt-faced bodies, it was explained that in heat transfer analogy the Nusselt number scales with $Re^{2/3}$ (Hwang et al. 1996, Marty et al. 2008).

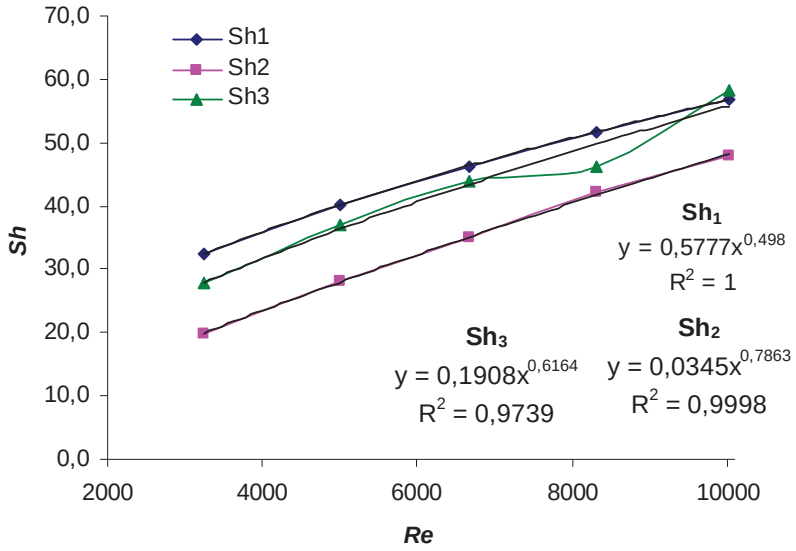

Fig.VI-20: Calculated Sherwood numbers as a function of the Reynolds number and their trend line as a power series.

As a result of our experiments we can express the average Sherwood number

$$Sh = 0.225\,\mathrm{Re}^{2/3}\,Sc^{1/3} \qquad \text{(VI-17)}$$

The Schmidt number (*Sc)* was found constant during the experimental measurements, and it was already given in the Tables from VI-1B-5B in column 24. If figure VI-20 is re-plotted after dividing the Sherwood numbers by the dependence in Reynolds number as (Hwang et al. 1996)

$$Sh_i \Big/ \mathrm{Re}^{m_i} = X_i \quad \text{where } i = 1, 2, 3 \qquad \text{(VI-18)}$$

We have taken, for X_1, $m_1 = ½$, for X_2, $m_2 = 4/5$, and for X_3, $m_3 = 2/3$. It is noteworthy that Fig. VI-21 underscores 3 different flow regions:

- laminar boundary flow over a thin flat plate (X_1)
- turbulent flow over a similar flat plate (X_2)

- present moderate turbulent boundary layer flow over a non mono-block geometry (X_3)

Evidently, the coefficient for X_3 presents a slight dip at 2.5 m/s, however, all other values lead to a constant value. It has already been discussed that the flow profile on the active condensing flat plate seemed to be weekly turbulent, and that the turbulence was increased with an increase in the mean entrance velocity.

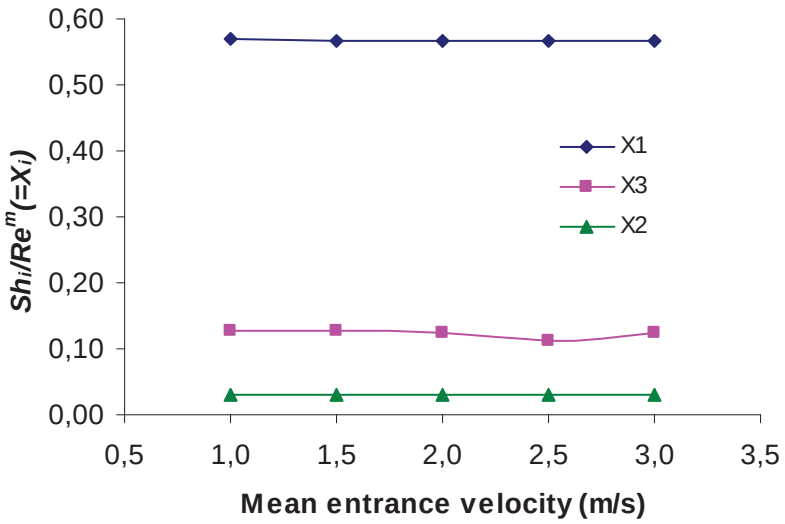

Fig.VI-21: Re-plotted data of figure VI-20, by using Sh_i / Re^{m_i} as ordinate and mean entrance velocity as abscissa.

Various data have already shown similar behaviour, a raise in mass flux coefficients (N_A) with an increase in the mean entrance velocity. The mass transfer study by Sørensen (1969) on truncated slabs of various thicknesses showed that mass transfer coefficients do not only depend on the air velocity and distance from the leading edge, but also on the thickness of the slabs. We have only studied velocity variations, as the thickness of our experimental body was constant for all velocity measurements.

Furthermore, Marty et al. (2008) talked about the flow behaviour on the surface of a blunt-faced body, they stated that because of the reattachment of the flow at a distance from the leading edge located between 6e/2 and 13e/2 (where e is the thickness of the slab), there was a sudden increase in flow pressure, which caused locally higher transfer coefficients. Consequently, there is a possibility that the growth of the drops and for the coalescence

phenomenon little faster at the reattachment zone in comparison to other parts of the plate due to higher mass transfer coefficients; usually we have noticed the formation of big drops between the centre part and the rear edge of the flat plate. Moreover, it was mentioned by several workers (Hwang et al. 2001, Sun 2001) that this distance is around the reattachment area of the flow, called 'reattachment zone', and pointed out that the transfer coefficients were higher normally around two regions, at the leading edge, as opposed to the training edge, and towards the reattachment zone. They performed the mass transfer experiments on a blunt-faced flat plate of finite length by naphthalene sublimation technique and found the velocity dependence of the results.

6.7 Image analysis

The visual observation of the images taken during the condensation experiments has shown some interesting phenomena about the condensation process. The initial growth of drops and the coalescence process were found to be as described by Beysens (1995, 2006). The surface of the aluminium metal flat plate was not well polished; only mechanical filing was done on the edges, and then just cleaned with ethyl alcohol by wipe out the substrate before starting each experiment. Dropwise condensation developed from the very beginning, as it can be observed from the fig.VI-22 (a, b, c, d). The fusion or the coalescence of two drops can take place, because they touch each other at their perimeter, and form a bigger drop, whose volume is the sum of the volumes of the initial two drops, and also its surface energy is lowered by the coalescence incident. Afterwards more free space as available for further condensation and growth, which is the consequence of a coalescence event, as the new big drop grows mainly in thickness or in the third dimension (Beysens, 2006). The photographs of the condensing plate are given for visual observation in fig.VI-22 (a-d) for all the velocities, from the beginning to the end of the experiment. The photographs are not available for each reading; however, there are enough to conclude that the drops distributions on the surface of the flat plate were not homogeneous, as a result of the nucleation process that developed, and not symmetrical either. As already discussed in chapter III, the temperature distribution on the plate surface presents a temperature gradient from the centre part to the outer sides, which is mainly due to the mounting in series of the unit Peltier elements, which in turn a stronger heat flux at the centre, and may be also due to the contact between the Peltier module and the plate (due to the effect of concavity in either surface) or the effect of the thickness of the thermal paste in between, which is not perfectly uniform.

CEL-19 RH 42 %											
5.2		0.4g 42 2.5h 4.9	0.5g 42 3.0h 5.0	0.7g 42 4.5h 5.4	0.8g 42 5.5h 6.0	1.0g 42 6.5h 5.2	1.2g 42 7.5h 5.3				
CEL-20 RH 55 %											
7.6										2.4g 55 6.5h 7.8	
CEL-21 RH 50 %											
3.6									2.3g 50 7.2h 3.3		2.5g 50 7.5h 3.4
CEL 22 RH 45 %											
3.6	0.1g 45 2.0h 3.7		0.5g 45 5.0h 2.8								
CEL-23 RH 50 %						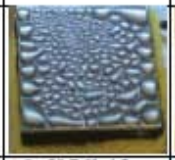					
4.3						1.0g 50 7.0h 4.2	1.1g 50 7.5h 4.3				
CEL-24 RH 46 %											
9.6	0.1g 46 0.2h 9.1	0.4g 47 0.9h 9.2	0.5g 47 1.1h 9.3	0.7g 47 1.6h 9.5	0.8g 47 2.0h 9.6	1.0g 48 2.6h 10	1.1g 48 2.9h 10	1.9g 52 4.7h 9.6	2.3g 53 5.6h 10	2.7g 53 6.4h 9.3	2.9g 54 6.9h 9.4

Fig.VI-22 (a): Images of condensing plate for **velocity 1.0 m/s.**

CEI-36 RH 42 %											
6.7		1.0g 42.6 2.5h 6.8		1.5g 42.6 3.7h 7.1	1.8g 42.6 4.5h 7.3	2.0g 42.6 5.0h 7.1					
CEI-46 RH 37 %											
7.1							2.8g 34 7.6h 6.2				
CEI-47 RH 32 %											
6.6					1.8g 30 6.1h 6.8						
CEI-51 RH 46 %											
8.2								2.9g 48 5.3h 9.1			
CEI-52 RH 46 %											
8.8										3.1g 46 4.9h 8.5	
CEI-53 RH 44 %											
8.7									3.0g 42 5.0h 8.3		
CEI-54 RH 48%											
9.7											3.3g 49 4.5h 9.7
CEI-56 RH 55 %											
10.1										3.1g 54 4.9h 10.3	3.6g 55 4.3h 10.2

Fig.VI-22 (b): Images of condensing plate for **velocity 2.0 m/s.**

Fig.VI-22 (c): Images of condensing plate for **velocity 2.5 m/s.**

Note for Fig.VI-22 (a-d): The first Column represents experiment no (such as CEI- X, whose details are given in the Tables), average humidity (RH %), and average temperature difference (ΔT_c). The row below the each image gives amount of condensate on the plate, relative humidity at that time, time of experiment, and the local ΔT_c.

CE I-69 RH 60 %			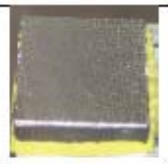	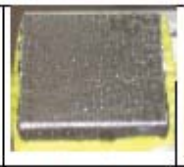							
8.1	0.0g 64 0.0h 7.9	0.4g 64 0.4h 8.0	0.7g 62 0.6h 8.0	1.1g 61 1.0h 8.1	1.9g 60 2.0h 8.2	2.0g 59 2.1h 8.2	2.2g 59 2.3h 8.2	2.3g 59 2.5h 8.2	3.1g 57 3.5h 8.2	3.2g 57 3.6h 8.2	3.5g 56 4.0h 8.2
CE I-61 RH 37 %											
6.5						2.0g 37 4.7h 6.9					
CE I-62 RH 35 %											
6.9						2.1g 34 3.8h 6.7					
CE I-60 RH 39 %											
6.3						2.0g 38 4.1h 6.3					
CE I-59 RH 44 %											
6.4					1.8g 41 4.5h 7.0						
CE I-42 RH 35 %											
6.6						2.1g 34 5.0h 6.9		2.5g 34 5.9h 7.0			
CE I-40 RH 21 %											
4.9				1.2g 21 5.5h 4.9							

Fig.VI-22 (d): Images of condensing plate for **velocity 3.0 m/s.**

Fig.VI-23 (a, b) shows the results of the temperature distribution experiments on the same plate at 23.4 °C ambient temperature in dry conditions, and one at 43% RH. It is notable that the thermal distribution presents a minimum near the centre of the plate and is not symmetric as all. In most cases, the minimum temperature region is scattered from the middle part to the right side of the plate, as in fig.VI-23 (a) where the contour moves towards the lower corner or in VI-23 (b) where it moves towards the upper corner. Hence the left upper corner appears as slightly warmer, which in turn should induce a weaker condensation flux. In fact, when looking at the condensation images (Fig.VI-22 and VI-24) can be observed in many patterns (particularly in the first phase of the process) much smaller drops in that specific area. That effect could be due to the geometry and some non-uniformity in the joint layer thickness (conductive paste) between the plate and the thermoelectric module.

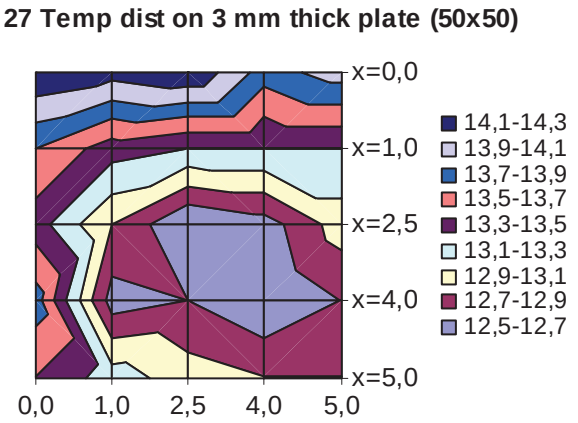

(a)

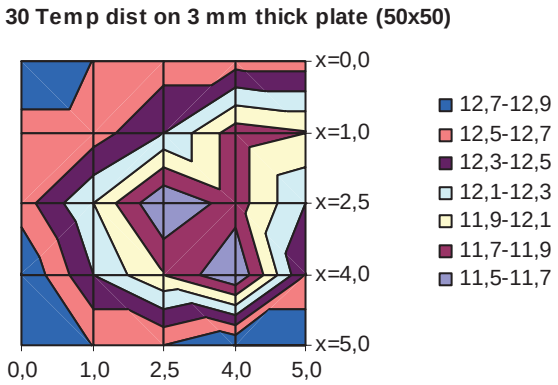

(b)

Fig.VI-23: The thermal distribution on the surface of the flat plate at 23.4 °C ambient temperature, and (a) 43% relative humidity (b) 33% relative humidity.

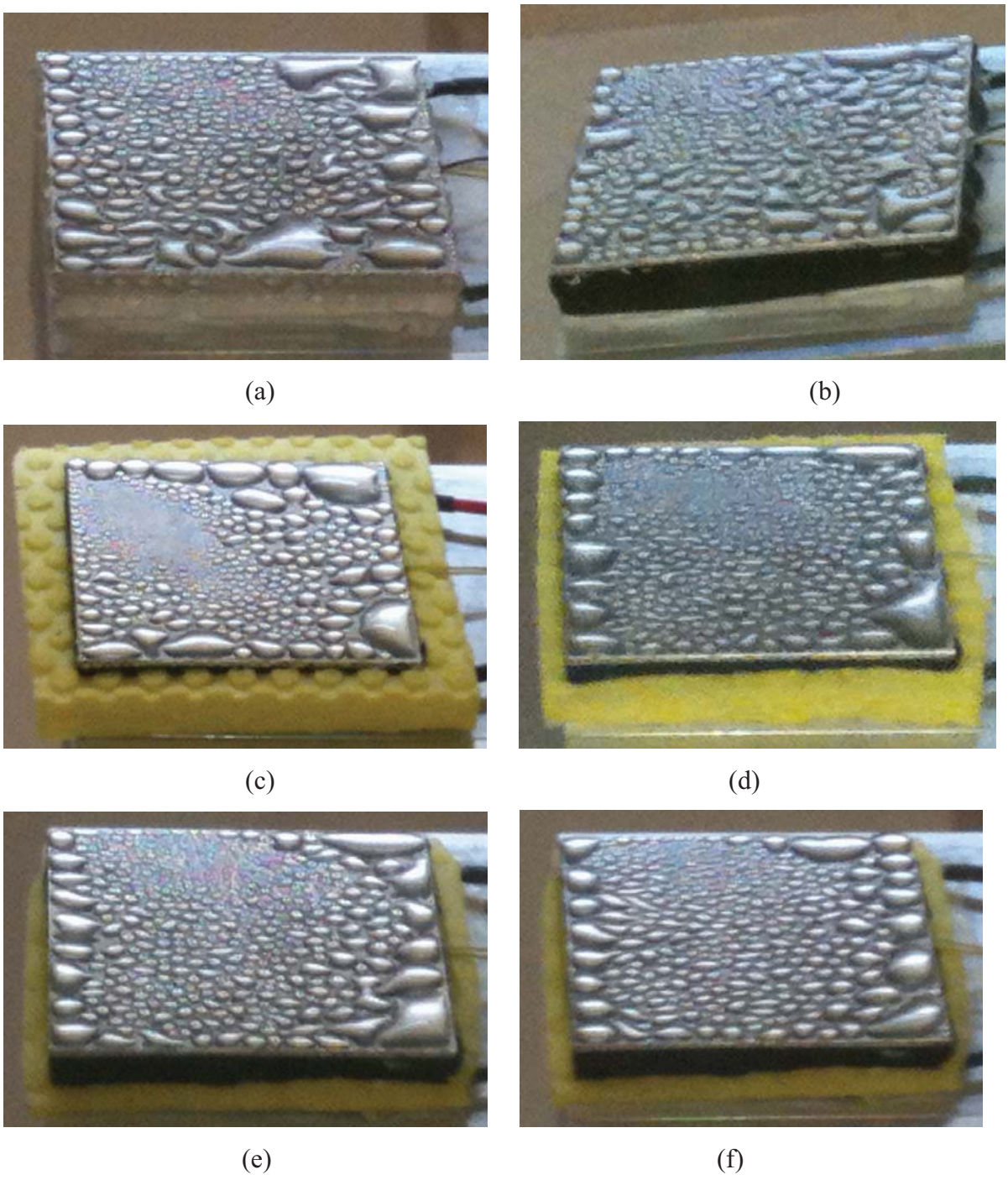

(a) (b)

(c) (d)

(e) (f)

Fig.VI-24: Photographs of the condensing plate (a) without sponge and tape (b) with only tape on its vertical surface (c) with a 7 mm wide and 6 mm thick sponge around the plate (d) with a 3 mm wide and 6 mm thick sponge (e-f) with a 3 mm wide and 3 mm thick sponge around the plate.

As I have mentioned that the asymmetry in the drop distribution may be an effect of the flow field also, because the strip of sponge that surrounded the vertical side of the Peltier

element and the plate has shown, such effects during the optimisation experiments performed for the design of the sponge (thickness, localisation). Fig.VI-24 (a-f) given here shows the patterns of the drop growth on the surface of the plate under different flow conditions due to different configurations of sponge application for a 1.0 m/s mean entrance velocity. Fig.VI-24 (a) represents the condensation pattern without sponge, (b) on applying a plastic tape on the vertical side of the plate to reduce the condensation on this surface, (c) with a 7 mm wide and 6 mm thick layer of sponge applied at the level of the flat plate surface, (d) a 3 mm wide and 6 mm thick sponge little below the level of the plate surface, (e-f) a 3 mm wide and 3 mm thick optimised sponge applied below the plate thickness just above the Peltier element in two different experiments. These condensation patterns are for similar amounts of condensation (0.9-1.1 g).

As seen in the photographs Fig.VI-24, the sponge configuration affects noticeably the condensing drop distribution, as the flow field. The photographs of the condensing active plate have been organized according to the velocity and experiment-wise and given for visual observations. They are arranged in the order of increasing mass on the plate surface from left to right, and the details of the experiment are given below each image (amount of condensate on the plate, relative humidity, time of the experiment when photographs was taken in hours, temperature difference ΔT_c). At a glance four main condensation regimes can be distinguished:

i) Up to the 1.5g a drop dominated distribution can be observed, and above it the formation of bigger drops starts and less free space is left for condensation on the metal surface.
ii) The main drops spread over about more than 1/5 of the surface in most of the experiments or it can be noticed that two or three big drops cover more than $1/4^{th}$ of the plate at all speeds.
iii) Above 3.0 g, a big mass is located at the rear edge, which dominates more than ½ of the plate or little more.
iv) At the end (above 3.5 g) most of the plate is covered by water.

More precisely, a few comments can be added:

- The condensation starts mainly at the leading and trailing edges and also along the other sides or at the corners. This is probably due to the manufacturing process of the

plates that produced edges not perfectly smooth, but slightly rough, as manufacturing only involve filing, and no polishing. As a result drops could stick to the edges and avoid moving towards the other sides, attracting very small drops, which would in turn be the first to large after coalescence. Such an effect has not been seen on the visualisations of the flow field.

- Condensation proceeds more or less according to both the thermal distribution on the plate and the flow field. As we have already discussed, the reattachment zone towards the rear edge of the plate could be seen in most experiments with bigger drops of the condensate developing in the rear. The flow field affects the mass transfer coefficients, for which a minor variation between the front and rear parts can produce inhomogeneous conditions for condensation and generate larger amount of condensate in the rear part of the plate. Then big masses of condensate grow in the rear, which results in an increased thermal inertia and thus in some type of a storage of cold energy that can reinforce the condensation flux in that area and the coalescence process that attracts all drops towards these big masses.
- Despite the film distribution of the water condensate (regime iv), I have found a similar growth rate of condensation. However, the active surface area available for condensation should be getting smaller as condensation proceeds at the water/air interface. That effect is not well understood with the current data, a better explanation would require specific experiments of data acquisition, like heat flux absorbed by the Peltier element, evolution of the air temperature very near to the condensing interface, and temperature profile within the film. The current hypothesis could be explained by an increase of the flux absorbed by the Peltier element, a lower decrease of the interface temperature.
- As the flow velocity increases from 1.0 to 3.0 m/s one can notice the lengthening of the drops along the flow direction from nearly circular shapes at 1.0 m/s to elongated drops, like channels, at 3.0 ms^{-1}. A mean aspect ratio of at least 4 (length/width) can be measured beyond 1.0 g.
- When a big mass of condensate has developed and the plate is almost covered by a film, one can see (4.2 g at 2.5 m/s for example) the development of the boundary layer along the leading edge, the wake effect at the trailing edge (water is pushed “inside” the plate) and some attraction towards the centre on the sides/parallel to the main flow directions.

6.8 Flow patterns

From weakly turbulent, (at the entrance of the test cell) the flow become fully turbulent and three dimensional around our condensing unit. The profiles detailed in chapter IV showed the turbulent nature over the plate in vertical planes parallel to the flow direction. Other visualisation shows, on a vertical plane, a recirculation zone from the leading edge to about 2/3-3/4 of the plate (Fig.VI-25 (4)), where a reattachment zone appears and a second vortex develops afterwards.

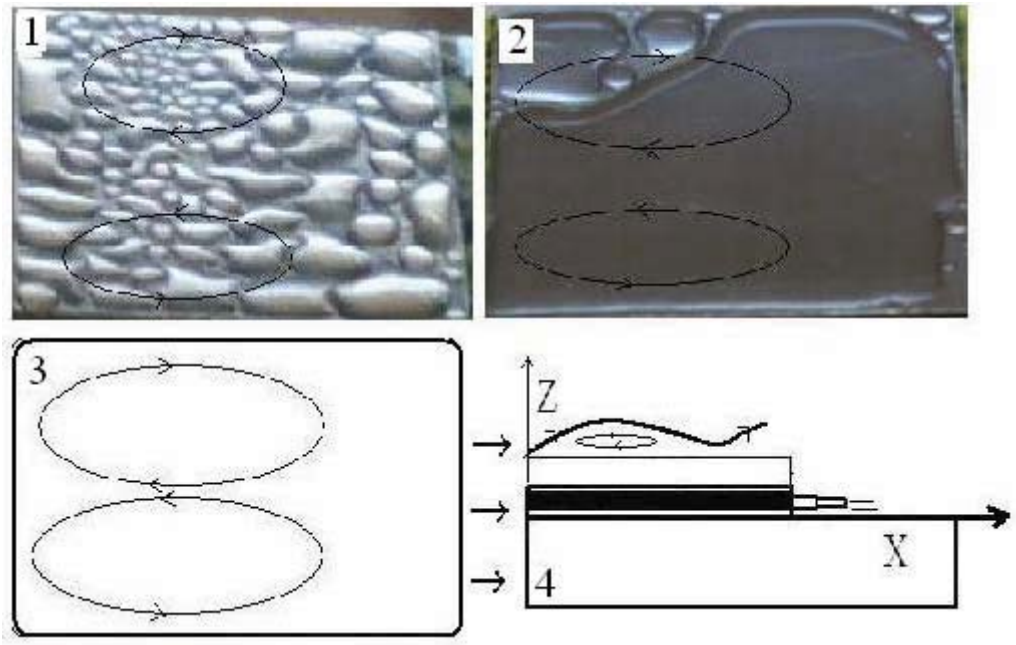

Fig.VI-25: Photographs of the plates with condensate (1, 2) shows flow pattern, and (3, 4) shows schematic of the plate with horizontal and vertical flow patterns on the plate surface.

Observations from above indicate 2 counter-rotating vortices that extend from the leading edge to near the reattachment zone (Fig.VI-25 (3)) above the plate.

This particular flow configuration can be observed on the condensation drops configuration at 1.0 m/s at the beginning of the process (up to 1.0 g), and slightly at 2.5 m/s. The drops are like pulled out by those 2 counter-rotating vortices and pushed towards the rear part (2/3 to 3/4 of the length). Then the coalescence phenomenon causes big masses of water to develop in that rear part (Fig.VI-25 (1, 2)). At 3.0 m/s, mainly

elongated (“channels”) drops are observed at first glance, which could represent the emphasized shear due to the air flow on condensate.

6.9 Conclusion

The evaluation of local mass transfer coefficients by condensation of humid air on a blunt-faced flat plate has been investigated for the values of Reynolds number (3 to 10) × 10^3. The variation of the flow velocity inside the wind tunnel showed a significant effect on the mass transfer coefficient, evaluated by the Sherwood number. The empirical relation presented as equation VI-3 to predict the surface temperature, which is one of the key parameters as it is directly related to the driving force for mass transfer, has given a good agreement with the experimental data. For the velocity range from 1.0 to 3.0 m/s the condensation mass flux proved to have a better proportionality relation with partial pressure difference as with the temperature difference imposed on the plate, which was expected as partial pressure also counts for relative humidity. In conclusion the experimental technique used in here has the capabilities to predict the local mass transfer coefficients by condensation of humid air. Some improvements to the technique could concern the size of the heat sink (not wider than the condensing module), the shape /position /size of the sponge which should be redesigned with aerodynamics purposes.

Conclusion - Future prospects

The use of thermoelectricity to induce an isothermal surface coupled with a precise weighing to measure the mass of condensate produced by condensation of humid air has proved to be successful for the evaluation of local mass transfer coefficients in a well controlled environment. This study focused on the characterization of condensation on a flat horizontal plate of small size in a low *Re* turbulent flow, which corresponds to configurations that can be encountered in a space greenhouse or a manned capsule. The velocity profiles on the surface of the blunt-faced flat plate have been investigated. Condensation experiments in an open uncontrolled environment and in a regulated environment within a closed circuit wind tunnel have been analyzed. The significant and important findings are summarized below:

- The use of a Peltier module to produce a homogeneous surface temperature for the condensation of humid air on a small size plate proved to be efficient.
- Even if the efficiency of a thermoelectric module is not very good nowadays; its solid state nature, effectiveness and reliability which are also not affected by the orientation of the module makes it very useful for our application.
- The best configuration involves a Peltier module sandwiched between a heat exchanger (underneath) and a thin, highly conductive plate (on top) that was adjusted to the size of the thermoelectric module for thermal homogeneity.
- The availability of a closed wind tunnel facility for low air velocities (1-3 m/s) that was also regulated in temperature and humidity is needed to evaluate accurately the mass transfer coefficients around small obstacles with precise measurements of the velocity profiles and turbulence intensity around the obstruction and also to validate low *Re* turbulent models to be used in CFD.
- This global experimental set-up will be very helpful for the development of theoretical models to predict local gas/liquid mass transfer at interfaces for various geometries.
- Above the plate a thick boundary layer was observed, that included 2 recirculation vortices in the vertical plane and also 2 extended counter-rotating cells along the flow direction in the horizontal plane.
- The understanding of the coalescence and growth of the condensate drops phenomena is important, because they affect the velocity profile and turbulence intensity very close to the surface of the plate and vice-versa.

- The flow that developed above the blunt-faced flat plate appeared to be very intricate, transient and three-dimensional and also coupled with a turbulent wake.
- These 2 perpendicular flow features can be seen on condensation patterns; as depicted by the drop distributions.
- The mass transfer coefficients by condensation of humid air on a blunt-faced flat plate have been investigated for the values of Reynolds number from 3000 to 10^4.
- The variation of the mean flow velocity inside the wind tunnel showed a significant effect on the mass transfer coefficients, hence on the Sherwood number.
- The empirical relation presented as equation VI-3 to predict the surface temperature has permitted to estimate a mass flux in good agreement with the experimental data.
- The linear fitting of the behaviour of the condensation mass flux versus the velocity range (from 1.0 to 3.0 m/s) is more accurate with the partial pressure difference than with the temperature difference imposed on the plate.
- The experimental value of the Sherwood number (*Sh*) reflects a mixed laminar / turbulent flow regime with dependence in $Re^{2/3}$.

In conclusion, the experimental technique used in here has the capability to predict "local" mass transfer coefficients by condensation of humid air.

This work consisted in an initial study in our laboratory for the estimation of gas/liquid local mass transfer coefficients. It was focused on the condensation of humid air on a flat horizontal plate of small size. An experimental set-up was developed and gave good results that allowed a better understanding of such a complex phenomenon (3D weakly turbulent flow, with concomitant heat and mass transfer and change of phases).

However, this setup could be improved by optimizing the set-up and /or improving the visualization technique and the data processing like:

- reducing the size of the heat sink and its geometry (width);
- improving the aerodynamic shape of the condensing unit;
- improving the feasibility to apply other complex geometries;
- measuring the height of the drops;
- performing some type of image processing on the condensation patterns;
- performing velocity measurements by Particle Image Velocimetry (PIV);

- performing temperature measurements with a micro-sensor just above the plate or condensation interface.

This technique is now available to be used with more complex structures, which will help in developing the theoretical models for further studies. They could be vertical flat plate structures, cylindrical or semi-cylindrical one or porous objects, which have resemblance to the inside structures of space vehicles or BLSS (biological life support system) such as plant leaves or solid walls.

References

Abu-Orabi M, 1998, Modelling of heat transfer in dropwise condensation, *Int. J. Heat Mass Transfer*, 41, 81-87.

Al-Diwany HK, Rose JW, 1973, Free convection film condensation of steam in the presence of noncondensing gases, *Int. J Heat Mass Transfer*, 16, 1359-1369

Altenkirch E, 1909, Uber den Nutzeffeckt der Thermosaule, *Physikalische Zeitschrifr,* 10, 560.

Altenkirch E, 1911, Electrothermische Kalteerzeugung und Reversible Electrische Heizung, *PhysikalischeZeitschrifr,* 12, 920.

Araki H, Kataoka Y, Murase M, 1995, Measurement of condensation heat transfer coefficient inside a vertical tube in the presence of noncondensable gas, *J. Nucl. Sci. Technol.*, 32, 517–536.

Asano K, 2006, Mass Transfer-From fundamentals to modern industrial applications, Wiley-VCH, Weinheim, Germany.

Asano K, Nakano Y, 1979, Forced convection film condensation of vapours in the presence of noncondensable gas on a small vertical flat plate, *J Chem Engr of Japan*, 12, 196-202.

Bagian James (chair) et al, 1997, Committee on Advanced technology for human support in space, National Academy Press, Washington D.C., No. 97-68305, ISBN 1-800-624-6242.

Bakhmeteff BA, 1932, Hydraulics of Open Channels, McGraw-Hill, New York, 39–41

Bakhmeteff BK, 1966, Hydraulics of Open Channel, McGraw-Hill, New York, 39-41.

Balasubramaniam R, **Nayagam V, Hasan MM, Khan L**, 2006, Analysis of heat and mass Transfer during Condensation over a Porous Substrate, *Ann. N.Y. Acad. Sci.* 1077: 459–470.

Barr A, Gillepsie TJ, 1987, Maximum wetness duration for water drops on leaves in the field, *Agricultural and forest meteorology*, 41 (3-4), 267-274.

Barry JJ, 1987, Effects of interfacial structure on film condensation, *PhD Thesis*, University of Wisconsin, USA.

Bartsev SI, Gitelson JI, Lisovsky HM, Mezhevikin VV, Okhonin VA, 1997, Perspectives of different type biological life support systems (BLSS) usage in space missions, *Acta Astronautica,*39(8), 617-622.

Benitez Jaime, 2009, Principles and modern applications of mass transfer operations, Wiley-Blackwell (an imprint of John Wiley & Sons Ltd) ISBN-10: 0470181788.

Bernett MK, Zisman WA, 1970, Confirmation of spontaneous spreading by water on pure gold, *J. Phys. Chem.*, 74, 2309-2312.

Beysens D, Knobler CM, 1986, Growth of Breath Figures, *Phys. Rev. Lett.*, 57, 1433-1436

Beysens D, 1995, The formation of dew, *Atmospheric Research*, 39, 215-237.

Beysens D, 2006, Dew nucleation and growth, *C. R. Physique*, 7, 1082-1100.

Bierschenk J, Gilley M, 2006, Assessment of TEC thermal and reliability requirements for thermoelectrically enhanced heat sinks for CPU cooling applications, International Conference on Thermoelectrics, 254–259.

Bird RB, Stewart WE, Lightfoot EN, 2002, Transport Phenomena, John-Wiley & Sons Inc., NY, USA.

Brain P, Butler, DR, 1985, A model of drop size distribution for a system with evaporation, *Plant, Cell & Environment*, 8 (4), 247–252.

Briscoe B, Galvin K, 1991, *J. Solar Energy*, 46, 191–197.

Bromley LA, 1952, Effect of heat capacity of condensate, *Ind. Eng. Chem.,* 44, 2966-2969.

Butterworth D, Sardesai RG, Griffith P, Bergles AE, 1983, Condensation, *Heat exchanger design handbook, Hemisphere, Washington, DC*, *Chapter 2.6*.

Cadiergues R, 1978, Propriétés de l'air humide et de l'eau – Justification de nouveaux choix, Promoclim.

Carey VP, 1992, Liquid–Vapour Phase Change Phenomena, Hemisphere Publishing (1992).

Cavallini A, J Smith R, Zecchin R, 1974, A dimensionless correlation for heat transfer in forced convection condensation, in: Sixth International Heat Transfer Conference, Tokyo, Japan, pp. 309–313.

Cess RD, 1960, Laminar film condensation on a flat plate in the absence of body force, *Zeitschrift fur Angewandte und Physik*, 11, 426-433.

Chang H-C, 1994, Wave evolution on a falling film. *Ann. Rev. Fluid Mech.* **26**, pp. 103–136.

Chang TB, 2005, Laminar film condensation on a horizontal plate in a porous medium with surface tension effects, *Journal of Marine Science and Technology*, 13 (4), 257-264.

Chen JM, Chiou CC, 1997, Flow past a blunt flat plate subjected to the disturbance of incident vortex street, *J. Wind Eng. Ind. Aerod.*, 66, 179–196.

Chen Michael Ming, 1961, An analytical study of laminar film condensation part I-flat plates, *J. Heat Transfer*, 83Series C, 48-55.

Chilton TH, Colburn AP, 1934, Mass transfer (absorption) coefficients. Prediction from data on heat transfer and fluid friction, *Industrial and Engineering Chemistry* 26(11), 1183-1187.

Cho DC, Stein RP, 1988, Steam condensation on the underside of a horizontal surface, *Proc 3rd Int. Topical Meeting on Nuclear Power Plant Thermal Hydr. Operations*.

Chu KJ and Dukler AE, 1974a, Statistical characteristics of thin, wavy films: Part II.

Studies of the substrate and its wave structure. *AIChE J.* 20, 695–706.

Chu KJ and Dukler AE, 1974b, Statistical characteristics of thin, wavy films: Part III. Structure of the large waves and their resistance to gas flow. *AIChE J.* 21 (1974), 583–593.

Chun KR, Seban RA, 1971, Heat transfer to evaporating liquid films. *J. Heat Transfer* 93, 391–396.

Collier JG, Thome JR, 1996, Convective boiling and condensation, 3rd ed., Oxford University Press, Inc., New York.

Corradini ML, 1997, Fundamentals of Multiphase flow, online edition.

Cunningham RE, Williams RJJ, 1980, *Diffusion in gases and porous media / R.E. Cunningham and R.J.J. Williams*, Plenum Press, New York

Dalkilic AS, Yildiz S, Wongwises S, 2009, Experimental investigation of convective heat transfer coefficient during downward laminar flow condensation of R134ain a vertical smooth tube, *Int. J heat ass Transfer*, 52, 142-150.

Dallmeyer H, 1970, Stoff-und warmeubertragung beider kondensation eines dumpfes aus einem gemisch mit einem licht kondensierenden gass in laminarer und turbulenter stromungsgrenzschicht, *VDI-Forschungsheft*, 539, 5-24.

Das AK, Kilty HP, Marto PJ, Andeen BG, Kumar A, 2000, The use of an organic self-assembled monolayer coating to promote dropwise condensation of steam on horizontal tubes, *ASME J. Heat Transfer*, 122, 278-286.

Dehbi AA, 1991, Analytical and experimental investigation of the effects of noncondensable gases on steam condensation under turbulent natural convection conditions, *PhD Thesis*, Dept. of Nuclear Engineering, MIT, USA.

Deissler RG, 1955, Analysis of Turbulent Heat Transfer, Mass Transfer, and Friction in Smooth Tubes at High Prandtl and Schmidt Numbers", *NACA Reports*, 1210.

Denny VE, Jousionis VJ, 1972, Effects of noncondensable gas and forces flow on laminar film condensation, *Int. J Heat Mass Transfer,* 15, 315-326.

Denny VE, Mills AF, Jusionis VJ, 1971, Laminar film condensation from a steam-air mixture undergoing forced flow down a vertical surface, *J Heat Transfer,* 93, 297-304.

Denny VE, South III V, 1972, Effects of forced flow, noncondensable and variable properties on film condensation of pure and binary vapours at the forward stagnation point of a horizontal cylinder, *Int. J Heat Mass Transfer,* 15, 2133-2142.

Deshpande RY, Hubbard KG, Coyne DP, Syteadman JR, Prankhurst AM, 1995, Estimating leaf wetness in dry bean canopies as a prerequisite to evaluating white mold disease, *Agronomy Journal* 87:613-619.

Dhir VK, Lienhard JH, 1971, Laminar film condensation on plane and axisymmetrics bodies in non-uniform gravity, *J. Heat Transfer*, 93, 97.

Dobson MK, Chato JC, 1998, Condensation in smooth horizontal tubes, *J. Heat Transfer Trans. ASME* (1998), 193–213.

Drew TB, 1954, see McAdams WH, Heat Transmission (3rd ed.), McGraw-Hill, New York.

Duminil M, 2006, Techniques de l'Ingénieur, traité Génie énergétique, B. Air Humide, B 2 230 01-26.

DuVuono AC, Christensen RN, 1984, Experimental investigation of the pressure effects on film condensation of stem-air mixtures at pressure above atmospheric, fundamentals of phase change; boiling and condensation, *The Winter Annual Meeting of ASME*, New Orleans, Louisiana, HTD-38.

Erb RA, Thelen E, 1966, Dropwise condensation characteristics of permanent hydrophobic systems, *US Office of Saline Water R&D Report No.184*, 54-57.

Fatica N, Katz DL, 1949, Dropwise condensation, *Chem. Engr. Prog.* 45(11), 661-674.

Fontaine JP, Tiwari A, 2009, Rapport Lot 1 - N° de gestion de lot: 6000010798 – Convention CNES N° 70729/00.

Fontaine JP, Tiwari A, 2010, N° Evt2, N° de gestion de lot: 6000010798 – Convention CNES N° 70729/00.

Fritter D, Knobler CM, Beysens DA, 1991, Experiments and simulation of the growth of droplets on a surface (breath figures), *Phys. Rev. A*, 43, 2858-2869.

Fujii T, Uehara H, 1972, Laminar filmwise condensation on a vertical surface, *Int. J Heat Mass Transfer,* 15, 217-233.

Ghisalberti L, Kondjoyan A, 2002, Complete map out of the heat transfer coefficient at the surface of two circular cylinders H/D = 3.0 and 0.3 subjected to a cross-flow of air, *Int. J. Heat and Mass Transfer,* 45, 2597-2609.

Gerstmann J, Griffith P, 1967, Laminar film condensation on the underside of horizontal and inclined surfaces, *Int. J Heat Mass Transfer*, 10, 567-580.

Goldsmid HJ, Gopinathan K, Matthews DN, Taylor KNR, Baird CA, 1988, High Tc superconductors as passive thermoelements, J. *Phys. D, Appl. Phys.,* 21 (2), 344.

Goldsmid HJ, Douglas RW, 1954, The use of semiconductors in thermoelectric refrigeration, *Br.* J. *Appl. Phys.,* 5(l l), 386.

Goldsmid HJ, 1986, Electronic Refrigeration, Pion Limited, London, 1986.

Goldstein R, Cho H, 1995, A Review of Mass Transfer Measurements Using Naphthalene Sublimation, *Exp. Thermal and Fluid Science*, 10, 416 - 434.

Grace J, 1977, Plant Responses to Wind, Academic Press, London.

Graham C, Griffith P, 1973, Drop size distributions and heat transfer in dropwise condensation, *Int. J Heat Mass Transfer*, 16, 337-346.

Gros JB, Poughon L, Lasseur C, Tikhomirov AA, 2003, Recycling efficiencies of C, H, O, N, S, and P elements in a biological life support system based on microorganisms and higher plants, *Adv. Space Res.*, 31(1), 195-199.

Haraguchi T, Shimada R, Kumagai S, Takeyama T, 1991, The effect of polyvinylidene chloride coating thickness on promotion of dropwise steam condensation, *Int. J. Heat Mass Transfer*, 34, 3047-3054.

Haraguchi T, 1992, Microscope observations of the initial droplet formation mechanism in dropwise condensation, *Heat Transfer Japan Res.*, 21, 573-585.

Hasan MH, Toh KC, 2007, Optimization of a thermoelectric cooler–heat sink combination for active processor cooling, in: Electronic Packaging Technology Conference, 848–857.

Hirschfelder JO, Curtis CF, Bird RB, 1952, *Molecular theory of gases and liquids*, John Wiley and Sons, 441-610.

Holden KM, Wanniarachchi A, Marto PJ, Boone DH, Rose JW, 1987, The use of organic coatings to promote dropwise condensation of steam, *ASME J Heat Transfer,* 109, 768-774.

Huber L, Gillespie TJ, 1992, Modelling leaf wetness in relation to plant disease epidemiology, *Annual Review of Phytopathology,* 30, 553-77.

Hwang KS, Sung HJ, Hyun JM, 1996, Mass transfer measurement from a blunt-faced flat plate in a uniform flow, *Int. J. Heat Fluid Flow*, 17, 179–182.

Hwang KS, HJ Sung, Hyun JM, 2001, An experimental study of large scale vortices over a blunt-faced flat plate in pulsating flow, *Experiments in Fluids,* 30, 202-213.

Incropera FP, DeWitt DP, 1990, Fundamentals of Heat and Mass Transfer, 3rd ed. John Wiley & Sons, Inc., New York.

Jacobs HR, 1966, An integral treatment of combined body force and forced convection in laminar film condensation, *Int. J Heat Mass Transfer,* 9, 637-648.

Jaffrin A, Makhlouf S, Scotto la Massese C, Bettachini A, Voisin R, 1989, *Agronomie*, 9, 729-741.

Jakob M, 1936, Heat transfer in evaporation and condensation, *Mech. Eng.*, 58, 729-739.

Johnson RC, 1998, The handbook of fluid dynamics, CRC press, USA.

Ka'rman T von, 1939, The analogy between Fluid Friction and Heat Transfer, *Transactions of the American Society of Mechanical Engineers*, 61, 705–710.

Kananeh AB, Rausch MH, Fröba AP, Leipertz A, 2006, Experimental study of dropwise condensation on plasma-ion implanted stainless steel tubes, *Int. J. Heat and Mass Transfer*, 49, 5018-5026.

Kang HC, Kim MH, 1992a, Measurement of three-dimensional wave form and interfacial

area in an air-water stratified flow, *Nucl. Engrg Des.* 136**,** 347–360.

Kang HC, Kim MH, 1992b, The development of a flush-wire probe and calibration method for measuring liquid film thickness, *Int. J. Multiphase Flow*, 18, 423–437.

Kellenbenz J, Hahne E, 1994, Condensation of pure vapours and binary vapour mixtures in forced flow. *Int. J. Heat Mass Transfer*, 37, 1269–1276.

Kim MH, Corradini ML, 1990, Modelling of condensation heat transfer in a reactor containment, *Nuclear Engineering and Design,* 118, 193-212.

King LV, 1914, On the convection of heat from small cylinders in a stream of fluid: determination of the convective constants of small platinum wires with applications to hot wire anemometry, *Proc. R. Society London*, 90, 563-570.

Kitaya Y, Shibuya T, Yoshida, Kiyota M, 2004, Effects of air velocity on photosynthesis of plant canopies under elevated CO_2 levels in a plant culture system, *Advances in space research*, 34, issue 7, 1466-1469.

Koch G, Zhang D, Leipertz A, 1997, Condensation of steam on the surface of hard coated copper discs, *Heat Mass Transfer*, 32, 149-156.

Koch G, Kraft K, Leipertz A, 1998a, Parameter study on the performance of dropwise condensation, *Rev. Ge´n. Therm.*, 37, 539-548.

Koch G, Zhang D, Leipertz A, 1998b, Study on plasma enhanced CVD coated material to promote dropwise condensation, *Int. J. Heat Mass Transfer*, 41, 1899-1906.

Koh JC, Sparrow EM, Hartnett JO, 1961, The two-phase boundary layer in laminar film condensation, *Int. J Heat Mass Transfer*, 2, 69-82.

Koh JC, 1962, Laminar film condensation of condensable gases and gaseous mixture on a flat plate, *Proc 4th USA Nat Cong Appl Mech,* 2, 1327-1336.

Kondjoyan A, 1993, Contribution à la connaissance des coefficients de transfert de chaleur et de matière à l'interface air-solide, Thèse de Docteur de l'ENSIA.

Kondjoyan A, Daudin, JD, 1995, Effect of free stream turbulence intensity on heat and mass transfer at the surface of a circular cylinder and an elliptical cylinder, axis ratio 4, *Int. J. Heat Mass Transfer*, 38 (10), 1735-1749.

Kondjoyan A, Daudin JD, 1997, Heat and mass transfer coefficients at the surface of a pork hindquarter, *J. Food Eng*., 32, 225.

Kondjoyan A, 1999, L'échange de chaleur et d'eau à l'interface air/solide, Habilitation à Diriger des Recherches de l'Université Blaise Pascal.

Kondjoyan A, Péneau F, Boisson H-C, 2004, Development of flat-plate thermal and velocity boundary layers under highly turbulent and instable air flows: Reynolds numbers ranging from 8400 to 127000, *Int. J Therm. Sc.*, 43, 1091–1100.

Korthals RL, Christianson LL, Knight SL, 1990, Evaluation of environmental parameters

within controlled environments, ASAE paper No. 90-4034, ASAE, St. Joseph, MI 49085-9659.

Kroger DG, Rohsenow WM, 1968, Condensation heat transfer in the presence of non-condensable gas, *Int. J Heat Mass Transfer*, 11, 15-26.

Kuhn SZ, Schrock VE, Peterson PF, 1997, An investigation of condensation from steam–gas mixtures flowing downward inside a vertical tube, *Nucl. Eng. Des.*, 177, 53–69.

Kutateladze SS, Gogonin II, 1979, Heat transfer in film condensation of slowly moving vapour, *Int. J. Heat Mass Transfer,* 22, 1593–1598.

Kutsuna H, Inoue K, Nakanishi S, 1987, Filmwise condensation of vapour containing noncondensable gas in a horizontal duct, *Int. Symposium on Heat Transfer*, Beijing, China.

Kwang-Tzu Yang, 1966, Laminar film condensation on a vertical non-isothermal plate, *J. Appl. Mech (Trans ASME)*, 33, 203-205.

Lasseur Ch, Verstraete W, Gros JB, Dubertret G, Rogalla F, 1996, MELISSA: A potential experiment for a precursor mission to the Moon, *Advances in Space Research*, 18 (11), 111-117.

Le Fevre EJ, Rose JW, 1965, An experimental study of heat transfer by dropwise condensation, *Int. J heat Mass Transfer,* 8*,* 1117-1133.

Le Fevre EJ, Rose JW, 1966, A theory of heat transfer by dropwise condensation, *Proc. 3rd Int. Heat Transfer Conf.,* Chicago, 2, 362-375.

Lee KY, Kim MH, 2008, Effect of an interfacial shear stress on steam condensation in the presence of a noncondensable gas in a vertical tube, *Int. J. Heat Mass Transfer* 51**,** 5333–5343.

Leipertz A, Koch G, 1998, Dropwise condensation of steam on hard coated surfaces, *Proc. of the XIth Int. Heat Transfer Conf.*, 6, 379-384.

Leppert G, Nimmo B, 1968, Laminar Film Condensation on Surface Normal to Body or Inertial Forces, *J. Heat Tran.*, 80, 1, 178-179.

Lhomme JP, Jimenez OF, 1992, Estimating dew duration on banana and plantain leaves from standard meteorological observations, *Agricultural and Forest Meteorology*, 62, 263–274

Liao Y, Vierow K, Dehbi A, Guentay S, 2009, Transition from natural to mixed convection for steam–gas flow condensing along a vertical plate, *Int. J. Heat Mass Transfer* 52, 366–375.

Ma X, Chen J, Xu D, Lin J, Ren C, Long Z, 2002, Influence of processing conditions of polymer film on dropwise condensation heat transfer, *Int. J Heat Mass Transfer*, 45, 3405-3411.

Ma X, Wang B, Xu D, Lin J, 1999, Lifetime test of dropwise condensation on polymer-

coated surfaces, *Heat Transfer- Asian Res.*, 28, 551-558.

Ma X, Xu D, Lin J, 1993, Dropwise condensation on super thin polymer surface, *J. Chem. Indust. Eng.* (China), 44, 165-170.

Ma X, Xu D, Lin J, 1994, A study of dropwise condensation on the ultra thin polymer surfaces, *Proc. 10th Int. Heat Transfer Conf.*, 3, Brighton, England, 359-364.

Ma X, Zhou XD, Lan Z, Li YM, Zhang Y, 2008, Condensation heat transfer enhancement in the presence of non-condensable gas using the interfacial effect of dropwise condensation, *Int. J Heat Mass Transfer*, 51, 1728-1737.

Maa JR, 1978, Drop size-distribution and heat flux of dropwise condensation, *Chem. Engr. J.*, 16, 171-176.

Maheshwari NK, Saha D, Sinha RK, Aritomi M, 2004, Investigation on condensation in presence of a noncondensable gas for a wide range of Reynolds number, *Nuclear Engineering and Design*, 227, 219-238.

Marcos-Martin MA, Bardat A, Schmitthaeusler R, Beysens D,1996, *Pharm. Technol. Eur.*, 8, 24-32.

Marto PJ, Looney DJ, Rose JW, Wanniarachchi A, 1986, Evaluation of organic coatings for the promotion of dropwise condensation of steam, *Int. J. Heat Mass Transfer*, 29, 1109-1117.

Marty Ph, Michel F, Tochon P, 2008, Experimental and numerical study of the heat transfer along a blunt flat plate, International Journal of Heat and Mass Transfer, 51, 13-23.

Mason EA, Monchick L, 1963, Survey of the equations of the state and transport properties of the moist gases. Humidity and Moisture – Measurement and control in science and industry, Int. Symposium humidity and Moisture, 3, Fundamentals and Standards, 257-272, Reinhold , NewYork.

Mayhew YR, 1987, Comments on the Paper, Theoretical Study of Laminar Film Condensation of Flowing Vapour, (by Shekriladze IG and Gomelauri VI), *Int. J Heat Mass Transfer,* 10, 107-108.

Mayhew YR, **Aggarwal JK**, 1973, Laminar film condensation with vapour drag on a flat surface, *Int. J Heat Mass Transfer,* 16, 1944-1949.

Mayhew YR, Griffith DJ, Phillips JW, 1965-66, Effect of vapour drag on laminar film condensation on a vertical surface, *Proc. Inst. Mech. Eng.,* 180, Part 3J, 280-289.

McAdams WH, 1954, Heat transmission, 3rd ed., McGraw-Hill, New York.

McCormick JL, Westwater JW, 1965, Nucleation sites for dropwise condensation, *Chem Eng Sci.*, 20, 1021-1031.

McCormick JL, Westwater JW, 1966, Drop dynamics and heat transfer during dropwise condensation of water vapour, *Chem Eng Prog Symp Ser*, 62(64), 120-134.

Mergeay M, Verstraete W, Dubertret G, Lefort-Tran M, Chipaux C, Binot R., 1988, "MELISSA - a microorganisms based model for CELSS development" Proceedings of the 3rd symposium on space thermal control & life support system, Noordwijk, The Netherlands, October 3-6, 1988.

Merigoux R, 1937, *Rev. Opt.,* 9, 281.

Mills AF, Seban RA, 1967, The condensation coefficient of water, *Int. J Heat Mass Transfer*, 10, 1815-1827.

Minkowycz WJ, Sparrow EM, 1966, Condensation heat transfer in the presence of noncondensables, interfacial resistance, variable properties and diffusion, *Int. J Heat Mass Transfer*, 9, 1125-1144.

Monteith JL, 1957, Dew, *Q. J. Royal Meteorol. Soc.*, 83, 322-341.

Monteith JL and Unsworth MH, 1990, In: Principles of Environmental Physics, Edward and Arnold Publishing Co, London, p. 291.

Mori K, Fujita N, Horie H, Mori S, Miyashita T, Matsuda M, 1991, Heat transfer promotion of an aluminium-brass cooling tube by surface treatment with triazinethiols, *Langmuir*, 7(6), 1161-1166.

Nikolayev V, Beysens D, Gioda A, Milimouk I, Katiushin E, Morel JP, 1996, *J. Hydrology*, 182, 19-35.

Nimmo B, Leppert G, 1970, Laminar Film Condensation on a Finite Horizontal Surface," *Proceedings of 4th International Heat Transfer Conference*, 402-403.

Nusselt WA, 1916, The surface condensation of water vapour, *Zieschrift Ver. Deut. Ing.,* 60, 541-546.

O'Neill GA, Westwater JW, 1984, Dropwise condensation of steam on electroplated silver surfaces, *Int. J. Heat Mass Transfer*, 27, 1539-1549.

Oh S, Revankar ST, 2005, Boundary layer analysis for steam condensation in a vertical tube with noncondensable gases, *Int. J. Heat Exchangers,* 6, 1–31.

Oh S, Revankar ST, 2006, Experimental and theoretical investigation of film condensation with non-condensable gas, *Int. J. Heat Mass Transfer,* 49, 2523-2534.

Ota T, Kon N, 1974, Heat transfer in the separated and reattached flow on a blunt flat plate, *J. Heat Transfer*, 75, 459–462.

Ota T, Itasaka M, 1976, A separated and reattached flow on a blunt flat plate, *ASME J. Fluid. Eng.*18, 79–86.

Othmer DF, 1929, The condensation of steam, *Ind. Eng Chem*, 21, 6, 577-583.

Pang Guoxin, Dale J Doug, Kwok Daniel Y, 2005, An integrated study of dropwise condensation heat transfer on self-assembled organic surfaces through Fourier transform infra-red spectroscopy and ellipsometry, *Int. J Heat Mass Transfer*, 48, 307-316.

Park HS, No HC, 1999, A condensation experiment in the presence of noncondensables in a vertical tube of a passive containment cooling system and its assessment with RELAP5/MOD3.2, *Nucl. Technol.* 127, 160–169.

Park SK, Kim MH, and Yoo KJ, 1997, Effects of a wavy interface on steam-air condensation on a vertical surface, *Int. J. Multiphase*, 23, 1031-1042.

Pasquill F, 1949, *Quart. J. R. Met. Soc*., 75, p. 249, and 1949, *Proc. Roy. Sac. A*, 198, 116.

Peltier JCA, 1834, Nouvelles experiences sur la caloricité des courants electrique, *Ann. Chem. Phys.*, 56, 371.

Peter C, Wayner Jr, 2002, Nucleation, growth and surface movement of a condensing sessile droplet, *Colloids Surf A.*, 206, 157-165.

Peterson AC, Westwater JW, 1966, Dropwise condensation of ethylene glycol, *Chem Eng Prog Symp Ser.,* 62(64), 135-142.

Phelan PE, Chiriac VA, Lee TYT, 2002, Current and future miniature refrigeration cooling technologies for high power microelectronics, *IEEE Transactions on Components and Packaging Technologies*, 25 (3) (2002) 356–365.

Poots G, Miles R, 1967, Effects of variable physical properties on laminar film condensation of saturated steam on a vertical flat plate, *Int. J Heat Mass Transfer,* 10, 1677-1692.

Popov VD, 1951, Heat Transfer During Vapour Condensation on a Horizontal Surfaces, *Trudy Kiev. Teknol. Inst.Pishch, Prom*. 11, 1, 87-97.

Rausch MH, Froba AP, Leipertz A, 2008, Dropwise condensation heat transfer on ion implanted aluminium surfaces, *Int. J Heat Mass Transfer,* 51, 1061-1070.

Rauscher JW, Mills AF, Denny VE, 1974, Experimental study of film condensation from steam-air mixtures flowing downward over a horizontal tube, *J. Heat Transfer*, 96, 83-88.

Robinson JA, Windebank SR, 1988, Measurement of condensation heat transfer coefficients in a steam chamber using a variable conductance heat pipe, *Proc 2nd UK National Conference on Heat Transfer*, 1, 617-637.

Rohsenow WM, 1956, Heat transfer and the temperature distribution in laminar film condensation, *Trans. ASME*, 78, 1645-1648.

Rose JW, 1969, Condensation of a vapour in the presence of a noncondensing gas, *Int. J Heat Mass Transfer,* 12, 233-237.

Rose JW, 1979, Boundary layer flow with transpiration of an isothermal flat plate, *Int. J Heat Mass Transfer,* 22, 1243-1244.

Rose JW, 1980, Approximate equations for forced convection condensation in the presence of a noncondensing gas on a flat plate and horizontal tube, *Int. J Heat Mass Transfer,* 23, 539-546.

Rose JW, 1981, Dropwise condensation theory, *Int. J. Heat Mass Transfer*, 24, 191-194.

Rose JW, 1988, Some aspects of condensation heat transfer theory, *Int. Commun. Heat Mass Transfer*, 15, 449-473.

Rose JW, 1994, Dropwise condensation, *Heat Exchanger Design Handbook Update*, 2.6.5.

Rose JW, 1998, Condensation heat transfer fundamentals, *Trans IChemE.*, 76, 143-152.

Rose JW, 1999, Condensation heat transfer, *Heat and Mass Transfer*, 35, 479-485.

Rose JW, Glicksman LR, 1973, Dropwise condensation- the distribution of drop sizes, *Int. J. Heat Mass Transfer*, 16, 411-425.

Rossie K, 1953, Die diffusion von wasserdampf in Luft bie Temperaturen bis 300 C, Forch. Ing. Wesen 19, 49-58.

Rowe DM (Ed.), 1995, CRC Handbook of Thermoelectrics, CRC Press.

Ruckenstein E, Metiu H, 1965, On dropwise condensation on the solid surface, *Chem Eng Sci.*, 20, 173-179.

Schlichting H, 1968, "*Boundary Layer Theory"*, 6th edition, p. 560–595, 596–606, McGraw-Hill.

Schwarzkopf, Steven H, 1994, "Design of a Controlled Ecological Life Support System." *Bioscience* 42, 526–535.

Seebeck TJ, 1822-1823**,** Magnetic polarization of metals and minerals, *Abhandlungen der Deutschen Akademie der Wissenschafrenzu Berlin, pp.*265-373.

Shekriladze IG, Gomelauri VI, 1966, Theoretical study of laminar film condensation of flowing vapour, *Int. J Heat Mass Transfer,* 9, 581-591.

Shigechi T, Kawae N, Tokita Y, and Yamada T, 1990, Film Condensation Heat Transfer on a Finite-Size Horizontal Plate Facing Upward, *JSME Series B*, 56, 1, 205-210.

Siddique MS, Golay MW, Kazimi MS, 1993, Local heat transfer coefficients for forced-convection condensation of steam in a vertical tube in the presence of a noncondensable gas, *Nucl. Technol.*, 102, 386–402.

Sidorenko NA, Mosolov AB, 1992, Cryogenic thermoelectric coolers with passive high Tc superconducting legs, *Proc. XIth Int. Conf Thermoelectrics,* University of Texas at Arlington, October 7-9, 289.

Siow EC, Ormiston SJ, Soliman HM, 2002, Fully coupled solution of a two-phase model for laminar film condensation of vapor–gas mixtures in horizontal channels, *Int. J. Heat Mass Transfer,* 45, 3689-3702.

Sleger L, Seban RA, 1969, Nusselt condensation of n-butil alcohol, *Int. J Heat Mass Transfer*, 12, 237-239.

Song Y, Xu D, Lin J, 1990, Study on dropwise condensation mechanism, *J Chem Eng Chin*

Univ, 4, 240-246.

Sørensen A, 1969**,** Mass transfer coefficients on truncated slabs, Chemical Engineering Science, 24, 1445-1460.

South III V, Denny VE, 1972, The vapour shear boundary condition for laminar film condensation, *Trans. ASME*, 94, 248-249.

Sparrow EM, Eckert EG, 1961, Effects of superheated vapour and noncondensable gases on laminar film condensation, *AIChE J*, 7, 473-477.

Sparrow EM, Gregg JL, 1959, A boundary layer treatment of laminar film condensation, *J. Heat Transfer*, 21Series C, 13-18.

Sparrow EM, Lin SH, 1964, Condensation heat transfer in the presence of a noncondensable gas, *J Heat Transfer,* 86, 430-436.

Sparrow EM, Minkowycz WJ, Saddy M, 1967, Forced convection in the presence of noncondensables and interfacial resistance, *Int. J Heat Mass Transfer,* 10, 1829-1845.

Spencer DL, Chang KI, Moy HC, 1970, Experimental investigation of stability effects in laminar film condensation on a vertical cylinder, *4th Int. Heat Transfer Conference*, Paris-6, Paper Cs 2.3.

Stern S Alan, 1999, "The lunar atmosphere: History, status, current problems and context. *Rev. Geophys.* 37 (4): 453–491.

Sun ZF, 2001, Numerical simulation of flow in an array of in-line blunt boards: mass transfer and flow patterns, *Chem. Eng. Sc.*, 56, 1883-1896.

Tammann G, Boehme W, 1935, Die Zahl der wassertrcpfchen bei der kondensation auf verschiedenen festen stiffen, *Ann Physik*, 5, 77-80.

Tamponnet C, Savage C, 1994, Closed ecological systems, *J. Biol. Educ.*, 28, 167-173.

Tanaka H, 1975a, A theoretical study of dropwise condensation, *Trans. ASME J. Heat Transfer*, 97, 72-78.

Tanaka H, 1975b, Measurements of drop-size distributions during transient dropwise condensation, *Trans ASME J Heat Transfer*, 97, 341-346.

Tanaka H, 1979, Further development of dropwise condensation theory, *Trans. ASME J. Heat Transfer*, 101, 603-611.

Thome JR, Hajal J El, Cavallini A, 2003, Condensation in horizontal tubes, part 2: new heat transfer model based on flow regimes, *Int. J. Heat and Mass Transfer*, 46, 3365–3387.

Thomson W, 1851, On a mechanical theory of thermoelectric currents, *Proc. Roy. Soc. Edinburgh,* 91, 1851.

Thornthwaite CW, Holzman B, 1942, *U.S. Dept. Agric. Tech. Bull*., 817.

Tianqing Liu, Chunfeng Mu, Xiangyu Sun, Songbai Xia, 2007, Mechanism study on

formation of initial condensate droplets, *AIChE Journal*, 53, 1050-1055.

Tiwari A, Fontaine J-P, 2009, Towards the prediction of heat and mass transfer in an air-conditioned environment for a life support system in space, *Water, Air, & Soil Pollution: Focus*, 2009, 9, No. 5-6, 539-547.

Tiwari A, Fontaine J-P, Lafon P, Kondjoyan A, 2010, Experimental modelling for the prediction of heat and mass transfer in an airconditioned space environment for life support systems, *40th ICES -2010*, Bercelona, Spain, (AIAA2010-6171).

Tiwari A, Lafon P, Kondjoyan A, Fontaine J-P, 2011, An air-conditioned wind tunnel environment for the study of mass and heat flux due to condensation of humid air, Chapter 4, In: *Wind Tunnels: Aerodynamics, Models and Experiments*, Editor- JD Pereira, Nova Science Publishers, Inc., New York, USA, 2011 (ISBN 978-1-61209-1)

Umur A, Griffith P, 1965, Mechanism of dropwise condensation, *J Heat Transfer*, 87, 275-282.

Vedernikov MV, Kuznetsov VL, Ditman AV, Melekh BT, and Burkov AT, 1991, efficient thermoelectric cooler with a thermoelectrically passive high T_c, superconducting leg, *Proc. Xth Int.Conf: Thermoelectrics,* Cardiff, Wales, September 10-12, 96.

Vemuri S, Kim KJ, 2006, An experimental and theoretical study on the concept of dropwise condensation, *Int. J. Heat Mass Transfer*, 49, 649–657.

Vierow KM, Schrock VE, 1991, Condensation in a natural circulation loop with noncondensable gases: Part I-Heat Transfer, in: Proceedings of the International Conference on Multiphase Flow, Tsukuba, Japan, 183–186.

von Karman T, 1939, The analogy between fluid friction and heat transfer, Trans. ASME, 61, 705-10.

Waligora JM, Michael RP, Richard LS, 1994, Spacecraft Life Support Systems. In *Space Physiology and Medicine.* A. E. Nicogossian, C. Leach Huntoon, and S. L. Pool, eds. Philadelphia, PA: Lea & Febiger, 109–127.

Walladares OG, 2003, Review of in-tube condensation heat transfer correlations for smooth and microfin tubes, *Heat Transfer Eng.* 24, 6–24.

Wang GQ, Zhao Q, Li G, Fu F, Li S, 1992, Vertical dropwise condensation shell and tube heat exchanger for steam with water cooling, *Patent no. 91201592.6*, *China Patent Bureau, (Patent Authority, Dalian Universtity of Technology/Dalian Power Station)*.

Wang S-C, Yang Y-T, Chen C-K, 2003, Effect of uniform suction on laminar filmwise condensation on a finite-size horizontal flat surface in a porous medium, *Int. J. Heat Mass Transfer*, 46, 4003–4011.

Weast RC, (Ed.) 1986, Handbook of Chemistry and Physics, CRC-USA.

Wheeler RM, Mackowiak CL, Stutte GW, Sager JC, Yorio NC, Ruffe LM, Fortson RE, Dreschel TW, Knott WM, and Corey KA, 1996, NASA's biomass production chamber : A testbed for bioregenerative life support studies, *Advances in Space*

Research, 18 (4-5), 215-224.

Whitley RH, 1976, Condensation heat transfer in a pressurized water reactor dry containment following a loss of coolant accident, *MS Thesis*, University of California at Los Angeles.

Woodruff DW, Westwater JW, 1979, Steam condensation on electroplated gold: effect of plating thickness, *Int. J. Heat Mass Transfer*, 22, 629-632.

Woodruff DW, Westwater JW, 1981, Steam condensation on various gold surfaces, *ASME J. Heat Transfer*, 103, 685-692.

Wu WH, Maa JR, 1976, On the heat transfer in dropwise condensation, *Chem. Eng. J.,* 12, 225-231.

Yabuki K and Miyagawa H, 1970, Studies on the effect of wind speed on photosynthesis. *Jpn. J. Agric. Met.,*26, 137–142 (in Japanese with English summary).

Yang SA and Chen CK, 1992, Laminar film condensation on a finite size horizontal plate with suction at the wall, Appl. Math. Modelling, 16, 325-329.

Yang YT, Chen CK, and Hsu PT, 1997, Laminar film condensation on a finite size horizontal wavy disk, Appl. Math. Modelling, 21, 139-144.

Yun R, Heo Haeheok, Kim Yongchan, 2006, Effects of surface roughness and tube materials on the filmwise condensation heat transfer coefficient at low heat transfer rates, *Int. Commun heat mass Transfer,* 33, 445-450.

Zhang HY, Mui YC, and Tarin M, 2010, Analysis of thermoelectric cooler performance for high power electronic packages, *Appl. Therm. Eng.,*30, 561–568.

Zhao Q, Zhang D, Li SF, Xu D, Zhang GB, Lin J, 1991a, New surface materials with dropwise condensation, *Proc. IVth World Cong. Chem. Eng.*, Sessions 8.3-10.

Zhao Q, Zhang D, Li SP, Xu D, Lin J, 1991b, Dropwise condensation of steam on ion-plating surfaces, *Proc. of the Int. Conf. on Petroleum Refining and Petrochemical Processing*, 2, 1049-1052.

Zhao Q, Zhang D, Lin J, 1991c, Surface material with dropwise condensation made by ion implantation technology, *Int. J Heat Mass Transfer*, 34, 2833-2835.

Zhao Q, Wang Q, 1993, Vertical dropwise condensation shell and tube heat exchanger for steam with water cooling, *Patent no. 91100529.3*, *China Patent Bureau, (Patent Authority, Dalian Universtity of Technology/Dalian Power Station)*.

Zhao Q, Burnside BM, 1994, Dropwise condensation of steam on ion implanted condenser surfaces, *Heat Recov. Syst. CHP,* 14(5), 525-534.

Zhao Q, Liu JJ, Bai T, Lin JF, Cui BY, Shen JL, Fang NT, 1994, Dropwise condensation of steam on vertical and horizontal U-type tube condensers, *Proc.10th Int. Heat Transfer Conf.*, 117-121.

Internet references

http://en.wikipedia.org/wiki/Mars (27th September, 2011)

http://en.wikipedia.org/wiki/Atmosphere_of_Mars#cite_note-mean_molar_mass-3 (27th September, 2011)

http://sp.uconn.edu/~mdarre/NE-127/NewFiles/psychrometric_inset.html (27th September, 2011)

Publications

Scientific Publications

1. **Akhilesh Tiwari**, P Lafon, A Kondjoyan and JP Fontaine, 2011, An air-conditioned wind tunnel environment for the study of mass and heat flux due to condensation of humid air, Chapter 4, In: *Wind Tunnels: Aerodynamics, Models and Experiments*, Editor- JD Pereira, Nova Science Publishers, Inc., New York, USA, 2011 (ISBN 978-1-61209-1).

2. **Akhilesh Tiwari**, P Lafon, A Kondjoyan and J-P Fontaine, 2010, Experimental modeling for the prediction of heat and mass transfer in an air-conditioned space environment for life support systems, *Proceedings of the 40th ICES-2010*, Barcelona, Spain, AIAA2010-6171.

3. **Akhilesh Tiwari** and J-P Fontaine, 2009, Towards the prediction of heat and mass transfer in an air- conditioned environment for a life support system in space, *Water, Air & Soil Pollution Focus*, 9, 539-547.

Conferences communications

1. **Akhilesh Tiwari**, Alain Kondjoyan and Jean-Pierre Fontaine, 2011, Driving phenomena for water condensation from humid air on a solid surface - Application to a bioprocess, International Conference on New Horizons on Biotechnology (NHBT-2011), 21-24 Nov 2011, Trivandrum, India.

2. **Akhilesh Tiwari**, Alain Kondjoyan and Jean-Pierre Fontaine, 2011, Caractérisation du transfert de masse par condensation sur une plaque horizontale en environnement climatisé, GdR MFA, 6-9 November, 2011, France.

3. **Akhilesh Tiwari** and J-P Fontaine, 2010, Utilisation de l'effet Peltier pour des expériences dédiées à la caractérisation des coefficients de transfert lors de condensation d'air humide, Journées de l'Ecole Doctorale des Sciences Pour L'Ingénieur, 28-29 April, 2010, University of Blaise Pascal, Clermont-Fd, France.

4. **Akhilesh Tiwari**, P Lafon, A Kondjoyan and J-P Fontaine, 2010, Experimental modeling for the prediction of heat and mass transfer in an air-conditioned space environment for life support systems, 40th International Conference on Environmental Systems (ICES), 11 - 15 Jul 2010, Hotel Fira Palace, Barcelona, Spain.

5. **Akhilesh Tiwari** and J-P Fontaine, 2009, The study of heat and mass transfer through condensation experiments, in Challenges in Environmental Science and Engineering, CESE-2009, 14-17 July 2009 at Townsville, Australia.

6. J-P Fontaine and **Akhilesh Tiwari**, 2008, Mass transfer prediction and measurement for condensation and evaporation phenomena in air-conditioned space environment, 3rd International Congress on Bioprocesses in Food Industries (ICBF 2008), 6-8 November 2008, at Osmania University, Hyderabad.

In: Wind Tunnels: Aerodynamics, Models and Experiments ISBN 978-1-61209-204-1
Editor: Justin D. Pereira © 2011 Nova Science Publishers, Inc.

Chapter 4

AN AIR-CONDITIONED WIND TUNNEL ENVIRONMENT FOR THE STUDY OF MASS AND HEAT FLUX DUE TO CONDENSATION OF HUMID AIR

Akhilesh Tiwari[1*], Pascal Lafon[1], Alain Kondjoyan[2] and Jean-Pierre Fontaine[1]

1. Clermont Université, Université Blaise Pascal, Laboratoire de Génie Chimique et Biochimique (LGCB), BP10488, F-63000, Clermont Ferrand, France

2. Institut National de la recherché Agronomie (INRA), UR Qualité des Produits Animaux, F-63122, Saint Genès Champanelle, France

ABSTRACT

The development of an artificial ecosystem inside a closed environment is one of the future challenging problems, which is mandatory for the long duration manned space missions like lunar base or mission to Mars. Plants will be essential companion life forms for such space missions, where human habitats must mimic the cycles of life on earth to generate and recycle food, oxygen and water. Thus the optimized growth of higher plants inside the closed environment is required to obtain efficient biological life support systems. The stability and success of such systems lie on the control of the hydrodynamics and on an accurate characterisation of the coupled heat and mass transfer that develop at interfaces (solids, plants,..) within the space habitat. However, very few data can be found on the precise characterization / prediction of the mass transfer at interfaces, and more particularly in space. In most studies the mass flux is deduced from the measured / calculated heat flux by a heat and mass transfer analogy.

Hence, we have developed a ground based experimental set-up to measure the air flow velocities and concomitant mass transfer on specific geometries under controlled air flow conditions (flow regime, hygrometry, temperature). The final goal is to derive a theoretical model that could help for the prediction of the hydrodynamics and coupled heat/mass transfer on earth, and eventually in reduced gravity. We have used a closed-circuit wind tunnel for our experiments, which can produce very laminar to turbulent flows with controlled temperature and hygrometric parameters inside the test cell. The

* E-mail : akhilesh.tiwari77@gmail.com

initial experiments have been performed in dry air with an average velocity between 0.5-2.5 $m.s^{-1}$. The velocity profiles near a clean aluminium flat plate in horizontal or vertical positions have been studied for low Reynolds number flows by hot wire anemometry. The measurements with the horizontal plate showed a boundary layer thickness in agreement with the Blasius' solutions. Condensation of humid air was induced on an isothermal flat plate, which was cooled by thermoelectricity. The mass transfer on the plate was controlled and recorded with a precise balance. The obtained results are analyzed, and compared to the available data on condensation.

INTRODUCTION

Human life is precious and its existence on Earth is characterised by few very important factors or parameters. The availability of these parameters on the earth is monitored and recycled by nature itself. The basic functions that sustain life on earth are breathable air, food, usable water, optimum temperature and pressure, and also recycling of waste. To maintain human life away from earth, we have to recreate a sustainable environment, with the above-mentioned life supporting basic systems. Today's technology is capable of supporting human crews in space for missions in low earth orbit (LEO) of short or indefinite duration as long as resupply is readily available, as evidenced by the International Space Station (ISS). All crewed space missions rely on resupply from Earth for some or nearly all of the required consumable resources (oxygen, water, food). The technology used on the ISS is capable of recovering water from humidity condensate, waste hygiene water, and crew urine with 80 to 90 percent efficiency [1]. The air and water treatments are performed with physico-chemical processes. However, no space-qualified technologies are capable of recycling food or oxygen from waste materials, and wastes have to be discarded or stored for return to Earth. Resupplying future missions beyond LEO, missions to Mars or to the moon for example, will be even more intricate, if not impossible.

The major advantage of a bio-regenerative life support system (BLSS) is that it does not need to be resupplied with food, water, and air, nor does it require expendable water or air filtration systems as present-day mechanical spacecraft life support systems do [2-4]. Indeed, throughout the history of manned-space flight, one of the key problems has been the development of bio-regenerative life support systems (BLSS), to provide autonomy to piloted spacecraft and planetary outposts for multiyear missions [5]. The importance of recycling within the spacecraft, with crews consuming the products of autotrophic synthesis, needs recycling of materials, requires exchanges between photoautotrophic organisms, which synthesize organic substances using solar or artificial light, and heterotrophic organisms. Hence, growing plants is a vital component and its performance in BLSS for space missions will be principally dependent on the progress of plant cultivation technology for space and the achievement of associated equipment. The growth of higher plants in a green house is optimized by the environmental conditions among which the effect of ventilation, condensation and evaporation phenomena on the surfaces of leaves, plants, windows, and walls. Our study is devoted to the control of the hydrodynamics and concomitant heat and mass transfer (gas /liquid) at interfaces.

Furthermore, condensation on solid walls or on plants has to be controlled to provide optimized living conditions (for astronauts or plants), although the humidity level may be

particularly high in a greenhouse (75-80%). Air-conditioning systems have always been known as good solutions to prevent condensation while maintaining optimized conditions for life, but an adapted ventilation system (forced convection) is needed, particularly in a micro-gravity or reduced gravity environment. Thus, a precise control of the hydrodynamics and the concomitant heat, humidity and mass transfer developing in the space station has to be performed. Numerical simulation or theoretical models could give insights into the dynamics of transport phenomena and assist in the design of an optimized and reliable air-conditioning system. However, a precise mathematical model requires the knowledge of the local mass transfer coefficient (for condensation or evaporation) for the specific configurations, and a validated turbulent model. Such data can only be given by experimental works or by literature. We have developed an experimental set-up to measure mass flux in a closed loop wind tunnel, where temperature and humidity are regulated.

EXPERIMENTAL MATERIAL AND METHODS

A wind tunnel is used to generate and control the mass flux of humid air that condenses on the active surface, which is a square flat plate. The temperature of this plate is kept constant below the dew point by an arrangement of thermoelectric cooling in order to induce a steady flow of condensation on the air/plate interface, and the produced condensate is regularly measured by weighing the whole system. The system consists of square shaped Peltier modules sandwiched between a square shaped aluminium flat plate and a heat exchanger device, and a temperature regulator which provides the power supply of the thermoelectric Peltier module. The overall arrangement is placed in the experimental cell of a wind tunnel in which the hydrodynamics, temperature and hygrometry are controlled.

Wind Tunnel

The wind tunnel facility built by INRA-Theix under the direction of Dr Kondjoyan [6] aimed to generate from nearly laminar to highly turbulent flows. The detailed description of the wind tunnel is given in the literature [6-8]. The data for laminar flows were compared in these studies for turbulent flows are similar to those encountered in industrial and outdoor environments. The temperature, humidity and wind velocity can all be regulated inside the wind tunnel.

The main characteristics of the wind tunnel are:

- The testing chamber has a cross section of 0.8 m x 0.8 m and a length of 1.6 m in the direction of the flow.
- It was designed to generate average air flow velocities from 0.5 $m.s^{-1}$ to 5.0 $m.s^{-1}$ and turbulence intensity ranging between 1% and 20%.
- Temperature and humidity (characterized by the dew point) are controlled with an accuracy of ±0.1°C (air temperatures and dew point are homogeneous to 0.1°C within the area where the experimental set-up is located).

The wind tunnel is shown schematically in Figure 1. It is a closed loop of 12 m long and 4 m high. The flow is initially made as laminar as possible and to get a very little turbulence intensity in the order of 1% in the test chamber (1), the diffusers (2, 6, 8 and 10) and elbows (4 and 7) were designed to bring the air of the ventilator (5) to the damping screen (11) without generation of turbulence due to separations on the walls of ducts. The fine mesh grid located in the damping chamber dissipates turbulence by viscous effects. The contraction area (12) makes the flow more uniform at the entrance of the experimental chamber through a contraction ratio of 9. Two drawers (12, 14) located respectively upstream and downstream of the contraction area may optionally be used as generators of turbulence by adding or removing extra perforated plates, perpendicular to the direction of the flow. The use of two drawers at different distances from the experimental test chamber strongly increases the possibility of obtaining flows whose turbulence intensity is uniform around the experimental set-up.

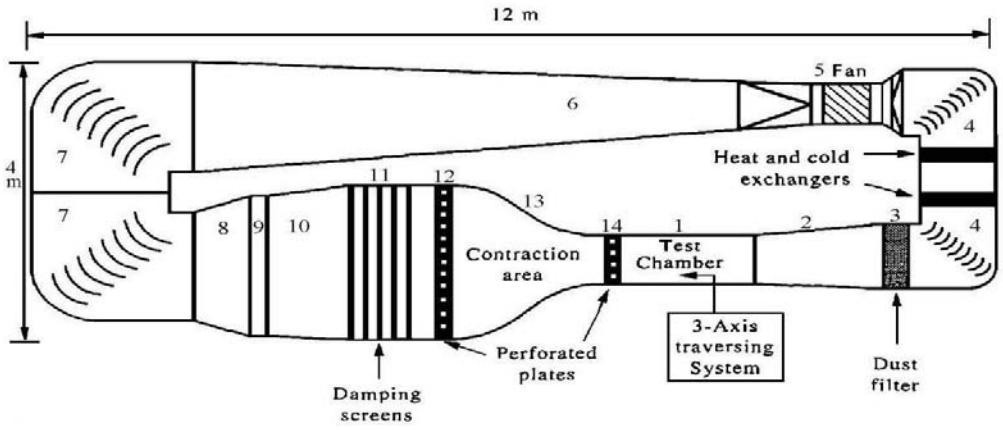

Figure 1. Schematic of wind tunnel.

Two devices of air-conditioning assistant are associated with the wind tunnel installation to ensure the temperature and humidity control. The measurement of the dew point is carried out using a cooled mirror hygrometer with a precision of ±0.1°C (Dew 10 of National Instrument). The wind tunnel is a closed loop, sealed, strongly isolated and the devices of conditioning are located upstream of the ventilator.

The hydrodynamic homogeneity of the experimental test chamber was validated by velocity measurements taken in many points of this chamber, these measurements showed that the mean velocities differ by less than 5% within the total volume, the intensity of turbulence varies by less than 3% in the area, where we should place our experimental prototype of condensation. Previous measurements showed a very good uniformity in temperature and humidity in the test area, the variations were lower than ±0.1°C for the temperature of the air and the dew point, even for a nearly laminar flow [7].

Measurement of Wind Velocity

The characterization of the flow, mean flow velocity and fluctuations, was carried out by constant temperature hot wire anemometry. The hot wires are normally 5 µm in diameter and 1.25 mm long suspended between two needle-shaped prongs. The sensor possesses flow sensitivity and wide frequency response in turbulent flow. Miniature wire probes with offset prongs and with the sensor perpendicular to the probe axis (DANTEC 55P15) were selected as they are designed for measurements within the boundary layer. This shape of prongs allows measurements close to a solid wall without disturbance from the body of the probe, which remains beyond the boundary layer. The wind tunnel is equipped with a three-axis traversing system that enables the displacement of the hot wire probe in an area of chosen dimension and location with a selected displacement in the order of about 0.01 mm.

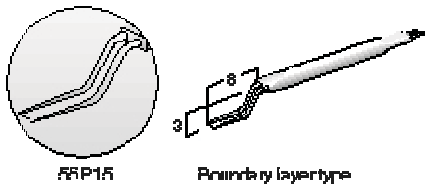

DANTEC 55P15.

Figure 2. Hot wire sensor probe.

A telescope (magnification ×24) placed at a distance (about 3 m) was used to locate the probe, with precision (± 0.05 mm), close to the plate and to avoid any contact. (See figure 2)

The hot wires available were calibrated with room temperature for velocity measurements averaged ranging between 0.5 $m.s^{-1}$ to 5 $m.s^{-1}$ with an accuracy of 1-3%. Below 0.4 $m.s^{-1}$ hot wire measurements lack accuracy because of thermal exchange. The data acquisition for the localization of the hot wire probe and the average velocity fluctuations was recorded using a computer connected to the system. A photograph of the test chamber, where we have placed our set-up is shown in figure 3.

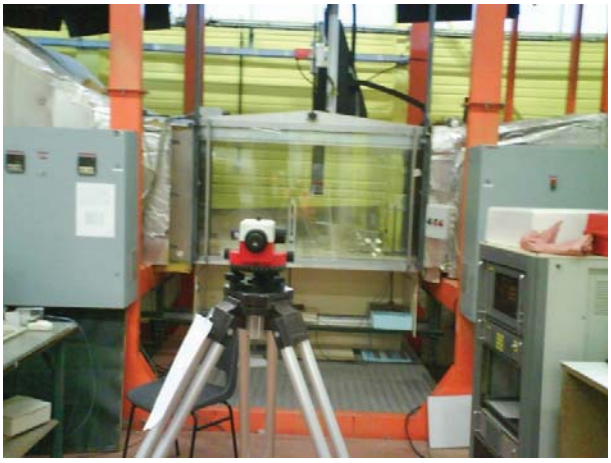

Figure 3. A view of the test chamber with telescope.

Condensation Unit

The whole system of cooling a square flat plate is shown in Figure 4. The temperature of the active surface is controlled by a Peltier element owing to a thermistor (1), which is itself inserted inside the square aluminium flat plate near its geometrical centre for the regulation of the input current of the Peltier element.

The aluminium flat plate (2) is glued on a Peltier module (3) of the same size, with a thermal adhesive, loaded with micronized silver (Arctic Silver – Premium Silver). The preliminary tests were carried out by pasting the aluminium flat plates with a thermal paste. The other side of the Peltier module is pasted on a heat sink (4). This heat sink made up of single-piece extruded aluminium has a strong density of wings aligned with the direction of the flow to reinforce the convective exchange. To increase the effectiveness of the Peltier module, the use of a heat sink on the hot side of the Peltier plate is a key parameter. The objective is to dissipate the heat flux produced on the "hot" side of the Peltier module in order to maintain this side at a temperature as close as the ambient temperature $T_{a,}$ which can be used as a reference temperature. The value of the electric current in a Peltier module theoretically makes it possible to create an absorption of heat on one side ("cold") and an equivalent heat emission on the opposite side ("hot"). Keeping this surface at room temperature, which is the reference temperature, makes it possible to create the necessary temperature difference with the dew point T_d in order to induce the desired rate of condensation on the cold surface temperature T_s. Indeed, the rate of condensation is directly related to this difference in temperature $\Delta T=T_d- T_s$.

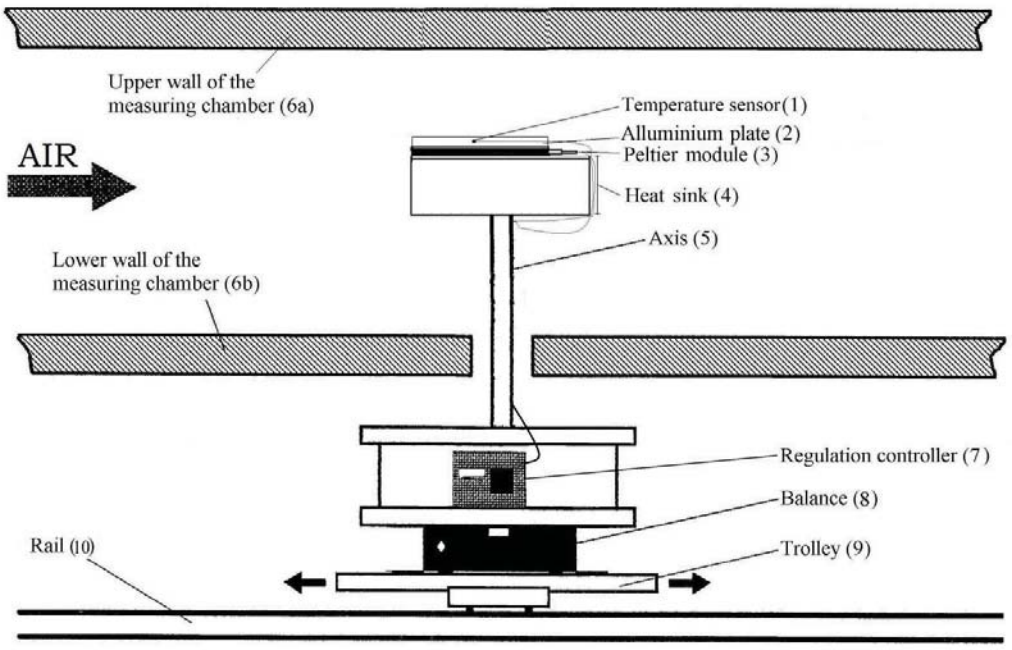

Figure 4. Schematic of the whole condensation unit.

In order to control this rate of condensation, we need, on the one hand, to maintain this temperature contrast constant ($\Delta T=T_d-T_s$) throughout the experiment. For this purpose, a thermistor of small size (1) is inserted in the plate to measure the temperature in its centre under the plate/air interface. It is connected to the temperature regulation controller (7), which adjusts the electric current transmitted to the Peltier module to maintain T_s constant. In addition, to obtain a uniform mass flux on the whole surface for a precise measurement of the rate of mass flux, we must maintain the temperature of the active surface (plate/air) as isothermal as possible. Aluminium plates (strong thermal conductivity) of thickness 2, 3, 4, 5 mm were studied. The 3 mm thickness make it possible to homogenize the thermal distribution obtained directly on the cold surface, the one produced at the ceramic Peltier module side (variations of several degrees Celsius for a 50 mm x 50 mm plate) with a weak inertia.

A programmable temperature regulation controller (LFI-3751 of Wavelength Electronics) for the Peltier module was chosen for its stability over time and accuracy (± 0.1°C). In addition, it is possible to add an auxiliary thermistor sensor (for the study of temperature difference inside and on the upper surface eventually).

The main goal of this study is to evaluate local mass transfer coefficients. Thus, we must study acive surfaces of small sizes for the measurement to be considered local and for the surface to be nearly isothermal, but which are however sufficiently large in order to condense a quantity of water that can be recorded with a precise balance. Plates measuring 30 mm x 30 mm, 40 mm x 40 mm and 50 mm x 50 mm were considered.

Thermoelectric Cooler (TEC) – Peltier Element

The idea behind the Peltier effect [9-11] is that, whenever a direct current flows through the circuit of heterogeneous conductors, heat is either released or absorbed at the conductors' junctions, which depends on the current polarity. The amount of heat is proportional to the current that passes through the conductors. The basic TEC unit is a thermocouple, which consists of a p-type and a n-type semiconductor elements, or pellets, which are traditionally made of Bismuth Telluride (Bi_2Te_3)-based alloy and normally copper commutation tabs are used to interconnect these pellets. Thus, a typical TEC consists of thermocouples connected electrically in series and sandwiched between two Alumina ceramic plates. The number of thermocouples may vary greatly from several elements to hundred of units.

Specifications of Used Peltier Modules

The Peltier Modules were manufactured by KRYOTHERM, Russia, the different parameters are given below.

Table 1. Different parameters of single stage thermoelectric coolers

	I_{max} Amps	Q_{max} Watts	U_{max} Volts	ΔT_{max} (K)	R_{ac} Ohm	No of thermo-couples	Dimensions (mm x mm x m)
Snow Ball – 71-S	3.6	36	16.1	71	3.2	71	30 x 30 x 3.6
ICE-71 HT(120) E L3	8	80	16.1	71	1.5	71	40 x 40 x 3.4
TB-127-2.0-2.5	7.6	76.0	16.3	72	1.65	127	48 x 48 x 4.8

ΔT_{max} = Maximum achievable temperature difference between the hot and cold side of a thermoelectric cooler

I_{max} = Input current through a thermoelectric cooler resulting in greatest ΔT (ΔT_{max})

U_{max} = Voltage on a thermoelectric cooler contacts at ΔT_{max}

Q_{max} = Maximum cooling capacity of a thermoelectric cooler. It is determined at maximum current through a thermoelectric cooler and at zero temperature difference between hot and cold sides

R_{ac} = Electric resistance of a thermoelectric cooler measured at an alternating current with the frequency of 1 kHz.

Advantages and Disadvantages of Using a Peltier Module as Cooling Devices Advantages:

- A Thermoelectric cooler module has no moving part, therefore, it needs virtually no maintenance;
- Capability of modules to operate for more than hundred thousand hours of steady-state operation;
- Compactness and lightness;
- Very fast response time;
- No orientation / position dependence;
- Reliability.

Disadvantages

- Heat dissipation, which requires heat sinks and fans;
- Control of the reference temperature;
- Non-uniformity of the cold power produced at the ceramic interface;
- Condensation inside the Peltier elements.

To prevent condensation inside the Peltier elements the Peltier modules have been sealed with Silicon and Epoxy.

Weighing

The whole experimental arrangement with the condensation unit, the temperature regulator and all the connecting wires is placed on a weighing balance (Figure 3). Also, it is

maintained in the measuring chamber by a shaft (5) fixed itself at the balance pan (8). There are two horizontal parallel plates connected by four screws and placed on the balance, in between these two plates the temperature regulation controller (7) is placed. The wire of the Peltier module and the thermistor inserted in the active plate (1) walk along the axis and are connected to the temperature controller. The balance is put on a mobile platform, a trolley (9) which makes it possible to slide the whole system on a rail (10). This device allows a continuous signal acquisition recorded by a precision balance (Mettler 30, precision of ±0.1 g), which is connected to the computer for monitoring the increase in mass as the humid air will condense on the active surface.

EXPERIMENTAL RESULTS AND DISCUSSIONS

Velocity and Turbulent Intensity Profiles in Dry Conditions

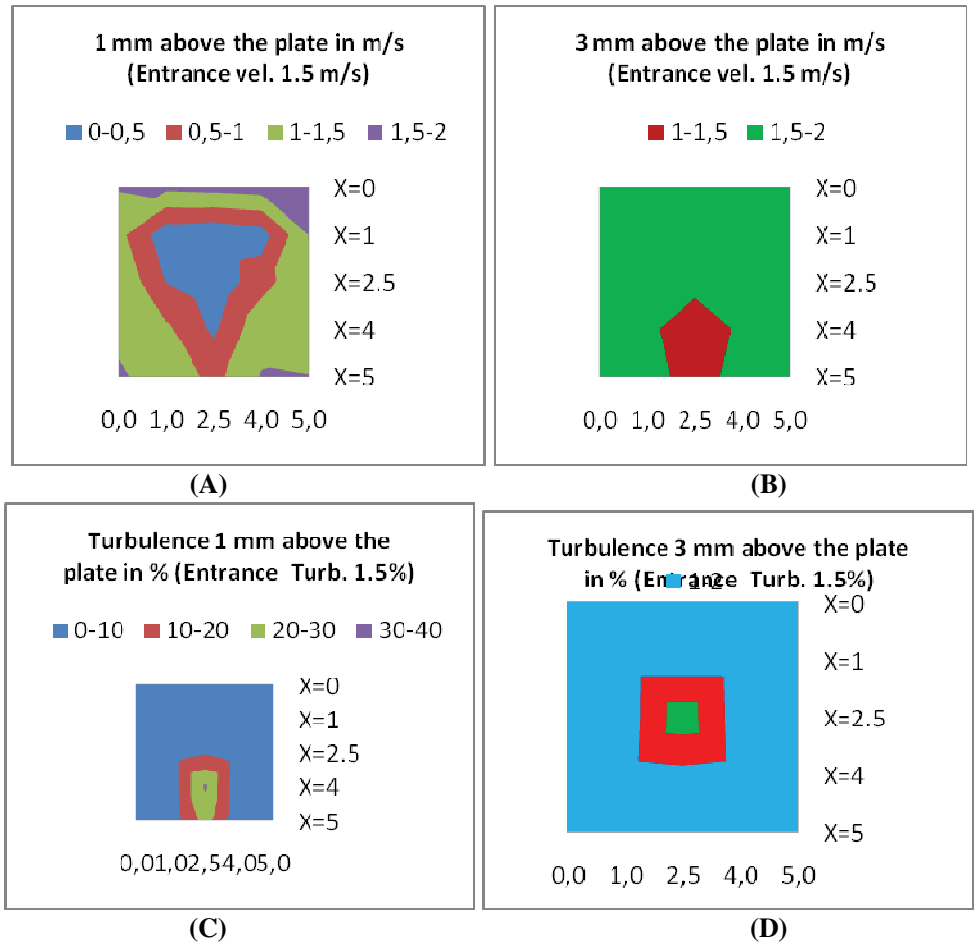

Figure 5 (a-d). Comparative surface plots above the flat plate in horizontal position at 1 mm (a, c) and at 3 mm (b, d): (a-b) velocity profiles in metre per second and (c-d) turbulence intensity in per cent.

Preliminary experiments have been performed inside the wind tunnel for the study of velocity and turbulence intensity profiles in dry conditions at room temperature ($T_a \approx 22°C$) [12-13]. The mean velocity measurements have been performed at 1 mm and 3 mm above the surface of the horizontal plate. The surface plots of the velocity profile are given in figure 5(a, b) and for the turbulence intensity in figure 5(c, d) for mean velocity of 1.5 $m.s^{-1}$. The experiments were performed for a mean entrance velocity of 0.5, 1.1, 1.5, and 2.0 $m.s^{-1}$ and the wind velocity as well as the turbulence intensity were measured. It is observed from figure 5(a, b) that, on moving from the surface of the flat plate to free stream velocity, the fluctuations in the velocity decrease and the shape of the velocity profile is almost conical, and centred towards the middle to back part of the flat plate. It is also observed in figure 5(c, d), that the maximum turbulence intensity at 1 mm above the surface of the plate reaches 30-40%, and at 3 mm above the surface drops to 3-4%, whereas the turbulence intensity at the entrance of the tunnel was about 1.5%. Slightly above a height of 3.2 mm of the plate, the turbulence intensity suddenly reached the range of the turbulence intensity measured at the entrance of the tunnel (1.5%), which shows that the probe was outside the boundary layer. The symmetry of the measured profiles (velocity and turbulence intensity) reflects the accuracy of the experimental set-up (position, manufacturing etc.). All our results showed that we observe the development of a boundary layer on top of the aluminium plate. This boundary layer could not be considered as the classical laminar boundary layer on a flat plate. Even if the upstream edge of the plate was thin (3 mm in thickness) it generated vortices which increased turbulence near the plate wall. Actually turbulence intensities up to 30-40% were measured in the wind tunnel above the plate which revealed the development of those turbulent vortices. In this case it was shown in literature [14] that close to the wall the velocity profile was similar to that of a classical laminar boundary layer, even if the velocity gradient increased with turbulence, while the contact region between the free stream and the boundary layer became less distinct similarly to the outer region of a turbulent boundary but without any logarithmic behaviour of the velocity profile. It was also shown in literature that the global boundary layer thickness including the outer turbulent part was a little bit increased compared to thickness of a classical laminar boundary layer. This thickening of the boundary layer due to free stream turbulence was always very small (10% to 20%). Boundary layer thickness was measured in our study for different air flow velocities by considering that the end of the boundary layer was reached when the turbulence intensity was the same as in the upstream flow. Results are compared with Blasius' solution ($\delta_x \cong 4.64\sqrt{\upsilon x/U}$) [15] in figure 6. In agreement with previous literature boundary layer thickness was close to Blasius' solution.

Table 3. Values of parameters used in calculations and taken at the time of the experiment

Parameter	Range
Atmospheric pressure, mbar	920-924
Dew point temperature, °C	< 7.0 °C
Density of air, kg/m^3	1.202
Kinematic viscosity, m^2/s	1.525×10^{-5}

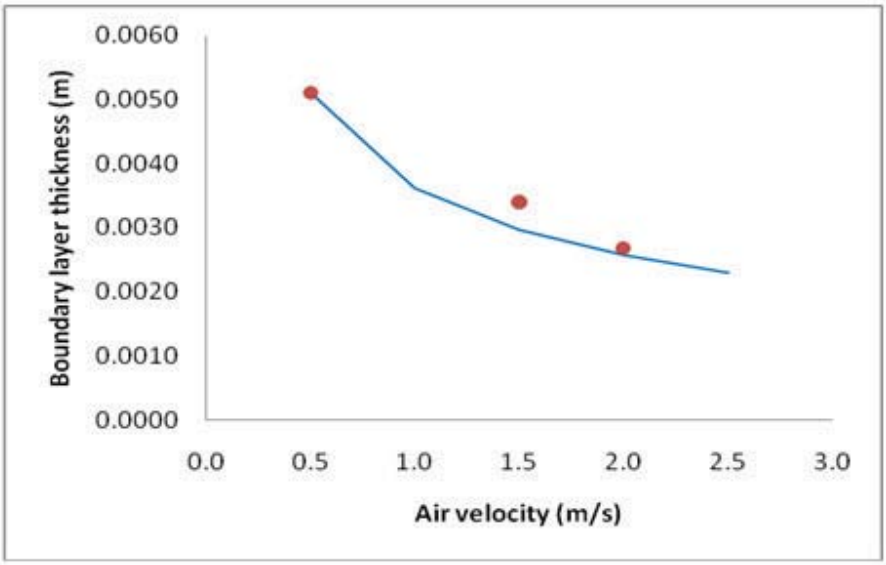

Figure 6: Comparative plot of boundary layer thickness calculated by using Blasius solution (*continuous line*) and (*observed experimentally*) on a plate of surface area 5 cm x 5 cm.

Condensation Experiments in Ambient Conditions

Some experiments for condensation on the surface of a flat square plate were carried out in a closed room in which the hygrometric and hydrodynamic parameters varied according to the inside ambient weather conditions, except for a fan which was used to produce the air turbulence for the heat exchanger. The condensation unit was put directly on top of a balance (Ohaus Navigator-N24120). A non laminar flow of humid air was generated on the active surface by a very small fan (same size as the heat exchanger) of 12 V power supply. The average air velocity was almost constant during all the experiments. More than 15 experiments were carried out with three different sizes of the plates. Each experiment was performed in different ambient atmospheric conditions.

The measurements of the temperature distribution on the surface of the flat plate and on the surface of the Peltier element only were carried out in the ambient air and they showed that the top surface temperature was more or less homogeneous for 3 mm thick plate (variation of less than 1°C for a 3 mm thick plate of 5 cm x 5 cm): it was observed in a local temperature distribution measurement with 25 equidistant points on the surface of 5 cm x 5 cm or 4 cm x 4 cm plates, and with 17 points on the 3 cm x 3 cm that the variation in temperature on the active surface was higher for thinner plates (1 mm and 2 mm thickness). Also the similar local temperature distribution measurements directly on the ceramic surface of the Peltier element (without the aluminium plate) showed a temperature difference larger by 1.5°C for the 5 cm x 5 cm plate. In all cases the temperature was minimum at the centre and maximum at the boundaries.

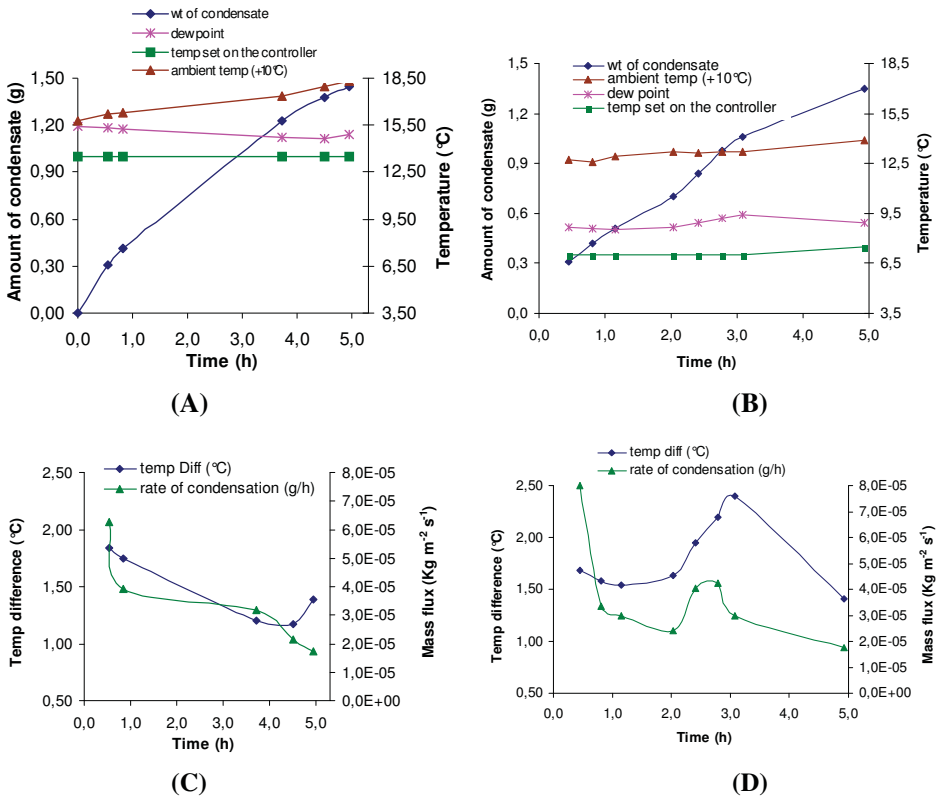

Figure 7: a-b) Amount of condensate and temperature as a function of time. The value of ambient temperature is also given in the graph after reducing 10°C to fit in scale. c-d) The temperature difference and mass flux as a function of total time.

Figure 7 (a-d) shows the plots of condensation experiments carried out on two different days with variable hygrometric and hydrodynamic atmospheric conditions. These experiments were performed on a horizontal aluminium square flat plate of 50 cm x 50 cm in open environment and for temperature differences, $\Delta T = T_d - T_s$ (between the surface temperature (T_s) and the dewpoint (T_d)) of approximately 1.50 °C. The variation in relative humidity was 2 to 12% and in ambient temperature less than 10% according to the local weather conditions during day time, sometimes both data increased or decreased simultaneously, other times one increased and the other decreased, which varied the dewpoint temperature by less than 1°C up or down during the experiment. However, it was important to maintain the temperature of the active surface sufficiently below the dewpoint for the condensation of water vapour in air to proceed.

It is observed from figure 7(a), the mass increase versus time and that the temperature difference ΔT varies from 1.2°C to 1.8°C. The ambient temperature is increased by 8% and the relative humidity decreased by almost 15% during the 5 h experiment, which provided a decrement in the initial dewpoint value of about 0.5 °C. The amount of condensate collected during this time was 1.5 g with an average rate of condensation of 0.26 g/h. Figure 7(b) shows a similar experiment, in which the temperature difference ΔT was first decreased then went up almost 0.7°C and then was decreased by 0.8°C, because the ambient temperature

went up 5%, but the relative humidity was slightly increased and then decreased with a variation of almost 5%. The dewpoint decreased for about 1 h and then increased, but the difference was less than 1°C during the 5 h experiment, which resulted in a collection of 1.4 g of condensate.

Figure 7 (c, d) shows the rate of condensation and temperature difference as a function of the total time of the experiments. Figure 7(c) indicates that the rate of condensation follows the trend of the temperature difference except after 4 h, where the measured rate of condensation decreased even though the temperature difference increased. Figure 7(d) shows that the rate of condensation has more or less a similar behavior as the temperature difference ΔT. As the temperature difference starts decreasing, the condensation rate decreases significantly, because of the low temperature difference and the reduced active surface area left on the surface of the plate as the interface condensate/air may not be cold enough to induce condensation.

The figures 8(a-b) shows similar plots as 7(a-b) but measured inside the wind tunnel and with slightly higher temperatures to get similar rates of condensation. The Reynolds number $\mathrm{Re} = (\rho_\infty v L)/\mu_\infty$ was in the range of 3800 – 4000 and the Schmidt number $Sc = \mu_\infty /(\rho_s D)$ was 0.6. Figure 8 (a) shows again that the mass flux of condensation varies according to the temperature difference ΔT represented on the graph by the dewpoint variation (as T_s is constant). Two main trends can be observed: (i) a mass rate of 0.36 g/h for $0 \le t \le 2.5$ h (ii) a mass rate of 0.2 g/h for $5 \le t \le 8$ h. The trend (i) corresponds to the early condensation period when drops grow all over the surface and coalesce according to the well known process [16-17]. The trend (ii) corresponds to a lower mass increase as the surface of the plate is covered by large mass of water leaving a much smaller active area for most of the condensation to proceed, as a much lower condensation rate develops at the condensate/ air interface. Figure 8(b) shows a more linear trend during the 8 h experiment with a mass rate of about 0.4 g/h, but a slight decrease seems to be seen at the end of the experiment.

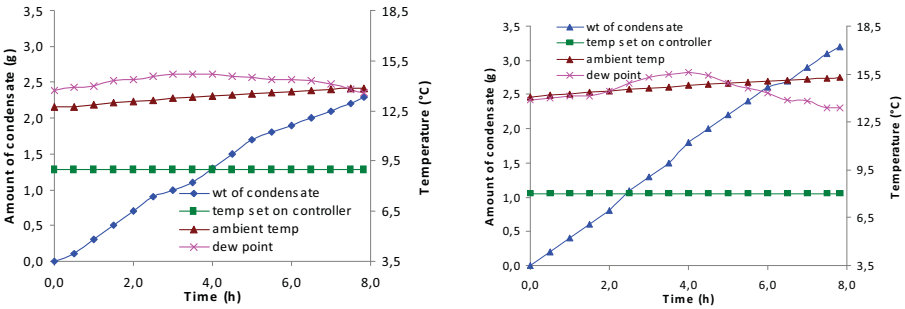

Figure 8: a-b) Amount of condensate and temperature as a function of time inside the wind tunnel.

Figure 9(a) shows the variation of the amount of condensate versus time for several average temperature differences ΔT in an open environment. The trends are affected by the hygrometric ambient conditions, which are not completely stable as we did not perform the experiments in air-conditioned environments. The figure 9(b) indicates more regular variations inside the controlled wind tunnel for three different temperature differences, which

indicates that on increasing the temperature difference the amount of condensate also increases accordingly. However, the main behavior indicates the sensitivity of the slope and, thus, of the mass flux to the temperature difference as expected. The evaluation in time is also influenced by the active area which decreases with time as condensation covers more and more the flat plate and after long duration we can observe some type of saturation as most of the plate surface is covered with water. It is also worth noting that the shape of the condensate is also strongly influenced by the physico-chemical properties of the aluminium plate (contact angle, etc.). Initially drop-wise condensation is induced (Figure 10(1)), but after a few hours (Figure 10 (3)), a large part of the plate is covered by mainly 4-5 big drops of water which can flow out of the plate or be thrown out by the air flow. These complex phenomena greatly affect the heat-mass transfer at the surface of the plate. In the future condensation process will be analyzed step by step trying to characterize as much as possible the formation of condensate.

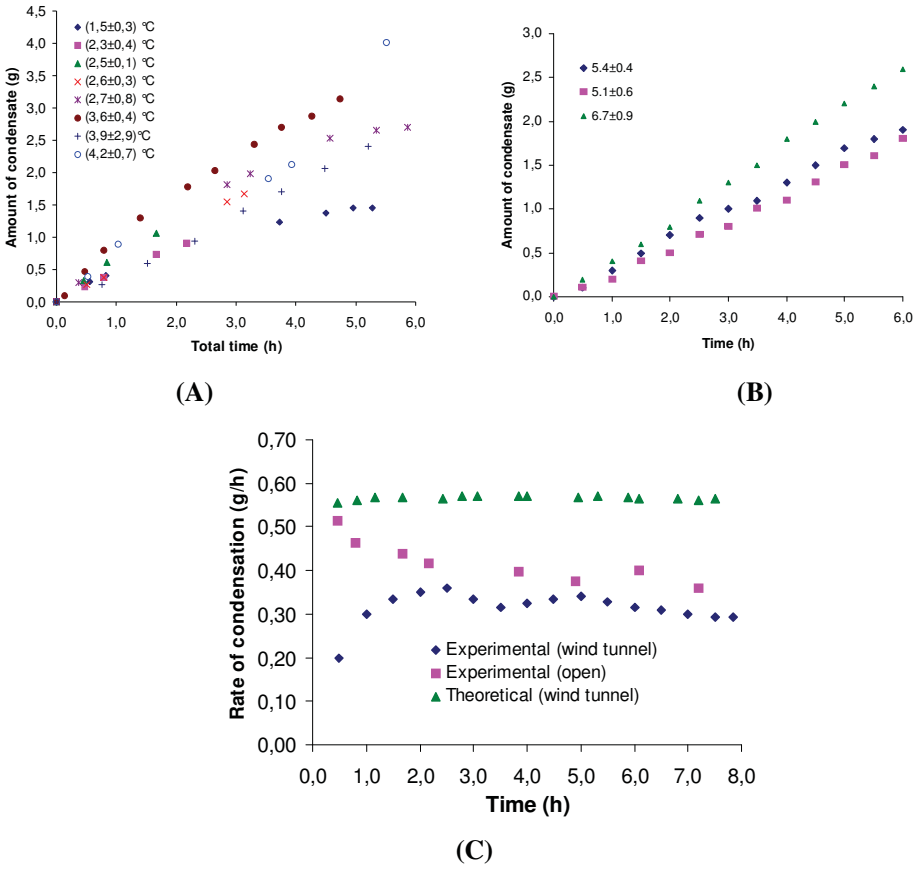

Figure 9. (a) Amount of condensate as a function of total time of experiment for 8 experiments in open environment (b) inside the wind tunnel for 3 experiments at given temperature differences (c) comparative rate of condensation as a function of time measured experimentally in open air and wind tunnel and calculated theoretically for wind tunnel.

The figures 9(c) shows the variation of the theoretical and experimental values of the rate of condensation versus total time. The theoretical diffusion coefficients were calculated here by using the binary diffusion coefficient of water vapour in air from the kinetic theory of gases [18]. The mass flux of water vapour in air was calculated by using the formula [19]:

$$N_{WV} = \frac{Sh\rho_s D(\omega_\infty - \omega_s)}{L(1-\omega_s)}$$

where the average Sherwood number is computed from, $Sh(1-\omega_s) = 0.664\,\mathrm{Re}^{\frac{1}{2}}\,Sc^{\frac{1}{3}}$ and the Reynolds number (Re) and the Schmidt number (*Sc*) are standard dimensionless numbers, where the Sherwood number is expressed with mass fraction and not with concentration.

From the observation of plot 9(c), we can say that the rate of condensation was not constant with time. For the first hour of the experiment it went down in the open environment, and then was decreased gradually. It differs in the wind tunnel for the first 2.5 h when the rate was increased, because the temperature difference was increased by 15%, and then a similar trend is seen. It is worth noting that the rate of condensation is proportional to the active surface and that this area decreases with time as condensation develops. Moreover, some evaporation takes place at the water / air interface. The theoretical value of the mass flux is almost constant during the whole experiment because the effect of the condensate collected on the surface was not considered in the theory.

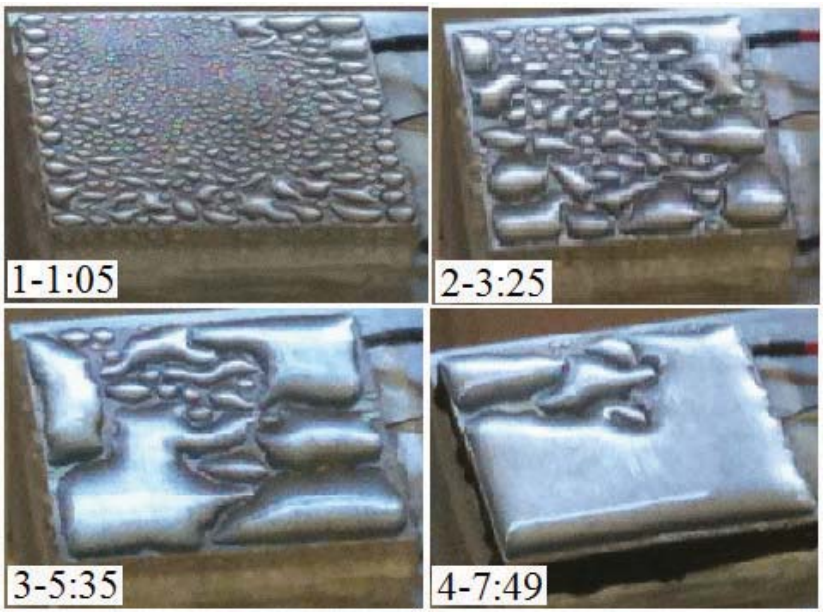

Figure 10. (1-4) Photographs of the flat plate with condensation on it at different duration of time (in hours) from starting point of condensation.

CONCLUSION

The above experimental findings show that the use of a wind tunnel is needed for the precise characterization of mass transfer by condensation of air on surfaces and that it will provide a very powerful tool to establish a theoretical model for the prediction of such phenomena. Also the concept based on thermoelectric cooling and weighing the growing mass of condensation to study mass transfer is validated. To be more accurate further experiments are being performed in the wind tunnel. Indeed, we have performed experiments in a closed wind tunnel, in which, it is possible to control the psychometric parameters (relative humidity, temperature) and to generate almost laminar to turbulent flows. The results in dry conditions determined the velocity profile above a flat horizontal plate and estimated a boundary layer thickness, which fits with Blasius' solutions. More complete results will allow in developing a theoretical model for the mass transfer flux of condensation at interfaces.

NOMENCLATURE

T	=	temperature, K
L	=	characteristic length of the plate, m
C_p	=	specific heat capacity, J/ kg K
h	=	heat transfer coefficient, J/m^2 K s
N	=	mass flux, Kg/m^2 s
D	=	binary diffusion coefficient at interface m^2/s
Tu	=	turbulence intensity of air, %
U	=	mean air velocity in the free stream, m/s
u	=	velocity fluctuations around U in the main flow direction, m/s
T_c	=	temperature constraint set on controller, °C
x	=	distance from the starting edge of the plate, m

Dimensionless Quantity

Sh	=	Sherwood number
Re	=	Reynolds number
Sc	=	Schmidt number

Greek

ρ	=	density, kg/m^3
μ	=	dynamic viscosity, Pa s
ω	=	mass fraction of water vapour in air
Δ	=	difference
ν	=	kinematic viscosity, m^2/s
δ	=	boundary Layer thickness, m

Subscripts

∞	=	value at ambient temperature or free flow temperature
wv	=	water vapour
s	=	surface or interface of air and flat plate
d	=	dewpoint

ACKNOWLEDGMENTS

The authors are grateful to the Centre National d'Etudes Spatiales (CNES), France for providing financial support. They also thank Prof. Jean Bernard Gros, LGCB for fruitful discussions.

REFERENCES

[1] Advanced Technology for Human Support in Space, National Academy Press, No. 97-68305, 1997.
[2] Mergeay, M.; Verstraete, W.; Dubertret, G.; Lefort-tran, M.; Chipaux, C.; Binot, R. Proc. 3rd Symp. Space Thermal Control and Life Support Systems. Noordwijk, The Netherlands. pp 65-68.
[3] Gros, J. B.; Poughon, L.; Lasseur, C.; Tikhomirov, A. A. Adv. Space Res. 2003, 31(1), pp. 195-199.
[4] Bérangère F.; Poughon, L.; Creuly C.; Cornet, J-F. ; Dussap, C-G. & Lasseur, C. Appl Biochem Biotechnol 2008, 151, 686–699.
[5] Erokhin, A.N.; Berkovich, Yu A.; Smolianina, S.O.; Krivobok, N.M.; Agureev, A.N.; Kalandarov, S.K. Advances in space Research 2006, 38, 1240–1247.
[6] Kondjoyan, A. Contribution à la connaissance des coefficients de transfert de chaleur et de matière à l'interface air-solide ; Thèse de Docteur de l'E.N.S.I.A., 1993.
[7] Kondjoyan, A.; Daudin, J.D. Int. J. Heat Mass Transfer, 1995, 38(10), 1735-1749.
[8] Kondjoyan, A. L'échange de chaleur et d'eau à l'interface air/solide, Habilitation à Diriger des Recherches de l'Université Blaise Pascal, 1999.
[9] Peltier, J. C. A. Ann. Chem. Phys. 1834, 56, 371.
[10] Rowe, D.M. Handbook of thermoelectrics, CRC Press Inc., 1995.
[11] Goldsmith, H.J. Electronic refrigeneration, Pion Ltd, London, 1986.
[12] Tiwari, A.; Fontaine, J-P. Water, Air, & Soil Pollution: Focus, 2009, 9, No. 5-6, 539-547.
[13] Tiwari, A.; Fontaine, J-P., Lafon, P.; Kondjoyan, A. 40th ICES -2010, Bercelona, Spain, (AIAA2010-6171).
[14] Kondjoyan, A.; Peneau, F.; Boisson, H-C. Int. J. Therm. Sci. 2002, 41, 1-16.
[15] Bird, R.B.; Stewart W.E.; Lightfoot, E.N. Transport Phenomena, John-Wiley & Sons Inc., NY, USA, 2002.
[16] Beysens, D. Atmospheric Research 1995, 39, 215-237.
[17] Beysens, D. C R Physique 2006, 7, 1082-1100.

[18] Hirschfelder, J.O.; Curtis, C.F.; Bird, R.B. Molecular theory of gases and liquids, John Wiley and Sons, 1952, pp. 441-610.
[19] Asano, K. Mass Transfer- from fundamentals to modern industrial applications, Wiley-VCH, Verlag GmbH & Co. KGaA, Weinheim, 2006, chapter 3.

Experimental modelling for the Prediction of Heat and Mass Transfer in an Air-Conditioned Space Environment for Life Support Systems

Akhilesh Tiwari[1], Jean-Pierre Fontaine[2] and Pascal Lafon[3]
Clermont Université, Université Blaise Pascal, Laboratoire de Génie Chimique et Biochimique (LGCB), BP10488, F-63000, Clermont Ferrand, France.

and

Alain Kondjoyan[4]
Institut National de la recherché Agronomie (INRA), UR Qualité des Produits Animaux, F-63122, Saint Genès Champanelle, France

For the success of long-term space flights, and the establishment of permanent bases in space, a well controlled self sustained environment is required. In order to optimize a closed-loop bio-regenerative life support system, it is necessary to control the hydrodynamics and the coupled heat and mass transfer, which develops in a space habitat concerned with humans and plants. Thus, we have proposed an experimental set up that can gives us accurate predictions of heat and mass transfer at interfaces. We intend to introduce later on the measured heat and mass transfer coefficients in a global theoretical model. More precisely, this study focuses on the condensation phenomena of humid air on specific and simple geometries. For that purpose we induce condensation on an active surface maintained isothermal, and measure the mass transfer. The experiments were carried out in a wind tunnel, where a low turbulent flow develops and the temperature and hygrometric distributions are also well controlled. We have already studied the velocity profiles on vertical and horizontal flat plates with and without condensation. Velocity profiles within the boundary layer have already been discussed in dry conditions.

Nomenclature

T	=	temperature, K
L	=	characteristic length of the plate, m
C_p	=	specific heat capacity, $J.kg^{-1}.K^{-1}$
h	=	heat transfer coefficient, $J.m^{-2}.K^{-1}.s^{-1}$
N	=	mass flux, $Kg.m^{-2}.s^{-1}$
D	=	binary diffusion coefficient at interface $m^2.s^{-1}$
Tu	=	turbulence intensity of air, %
U	=	mean air velocity in the free stream, $m.s^{-1}$
u	=	velocity fluctuations around U in the main flow direction, $m.s^{-1}$
T_c	=	temperature constraint set on controller, °C

Dimensionless quantity

Sh	=	Sherwood number
Re	=	Reynolds number

[1]Research Scholar, Laboratoire de Génie Chimique et Biochimique, akhilesh.tiwari77@gmail.com
[2]Professor & Head, Génie Physique, J-Pierre.FONTAINE@univ-bpclermont.fr
[3]Research Scientist, Institut National de la Recherche Agronomique (INRA), alain.kondjoyan@clermont.inra.fr
[4]PREN, lafon@polytech.univ-bpclermont.fr

Pending final paper processing, any questions regarding copyright status and permission to reprint or reuse this paper must be directed to AIAA.

Sc = Schmidt number

Greek

ρ = density, $kg.m^{-3}$
μ = dynamic viscosity, Pa.s
ω = mass fraction of water vapour in air
Δ = difference
ν = kinematic viscosity, $m^2.s^{-1}$
δ = boundary Layer thickness, m

Subscripts

∞ = value at ambient temperature or free flow temperature
wv = water vapour
s = surface or interface of air and flat plate
d = dewpoint

I. Introduction

THE classical analysis of laminar film condensation on a vertical or inclined surface was first performed by Nusselt [1]. In that analysis Nusselt made four major assumptions and predicted the heat transfer coefficient. Then the problem of laminar film condensation has been studied by any authors like Rohsenow [2], Chen [3], and Denny and Mills [4] etc. and a variety of theoretical expressions and correlations of experimental data have been given in the literature for isolated vertical and horizontal surfaces. Some researchers have extended the analysis by removing the restricted assumptions [2-6]. The earliest attempt to consider the condensation heat transfer rate on a horizontal surface was experimentally done by Popov [7]. Gerstmann and Griffith [8] then investigated the condensation on the underside of a horizontal plate both theoretically and experimentally. The case of the upper side condensation of a horizontal plate was first studied by Leppert and Nimmo [9] and Nimmo and Leppert [10]. The film condensation thickness at the plate edge is either assumed or specified by the particular boundary condition. Shigechi *et al*. [11] obtained the condensate thickness and heat transfer results on a horizontal plate by adjusting the inclined angle of the vapour-liquid interface at the plate edge. Yang and Chen [12] used the concept of minimum mechanical energy [13] to search the boundary condition at the edge of the horizontal plate. Yang et al. [14] considered the condensation on a finite-size horizontal wavy disk and on a plate facing upward based on the Bakhmeteff's [13] assumption used by, which is the minimum mechanical energy with respect to the boundary layer thickness at the edge of the plate.

The condensate film characteristics depend on its flow field and the nature of the condensing surface, e.g. roughness, wetting, and orientation. The surface finish has a major effect on the mode of condensation for a downward facing surface and it is the wetting characteristics of the surface that ultimately determine this. Dropwise condensation (DWC) is likely to exist on non-wetting surfaces and filmwise condensation (FWC) is likely on wetting surfaces. In dropwise condensation mode with polished metal surfaces, the heat transfer characteristics are likely to change with time due to the oxidation of the surface or tarnishing. Thus, one cannot precisely know the wetting characteristics as surface aging occur. Filmwise condensation is currently used by industry while dropwise condensation is an alternative that is under development [15].

Schmidt [16] reported that heat transfer coefficients in DWC are significantly larger than in FWC. In film condensation, the surface is blanketed by a liquid film of increasing thickness that serves as a resistance to heat transfer. The heat of vaporization released, as the vapour condenses, must diffuse through this resistance before it can reach the solid surface and be transferred to the medium on the other side. In DWC, part of the surface is in contact with vapour leading to higher heat transfer rates. In attempting to predict or correlate heat transfer rates with DWC on solid surfaces or in evaluating experimental results, a number of possible complicating factors should be taken into consideration: the effects of non-condensable gases, promoter surface thermal properties and droplet removal mechanism. Since, the discovery of the advantages of DWC, many trials have been made to induce this form of condensation on metallic surfaces, but up to now none of the methods could be established in real technical applications because in most cases long term stability over several years cannot be obtained [17-18].

However, even if condensation has been extensively studied, today's knowledge lacks accurate data for gas/liquid mass transfer on solid walls as most of the studies have focused on heat transfer coefficients only. The mass transfer coefficients were deduced by a heat-mass transfer analogy. Our objective is to determine the mass

transfer coefficients related to simple geometries in order to develop a theoretical model that could be implemented in a computational fluid dynamics later on.

We have investigated velocity profiles in a wind tunnel and the boundary layer thickness on the surface of a horizontal flat plate in dry conditions. In humid air, we performed experiments of condensation on the surface of a horizontal flat plate to study the mass transfer coefficients. The final goal is to measure the local mass transfer coefficients on horizontal or vertical flat plate. We describe herein the experimental apparatus, procedure and then the data reduction methods are discussed. The results from the temperature distributions on the surface of a flat aluminium plate and the overall mass of condensate collected are then shown and discussed.

II. Experimental Material and Methods for Mass Flux Measurements

To generate and control the mass flux of humid air that condenses on the surface of a flat plate, we have developed a system based on a controlled thermoelectric cooler. The temperature of the plate is kept constant in order to induce a steady flow of condensation on the plate/air interface, and the produced condensate is regularly monitored by weighing the whole system. The system consists of square shaped Peltier modules sandwiched between a square shaped aluminium flat plate and a heat exchanger device, in addition to a temperature regulator with the power supply of thermoelectric Peltier module. The overall arrangement is placed on a weighing balance to measure the weight of condensate collected. The experiments were carried out in a laboratory room inside the building, where the local hygrometric parameters were varying according to the inside weather conditions. The condensation experiments were performed in the months of August and September, when the average humidity inside the room was approximately 35-50% and ambient temperature 20-30°C. The variation in relative humidity and ambient temperature during the time of the experiment was 10-15%.

A. Measurement of Wind Velocity, Humidity and Temperature

The characterization of the flow, mean flow velocity and fluctuations, were carried out by a constant temperature hot wire anemometer. For wind velocity measurement we have used two channel current/voltage sensor and temperature sensor (Testo 175 S2). The relative humidity and ambient temperature were measured using Testo-175 H2 two channel humidity and temperature sensor.

B. Condensation Unit

The temperature of the active surface is controlled by a Peltier element and a temperature sensor (thermistor or platinum sensor), which is itself inserted inside the aluminium flat plate (middle) for the regulation of the input current of the Peltier element adapted by the controller (LFI – 3751, Wavelength Electronics), as sketched on Figure 1.

A square polished aluminium flat plate (2) was glued on a Peltier module (3) of the same size, with a thermal adhesive, loaded with micronized silver (Arctic Silver – Premium Silver) thermal adhesive. Preliminary tests were carried out by pasting aluminium flat plates with a thermal paste. The other side of the Peltier module was pasted on a heat sink (4). This heat sink, made up of single-piece extruded aluminium, had a strong density of wings aligned with the direction of the flow to reinforce the convective exchange. To increase the effectiveness of the Peltier module, the use of a heat sink on the hot side of the Peltier plate is a key parameter. The objective is to dissipate the heat flux produced on the "hot" side of the Peltier element in order to maintain this side at a temperature as close as the ambient temperature T_a, which can be used as a reference temperature. The value of the electric current in a Peltier module theoretically makes it possible to create an absorption of heat on one side ("cold") and an equivalent heat emission on the opposite side ("hot"). By keeping this surface at room temperature, which is the reference temperature, it is possible to create the necessary temperature difference with the dew point T_d in order to induce the desired rate of condensation on the cold surface temperature T_c. Indeed, the rate of condensation is directly related to this difference in temperature $\Delta T_c = T_d - T_c$.

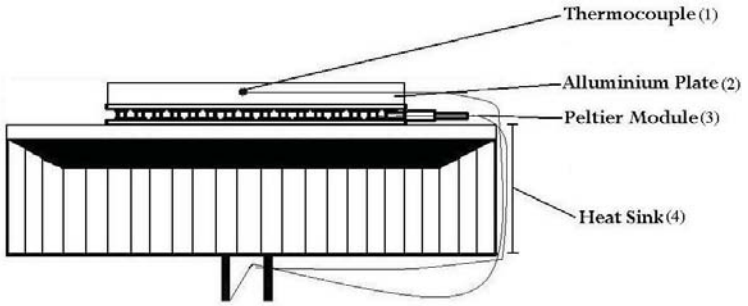

Figure 1. Schematic side view of the condensation unit, which faces the airflow.

In order to control this rate of condensation, we need, on the one hand, to maintain this temperature contrast constant $\Delta T_c = T_d - T_c$ throughout the experiment. For this purpose, a thermistor of small size (1) is inserted in the plate to measure the temperature in its centre under the plate/air interface (approximately 0.5 mm below the surface), it is connected to the temperature regulation controller, which adjusts the electric current transmitted to the Peltier module to maintain T_s constant. In addition, to obtain a uniform mass flux on the whole surface for a precise measurement of the mass flux, we must maintain the temperature of the active surface (plate/air) as isothermal as possible. Aluminium plates of strong thermal conductivity of 3 mm thickness were studied. We have already tested 1 mm and 2 mm thickness aluminium plates but the homogeneity in the 3 mm thick plate was better than in the others. The thickness of the aluminium plates act like a thermal buffer and induces a more homogeneous thermal distribution on the plate/air interface, than the one produced at the ceramic Peltier module side (variations of several degrees Celsius for a 5 cm x 5 cm plate).

A programmable temperature regulation controller (LFI-3751 of Wavelength Electronics) for the Peltier module was chosen for its stability over time and accuracy (± 0.1°C).

The main goal of this study is to evaluate the local mass transfer coefficients. Thus, we must study active surfaces of small sizes, but which are however sufficiently large to condense a quantity of water that can be weighted with precision. Plates measuring 3 cm x 3 cm, 4 cm x 4 cm and 5 cm x 5 cm were considered.

A Peltier Element is typically used to get a low or high temperature with a very fast response time, and a good temperature control with a solid state heating and cooling having no associated liquids only by using current. It consists of a number of small thermoelectric elements connected electrically in series. Typical commercially available thermoelectric elements are made by P-type and N-type bismuth telluride (Bi_2Te_3) alloy semiconductors. A few hundred small Bi_2Te_3 blocks are sand-witched between two ceramic plates. The working principle of these thermoelectric devices is well described by Kraftmakher [19].

In this study, three different sized Peltier elements were used, which have a different number of thermocouples. (See table 1)

Table 1.

Peltier Elements used in this experiment:

Peltier element	supplier	no of thermocouples	Dimensions (mm x mm x mm)
1. TB-127-2.0-2.5	Kryotherm (Russia)	127	48 x 48 x 4.8
2. ICE-71	Kryotherm (Russia)	71	40 x 40 x 3.4
3. Snowball – 71	Kryotherm (Russia)	71	30 x 30 x 3.6

C. Weighing

The condensation unit was placed horizontally, with its active surface upside in the centre of the pan of the weighing balance. The wires of the Peltier module and the thermistor inserted in the active plate (1) walked along the same plane on a solid base and were connected to the temperature controller. The balance was placed on a solid platform. The portable balance allowed a continuous display of weight recorded (Ohaus Navigator Balance N24120, precision of ±0.01 g), for monitoring the increase in mass as the humid air will condense on the active surface.

III. Experimental Set-up for Velocity Measurements

For boundary layer velocity measurements a closed circuit wind tunnel was used, its installation was 12 m long and 4 m high as given in figure 2(a), which has already been described in detail [20]. The wind velocity inside the tunnel varies from almost laminar to very turbulent flows. The test chamber measured 0.8 m x 0.8 m with a length in the flow direction of 1.50 m. A three-axis traversing system enabled the displacement of a probe within the test chamber. The mean flow velocity and fluctuations were measured using a constant temperature hot wire anemometer (5 µm in diameter and l.25 mm in length). The sample frequency was chosen between 0.5 kHz and 2 kHz. Calibration of each wire probe with air temperature enabled mean velocity measurements to be made with an accuracy of l-3% in the range of 0.4-5.0 $m.s^{-1}$. Below 0.4 $m.s^{-1}$ hot wire measurements lack accuracy because of thermal exchange. In the clear test chamber the mean velocity at any point within the chamber was differed by less

than 0.5% from its average value over the entire chamber. The turbulence intensity was less than 1.3% and uniform in a part of the test chamber large enough to contain the sample.

A horizontal square flat plate was located inside the test chamber of the wind tunnel and subjected to air flows of different mean velocities. . It was a well polished square shaped flat plate of aluminium held in position by cylindrical rod glued perpendicularly on its back. The surface area of the plate was 5 cm x 5 cm and 3 mm thick as shown in figure 2(b). It was located in the centre of the test chamber i.e., 40 cm above the base of the tunnel, 40 cm down from the upper surface of the tunnel, and 74 cm downstream from its start.

The measurements were performed using an "offset" prong probe (DANTEC, 55P15). Repeated calibrations of the response of the hot wire system with respect to air temperature ensured that the absolute error on the velocity measurements was less than ±0.1 m.s^{-1}. The turbulence intensity (*Tu*) and the free stream flow were determined $Tu = \sqrt{\overline{u}^2}/U$. On the flat plate we have taken 25 points as shown in the top view of the flat plate in figure 2(b). The Z was fixed and then the probe was conveyed at 0.01 m towards Y, and at a given distance X of 0.01, 0.025, 0.04 or 0.05 m from the leading edge of the plate. A telescope (×24) was used to accurately locate the point of contact (the error of this visual observation through the magnifying glass was +/−0.05 mm). From this point upward the air velocity and fluctuation in the main flow direction were measured at 3 mm and until the frontier of the boundary layer was reached (average velocity value became constant).

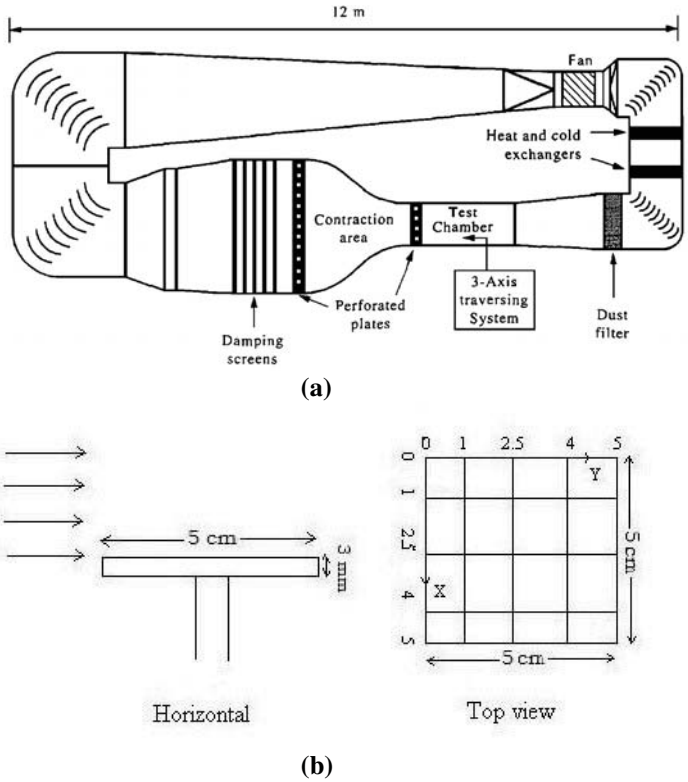

Figure 2. a) Schematic representation of the wind tunnel b) position and flow profile of flat plate

IV. Results and Discussions

A. Velocity measurements

The mean velocity measurements have been performed at 1 mm and 3 mm above the plate surface. The surface plots of the velocity profile are given for the flat plate in horizontal position in figure 3(a, b) and the turbulence intensity is given for the same positions in figure 3(c, d). The experiments were performed for a mean entrance velocity of 0.5, 1.1, 1.5, and 2.0 m.s^{-1} and the wind velocity as well as the turbulence intensity was measured and here we have given the data only for 1.1 m/s mean velocity and its turbulence intensity. It is observed from the figure 3(a, b) that, on moving from the surface of the flat plate to free stream velocity, the fluctuations in the velocity decrease and the shape of the velocity profile is almost conical, and centred towards the middle to back part of the flat plate. It is also observed in figure 3(c, d), that the maximum turbulence intensity at 1 mm above the surface of the plate reaches 10-15%, and at 3 mm above the surface drops to 8-10% and at the same time the turbulence intensity at the entrance of the tunnel was 1.7% for both cases. We have tested the readings for a height of 5 mm and little more above the surface of the plate; the turbulence intensity at 5 mm started decreasing and then suddenly reached the range of the turbulence intensity measured at the entrance of the tunnel, which shows that the probe was outside the boundary layer. We have calculated the boundary layer thickness using Blasius' solution ($\delta \cong 4.5\sqrt{\upsilon L/U}$), and obtained results close to the ones observed experimentally (3-9%). The plot is given in the figure 5(b) for comparison with the Blasius' solution.

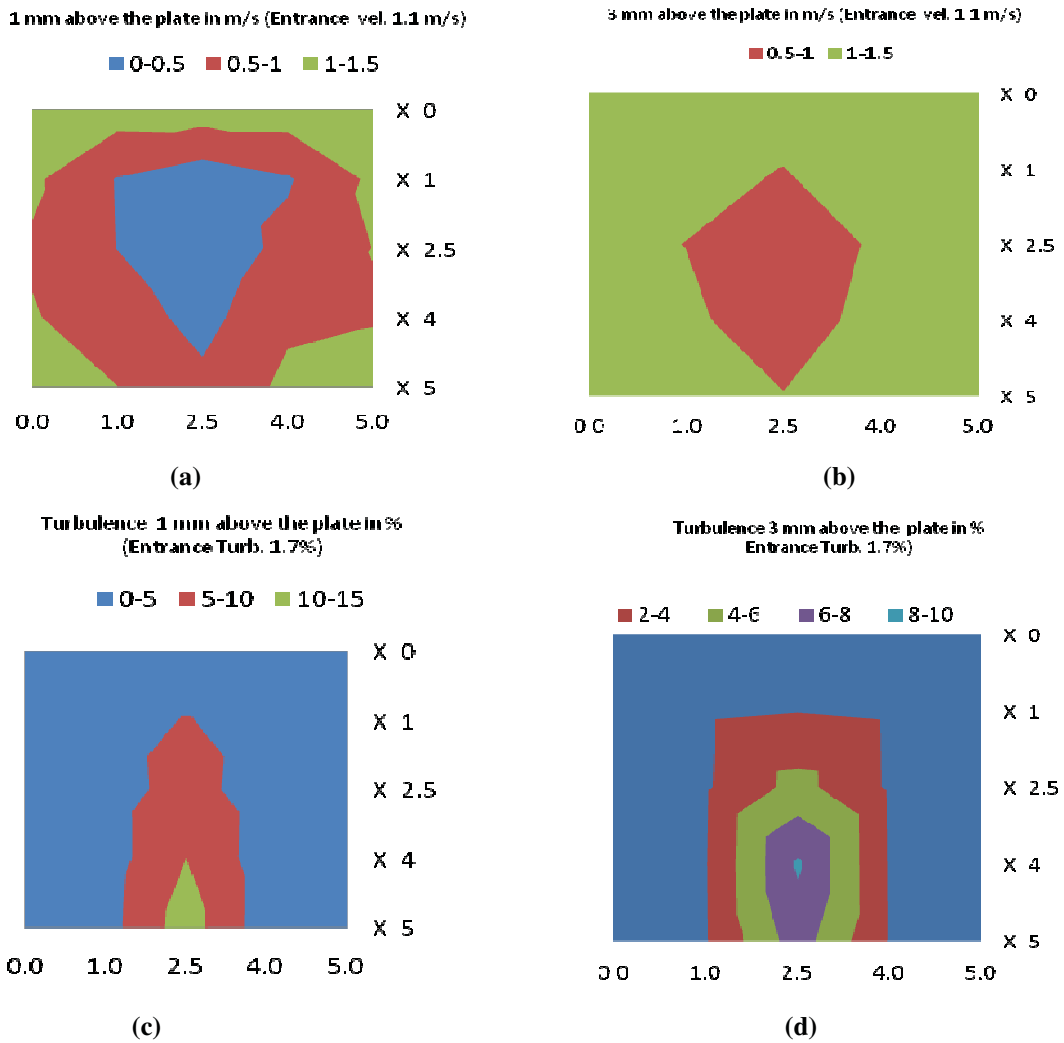

Figure 3. (a-d) Comparative surface plots for the flat plate in horizontal position (a-b) velocity profiles in metre per second for ambient temperature 21.8°C and (c-d) turbulence intensity in per cent.

B. Condensation Measurements

We tested our set-up in a closed room in which the hygrometric and hydrodynamic parameters varied according to the inside ambient conditions, except for a fan which was used to produce the air turbulence on the flat plate. An air flow of about 1 m/s was generated on the active surface by a very small fan of 12 V power supply. The average air velocity was almost constant during all the experiments. More than 15 experiments were carried out on three different sizes of the plates. Each experiment was carried out in different ambient air conditions.

Preliminary experiments in the air have shown that the top surface temperature was more or less homogeneous (variation below 1°C for a 3 mm thick plate of 5 cm x 5 cm). The variation in temperature on active surface was higher for thinner plates. The local temperature distribution measured at 25 equidistant points on the surface of 5 cm x 5 cm and 4 cm x 4 cm plates, and at 17 points on the 3 cm x 3 cm. The same local temperature distribution measurements were also performed on the ceramic surface of the Peltier element (without the aluminium plate), the temperature difference was found to be more than 1.5 °C higher for the 5 cm x 5 cm plate. The temperature on the ceramic surface of the Peltier or on the plate was minimum at the centre and maximum at the boundaries.

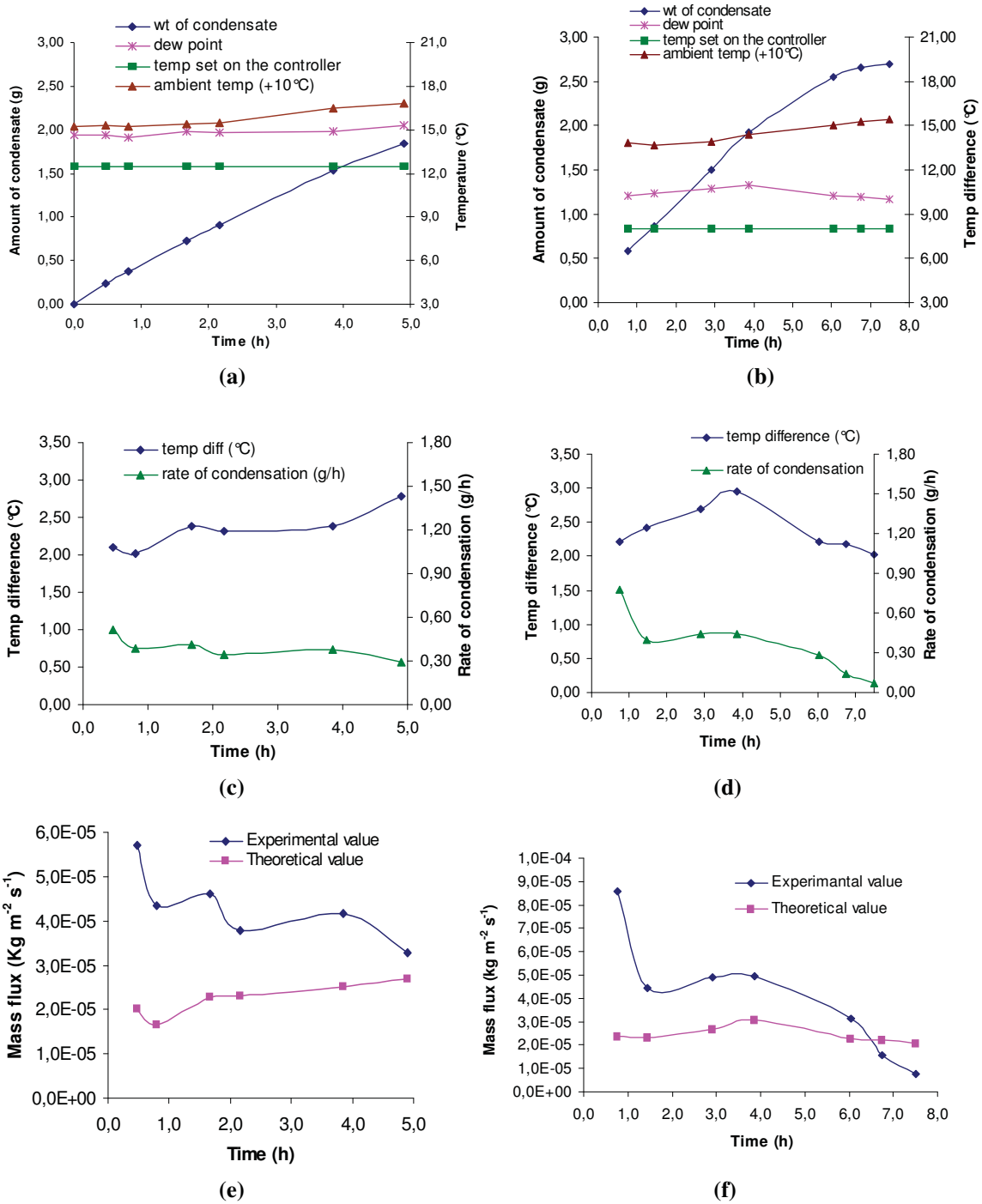

Figure 4. a-b) Amount of condensate and temperature as a function of time. The value of ambient temperature is also given in the graph after reducing 10°C to fit in scale. c-d) The temperature difference and rate of condensate as a function of total time. e-f) Mass flux as a function of time, the experimental values are compared with calculated ones.

The plots of condensation profiles for two experiments performed on different days are given in figure 4 (a, c, e) and 4 (b, d, f) and their comparison with theoretical calculations including some other experiments as figure 5(a). These results were obtained on the horizontal aluminium surface of 5 cm x 5 cm. The Reynolds number (Re) was in

the range of 3800 – 4000 and the Schmidt number was 0.6. These experiments were performed for temperature differences, ΔT_c (between the temperature set on the controller and the dewpoint) ranging from 1.50 °C to 4.5 °C. The relative humidity and ambient temperature varied from 2 to 15% inside the building according to the local weather conditions during day time, sometimes both data increased or decreased simultaneously, other times one increased and the other decreased, which varied the dewpoint temperature from 0 to 3°C up or down. However, it was important to maintain the temperature of the active surface sufficiently below the dewpoint for the condensation of water vapour in air to proceed. This was done with the help of the temperature regulation controller.

It is observed from figure 4 (a) that the temperature difference ΔT_c varied from 2.1°C to 2.8°C. The ambient temperature increased by 6% and the relative humidity decreased by almost 6% during the 5 h experiment, which provided an increment in the initial dewpoint of about 0.7 °C. The amount of condensate collected during this time was 1.84 g with an average rate of condensation of 0.38 $g.h^{-1}$. Figure 4(b) shows a similar experiment, In which temperature difference ΔT_c first went up almost 0.7°C and then decreased 0.9°C, because the ambient temperature went up 6%, but the relative humidity slightly went up and then down and the variation was almost 10%. The dewpoint increased for about 4 h and then decreased, but the difference ranged between 2°C and 3°C during the 7.5 h of experiment, which resulted in a collection of 2.7 g of condensate.

Figure 4 (c, d) shows the rate of condensation and temperature difference as a function of the total time of the experiments. Figure 4(c) shows that the rate of condensation follows the trend of the temperature difference except after 4 h, where the measured condensation rate decreases the rate even if the temperature difference increases. figure 4(d) shows a similar tendency maintained after 1.5 h. As the temperature difference starts decreasing, the condensation rate decreased significantly, because of reasons, low temperature difference and very low active surface area on the surface of the plate.

The figures 4(e, f) give here shows the variation of the theoretical and experimental values of mass flux with total time of experiment. The theoretical values were calculated here by using the binary diffusion coefficient of water vapour in air from the kinetic theory of gases [21]. The mass flux of water vapour in air was calculated by using the formula [22]

$$N_{WV} = \frac{Sh\rho_s D(\omega_\infty - \omega_s)}{L(1-\omega_s)} \tag{1}$$

Where the Sherwood number is computed from: $Sh(1-\omega_s) = 0.664\,\mathrm{Re}^{\frac{1}{2}}\,Sc^{\frac{1}{3}}$, where the Reynolds number $\mathrm{Re} = (\rho_\infty vL)/\mu_\infty$ and Schmidt number $Sc = \mu_\infty/(\rho_s D)$ are standard dimensionless numbers.

From the observation of figures 4(e, f), we can say that the mass flux tend to decrease with time. In the first hour of the experiment it went down sharply, and then as decreased gradually. Its worth noting that the mass flux is proportional to the active surface and that this area decreases with time as condensation develops – Thus, a sharp decrease is obtained at the early stage of the experiment. Moreover, some evaporation takes place at the water / air interface. The theoretical value of the mass flux is almost constant during the whole experiment because the effect of the condensate collected on the surface was not considered in the theory.

Figure 5(a) shows the variation of the amount of condensate versus time for several average temperature differences ΔT_c. The trends are affected by the hygrometric ambient conditions, which are not completely stable as we did not perform the experiments in air-conditioned environments. However, the main behaviour indicates the sensitivity of the slope and of thus the mass flux to the temperature difference as expected. The evaluation in time is also influenced by the active area which decreases with time as condensation covers the flat plate. After 3 hours half of the plate is covered by water for $\Delta T_c = (2.7 \pm 0.8)$ °C and after long duration we can observe some type of saturation as most of the plate surface is covered with water.

V. Conclusion

We have proved the concept based on thermoelectric cooling and weighing to study mass transfer that occurs during condensation experiments is valid. To be more accurate the results need to be obtained in an environment in which the temperature and the humidity levels are controlled. Thus we have performed experiments in a closed wind tunnel, in which, it is possible to control the psychometric parameters (relative humidity, temperature) and to generate almost laminar to turbulent flows. In dry conditions we have determined the velocity profile above a flat horizontal plate and estimated the boundary layer thickness. The results fit with the Blasius' solutions. Experiments in the wind tunnel in humid air are ongoing. The results will allow in developing a theoretical model for the mass

transfer flux of condensation. Here we have performed experiments further to do it in wet conditions by condensation on the surface of the plate inside building environment and further we will do it in closed environment of wind tunnel, where hygrometric parameters will be fully controlled. The dependence of mass flux on the temperature difference and other parameters will helpful to characterize the theoretical model.

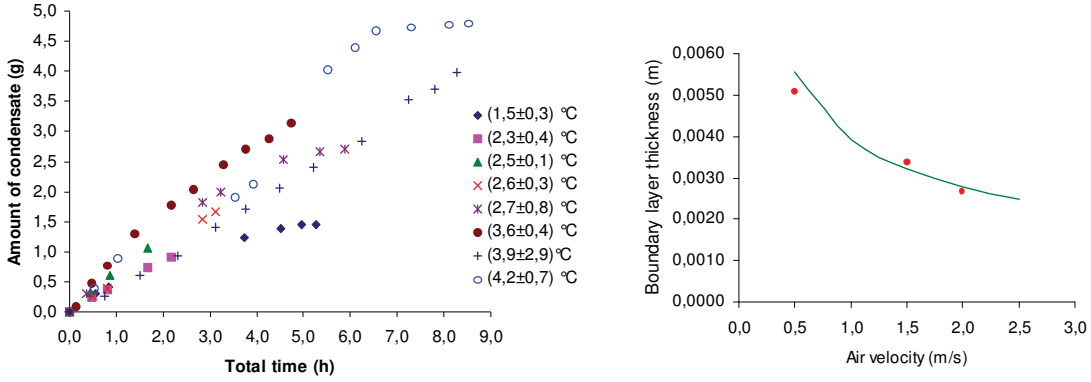

(a) **(b)**

Figure 5. (a) Amount of condensate as a function of total time of experiment for 8 experiments (b) Comparative plot of boundary layer thickness calculated by using Blasius solution (*continuous line*) and (*observed experimentally*) on a plate of surface area 5 cm x 5 cm.

Acknowledgments

The authors (A.T. and J.P.F.) thank Prof. Jean Bernard Gros, LGCB for fruitful discussions and also to the Centre National d'Etudes Spatiales (CNES), France for providing financial support.

References

[1]Nusselt, W., "Die Oberflachen Kondensation des Wasserdampes," *Zeitsehrift des Vereines DeutscherIngenieure*, Vol. 60, No. 2, 1916, pp.541-546.

[2]Rohsenow, W.M., "Heat Transfer and Temperature Distribution in Laminar Film Condensation," *J. Heat Trans-T. ASME*, Vol. 78, 1956, pp.1645-1648.

[3]Chen, M.M., "An Analytical Study of Laminar Film Condensation: Part 1-Flat Plates," *J. Heat Trans.*, Vol. 83, 1961, pp.48-54.

[4] Denny, V.E., Mills, A.F., "Non-similar solutions for laminar film condensation on a vertical surface", *Int. J. Heat Mass Trans,* Vol. 12, 1969, pp.965–979.

[5]Koh, J.C.Y., "On Integral of Treatment of Two Phase Boundary Layer in Flim Condensation," *J. Heat Transf.*, Vol. 83, 1961, pp.359-362.

[6]Koh, J.C.Y., Sparrow, E.M., and Hartnett, J.P., "The Two Phase Boundary Layer in Laminar Film Condensation," *Int. J. Heat Mass. Tran.*, Vol. 2, 1961, pp.69-82.

[7]Popov, V.D., "Heat Transfer during Vapour Condensation on a Horizontal Surfaces," *Trudy Kiev. Teknol. Inst.Pishch, Prom.* Vol. 11, No. 1, 1951, pp.87-97.

[8]Gerstmann, J. and Griffith, P., "Laminar Film Condensation on the Underside of Horizontal and Inclined Surfaces," *Int. J. Heat Mass Tran.*, Vol. 10, No. 2, 1976, pp.567-580.

[9]Leppert, G. and Nimmo, B., "Laminar Film Condensation on Surface Normal to Body or Inertial Forces," *J. Heat Tran.*, Vol. 80, No. 1, 1968, pp. 178 -179.

[10]Nimmo, B. and Leppert, G., "Laminar Film Condensation on a Finite Horizontal Surface," *Proceedings of 4th International Heat Transfer Conference*, 1970, pp. 402-403.

[11]Shigechi, T., Kawae, N., Tokita, Y., and Yamada, T., "Film Condensation Heat Transfer on a Finite-Size Horizontal Plate Facing Upward," *JSME Series B*, Vol.56, No. 1, pp. 205-210 (1990).

[12]Yang, S.A. and Chen, C.K., "Laminar Film Condensation on A Finite-Size Horizontal Plate with Suction at Wall," *Appl. Math. Model.,* Vol. 16, No. 1, 1992, pp.325-329.

[13]Bakhmeteff, B.K., *Hydraulics of Open Channel*, McGraw-Hill, New York, 1966, pp.39- 41.

[14]Yang, Y.T., Chen, C.K., Hsu, P.T., "Laminar film condensation on a finite size horizontal wavy disk", *Appl. Math. Modelling,* Vol. 21, 1997, pp.139–144.

[15] Pang G., Dale, J. D., Kwok, D. Y., "An integrated study of dropwise condensation heat transfer on self-assembled organic surfaces through Fourier transform infra-red spectroscopy and ellipsometry", *Int. J Heat Mass Transfer* Vol.48, 2005, p307.
[16] Schmidt, E., Schurig, W., Sellschopp, W., Versuche u¨ber die Kondensation von Wasserdampf in Film- und Tropfenform, *Tech. Mech. Thermodyn*., Vol. 1(2), 1930, p53.
[17] Rausch, M H., Froba, A.P., Leipertz, A., Dropwise condensation heat transfer on ion implanted aluminium surfaces, *Int. J. Heat Mass Transfer* Vol. 51, 2008, p1061.
[18]Tiwari, Akhilesh, and Fontaine, Jean-Pierre "Towards the prediction of heat & mass transfer in an air-conditioned environment for a life support system in space", *Water, Air, & Soil Pollution: Focus*, Vol. 9, No. 5-6, Dec. 2009, pp.539-547.
[19]Kraftmakher, Y., "Simple experiments with a thermoelectric module" *Eur. J. Phys.* Vol. 26, 2005, pp.959-967.
[20]A. Kondjoyan, J.D. Daudin, Heat and mass transfer coefficients at the surface of a pork hindquarter, *J. Food Eng*. Vol. 32, 1997, p.225.
[21]Hirschfelder J.O., Curtis C.F. and Bird R.B., *Molecular theory of gases and liquids*, John Wiley and Sons, 1952, pp. 441-610.
[22]Asano K., *Mass Transfer- from fundamentals to modern industrial applications,* Wiley-VCH, Verlag GmbH & Co. KGaA, Weinheim, 2006, chapter 3.

Water Air Soil Pollut: Focus (2009) 9:539–547
DOI 10.1007/s11267-009-9232-z

Towards the Prediction of Heat and Mass Transfer in an Air-Conditioned Environment for a Life Support System in Space

Akhilesh Tiwari · Jean-Pierre Fontaine

Received: 7 April 2009 / Revised: 5 July 2009 / Accepted: 2 September 2009 / Published online: 10 November 2009
© Springer Science + Business Media B.V. 2009

Abstract Long-term flights or the establishment of permanent bases in space provide serious challenges for life support systems. Plants are essential companion life forms for such space missions, where human habitats must mimic the cycles of life on earth to generate and recycle food, oxygen and water. Nowadays, the chemical–mechanical recycling systems used in the international space station are much more compact, less labour intensive and more reliable than plant-based systems, but these systems would be too expensive for the long-term human exploration. In order to improve living conditions for humans and plants, we need an accurate characterisation of the mass transfer phenomena related to condensation of humid air. We are interested in developing an experimental protocol, which would help us to establish a theoretical model describing the heterogeneous transfers along a wall or a plant in an air-conditioned environment. Initially, we started in dry conditions by measuring the velocity profiles within the boundary layer that develop on a horizontal or a vertical flat plate in a wind tunnel. The velocity ranged from 0.5 to 2.5 m s^{-1}. Existing coupled heat and mass transfer measurement results relevant to our applications are discussed.

A. Tiwari (✉) · J.-P. Fontaine
Laboratoire de Génie Chimique et Biochimique,
Université Blaise Pascal,
Polytech'Clermont-Ferrand, BP 206, CUST,
24 avenue des Landais,
63174 Aubiere, France
e-mail: akhilesh.tiwari77@gmail.com

Keywords Heat and mass transfer · Low Re convective flows · Velocity measurement

1 Introduction

The basic research on regenerative systems and understanding how to merge them require researchers to concentrate on both the biotechnological and the physicochemical processes that can be assimilated into a bioregenerative life support system (BLSS; Bartsev et al. 1997). After all, while plants could provide all the human necessities, realistic regenerative complexes will rely on machinery to regulate the system, supply the plants with nutrient solutions and process wastes. Hardware will also provide a backup in case the natural system should fail for any reason. The recycling of materials in these systems requires exchanges between photo-autotrophic organisms, which synthesise organic substances using solar or artificial light, and heterotrophic organisms, humans specifically, who consume the products of autotrophic synthesis. Hence, growing plants is an indispensable component of BLSS. The performance of BLSS for space missions will be principally dependent on the progress of space plant cultivation technology and the achievement of associated equipment. The vital element is a breathable atmosphere. A human in space, whether in a craft, station or suit, must have air. Choosing the composition of an artificial atmosphere, however, is difficult. Physiological, engineering, cost and safety factors must

be considered previously. A way of providing such living conditions in a confined environment is by using a well-controlled air-conditioned system.

Our main objectives are to study and control the ventilation of humid air inside an air-conditioned space environment for human life and the growth of higher plants. The other issues are quality and treatment of the air, control of condensation–evaporation phenomenon, characterisation of gas/plant transfer, hydrodynamics and concomitant heat and mass transfer and the influence on the growth of high plants. The related effects are health risks (nosocomial infections), mould, rot/corrosion, light transmission, etc. The water vapour condensation in such systems gives interaction between weakly turbulent air flows main stream velocities below 2 m s^{-1} and water vapour transfer at interfaces such as surface condensation.

Fundamental heat and mass transfer studies are needed to estimate the local heat and mass transfer coefficients. Very few experimental methodologies have been developed for the direct evaluation of convective mass transfer coefficients of air. An alternative method would be to conduct heat transfer experiments and use the heat and mass transfer analogy, such as the Chilton–Colburn analogy, to deduce mass transfer coefficients. However, the analogy requires that the Schmidt and Prandtl numbers be equal. One of the most popular mass transfer evaluation methods is the well-developed naphthalene sublimation technique (Goldstein and Cho 1995). The other one is the swollen polymer technique presented by Macleod and Todd (1973). The above techniques are complex to implement: the former relies on accurate values of the naphthalene properties whereas the latter on the properties of the swelling agent and on most of the chemical solvents used whose volatility changes with the change in temperature.

We are interested in measuring the mass transfer coefficients for the condensation of air on a flat plate. Our goal is then to define a theoretical model for the numerical simulation of the atmosphere of a space habitation including the condensation phenomena. At first, the measurements will be performed in a well-controlled wind tunnel. For the validation of our velocity measurement technique, we performed experiments in dry conditions near the surface of a polished flat plate kept in different positions, to determine the velocity profile and turbulence intensity near the surface of the flat plate for low Reynolds number ($1{,}600 \leq Re \leq 8{,}200$) flows. The results are needed to validate the low Re turbulent model used in the computational fluid dynamics (CFD) approach. In the present study, we also discuss key heat and mass transfer phenomena during condensation phases.

2 Existing Results on the Condensation of Air

Condensation results when the temperature is lowered below saturation values. In general, the tendency exists for condensation to occur when the partial pressure of a given component of a gaseous mixture at a given temperature exceeds the vapour pressure of the liquid form of that component at the given temperature. It can be considered as taking place either within the bulk material or on a cooled surface and is accompanied by simultaneous heat and mass transfer. Condensation is initiated by a nucleation process in a bulk vapour, and on a solid surface two kinds of mechanism have been proposed for the origin of the initial drops: (1) liquid fracture hypothesis and (2) surface nucleation hypothesis (Collier and Thome 1996). Although many experimental studies have been devoted to the origin of the mechanism of dropwise condensation (DWC), all of them have been performed with microscopy or a high-speed camera, which are limited to microscale above 100 nm. Recently, Tianquing et al. (2007) used an electron probe microanalyser to analyse the chemical composition of the magnesium surfaces. The hot condensate reacted with the magnesium to produce magnesium hydroxide. The average surface roughness was about 20 nm, as observed by atomic force microscope. The authors concluded that the distribution of sites where drops develop is not uniform and that the size of the initial condensate nuclei is in the range of 3–10 nm, which agree with thermodynamics for new phase formation.

The condensate film characteristics depend on its flow field and the nature of the condensing surface, e.g. roughness, wetting and orientation. The surface finish has a major effect on the mode of condensation for a downward-facing surface, and it is the wetting characteristics of the surface that ultimately determine this. DWC is likely to exist on non-wetting surfaces and filmwise condensation (FWC) is likely on wetting surfaces. In DWC mode with polished metal surfaces, the heat transfer characteristics are likely to change with time due to the oxidation of the surface or

tarnishing. Thus, one cannot precisely know the wetting characteristics as surface ageing occur. FWC is currently used by industry while DWC is an alternative that is under development (Guoxin Pang et al. 2005).

Condensation heat transfer is a vital process in the power generation industries as it is used to transfer a large quantity of heat. This paper focuses on the condensation of air on solid surfaces, with an emphasis on the evaluation of mass transfer.

2.1 Filmwise Condensation

Nusselt (1916) presented the first analytical solution for heat transfer on a plane surface during the FWC of a stationary saturated vapour with several assumptions (Collier and Thome 1996). Furthermore, many scientists solved this problem and included the effect of some of these assumptions (Poots and Miles 1967), such as effect of inertial forces, convection terms in liquid, momentum, interfacial shear forces and non-linear distribution of temperature. These results show that the interfacial shear stress can reduce heat transfer due to the effect of holdup of the condensate film for low values of Prandtl number ($Pr = \nu/\alpha = C_p\mu/k$), but this effect is small and steadily decreases with increasing Pr above unity. As a conclusion for pure steam-water condensation, Nusselt's assumptions can be accepted for a stationary vapour without non-condensable gas in practical engineering situations.

The buildup of non-condensable gas near the condensate film acts as a banner and inhibits the diffusion of the vapour from the bulk mixture to the liquid film and reduces the rate of heat, mass and energy transfer. The analysis by Sparrow and Lin (1964) indicate that the condensing rate is dependent on the bulk gas mass fraction and the vapour–gas mixture Schmidt number ($Sc=\upsilon/D=\mu/\rho D$). The numerical calculations show that the effect of the non-condensable gas increases with the increase of the Schmidt number.

Rose (1969) presented an approximate integral boundary layer solution to reduce the computation time, assuming uniform properties except for density in the buoyancy term like for the Boussinesq approximation. Plausible velocity and concentration profiles for the vapour–gas boundary layer were used, and it was assumed that these two layers had equal thickness. The results showed quite good agreement with those of Minkowycz and Sparrow (1966). To study the effect of moving vapour with a non-condensable gas, Sparrow et al. (1967) solved the conservation equations. The computed results reveal that interfacial resistance has a negligible effect on the heat transfer and that superheating has much less of an effect than in the corresponding free convection studies.

The experimental studies performed before mid-twentieth century for stationary pure vapour showed some difference (McAdams 1954) with the predictions of the Nusselt theory. The differences can be attributed to one or more of the following reasons: (1) significant forced-convection effects; (2) presence of non-condensable gas; (3) waviness and turbulence within the condensate film; and (4) presence of DWC. Mills and Seban (1967) condensed steam on a copper vertical flat plate. They supported the Nusselt theory for pure stationary vapour condensation.

The heat transfer coefficients have been observed to decrease significantly with increased non-condensable gas mass fraction under various conditions and test geometries. The degradation of heat transfer is caused by the accumulation of a non-condensable gas layer near the cold wall through which the vapour must diffuse. Othmer (1929) introduced air mole fraction below 7% and was the first to present definitive experiment on the effect of non-condensable gas on the rate of condensation of a vapour.

2.2 Dropwise Condensation

It is well known that if the condensate does not completely wet the solid surface, individual liquid droplets form instead of continuous condensate film. Schmidt et al. (1930) reported that heat transfer coefficients in DWC are significantly larger than in FWC. For the condensation of steam, the heat transfer coefficients measured in DWC have been a factor of 4 to 8 times larger (Collier and Thome 1996) than in FWC. In film condensation, the surface is blanketed by a liquid film of increasing thickness that serves as a resistance to heat transfer. The heat of vaporisation released, as the vapour condenses, must diffuse through this resistance before it can reach the solid surface and be transferred to the medium on the other side. In DWC, part of the surface is in contact with vapour, leading to higher heat transfer rates. In attempting to predict or correlate heat transfer rates

with DWC on solid surfaces or in evaluating experimental results, a number of possible complicating factors should be taken into consideration: the effects of non-condensable gases, promoter surface thermal properties and droplet removal mechanism. Since the discovery of the advantages of DWC, many trials have been made to induce this form of condensation on metallic surfaces, but up to now none of the methods could be established in real technical applications because in most cases long-term stability over several years cannot be obtained (Rausch et al. 2008).

Fatica and Katz (1949) were first to propose a model to compute the rate of heat transfer. In later attempts, different researchers have dealt with the problem of drop size distribution in a variety of ways. A detailed discussion and its theoretical and experimental developments were given by Rose (1994). The studies of different experimenters in different countries were in good agreement and indicated heat transfer coefficients for DWC of steam around ten and 20 times those for film condensation at power station condenser pressures and at atmospheric pressure, respectively. Moreover, the heat transfer coefficient was found to increase with increase in temperature difference or heat flux.

For producing DWC on metals, a reduction of their free energy in order to reduce wetting properties is necessary, which could either be obtained by applying hydrophobic layers of substances like organic and inorganic compounds, polymers, hard metal coatings or by the formation of surface alloys (Rausch et al. 2008).

The development of ultra-thin and stable coatings for DWC are still of interest to researchers. Ma et al. (2002) coated ultra-thin polymers that were created by plasma polymerization and dynamic ion beam mixed implantation method on vertical brass tubes for heat transfer experiments and studied the influence of processing conditions. The experimental results given by Vemuri and Kim (2006) using self-assembled monolayer technique for the coating of *n*-octadecyl mercaptan solution showed DWC for more than 2600 hours. These experiments indicated heat transfer enhancements up to 30 times higher than in film condensation.

The interest and the development of DWC waned following failures, despite the fact that many attempts have been made to find an industrially effective and reliable means of promoting DWC. However, Zhao et al. (1991) have given encouraging reports and proposed a means of process called "dynamic mixing magnetron sputtering/ion plating," which was successfully applied by using ion implantation of N, Ar, He, H and Cr in copper tubes. This technique has been successfully used in Dalian and Jilian power plants (Zhao and Wang 1993). A dropwise-promoted, vertical-tube condenser/feed heater has operated successfully since 1989 with an overall heat transfer coefficient of 6,000 W/m^2 K and with the same performance as a similar condenser operating under the same steam and coolant conditions and with twice the number of untreated tubes. Even if condensation of humid air has drown much attention, today's knowledge lack accurate data for gas/liquid transfer coefficients on solid walls (simple or complex shape), on plants or on human bodies.

3 Experimental Material and Methods

For boundary layer velocity measurements, a closed-circuit wind tunnel (Fig. 1) was used (Kondjoyan and Daudin 1997) to control the psychometric parameters such as relative humidity, ambient temperature and dew point. The wind velocity inside the tunnel varies from almost laminar to very turbulent flows. The contraction area ratio between the settling chamber and the test section was 9. The test chamber measured 0.8×0.8 m^2 with a length in the flow direction of 1.50 m. A three-axis traversing system enabled the displacement of a probe in an area of chosen dimension and location with a selected displacement step. The recording of the probe location and response was performed by a computer linked to the system. The mean flow velocity and fluctuations were measured using a constant temperature hot-wire anemometer. The hot-wire element was 5 μm in diameter and l.25 mm in length. The sample frequency was chosen between 0.5 and 2 kHz. Calibration of each wire probe with air temperature enabled mean velocity measurements to be made with an accuracy of l–3% in the range of 0.4–5.0 m s^{-1}. Below 0.4 m s^{-1}, hot-wire measurements lack accuracy because of thermal exchange. In the clear test chamber, the mean velocity at any point within the chamber was differed by less than 0.5% from its average value over the entire chamber. The turbulence intensity was less than 1.3% and uniform in a part of the test chamber large enough to contain the sample. Attention was paid to the

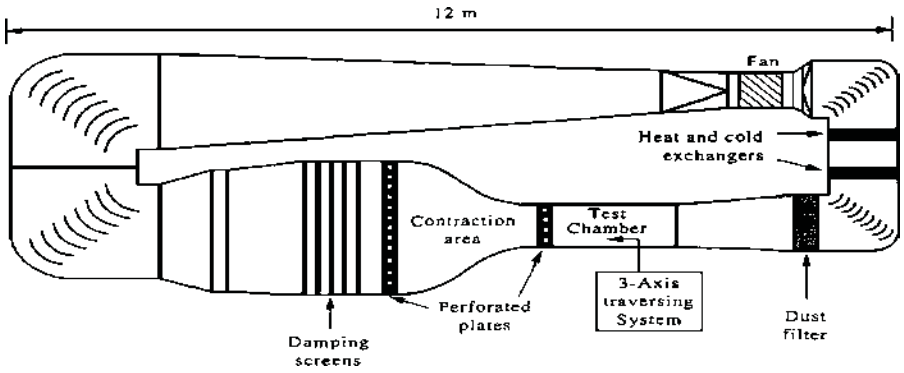

Fig. 1 Schematic representation of the wind tunnel

regulation of the air and dew point temperatures so that these values were maintained uniform across the experimental area in the range of ±0.l°C even when the flow was laminar.

A square flat plate was located inside the test chamber of the wind tunnel and subjected to air flows of different velocities. In a first set of experiments, the average velocity and fluctuated velocity profiles were measured in the boundary layer, which developed along the surface of the horizontal flat plate and parallel to the direction of air flow. In another set of experiments, the surface of the flat plate was taken as vertical and perpendicular to the direction of air flow.

The closed-loop wind tunnel installation was 12 m long and 4 m high as given in Fig. 1, which has already been described in detail (Kondjoyan and Daudin 1997). The flat plate used to study the velocity profile was 0.05 m long, 0.05 m wide and 0.003 m thick as shown in Fig. 2. It was located halfway up the test chamber, i.e., 0.40 m above the base of the tunnel, 0.40 m down from the upper surface of the tunnel and 0.74 m downstream from its start. It is a well-polished square-shaped flat plate of aluminium held in position by cylindrical rod glued perpendicularly on its back.

The hot-wire element was located between two prongs, which were themselves connected to a support. The measurements were performed using an "offset" prong probe (DANTEC, 55P15). Repeated calibrations of the response of the hot-wire system with respect to air temperature ensured that the absolute error on the velocity measurements was less than ±0.1 m s^{-1}. The measurement of a velocity profile began by choosing the frequency of the fan, which fixed the fan speed to reach an average air velocity of about 0.5 m s^{-1} inside the test chamber (this air velocity was measured accurately afterwards). The turbulence intensity (Tu) and the free stream flow were determined $Tu = \sqrt{\overline{u}^2}/U$. The traversing system was reset to zero in the flow direction X, Y and 0.001 m in Z, the surface by conveying the tip of the hot-wire prongs on a line parallel to the edge of the flat plate surface. On the flat plate, we have taken 25 points as shown in the top view of the flat plate in Fig. 2. The Z was fixed and then the probe was conveyed at 0.01 m towards Y and at a given distance X of 0.01, 0.025, 0.04 or 0.05 m from the leading edge of the plate. A telescope (×24) was used to accurately locate the point of contact (the error of this visual observation through the magnifying glass was ±0.05 mm). From this point upward, the air velocity and fluctuation in the main flow direction were measured at 0.003 m and until the frontier of the boundary layer was reached (average velocity value became constant).

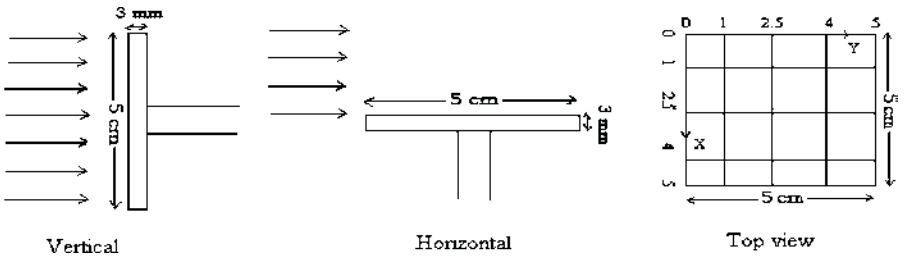

Fig. 2 Position and flow profile of flat plate

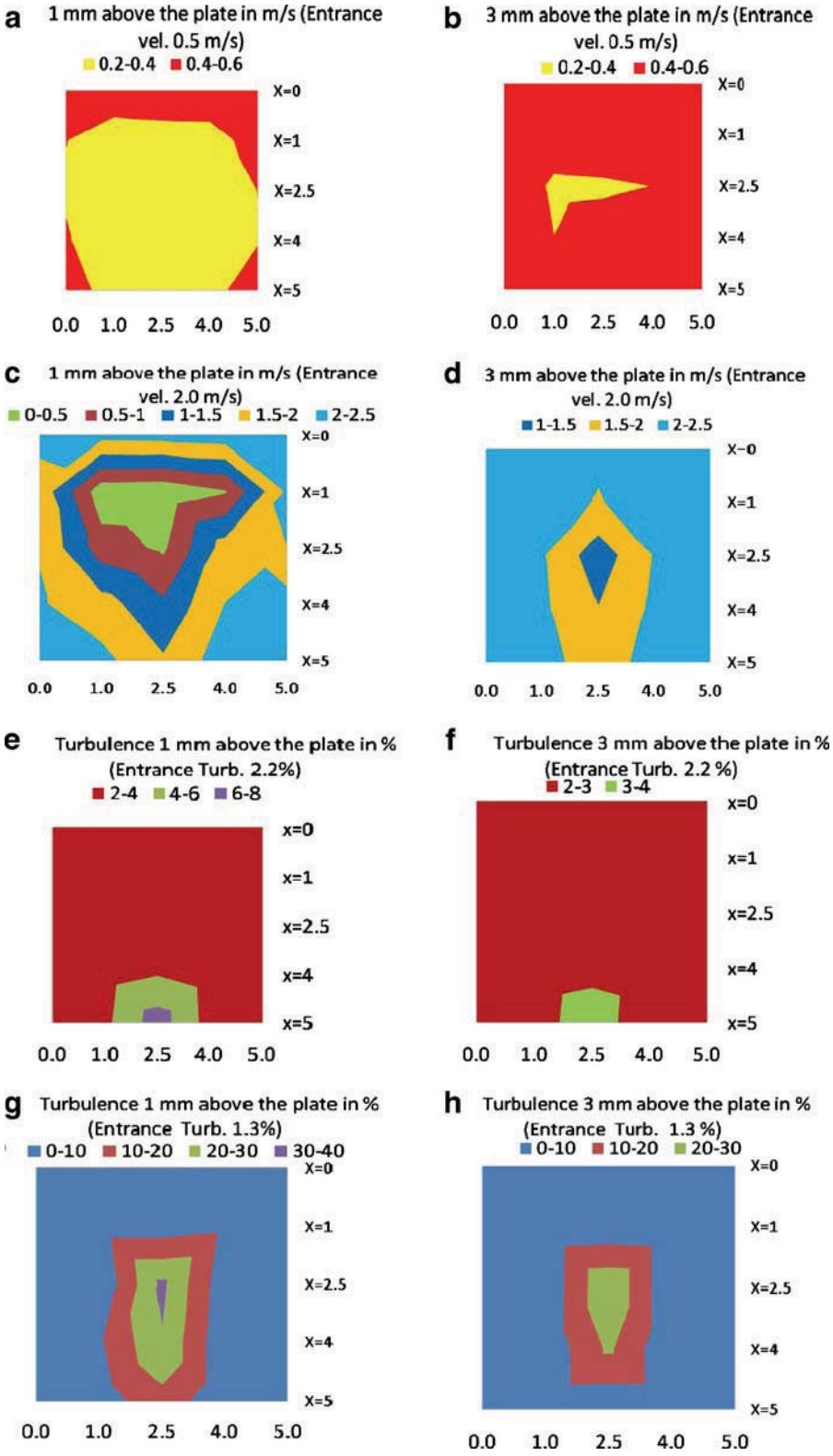

Fig. 3 **a**–**h** Comparative surface plots for the flat plate in horizontal position (**a**–**d**) velocity profiles in metre per second for (**a**, **b**) ambient temperature (T_a)=21.8°C and (**c**–**d**) at (T_a)=21.2°C and (**e**–**h**) turbulence intensity in per cent

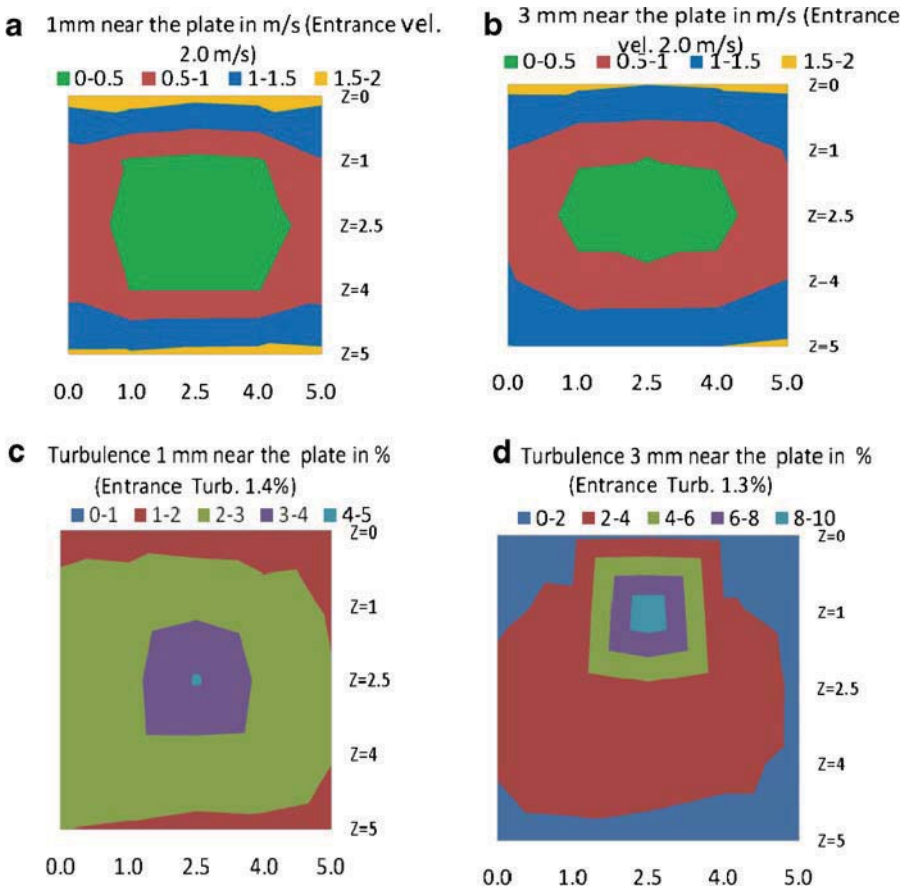

Fig. 4 **a**–**d** Comparative surface plots of a flat plate in vertical position (**a**, **b**) velocity profile in metre per second for (**a**) ambient temperature (T_a)=21.1°C and (**b**) at (T_a)=19.9°C (**c**–**d**) and turbulence intensity in per cent

4 Results and Discussions

We performed velocity measurements at 0.001 and 0.003 m away from the polished flat plate surface in both horizontal and vertical positions. Overall 25 measurement points for each height were considered as shown in the top view of the flat plate in Fig. 2. Velocity measurement using hot wire is known to be erroneous very close to the wall because of the influence of thermal exchanges by conduction and radiation between the wall and the wire (Brun 1995). When moving away from the wall, the velocity seems to decrease to a minimum and then to increase again.

The surface plots of the velocity profile are given for the flat plate in horizontal position in Fig. 3a–d and in vertical position in Fig. 4a, b. The turbulence intensity is given for the same positions in Fig. 3e–h and in Fig. 4c, d. The experiments were performed for a mean entrance velocity of 0.5, 1.1, 1.5 and 2.0 m s^{-1}, and the wind velocity as well as the turbulence intensity was measured. It is observed from Fig. 3a–d that, on moving from surface of the flat plate to free stream velocity, the fluctuations in the velocity decrease and the shape of the velocity profile is conical and centred towards the middle to back part of the flat plate. It is also observed in Fig. 3e–h that for a velocity of 0.5 m s^{-1} the maximum turbulence intensity at 0.001 m above the surface of the plate reaches 6–8%, and at 0.003 m above the surface it drops to 3–4%. In addition for 2.0 m s^{-1}, the maximum turbulence intensity is above 30% at 0.001 m height and more than 20% at 0.003 m above the flat plate. At the same

Table 1 Values of parameters used in calculations and taken at the time of the experiment

Parameter	Range
Atmospheric pressure, mbar	920–924
Dew point temperature, °C	1.2–6.6
Density of air, kg/m^3	1.202
Kinematic viscosity, m^2/s	1.525×10^{-5}

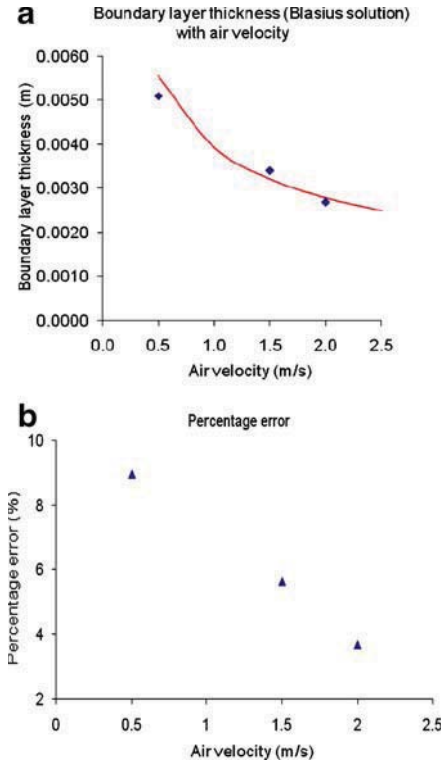

Fig. 5 **a** Comparative plots of boundary layer thickness calculated using Blasius solution (*continuous line*) and observed experimentally (*square points*); **b** its relative percentage error

time, the turbulence intensity at the entrance of the tunnel is 2.2% at 0.5 m s^{-1} and 1.4% at 2.0 m s^{-1}. We have taken the readings for a height of a little more than 0.005 m; the turbulence intensity at 0.005 m started decreasing and then suddenly reached the range of the turbulence intensity measured at the entrance of the tunnel, which shows that the probe was outside the boundary layer. The plots given in the Fig. 4a–d concern a vertical flat plate held perpendicular to the free stream flow. In this position, the velocity profile is always centred at the middle of the flat plate, where it is minimal, while the turbulence intensity increases as we move away from the surface of the flat plate. The middle part of the flat plate creates a hindrance in the path of free stream flow, which decreases the air velocity. As we go outside of the flat plate, the velocity increases and becomes similar to the velocity at the entrance of the wind tunnel. The turbulence intensity is obviously at its maximum in the middle part of the flat plate, but as we move away, the turbulence intensity decreases. When moving farther from the surface of the flat plate, the turbulence intensity is increased as long as the flow is still affected by the rebound effect. Figure 4c, d shows little asymmetry in the flow profile, which reflects the sensitivity of the boundary layer flow to the trailing edge of the flat plate. Hence, high-accuracy manufacturing is required in these conditions. We calculated the boundary layer thickness using Blasius' solution ($\delta \cong 4.5\sqrt{\upsilon L/U}$; see Table 1 for air properties) and obtained results close to the ones observed experimentally (3–9%). The plots are given in Fig. 5a, b for comparison with Blasius' solution and its relative error with the measured one.

5 Conclusion

We proved here that there is a need for an experimental facility that will evaluate accurately mass transfer coefficients around small obstacles with precise control and measurements of the velocity profiles and turbulence intensity around the obstacle. We have already tested this facility for a flat plate in dry conditions. At low-turbulence intensity, the average velocity profile inside the boundary layer can be described by Blasius solution even if the boundary layer is 5–10% thicker and if there is already production of turbulent fluctuations inside that layer. But for moderate turbulence intensity, the velocity boundary layer thickens a lot with the free stream velocity as well as the thickening of the displacement and momentum. The next step is to validate the low Re turbulence model used in the CFD approach to simulate the flow in a space environment (greenhouse or planetary outpost). Further studies will deal with the production of condensation and its accurate recording in order to deduce the mass transfer coefficients.

6 Symbols

k	Thermal conductivity, W/m K
D	Mass diffusivity, m^2/s
Tu	Turbulence intensity of air, %
L	Characteristic length of the plate, m
C_p	Specific heat capacity, J/kg K
U	Mean air velocity in the free stream, m/s
u	Velocity fluctuations around U in the main flow direction, m/s

Dimensionless quantity

Re Reynolds number
Pr Prandtl number
Sc Schmidt number

Greek

ρ Density, kg/m^3
μ Dynamic viscosity, Pa s
ν Kinematic viscosity, m^2/s
α Thermal diffusivity, m^2/s
δ Boundary layer thickness, m

Acknowledgements The authors gratefully acknowledge Dr. Alain Kondjoyan of the l'Institut National de la Recherche Agronomique (INRA) Lab in St. Genés Champanelle, France for allowing us to use their experimental facility and Mr. Cyril Chevarin for technical assistance. In addition, the authors thank Prof. Jean Bernard Gros, LGCB, for fruitful discussions. Authors are also thankful to the Centre National d'Etudes Spatiales (CNES), France, for providing financial support.

References

Bartsev, S. I., Gitelson, J. I., Lisovsky, H. M., Mezhevikin, V. V., & Okhonin, V. A. (1997). Perspectives of different type biological life support systems (BLSS) usage in space missions. *Acta Astronautica, 39*(8), 617.

Goldstein, R. & Cho, H. (1995). A review of mass transfer measurements using naphthalene sublimation. *Experimental Thermal and Fluid Science, 10*, 416.

Macleod, A. & Todd, R. B. (1973). Experimental determination of wall-fluid mass transfer coefficients using plasticized polymer surface coatings. *International Journal of Heat and Mass Transfer, 16*, 485.

Tianqing, L., Chunfeng, M., Xiangyu, S., & Songbai, X. (2007). Mechanism study on formation of initial condensate droplets. *AIChE Journal, 53*, 1050.

Guoxin Pang, J., Dale, D., & Kwok, D. Y. (2005). An integrated study of dropwise condensation heat transfer on self-assembled organic surfaces through Fourier transform infra-red spectroscopy and ellipsometry. *International Journal of Heat and Mass Transfer, 48*, 307.

Nusselt, W. A. (1916). The surface condensation of water vapour. *Zeitschrift Des Vereines Deutscher Ingenieure, 60*, 541.

Collier, J. G. & Thome, J. R. (1996). *Convective boiling and condensation* (3rd ed.). New York: Oxford University Press.

Poots, G. & Miles, R. (1967). Effects of variable physical properties on laminar film condensation of saturated steam on a vertical flat plate. *International Journal of Heat and Mass Transfer, 10*, 1677.

Sparrow, E. M. & Lin, S. H. (1964). Condensation heat transfer in the presence of a noncondensable gas. *Journal of Heat Transfer, 86*, 430.

Minkowycz, W. J. & Sparrow, E. M. (1966). Condensation heat transfer in the presence of noncondensables, interfacial resistance, variable properties and diffusion. *International Journal of Heat and Mass Transfer, 9*, 1125.

Rose, J. W. (1969). Condensation of a vapour in the presence of a noncondensing gas. *International Journal of Heat and Mass Transfer, 12*, 233.

Sparrow, E. M., Minkowycz, W. J., & Saddy, M. (1967). Forced convection in the presence of noncondensables and interfacial resistance. *International Journal of Heat and Mass Transfer, 10*, 1829.

McAdams, W. H. (1954). *Heat transmission* (3rd ed.). New York: McGraw-Hill.

Mills, A. F. & Seban, R. A. (1967). The condensation coefficient of water. *International Journal of Heat and Mass Transfer, 10*, 1815.

Othmer, D. F. (1929). The condensation of steam. *Industrial and Engineering Chemistry, 21*, 577.

Schmidt, E., Schurig, W., & Sellschopp, W. (1930). Versuche u¨ber die Kondensation von Wasserdampf in Film- und Tropfenform. *Technische Mechanik und Thermodynamik, 1*(2), 53.

Rausch, M. H., Froba, A. P., & Leipertz, A. (2008). Dropwise condensation heat transfer on ion implanted aluminium surfaces. *International Journal of Heat and Mass Transfer, 51*, 1061.

Fatica, N. & Katz, D. L. (1949). Dropwise condensation. *Chemical Engineering Progress, 45*(11), 661.

Rose, J. W. (1994). Dropwise condensation. Heat Exchanger Design Handbook Update, 2.6.5.

Ma, X., Chen, J., Xu, D., Lin, J., Ren, C., & Long, Z. (2002). Influence of processing conditions of polymer film on dropwise condensation heat transfer. *International Journal of Heat and Mass Transfer, 45*, 3405–3411.

Vemuri, S. & Kim, K. J. (2006). An experimental and theoretical study on the concept of dropwise condensation. *International Journal of Heat and Mass Transfer, 49*, 649.

Zhao, Q., Zhang, D., & Lin, J. (1991). Surface material with dropwise condensation made by ion implantation technology. *International Journal of Heat and Mass Transfer, 34*, 2833.

Zhao, Q., & Wang, Q. (1993). Vertical dropwise condensation shell and tube heat exchanger for steam with water cooling. Patent no. 91100529.3, China Patent Bureau (Patent Authority, Dalian University of Technology/Dalian Power Station).

Kondjoyan, A. & Daudin, J. D. (1997). Heat and mass transfer coefficients at the surface of a pork hindquarter. *Journal of Food Engineering, 32*, 225.

Brun, H. H. (1995). *Hot-wire anemometry—principles and signal analysis*. Oxford: Oxford Science.